QA: QA

ANL-EBS-GS-000001 REV 02

September 2007

Geochemistry Model Validation Report: Material Degradation and Release Model

Prepared for:
U.S. Department of Energy
Office of Civilian Radioactive Waste Management
Office of Repository Development
1551 Hillshire Drive
Las Vegas, Nevada 89134-6321

Prepared by:
Sandia National Laboratories
OCRWM Lead Laboratory for Repository Systems
1180 Town Center Drive
Las Vegas, Nevada 89144

Under Contract Number
DE-AC04-94AL85000

DISCLAIMER

This report was prepared as an account of work sponsored by an agency of the United States Government. Neither the United States Government nor any agency thereof, nor any of their employees, nor any of their contractors, subcontractors or their employees, makes any warranty, express or implied, or assumes any legal liability or responsibility for the accuracy, completeness, or any third party's use or the results of such use of any information, apparatus, product, or process disclosed, or represents that its use would not infringe privately owned rights. Reference herein to any specific commercial product, process, or service by trade name, trademark, manufacturer, or otherwise, does not necessarily constitute or imply its endorsement, recommendation, or favoring by the United States Government or any agency thereof or its contractors or subcontractors. The views and opinions of authors expressed herein do not necessarily state or reflect those of the United States Government or any agency thereof.

QA: QA

Geochemistry Model Validation Report: Material Degradation and Release Model

ANL-EBS-GS-000001 REV 02

September 2007

Model Signature Page/Change History

Complete only applicable items.

1. Total Pages: 240

2. Type of Mathematical Model

☒ Process Model ☐ Abstraction Model ☐ System Model

Describe Intended Use of Model

The results of the model will be used in criticality risk assessments to support the postclosure safety case.

3. Title

Geochemistry Model Validation Report: Material Degradation and Release Model

4. DI (including Revision No. and Addendum No.):

ANL-EBS-GS-000001 REV 02

	Printed Name	Signature	Date
5. Originator	Susan LeStrange	Susan LeStrange	9/19/07
6. Independent Technical Reviewer	David Sassani	David Sassani	9/19/07
7. Checker	Clinton Lum	Clinton Lum	9/19/07
8. QCS/Lead Lab QA Reviewer	Brian Mitchelltree	Brian Mitchelltree	9/19/07
9. Responsible Manager/Lead	Cliff Howard	Cliff Howard	9-19-07
10. Responsible Manager	Kathryn Knowles For Paul A Dixon	Paul A Dixon	9-19-07

11. Remarks

The contributing originators are as follows: Susan LeStrange (all sections), Sara Arthur (portions of Table 4-1 (FFTF, TMI, 5-DHLW/DOE SNF Long Waste Packages)), Harlan Stockman (all sections), Kaveh Zarrabi (Portions of Table 4-1 (N-Reactor, 2-MCO/2-DHLW Waste Package, Glass Pour Canisters, HLWG)), and Paul Mariner (Section 7.1.1). The contributing checkers are as follows: Clinton Lum (Sections 1 through 6, and 8), William Downs (Section 6 and 7), Emma Thomas, Kaveh Zarrabi, Sara Arthur. Checking assignments were made to preclude originators from checking their own work.

Change History

12. Revision No. and Addendum No.	13. Description of Change
00	Initial Issue.
01	The model was revised to incorporate new inputs and a new validation section.
02	The model was revised to incorporate revised inputs and to address DOE comments. This document addresses (1) CR 10727 (which indicates that the descriptions of seismic and igneous scenarios were switched in TWP) in Section 6.2.1, (2) CR 9424 (which indicates that N_2(aq) should be suppressed in adjusted-Eh runs) in Section 6.3.14, and (3) CR 7763 (which indicates that radionuclide solubility predictions at high pH do not agree with available solubility data) in Section 6.3.15. The changes are too extensive to show change bars. The Section number was corrected on page 3-1, paragraph 1. CH 9-27-07

INTENTIONALLY LEFT BLANK

CONTENTS

Page

CONTENTS (Continued)

Page

CONTENTS (Continued)

Page

INTENTIONALLY LEFT BLANK

FIGURES

Page

FIGURES (Continued)

Page

TABLES

Page

TABLES (Continued)

Page

ACRONYMS AND ABBREVIATIONS

B&W	Babcock & Wilcox
CDSP	codisposal waste package (used as a label for N-reactor)
CSNF	commercial spent nuclear fuel
DFA	driver fuel assemblies
DHLW	defense high-level waste
DOE	U.S. Department of Energy
DSNF	defense spent nuclear fuel
FFTF	Fast Flux Test Facility
GWd/MTU	gigawatt days per metric ton of uranium
HLWG	high-level waste glass
IPC	*In-Package Chemistry Abstraction* (report)
LiCon	low-density concrete (fill material)
LWBR	light water breeder reactor
MCO	multicanister overpack
MDR	material degradation and release
NRC	U.S. Nuclear Regulatory Commission
PWR	pressurized water reactor
RTA	*Radionuclide Transport Abstraction* (report)
SIT	specific-ion interaction theory
SNF	spent nuclear fuel
SRL	Savannah River Laboratory
TAD	transportation, aging, and disposal (canister)
TMI	Three Mile Island
TSPA	total system performance assessment
TSPA-LA	TSPA for the license application
TWP	technical work plan
YMP	Yucca Mountain Project

INTENTIONALLY LEFT BLANK

1. PURPOSE

The purpose of the material degradation and release (MDR) model is to predict the fate of the waste package materials, specifically the retention or mobilization of the radionuclides and the neutron-absorbing material as a function of time after the breach of a waste package during the 10,000 years after repository closure. The output of this model is used directly to assess the potential for a criticality event inside the waste package due to the retention of the radionuclides combined with a loss of the neutron-absorbing material. The output of this model is also used by the external accumulation model to assess the potential for accumulation of radionuclides outside the waste package. The scope of this report is to describe the development and validation of the MDR model and to use the model to analyze the degradation of commercial spent nuclear fuel (CSNF) waste packages and codisposal waste packages containing high-level waste glass (HLWG) and U.S. Department of Energy (DOE) spent nuclear fuel. This report was developed in accordance with *Technical Work Plan for: In-Package Geochemistry for Criticality Evaluations* (SNL 2006 [DIRS 179452]) requirements.

The model is based on the EQ3/6 computational code (V. 8.1. STN: 10813-8.1-00 [DIRS 176889]) and simulates the degradation of waste package components once aqueous solutions have entered the waste package. As a function of time, the model calculates: (1) dissolved concentrations, (2) mass and composition of corrosion products, and (3) quantity of intact waste package components (basket, fuel, etc.). The model is limited to the scenarios that involve seepage water entering the waste package—the seismic fault displacement and igneous scenarios. In the seismic scenario, the drip shield is displaced; waste package, cladding, and fuel containers fail; and seepage water flows through the waste package. In the igneous scenario, the drip shield is displaced, basalt fills the drift, and basalt-equilibrated water flows through the waste package.

INTENTIONALLY LEFT BLANK

2. QUALITY ASSURANCE

2.1 QUALITY ASSURANCE PROGRAM APPLICABILITY

Section 8.1 of *Technical Work Plan for: In-Package Geochemistry for Criticality Evaluations* (SNL 2006 [DIRS 179452]) indicates that this report is subject to quality assurance requirements because the activities involve "Performance of postclosure safety analysis, TSPA [total system performance assessment], and their inputs," as listed in Section 8 of Attachment 2 of SCI-PRO-002, *Planning for Science Activities*.

2.2 ELECTRONIC MANAGEMENT OF INFORMATION

The process-control evaluation for the electronic management of information was conducted in accordance with IM-PRO-002, *Control of the Electronic Management of Information*, as described by the technical work plan (TWP) (SNL 2006 [DIRS 179452], Section 8.5).

INTENTIONALLY LEFT BLANK

3. USE OF SOFTWARE

A list of controlled and baselined software used in this report is provided in Table 3-1 (in the model) and Table 3-2 (for validation), and the operating environments are provided in Table 3-3. The range of use for each software application is within that for which it was qualified. Each software code was selected because it is appropriate for use in geochemical modeling, uses the thermodynamic database qualified for use on the Yucca Mountain Project (YMP), and is subject to no limitations on the outputs due to the selected software (though there are limitations on the thermodynamic database used, which is discussed in more detail in Section ~~6.3.1.1~~ 6.3.13). SPR 9/27/07

Table 3-3 presents the computers and operating systems on which the software for this model was used. The use of the software was consistent with its intended use and within documented validation ranges. No software was used prior to qualification to develop any preliminary output. Microsoft Excel®, a commercial off-the-shelf software program, is used in this report; however, the results are not dependent on the software program used, so this software is exempt from requirements in IM-PRO-003, *Software Management*. Section 4 discusses formulas and inputs used in this model for all software. The outputs are discussed in Section 6. No other information is required for independent reproduction of the work.

Table 3-1. Computer Software Used

Software Name	Version	Software Tracking Number (Qualification Status)	Description and Components Used	Input and Output Files (Included in Output DTN: MO0705GEOMODEL.000)
EQ3/6	8.1 (2005)	STN: 10813-8.1-00 [DIRS 176889] (Qualified on Windows 2000)	EQ6: a FORTRAN reaction path code	input: *.6i output: *.6p, *.6o
			EQ3NR: a FORTRAN speciation-solubility code	input: *.3i output: *.3p, *.3o
			EQPT: a data file preprocessor in FORTRAN	input: *data0.** output: *data1.**
ASPRIN	1.0 (2004)	STN: 10487-1.0-00 [DIRS 179458] (Qualified on Windows 2000)	A postprocessor for EQ6 that computes the isotope fractions of actinides in waste package and reads the binary output file	input: *.bin output: *.txt
Microsoft Excel	SP2 (2003)	Commercial off-the-shelf software (Exempt)	Used in this document for graphical representation and arithmetical manipulations	input: *.txt, *.xls output: *.xls
Mathcad	13.0 (2005)	Commercial off-the-shelf software (Exempt)	Used to calculate the waste package–to-drift wall temperature difference	File: *.xmcd

Table 3-2. Computer Software Used in Validation

Software Name	Version	Software Tracking Number (Qualification Status)	Description and Components Used	Input and Output Files (Included in Validation DTN: MO0705MODELVAL.000)
EQ3/6	7.2b (1999)	UCRL-MA-110662 (LSCR198) [DIRS 153964] (Qualified on Windows 95 and HP-UX 10.20 B)	EQPT: a data file preprocessor in FORTRAN	input: *data0.** output: *data1.**
EQ6	7.2bLV (2002)	STN: 10075-7.2bLV-02 [DIRS 159731] (Qualified on Windows 2000 and NT)	EQ6: a reaction-path code that models water–rock interaction or fluid mixing in either a pure reaction progress mode or a time mode. Used for validation only	input: **.6i* pickup: **.6p* output: **.6o* **.elem_aqu.txt* **.elem_min.txt* **.elem_tot.txt* **.min_info.txt* **.bin*
PHREEQC	2.11 (2006)	STN: 10068-2.11-00 [DIRS 175698] (Qualified on Windows 2000)	A code for geochemical speciation, reaction path modeling, reactive transport, and surface-complexation modeling. Used for validation only	input: *. (no extension) output: **.out*

Table 3-3. Computers and Operating Systems

Computer Make	CPU #	Operating System	Software Used
Dell Optiplex GX260 (Susan LeStrange)	S884966	Windows 2000	EQ3/6 V. 8.1, ASPRIN V. 1.0, Microsoft Excel, Mathcad
Dell Optiplex GX260 (Kaveh Zarrabi)	S884946	Windows 2000	EQ3/6 V. 8.1, ASPRIN V. 1.0, Microsoft Excel
Dell Optiplex GX260 (Harlan Stockman)	S884922	Windows 2000	EQ3/6 V. 8.1, ASPRIN V. 1.0, Microsoft Excel
Dell Latitude D610 (Sara Arthur)	1R24M81	Windows 2000	EQ3/6 V. 8.1, ASPRIN V. 1.0, Microsoft Excel
Dell Optiplex GX300 (Patricia Bernot)	S884909	Windows 95	EQPT (EQ3/6 V. 7.2b, for validation only)
Dell Latitude D610 (Paul Mariner)	S874043	Windows 2000	PHREEQC V. 2.11 (for validation only)
Dell Optiplex GX260 (Clinton Lum)	S884908	Windows 2000	EQ6 V. 7.2bLV (for validation only)

NOTE: CPU = central processing unit.

4. INPUTS

This section lists the inputs used to develop this report. The information used to develop the model was not used to validate the model.

4.1 DIRECT INPUT

The information in the following sections is used as direct input to the MDR model, unless otherwise noted. Table 4-1 lists the data used in the MDR model.

Table 4-1. Summary of Direct Inputs

Identifier	Input	Reference[a]	Used in:[b]
Data0.ymp.R5	Thermodynamic data	DTN: SN0612T0502404.014 [DIRS 178850]	Section 6.3.13
J-13 Well Water	Water composition	DTN: MO0006J13WTRCM.000 [DIRS 151029]	Folder: EQ3\seismic pore waters\J-13, files: **.3i*
W1 Water	Water composition	DTN: GS030408312272.002 [DIRS 165226], Sample SD-9/1184.7-1184.8/UC	
W2 Water	Water composition	DTN: GS060908312272.004 [DIRS 179065], Sample HD-PERM-3/56.7-57.1/UC	
W3 Water	Water composition	DTN: MO0005PORWATER.000 [DIRS 150930], Sample ESF-HD-PERM-3	
Columbia Basin Basalt Water 1	Basalt water composition	Turney 1986 [DIRS 179852], Table 1 (p. 28), Table 2 (pp. 49 to 53)	Folder: EQ3\basalt waters, files: **.3i* Tables 4-3 and 4-4
Columbia Basin Basalt Water 2	Basalt water composition	Turney 1986 [DIRS 179852], Table 1 (p. 30), Table 2 (pp. 74 to 78)	
Iceland Basalt Water	Basalt water composition	Gislason and Eugster 1987 [DIRS 179957], Table 3, Sample SP01	Folder: EQ3\basalt waters, files: **.3i* Table 4-5
Drift Seepage Flux	Flux rates	DTN: MO0705TSPASEEP.000 [DIRS 180700], files: *seismic-FD.zip* and *Igneous.zip*	Section 6.3.4
Waste Package Temperature	Drift wall temperature	DTN: SN0703PAEBSPCE.006 [DIRS 181571], file: *WRIP calculations\Mathcad calculations of WRIP values\thermal-K, 10th percentile\Drift 5.xls* DTN: SN0703PAEBSPCE.006 [DIRS 181571], file: *WRIP calculations\Mathcad calculations of WRIP values\thermal-K, 90th percentile\Drift 3.xls*	Folder: temperature, file: *waste package temperature.xls*, Section 6.3.9 Table 4-6
	Waste package-to-drift wall temperature difference	SN0408T05093.007 [DIRS 171547], file: *2DComparison.mcd*	Folder: temperature, file: *DeltaT.xmcd*, Section 6.3.9

Table 4-1. Summary of Direct Inputs (Continued)

Identifier	Input	Reference[a]	Used in:[b]
High temperature Log K	Inputs for calculating log K for gadolinium and plutonium species for sensitivity calculation	Cantrell and Byrne 1987 [DIRS 181066], p. 555 Lide 2006 [DIRS 178081], p 4-64 Pankratz 1982 [DIRS 181065], p. 167 DTN: MO0302SPATHDYN.001 [DIRS 161886], files: *CpofCO2(fic)+P2O5(fic).xls* and *"YC Cp Regression vs Temp.xls*	Folder: Augment LogK, files: *Gd-CO3-complex-augmentk.xls, Solids_j_HWS_Gd.xls*, Appendix D
HLWG	Reaction rate	DTN: MO0502ANLGAMR1.016 [DIRS 172830], Table 8-1, Equations 50 and 51	Folder: CDSP (N-reactor), file: *CDSP WP_REV02.xls*
	HLWG composition and density	Allison 2004 [DIRS 168734], Table 3	Folder: glass, file: *CDSP_HLWGlass_2004.xls ;* Folder: CDSP (N-reactor), file: *CDSP WP_REV02.xls*
	Historical GlassSRL[c] composition	CRWMS M&O 2001 [DIRS 153263], Table 3	Section 4.1.3.3
	$f_{exposure}$[d]	DTN: MO0502ANLGAMR1.016 [DIRS 172830], Table 8-1	Folder: CDSP (N-reactor), file: *CDSP WP_REV02.xls*
N-reactor fuel	Reaction rate	DOE 2000 [DIRS 152658], Equation 2-39	Folder: CDSP (N-reactor), file: *CDSP WP_REV02.xls*
	Composition and density	DOE 2000 [DIRS 150095], Table 3-1 and Section 3.1.4	
CSNF pressurized water reactor (PWR)	Composition	BSC 2003 [DIRS 169110], Disk 1 of 9, folder: ATT III/LPM1/uniform_profile/3.5, file: *ft71-case10.N04*	Folder: CSNF, file: *CSNF Fuel REV02.xls*
	Reaction rate	DTN: MO0404ANLSF001.001 [DIRS 169007], Tables 8.1-2 and 8.1-3	Folder: CSNF, file: *CSNF WP and TAD.xls*, tab: CSNF rate
Fast Flux Test Facility (FFTF)	Fuel composition	INEEL 2002 [DIRS 158820], Table 1	Folder: FFTF, file: *CDSP_Long WP_FFTF_REV02.xls;* Folder: data0, file: *data0.ymp.R5.criticality*, and EQ6 input files
	Fuel reaction rate	DTN: MO0404ANLSF001.001 [DIRS 169007], Tables 8.1-2 and 8.1-3	
	DOE canister and internals	SNL 2007 [DIRS 179567], Table 4-9 Taylor 2005 [DIRS 180657], Appendix C INEEL 2002 [DIRS 158820], Section 3 and 4	
Three Mile Island (TMI) spent nuclear fuel (SNF)	Fuel composition and density	SNL 2007 [DIRS 179567], Table 4-1, No. 03-02, which points to BSC 2004 ([DIRS 172201], Table 5-12) Lide 2006 [DIRS 178081], p. 4-97 Wimmer 2001 [DIRS 158013], Table 3-1	Folder: TMI, file: *CDSP_Long_WP_TMI_REV02.xls;* Folder: data0, file: *data0.ymp.R5.criticality*, and EQ6 input files
	Fuel reaction rate	DTN: MO0404ANLSF001.001 [DIRS 169007], Tables 8.1-2 and 8.1-3	
	DOE canister and internals	DOE 2002 [DIRS 161752], Sections 1.3.1.1, 1.3.1.3.2 SNL 2007 [DIRS 179567], Table 4-9 Taylor 2005 [DIRS 180657], Appendix J SNL 2007 [DIRS 179567], Table 4-1, No. 03-02, which points to BSC 2004 ([DIRS 172201], Table 5-12) INEEL 2002 [DIRS 158820], Section 4 Wimmer 2001 [DIRS 158013], Figures 2-2 and 2-3, Tables 2-3 and 3-1	

Table 4-1. Summary of Direct Inputs (Continued)

Identifier	Input	Reference[a]	Used in:[b]
21-PWR CSNF waste package	Fuel assembly and waste package component dimensions	Punatar 2001 [DIRS 155635], pp. 2-3 and 2-5, Tables 2-2, 2-3, and 3-1, Figures 2-2, 2-3, 2-5, 2-6, and 2-7 SNL 2007 [DIRS 179394], Tables A-1 through A-7	Folder: CSNF, file: *CSNF WP and TAD.xls,* and EQ6 input files
5-DHLW[e] / DOE SNF – Long waste package	Waste package component dimensions	SNL 2007 [DIRS 179567], Table 4-9	Folder: FFTF, file: *CDSP_Long WP_FFTF_REV02.xls;* Folder: TMI, file: *CDSP_Long_WP_TMI_REV02.xls*, and in EQ6 input files
2-MCO / 2-DHLW waste package	Waste package component dimensions	DOE 2000 [DIRS 150095], pp. 24 to 28 SNL 2007 [DIRS 179567], Table 4-10	Folder: CDSP (N-Reactor), file: *CDSP WP REV02.xls*
Glass pour canisters	Glass pour canister dimensions	SNL 2007 [DIRS 179567], Table 4-10 DOE 1992 [DIRS 102812], Figure 3.4.2	Folder: CDSP (N-Reactor), file: *CDSP WP REV02.xls, CDSP_Long WP_FFTF REV02.xls*, *CDSP_Long_WP_TMI REV02.xls*
Periodic table	Atomic weights of elements and isotopes	Audi and Wapstra 1995 [DIRS 149625], pp. 409 to 480 Parrington et al. 1996 [DIRS 103896], p. 50	Folder: CDSP (N-Reactor), file: *CDSP WP REV02.xls, CSNF WP.xls, CDSP_Long WP_FFTF REV02.xls*, *CDSP_Long_WP_TMI REV02.xls*, and all EQ6 input files
Stainless Steel Type 316 and Type 316L	Corrosion rate	DTN: MO0409SPAACRWP.000 [DIRS 172059]	Folder: corrosion rates, file: *Steels and Alloys REV02.xls*
	Density	ASTM G 1-90 1999 [DIRS 103515], Table XI, p. 7	
	Composition	ASTM A 240/A 240M-03b 2003 [DIRS 165003], Table 1, p. 4	
Stainless Steel Type 304B4	Corrosion rate	DTN: MO0706ECTBSSAR.000 [DIRS 181380], Tables 5, 6, and 7	Folder: corrosion rates, files: *Steels and Alloys REV02.xls* and *304B4 INL results.xls*
	Density	Carpenter Technology Corporation 2003 [DIRS 179642]	
	Composition	ASTM A 887-89 2004 [DIRS 154062], p. 2; SNL 2007 [DIRS 179394], Section 4.1.1.5 (boron composition)	
Stainless Steel Type 304L	Corrosion rate	DTN: MO0409SPAACRWP.000 [DIRS 172059]	Folder: corrosion rates, file: *Steels and Alloys REV02.xls, CDSP_Long WP_FFTF_REV02.xls*, *CDSP_Long_WP_TMI_REV02.xls*
	Density	ASTM G 1-90 1999 [DIRS 103515], Table XI, p. 7	
	Composition	ASTM A 240/A 240M-03b 2003 [DIRS 165003], Table 1, p. 3	
Zircaloy-4	Density	ASM International 1990 [DIRS 141615], p. 666, Table 6	Folder: CSNF, file: *CSNF WP and TAD.xls*, tab 21-PWR Part 2

Table 4-1. Summary of Direct Inputs (Continued)

Identifier	Input	Reference[a]	Used in:[b]
Inconel 718	Density	Lynch 1989 [DIRS 154076], p. 496	Folder: CSNF, file: *CSNF WP and TAD.xls*, tab 21-PWR Part 2
Carbon Steel Type A516	Corrosion rate	DTN: MO0409SPAACRWP.000 [DIRS 172059]	Folder: corrosion rates, file: *Steels and Alloys REV02.xls, CDSP_Long WP_FFTF_REV02.xls*, *CDSP_Long_WP_TMI_REV02.xls*
	Density	ASTM A 20/A20M-99a. 1999 [DIRS 147578], Section 14, p. 9.	
	Composition	ASTM A 516/A 516M-01 2001 [DIRS 162723], Table 1, grade 70, ½" to 2" thickness, product analysis	
Aluminum Alloy Type 6061, Type 1100, Type 2024	Corrosion rate	DTN: MO0409SPAACRWP.000 [DIRS 172059]	
	Density	ASTM G 1-90 1999 [DIRS 103515], Table X1.1	
	Composition	ASTM B 209M-02 2002 [DIRS 162727], Table 1, p. 2	
Gadolinium metal	Density	Lide 2006 [DIRS 178081], p. 4-64	*CDSP_Long WP_FFTF_REV02.xls*
Nickel–gadolinium alloy	Corrosion rate (immersion tests)	DTN: MO0409SPAACRWP.000 [DIRS 172059]	Folder: corrosion rates, files: *Steels and Alloys REV02.xls; NiCrMoGdalloy.xls*
	Corrosion rate (potentiostatic tests)	DOE 2004 [DIRS 168434], p. 53	
	Composition and density	ASTM B 932-04 2004 [DIRS 168403], Table 1 and Section 8	*Steels and Alloys REV02.xls, CDSP_Long WP_FFTF_REV02.xls*
LiCon[f]	Composition and density	DOE 2002 [DIRS 161752], Section 1.2.1.3 and Table 5	Folder: TMI, file: *CDSP_Long_WP_TMI REV02.xls*
	High corrosion rate	Blenkinsop et al. 1985 [DIRS 181193], Tables 1, 2, and 3	Folder: corrosion rates, file: *LiCon.xls*
	Low corrosion rate	Dunster et al. 2000 [DIRS 181194], Table 2	
^{239}Pu Half-Life	Radioactive half-life	Parrington et al. 1996 [DIRS 103896], p. 48	Folder : CSNF, folder: CSNF Igneous, file : *decay.eq6*.

NOTES: [a] References used as "established fact" are justified in Section 4.1.11. Qualifications of outside references are found in Appendix G.
[b] Files and folders listed in column 4 are located in output DTN: MO0705GEOMODEL.000)
[c] GlassSRL = glass composition from the Savannah River Laboratory used in previous calculations.
[d] $f_{exposure}$ = an empirical factor that accounts for the effects of cracking, the extent to which water can penetrate cracks, and the reactivity of glass in cracks compared to free surface.
[e] DHLW = defense high-level waste.
[f] LiCon = type of low-density concrete.

4.1.1 Thermodynamic Databases

The thermodynamic database, *data0.ymp.R5* (DTN: SN0612T0502404.014 [DIRS 178850]), was used with the EQ3/6 software. This database is qualified for use for temperatures up to 200°C. The thermodynamic database has high-temperature data for most solids and aqueous species. However, when there are no high-temperature data for certain species, 25°C data are used. The database is appropriate for the MDR model because it includes the elements that

constitute the waste package, waste form, seepage, and gas compositions in the temperature range needed for the model.

4.1.2 Input Water Compositions

Table 4-2 summarizes the input water compositions used in the seismic scenario as direct input. J-13 well water composition was used to maintain consistency with previous work. The other three waters listed in Table 4-2 are pore water compositions that have been identified as representative of three of the four groups of waters to be used in TSPA calculations (SNL 2007 [DIRS 177412]; DTN: SN0703PAEBSPCE.007 [DIRS 180177], file *Cl_NO3_CDFs.xls,* tab: "34 TSw pore waters summary"; water compositions are highlighted in red on spreadsheet). The representative composition of the fourth group of waters, not included in the current modeling, is bounded by the composition of J-13 and the three water compositions as shown in *waters.xls* (output DTN: MO0705GEOMODEL.000, folder: EQ3\seismic pore waters). For simplicity, the water compositions are referred to as J-13, W1, W2, and W3.

Table 4-2. Seismic Scenario Input Water Compositions

Parameter	Units	Sample ID (Shorthand name in parentheses)			
		J-13 Well Water[a, e] (J-13)	SD-9/1184.7-1184.8/UC[b] (W1)	HD-PERM-3/56.7-57.1/UC[c] (W2)	ESF-HD-PERM-3[d] (W3)
Ca^{2+}	mg/L	13	19	59.9	97
Mg^{2+}	mg/L	2.01	0.7	16.7	17.4
Na^{+}	mg/L	45.8	59	123	62
K^{+}	mg/L	5.04	4.8	13.8	9
SiO_2	mg/L	61.0	42	—	75
NO_3^{-}	mg/L	8.78	16	57.4	10
Cl^{-}	mg/L	7.14	23	146	123
F^{-}	mg/L	2.18	2.2	1.3	0.76
SO_4^{2-}	mg/L	18.4	16	126	120
pH	pH	7.41 (8.23)	8.2 (8.28)	- (8.24)	8.31 (8.31)

Sources: [a] DTN: MO0006J13WTRCM.000 [DIRS 151029].
[b] DTN: GS030408312272.002 [DIRS 165226].
[c] DTN: GS060908312272.004 [DIRS 179065].
[d] DTN: MO0005PORWATER.000 [DIRS 150930].

NOTES: The SiO_2 value is calculated from the 28.5 mg/L of silicon given in DTN: MO0006J13WTRCM.000 [DIRS 151029].

For the pH parameter, the values in parenthesis are the pH values once the solution is equilibrated to log fCO_2 = –3.0 and 50°C (Output DTN: MO0705GEOMODEL.000, folder: EQ3\seismic pore waters\J-13).

For the igneous scenario, water that enters the waste package must first flow through basalt that has filled the drifts. The basalt may partially fill breached waste packages. Therefore, the seepage water entering the waste package is modeled as water equilibrated with basalt rocks. Three basalt water compositions were taken as input—two compositions from the Columbia River Basin basalt in the State of Washington (Tables 4-3 and 4-4) and one from a basalt unit in Iceland (Table 4-5). The samples from the Columbia Basin are from two basalt units, each of which is a combination of two other basalt units: (1) Wanapum and Brande Ronde basalts and (2) Saddle Mountains and Wanapum basalts. The samples were chosen such that most of the

element concentrations are close to the median value (Tables 4-3 and 4-4). The sample chosen from Iceland was collected from a spring (Table 4-5). The basalt waters are referred to as Columbia Basin 1 (Base Case), Columbia Basin 2 (CB2), and Iceland basalt (IB).

Table 4-3. Basalt Water Composition 1, Columbia Basin

		Summary of Water Samples from Adams County, Washington			Selected Sample (Base Case)
Parameter	Units	Maximum	Minimum	Median	Wanapum and Grande Ronde Basalts, Sample 19/31E-27G01D1
Sodium	mg/L	89	8.5	45	76
SiO_2 (aq)	mg/L	110	30	56	73
Calcium	mg/L	95	1.0	18	3.9
Potassium	mg/L	14	1.9	7.3	8.0
Magnesium	mg/L	45	0.1	8	0.5
Fluorine	mg/L	4.8	0.1	0.9	1.9
Chlorine	mg/L	110	2.1	11	13
SO_4	mg/L	180	2.2	21	21
$NO_2 + NO_3$	mg/L as N	30	<0.1	0.35	<0.1
Hydrogen	pH	9.4	7.3	8.2	8.6 (8.36)[a]

[a] The value in parentheses is the pH value once the solution is equilibrated to log fCO_2 = –3.0 and 50 °C (Output DTN: MO0705GEOMODEL.000, folder: EQ3\ basalt waters\Columbia Basin CSNF\BaseCase composition).

Source: Turney 1986 [DIRS 179852], Table 1 (p. 28), Table 2 (pp. 49 to 53).

Table 4-4. Basalt Water Composition 2, Columbia Basin

		Summary of Water Samples from Franklin County, Washington			Selected Sample (Columbia Basin 2)
Parameter	Units	Maximum	Minimum	Median	Saddle Mountains and Wanapum Basalts, Sample 14/31E-19B01
Sodium	mg/L	90	18	35	22
SiO_2 (aq)	mg/L	100	32	56	58
Calcium	mg/L	80	0.8	29	36
Potassium	mg/L	21	2.1	6.9	6.4
Magnesium	mg/L	57	0.3	18	21
Fluorine	mg/L	2.4	0.3	0.6	0.4
Chlorine	mg/L	55	3.4	18	17
SO_4	mg/L	150	<0.2	43	55
$NO_2 + NO_3$	mg/L as N	13	<0.1	1.9	2.0
Hydrogen	pH	8.8	7.4	7.8	8.0 (8.33)[a]

[a] The value in parentheses is the pH value once the solution is equilibrated to log fCO_2 = –3.0 and 50°C (Output DTN: MO0705GEOMODEL.000, folder: EQ3\ basalt waters\Columbia Basin CSNF\Columbia Basin 2).

Source: Turney 1986 [DIRS 179852], Table 1 (p. 30), Table 2 (pp. 74 to 78).

Table 4-5. Basalt Water Composition 3, Iceland

	Iceland Basalt Spring Water, Sample SP01	
Parameter	**Value**	**Units**
Sodium	15.8	ppm
SiO_2 (aq)	18.1	ppm
Calcium	4.35	ppm
Potassium	1.11	ppm
Magnesium	2.44	ppm
Fluorine	0.28	ppm
Chlorine	2.30	ppm
SO_4	8.6	ppm
Hydrogen	9.0 (7.89)[a]	pH

[a] The value in parentheses is the pH value once the solution is equilibrated to log fCO_2 = –3.0 and 50°C (output DTN: MO0705GEOMODEL.000, folder: EQ3\basalt waters\Iceland).

Source: Gislason and Eugster 1987 [DIRS 179957], Table 3.

4.1.3 Water Flux into the Repository Drift

The range of drift seepage flux expected for the seismic and igneous scenarios is presented in Figures 4-1 and 4-2. The values represent locations in the repository with the lowest seepage (PS1) and the highest seepage (PS5). The seepage rates result from TSPA GoldSim calculations (DTN: MO0705TSPASEEP.000 [DIRS 180700]). The drift seepage represents the water that enters the area defined by the diameter of the emplacement drift and the waste package length. The values shown are for the CSNF waste packages. Data are also available for codisposal waste packages, but the values are approximately the same (see output DTN: MO0705GEOMODEL.000, folder: seepage, file: *Igneous seepage.xls*, tabs: "25% Chart" and "95% Chart"). The values are used in Section 6.3.4 to estimate the seepage flux into a breached waste package.

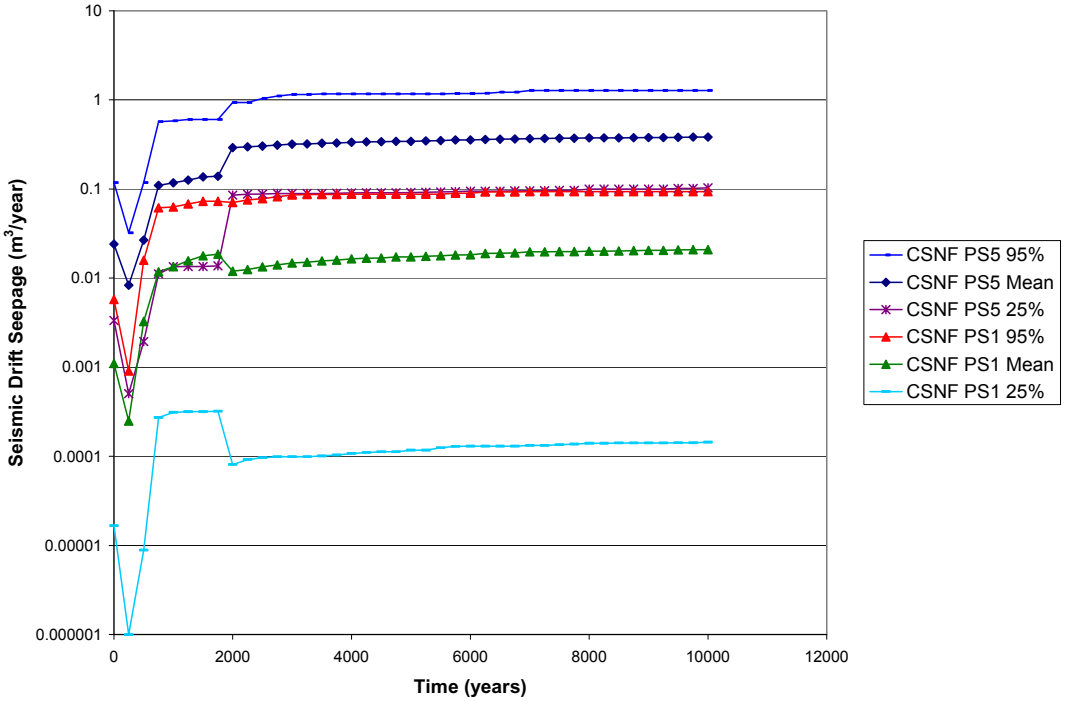

Source: Data from DTN: MO0705TSPASEEP.000 [DIRS 180700], File *seismic-FD.zip*; data plotted in output DTN: MO0705GEOMODEL.000, folder: seepage.

Figure 4-1. Seismic Drift Seepage

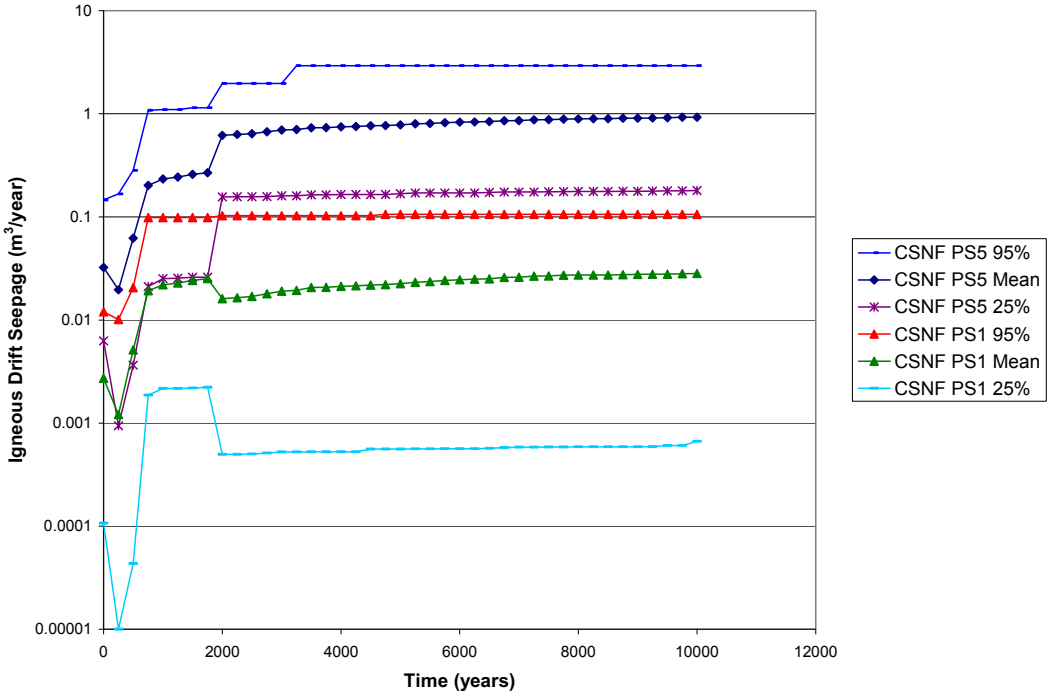

Source: Data from DTN: MO0705TSPASEEP.000 [DIRS 180700], File: *igneous.zip*; data plotted in output DTN: MO0705GEOMODEL.000, folder: seepage.

Figure 4-2. Igneous Drift Seepage

4.1.4 Temperature

The high and low drift-wall temperatures are outputs from the near-field chemistry model (DTN: SN0703PAEBSPCE.006 [DIRS 181571]) and are presented in Table 4-6. The high value comes from the middle of Drift 5, at the 10th percentile of thermal conductivity, whereas the low value comes from the coolest edge of Drift 3, which is at the edge of the repository. The location of the drifts within the repository footprint is presented in *In-Drift Natural Convection and Condensation* (SNL 2007 [DIRS 181648], Figures 6.3.5-11 and 6.3.5-9).

The temperature of the waste package surface and the drift wall, calculated by the FLUENT model in the in-drift natural convection and condensation model (SNL 2007 [DIRS 181648]), are provided in DTN: SN0408T05093.007 [DIRS 171547], file: *2DComparison.mcd*. Those values were used in Section 6.3.9 to calculate the average temperature difference between the waste package and the drift wall. The temperature difference and the drift wall temperature are used to calculate the waste package surface temperature for use in the EQ6 degradation calculations.

Table 4-6. Drift Wall Temperature

Time (years)	Temperature (°C), middle of Drift 5, 10th percentile thermal conductivity	Temperature (°C), Drift 3, edge2, 90th percentile thermal conductivity
50	44.31	24.11
51	95.43	24.13
52	111.73	24.15
55	131.65	24.20
60	142.81	24.29
65	146.64	24.41
70	146.94	24.61
80	145.61	25.21
90	142.88	25.96
100	140.12	26.74
120	135.52	28.23
150	129.98	30.05
200	124.76	32.18
300	120.05	34.63
400	116.97	36.00
500	114.18	36.83
600	111.49	37.33
700	108.88	37.62
800	106.34	37.74
900	103.89	37.76
1,000	101.52	37.68
1,100	99.67	37.56
1,200	97.87	37.41
1,300	95.99	37.23
1,400	94.02	37.01
1,500	91.93	36.77
2,000	84.52	35.52
3,000	75.11	33.54
5,000	65.88	31.56
7,000	60.59	30.55
10,000	54.81	29.50

Source: DTN: SN0703PAEBSPCE.006 [DIRS 181571], file: WRIP calculations\Mathcad calculations of WRIP values\thermal-K, 10th percentile*Drift 5.xls* tab: "middle, distance from center of drift: 2.75" and file: WRIP calculations\Mathcad calculations of\WRIP values\thermal-K, 90th percentile*Drift3.xls* tab: "Edge2, distance from center of drift: 2.75."

4.1.5 Waste Form Compositions and Degradation Rates

4.1.5.1 Commercial Spent Nuclear Fuel

The CSNF composition comes from *PWR Assembly End-Effect Reactivity Evaluation* (BSC 2003 [DIRS 169110], Disk 1 of 9, folder: ATT III/LPM1/uniform_profile/3.5, file: *ft71-case10.N04*), which starts with fresh fuel (UO_2) and calculates the composition of the irradiated fuel when it is discharged from the reactor (specified by burnup) and at specified times after discharge. The calculations were performed in that report (BSC 2003 [DIRS 169110]) using the SAS2H sequence and the ORIGEN sequence of the SCALE computer code system (SCALE V. 4.3 [DIRS 154059]). The calculation covers initial enrichment of 2 wt % to 5 wt % ^{235}U, and burnup of 0 gigawatt days per metric ton of uranium (GWd/MTU) to 50 GWd/MTU. The quantity of fuel in one assembly is based on the Babcock and Wilcox (B&W) 15 × 15-assembly design with the mass of type Mark B4. The Mark B4 design contains the greatest mass of uranium per assembly (Punatar 2001 [DIRS 155635], Table 3-1). The B&W 15 × 15 fuel assembly is one of the most reactive 21-PWR designs (B&W Fuel Company 1991 [DIRS 104439], p. II 6-6). A representative assembly for CSNF with an initial enrichment of 3.5 wt % ^{235}U and a burnup of 40 GWd/MTU was chosen by visual inspection of the central region of the CSNF assembly population illustrated in *21-PWR Waste Package with Absorber Plates Loading Curve Evaluation* (BSC 2004 [DIRS 172553], Figure 34).

Table 4-8 gives the gram-atom content of the simplified elements contained in the spent fuel. The calculated percentage of each isotope represented in the simplified composition is presented in Section 6.3.2. Table 4-8 does not contain all the radionuclides that are important to criticality. The complete list of principal isotopes that are considered important to criticality is provided in *Disposal Criticality Analysis Methodology Topical Report* (YMP 2003 [DIRS 165505], Table 3-1, p. 3-30). Table 4-9 contains the gram-atom content of the principal isotopes contained in the spent fuel, but not contained in the simplified composition of Table 4-8. The values in Table 4-9 are used in Section 6.3.2 to calculate inputs for two sensitivity calculations for the igneous scenario (*CSIGPI.6i, CSIGPI_R.6i, and CSIGPIss.6i*).

Table 4-8. Simplified Composition of CSNF

Isotope	Gram-atoms
^{234}U	4.33×10^{-2}
^{235}U	$1.15 \times 10^{+0}$
^{236}U	7.14×10^{-1}
^{238}U	$1.02 \times 10^{+2}$
^{237}Np	2.68×10^{-1}
^{239}Pu	5.93×10^{-1}
^{240}Pu	1.07×10^{-1}
^{242}Pu	7.39×10^{-2}
^{93}Zr	1.54×10^{-1}
^{95}Mo	2.46×10^{-1}
^{99}Tc	2.37×10^{-1}
^{101}Ru	2.37×10^{-1}
^{103}Rh	1.49×10^{-1}
^{105}Pd	1.18×10^{-1}
^{108}Pd	4.61×10^{-2}
^{107}Ag	7.65×10^{-5}
^{109}Ag	2.73×10^{-2}
^{133}Cs	2.65×10^{-1}
^{135}Cs	6.81×10^{-2}
^{138}Ba	2.90×10^{-1}
^{89}Y	1.55×10^{-1}
^{141}Pr	2.46×10^{-1}
^{143}Nd	1.78×10^{-1}
^{145}Nd	1.40×10^{-1}
^{148}Nd	7.80×10^{-2}
^{147}Sm	4.78×10^{-2}
^{149}Sm	1.12×10^{-3}
^{150}Sm	6.82×10^{-2}
^{152}Sm	2.57×10^{-2}
^{151}Eu	3.88×10^{-3}
^{153}Eu	2.53×10^{-2}
^{154}Gd	6.18×10^{-3}
^{155}Gd	1.31×10^{-3}
^{156}Gd	1.72×10^{-2}
^{158}Gd	4.66×10^{-3}
^{160}Gd	2.21×10^{-4}

Source: BSC 2003 [DIRS 169110], Disk 1 of 9, folder: ATT III/LPM1/uniform_profile/3.5, file: *ft71-case10.N04*; used in output DTN: MO0705GEOMODEL.000, file: *CSNF Fuel REV02.xls*, tab: "Complete Fuel Composition."

NOTE: The numerical designation of the radionuclides in the source is decoded in the file *CSNF Fuel REV02.xls*, tab: "Complete Fuel Composition."

Table 4-9. CSNF Principal Isotope Composition Not Included in Simplified Composition

Isotope	Gram-atoms
^{241}Am	6.94×10^{-6}
^{242}Am	3.88×10^{-26}
^{243}Am	7.62×10^{-3}
^{103}Rh	1.49×10^{-1}
^{107}Ag	7.65×10^{-5}
^{109}Ag	2.73×10^{-2}
^{143}Nd	1.78×10^{-1}
^{145}Nd	1.40×10^{-1}
^{148}Nd	7.80×10^{-2}
^{147}Sm	4.78×10^{-2}
^{149}Sm	1.12×10^{-3}
^{150}Sm	6.82×10^{-2}
^{152}Sm	2.57×10^{-2}
^{151}Eu	3.88×10^{-3}
^{153}Eu	2.53×10^{-2}

Source: BSC 2003 [DIRS 169110], Disk 1 of 9, folder: ATT III/LPM1/uniform_profile/3.5, file: *ft71-case10.N04*; used in Output DTN: MO0705GEOMODEL.000, file: *CSNF Fuel REV02.xls*, tab: "Complete Fuel Composition."

NOTE: The numerical designation of the radionuclides in the source is decoded in the file *CSNF Fuel REV02.xls*, tab: "Complete Fuel Composition."

The CSNF degradation rate law (DTN: MO0404ANLSF001.001 [DIRS 169007], Tables 8.1-2 and 8.1-3) is dependent on pH, O_2 partial pressure, total carbonate, and temperature. This rate, Log(F/A), is expressed in units of mg/m^2/day and is appropriate for temperatures less than 100°C, total carbonate concentrations greater than 2×10^{-4} molar, and an oxygen partial pressure from 0.002 atm to 0.2 atm. For low fCO_2 conditions (lower than a total carbonate molar concentration equal to 2×10^{-4} molar), the rate described in Equation 4-1 should be used with a total carbonate molar concentration equal to 2×10^{-4} molar (BSC 2004 [DIRS 169987], Section 8.2).

For pH > 6.8:

$$\text{Log (F)} = \text{Log (A)} + a_0 + a_1 \times \text{IT} + a_2 \times pCO_3 + a_3 \times pO_2 \qquad \text{(Eq. 4-1)}$$

For pH ≤ 6.8:

$$\text{Log (F)} = \text{Log (A)} + a_0 + a_1 \times \text{IT} + a_3 \times pO_2 + a_4 \times \text{pH} \qquad \text{(Eq. 4-2)}$$

where,

Log(F) = $\log_{10}$ fractional dissolution rate of the fuel (per day)
Log(A) = $\log_{10}$ of the fuel effective specific surface area (m^2/mg)
IT = inverse temperature (Kelvin^{-1})

pCO_3 = $-\log_{10}$ (total molar carbonate species concentration)
pO_2 = $-\log_{10}$ (oxygen partial pressure in atmospheres).

The values for Log(A), a_0, a_1, a_2, a_3, and a_4, are given in Table 4-10. This combined rate is appropriate for use for a pH range from 2 to 10.3 (BSC 2004 [DIRS 169987], Section 8.2). The rate equations are converted into terms suitable for EQ6 in *CSNF WP and TAD.xls*, tab "CSNF Rate."

Table 4-10. Commercial Spent Nuclear Fuel Rate Parameters

Model Parameter	Alkaline Parameter Value	Acidic Parameter Value
Log(A)	−7.3 (min), −6.7 (apex), −5.4 (max)	−7.3 (min), −6.7 (apex), −5.4 (max)
a_0	4.705	6.60
a_1	−1,093.826	−1,093.826
a_2	−0.102	N/A
a_3	−0.338	−0.338
a_4	N/A	−0.340

Source: DTN: MO0404ANLSF001.001 [DIRS 169007], Tables 8.1-2 and 8.1-3.

Summary Report of Commercial Reactor Criticality Data for Crystal River Unit 3 (Punatar 2001 [DIRS 155635], Table 2-2, p. 2-5) and *Total System Performance Assessment Data Input Package for Requirements Analysis for TAD Canister and Related Waste Package Overpack Physical Attributes Basis for Performance Assessment* (SNL 2007 [DIRS 179394]) provide inputs required to calculate the quantity and surface areas of waste package materials comprising the 21-PWR waste package. These calculations are contained in *CSNF WP and TAD.xls*. The 21-PWR assembly volume, calculated in *CSNF WP.xls*, is corroborated by a volume value of 0.081 m^3 from *Criticality Evaluation of Degraded Internal Configurations for the PWR AUCF WP Designs* (CRWMS M&O 1997 [DIRS 102824], Table 4.1-1).

4.1.5.2 N-Reactor Fuel

N Reactor (U-Metal) Fuel Characteristics for Disposal Criticality Analysis (DOE 2000 [DIRS 150095], Table 3-1 and Sections 3.1.4 and 4), for Mark IV fuel, provides the N-reactor fuel composition information and density, and the multicanister overpack (MCO) dimensions used in the MDR model. Praga (1998 [DIRS 172869]) corroborates the N-reactor fuel composition and the MCO dimensions information. Due to the poor N-reactor fuel cladding condition (DOE 2000 [DIRS 152658]), the fuel is always considered 100% exposed.

A linear degradation rate (i.e., constant reaction rate) of 1.12×10^5 mg/(m^2 d) at 50°C is used for the dissolution of the N-reactor fuel (calculated in output DTN: MO0705GEOMODEL.000, file: *CDSP_WP_REV02.xls*, worksheet "CDSP Rates"). This rate is five times the constant U-metal rate reported in *Review of Oxidation Rates of DOE Spent Nuclear Fuel, Part 1: Metallic Fuel* (DOE 2000 [DIRS 152658], Equation 2-39). That report (DOE 2000 [DIRS 152658]) also contains the N-reactor fuel degradation rate, which is the property of interest. Gray and Einziger (1998 [DIRS 109691], Section 4.3) document a rate of 1.3×10^4 mg/(m^2 d), thereby corroborating the rate from *Review of Oxidation Rates of DOE Spent Nuclear Fuel, Part 1: Metallic Fuel* (DOE 2000 [DIRS 152658]).

In the MDR model for defense spent nuclear fuel (DSNF), the EQ6 simulations were split into two stages. In the first stage, N-reactor fuel was corroded by interacting with seepage water for 1 year. The resulting EQ6 pick-up file was used to create the second-stage EQ6 input file. The second stage models the interaction of all waste package components with the minerals and solutions formed by corrosion of the fuel in the first stage. Using the above rate in EQ6 results in complete degradation of the DSNF within six months. Because this rate equates to essentially instantaneous degradation of the DSNF, it is also appropriate for the higher temperature simulations.

N Reactor (U-Metal) Fuel Characteristics for Disposal Criticality Analysis (DOE 2000 [DIRS 150095], Section 3.1.4 and Table 3-1) and *Total System Performance Assessment Data Input Package for Requirements Analysis for DOE SNF/HLW and Navy SNF Waste Package Overpack Physical Attributes Basis for Performance Assessment* (SNL 2007 [DIRS 179567]) provide the inputs required to calculate the quantity and surface areas of the waste package materials for the 2-MCO/2-DHLW (defense high-level waste) waste package (as shown in output DTN: MO0705GEOMODEL.000, folder: CDSP (N-reactor), file: *CDSP WP_REV02.xls*). The N-reactor rate is converted to EQ6 format in output DTN: MO0705GEOMODEL.000, folder: CDSP (N-reactor), file: *CDSP WP_REV02.xls*.

The EQ6 simulations use pure uranium metal to represent the N-reactor fuel. Although some of the N-reactor fuel has contains fission products, the pure metal (unburned) fuel is considered to be the most reactive for criticality calculations.

4.1.5.3 High-Level Waste Glass

Glass Composition—The base case HLWG composition in Table 4-11 comes from Allison (2004 [DIRS 168734], Table 3). The cover letter transmitting the data from DOE Savannah River Operations to John Arthur of the Office of Civilian Radioactive Waste Management indicates that this report contains the HLWG composition range that should be referenced. In previous calculations in support of criticality, such as *EQ6 Calculations for Chemical Degradation of N Reactor (U-metal) Spent Nuclear Fuel Waste Packages* (CRWMS M&O 2001 [DIRS 153263], Table 3), the HLWG composition presented in Table 4-12 was used. A sensitivity case for N-reactor (*CD_S_GS.6i*) using the composition in Table 4-12 was implemented to see how sensitive the model results are to differences in glass composition.

HLWG Degradation Rate—The HLWG degradation rate expression (DTN: MO0502ANLGAMR1.016 [DIRS 172830]) can be modeled with the "transition-state" rate law in EQ6, and is dependent on the pH value of the solution. (The logK for dissolution of HLWG is given a very high value in the thermodynamic database, so the transition-state saturation term is always approximately 1.) The rate law coefficients provided were deemed the "most probable" in *Defense HLW Glass Degradation Model* (BSC 2004 [DIRS 169988]). This rate is appropriate for temperatures less than 100°C. The exposure factor, $f_{exposure}$, is the value that is multiplied by the geometric surface area of the HLWG to achieve an effective surface area, which includes an increase in surface area due to fractures in the glass. The most likely value for $f_{exposure}$ is 4, and the maximum value is 17 (DTN: MO0502ANLGAMR1.016 [DIRS 172830], Table 8-1).

Table 4-11. HLWG Composition

Oxides	Batch 1A (Wt %)	Batch 1B (Wt %)	Batch 2 (Wt %)
Al_2O_3	4.60%	5.37%	4.22%
B_2O_3	8.71%	8.18%	7.31%
CaO	1.27%	1.39%	1.39%
Fe_2O_3	12.10%	10.50%	12.30%
Li_2O	3.68%	3.53%	3.29%
Na_2O	12.27%	11.50%	11.40%
MgO	2.12%	2.16%	2.35%
MnO	1.37%	1.76%	2.14%
P_2O_5	0.46%	0.63%	NM
SiO_2	50.33%	52.40%	48.70%
U_3O_8	1.08%	1.06%	3.57%

Source: Allison 2004 [DIRS 168734], Table 3.

Table 4-12. Historical HLWG Composition (GlassSRL)

Element	Mol/100g HLWG
Oxygen	2.70
Uranium	7.82×10^{-3}
Barium	1.08×10^{-3}
Aluminum	8.63×10^{-2}
Sulfur	4.01×10^{-3}
Calcium	1.62×10^{-2}
Phosphorus	4.89×10^{-4}
Silicon	7.76×10^{-1}
Boron	2.91×10^{-1}
Fluorine	1.66×10^{-3}
Iron	1.72×10^{-1}
Potassium	7.51×10^{-2}
Magnesium	3.33×10^{-2}
Sodium	5.77×10^{-1}

Source: CRWMS M&O 2001 [DIRS 153263], Table 3.

NOTES: GlassSRL = Defense HLWG produced at Savannah River Laboratory.

Mol/100g = moles of each element contained in 100 g of HLWG.

For acidic conditions (DTN: MO0502ANLGAMR1.016 [DIRS 172830], Section 8.1, Equation 50), the rate is given in Equation 4-3:

$$rate_G = k_{E\_acidic} \times 10^{-0.49 \cdot pH} \times \exp(-31 \text{ kJ/mol } / RT) \quad \text{(Eq. 4-3)}$$

For alkaline conditions (DTN: MO0502ANLGAMR1.016 [DIRS 172830], Section 8.1, Equation 51), the rate is given in Equation 4-4:

$$rate_G = k_{E\_alkaline} \times 10^{0.49 \cdot pH} \times \exp(-69 \text{ kJ/mol } /RT) \quad \text{(Eq. 4-4)}$$

where (DTN: MO0502ANLGAMR1.016 [DIRS 172830], Section 8.1):

$rate_G$ = the glass rate law in units of g/m^2/day

k_{E_acidic} = the glass degradation rate coefficient for acidic solutions: the minimum and most probable value of k_{E_acidic} is 8.41×10^3 g/(m^2 d), and the maximum value of k_{E_acidic} is 1.15×10^7 g/(m^2 d)

$k_{E\_alkaline}$ = the glass degradation rate coefficient for alkaline solutions: the minimum and most probable value of $k_{E\_alkaline}$ are 2.82×10^1 g/(m^2 d), and the maximum value of $k_{E\_alkaline}$ is 3.47×10^4 g/(m^2 d).

Glass Pour Canisters—The following references provide properties of interest for the glass pour canisters, and include canister dimensions: *Total System Performance Assessment Data Input Package for Requirements Analysis for DOE SNF/HLW and Navy SNF Waste Package Overpack Physical Attributes Basis for Performance Assessment* (SNL 2007 [DIRS 179567], Tables 4-9 and 4-10) and *Characteristics of Potential Repository Wastes* (DOE 1992 [DIRS 102812], Figures 3.4.1 and 3.4.2), These references contain the most detailed information available on the specific dimensions of the glass pour canister. In addition, assumptions have been made about the wall thickness and fill volume of these canisters (see Assumption 5.2, Section 5). These dimensions are used to calculate surface areas and volumes of the glass pour canisters and are converted to EQ6 inputs (output DTN: MO0705GEOMODEL.000, folder: CDSP (N-reactor), file: *CDSP WP REV02.xls*).

The HLWG rate is converted to EQ6 format in output DTN: MO0705GEOMODEL.000, folder: CDSP (N-reactor), file: *CDSP WP REV02.xls*.

4.1.5.4 Fast Flux Test Facility

FFTF (MOX) Fuel Characteristics for Disposal Criticality Analysis (INEEL 2002 [DIRS 158820], Table 1) is the source for the composition of the Fast Flux Test Facility (FFTF) fuel, which is used in output DTN: MO0705GEOMODEL.000, file: *CDSP_Long WP_FFTF_REV02.xls*, tab "Fuel."

Loo et al. 2004 ([DIRS 168999], Section 6.3) and *DSNF and Other Waste Form Degradation Abstraction* (BSC 2004 [DIRS 172453], Section 6.1.4 and Table 6-2) suggest the CSNF dissolution rate model be used for FFTF mixed uranium/plutonium oxide fuel. The CSNF dissolution rate model (see Section 4.1.3.1) was used to represent FFTF fuel in the degradation and release model. Since this fuel consists of UO_2 and $(U,Pu)O_2$, the CSNF rate should overestimate the FFTF degradation rate, since the dissolution of PuO_2 occurs about 10 times more slowly than UO_2 (or CSNF) dissolution (DOE 2003 [DIRS 166027], Section 2.3.2).

FFTF (MOX) Fuel Characteristics for Disposal Criticality Analysis (INEEL 2002 [DIRS 158820], Section 3 and 4), *Total System Performance Assessment Data Input Package for Requirements Analysis for DOE SNF/HLW and Navy SNF Waste Package Overpack Physical Attributes Basis for Performance Assessment* (SNL 2007 [DIRS 179567], Table 4-9), and *Using Fuel Parameters to Predict DOE SNF Canister Loadings* (Taylor 2005 [DIRS 180657], Appendix C), provide the inputs required to calculate the quantity and surface areas of the waste package components of the FFTF 5-DHLW Long DOE spent nuclear fuel (SNF) waste package in *CDSP_Long WP FFTF_REV02.xls*). *Using Fuel Parameters to Predict DOE SNF Canister Loadings* (Taylor 2005 [DIRS 180657], Appendix C) is the source for the dimensions and material of the nickel–gadolinium alloy basket, which holds the FFTF fuel inside of the DOE canister. These basket dimensions are corroborated by *Criticality Calculation for the Most Reactive Degraded Configurations of the FFTF SNF Codisposal WP Containing an Intact Ident-69 Container* (BSC 2002 [DIRS 164418], Section 5.1.2) and *DOE SNF Phase I and II Summary Report* (Radulescu et al. 2004 [DIRS 165482], Section 3.2.1).

Radulescu et al. (2004 [DIRS 165482], Table 10-2) state that the most reactive FFTF waste package configuration includes four driver fuel assemblies (DFAs) with an IDENT 69 fuel pin container in the central nickel-gadolinium basket position with one radial basket position void. The MDR model will also consider a sensitivity calculation for another reactive configuration consisting of five DFAs in the radial basket positions with the central basket position void (*FFTF5DFA.6i*). For the first of these reactive configurations, Radulescu et al. (2004 [DIRS 165482], Table 10-2) recommend the addition of at least 30.8 kg of gadolinium beyond the amount contained in the nickel-gadolinium basket, probably as aluminum-gadolinium shot (see Assumption 5.3, Section 5). This shot material will need to be added to FFTF waste packages inside the DOE canister around the DFAs and in the void basket position. A shot diameter of 3 mm was chosen (see Assumption 5.3, Section 5) to be consistent with the aluminum-gadolinium shot modeled for the Shippingport (Pennsylvania) light water breeder reactor (LWBR) spent fuel waste packages (Radulescu et al. 2004 [DIRS 165482], Table 10-14).

The composition for this material was based on that of aluminum Alloy 2024 (UNSA92024) with 15% added gadolinium. The source for the composition of aluminum Alloy 2024 shown in Table 4-14 is ASTM B 209M-02 (2002 [DIRS 162727], Table 1, p. 2). The density of the aluminum-gadolinium fill material was calculated from the densities of UNSA92024 (ASTM G 1-90 1999 [DIRS 103515], Table X1.1) and gadolinium metal (Lide 2006 [DIRS 178081], p. 4-64) in *CDSP_Long WP_FFTF_REV02.xls,* tab *Al-Gd shot* (output DTN: MO0705GEOMODEL.000, folder: FFTF). These densities are also given in Table 4-14.

Table 4-14. Composition and Density of Aluminum Alloy and Density of Gadolinium Metal

Element	Weight %[a]
Silicon	0.50
Iron	0.50
Copper	4.35 (3.8-4.9)
Manganese	0.6 (0.3-0.9)
Magnesium	1.5 (1.2-1.8)
Chromium	0.10
Zinc	0.25
Titanium	0.15
Aluminum	92.05 (remainder)
Total	100
Density[b]	2.78 (g/cm^3)
Density of gadolinium metal[c]	7.9 (g/cm^3)

Sources: [a] ASTM B 209M-02 2002 [DIRS 162727], Table 1, p. 2.
[b] ASTM G 1-90 1999 [DIRS 103515], Table X1.1.
[c] Lide 2006 [DIRS 178081], p. 4-64.

NOTE: For copper, manganese, and magnesium, the average value of the wt % range in parentheses was used.

4.1.5.5 Three Mile Island Fuel Assemblies

TMI Fuel Characteristics for Disposal Criticality Analysis (DOE 2003 [DIRS 164970]) provides an overall description of Three Mile Island (TMI) fuel assemblies and disposal canisters. The reference was used as corroboration, while several other references were used (listed in Table 4-1) to provide qualified inputs necessary for the calculations.

TMI consisted of 15 × 15 arrays of 225 rods, of which 208 were fuel rods composed of about 326 UO_2 pellets each (Wimmer 2001 [DIRS 158013]). The fuel rod cladding was made of Zircaloy-4, and the fuel assembly end fittings were made of Stainless Steel Type 304L. As a result of recovery and cleanup of a reactor core after the TMI accident in March 1979, core debris was placed in Stainless Steel Type 304L canisters large enough to contain one TMI assembly (DOE 2003 [DIRS 164970], Section 1). For this model, TMI fuel loading is considered to be one complete assembly to ensure the highest possible mass of uranium per TMI canister (DOE 2003 [DIRS 164970], Table 4). Only one such TMI canister can be placed in each DOE canister. The TMI DOE canister, thus, contains the following reactive components:

- Carbon Steel Type A516 impact plates
- Carbon Steel Type A516 (or Stainless Steel Type 316) sleeve/basket structure used to center the TMI canister inside the DOE canister (DOE 2003 [DIRS 164970], Section 4.1.4, Figure 13; Taylor 2005 [DIRS 180657], Appendix J)
- A Stainless Steel Type 304L TMI Type D fuel canister and top plate
- A Stainless Steel Type 304L center box structure within the TMI canister to hold the fuel assembly in place

- Low-density concrete (LiCon) fill material inside the TMI canister and outside of the center box structure
- A TMI SNF assembly composed of UO_2 with Stainless Steel Type 304L assembly end fittings.

The dimensions and characteristics of the TMI spent nuclear fuel waste package components and the DOE SNF canister dimensions were used to calculate the surface areas and quantities of the TMI waste package materials in *CDSP_Long_WP_TMI_REV02.xls* (output DTN: MO0705GEOMODEL.000, folder: TMI).

The fresh TMI fuel composition used for the MDR model has the composition of UO_2 (Wimmer 2001 [DIRS 158013]). Loo et al. (2004 [DIRS 168999], Section 6.8) suggest the CSNF dissolution rate model be used for uranium oxide DSNF. *DOE Spent Nuclear Fuel Information in Support of TSPA-SR* (DOE 2002 [DIRS 158405], Section 6.8) and *DSNF and Other Waste Form Degradation Abstraction* (BSC 2004 [DIRS 172453], Section 6.1.8 and Table 6-2) suggest that the CSNF rate law be used but that the fuel surface area be multiplied 100× for the TMI core debris material. The 100 × CSNF dissolution rate model (see Section 4.1.5.1) was used for TMI fuel in the degradation and release model with the effective specific surface area for CSNF (see Table 4-10).

Table 4-15 presents the composition, density, and degradation rates of LiCon, the low-density concrete fill material used inside the TMI canister and outside of the center box structure. LiCon is hydrated high-alumina cement with glass microsphere filler. *SNF Canister Characteristics for Criticality Analysis of a Dual Canister/Waste Package Disposal Strategy* (DOE 2002 [DIRS 161752], Section 1.2.1.3 and Table 5) is the source for the density and composition of the LiCon fill material for this analysis. The density and composition of the LiCon fill material in *SNF Canister Characteristics for Criticality Analysis of a Dual Canister/Waste Package Disposal Strategy* (DOE 2002 [DIRS 161752], Section 1.2.1.3 and Table 5) are very close to those given in *TMI Fuel Characteristics for Disposal Criticality Analysis* (DOE 2003 [DIRS 164970], Section 3.3 and Table A-6). The LiCon degradation rate was estimated as the carbonation rate observed for other high alumina concretes in laboratory experiments and structural materials (Blenkinsop et al. 1985 [DIRS 181193]; Dunster et al. 2000 [DIRS 181194]; Crammond and Currie 1993 [DIRS 181195]). Carbonation is the prime means of attack on high alumina concrete, converting hydrous calcium aluminates in the cured cement to calcite ($CaCO_3$) and aluminum hydroxide.

Table 4-15. Properties of LiCon Fill in TMI SNF Waste Package

Element	Number Density atoms/barn-cm[a]
Hydrogen	1.9351×10^{-2}
Oxygen	2.1531×10^{-2}
Sodium	1.4380×10^{-4}
Aluminum	2.8385×10^{-3}
Silicon	8.1796×10^{-4}
Magnesium	3.5859×10^{-5}
Calcium	1.3101×10^{-3}
Iron	1.3576×10^{-5}
Density[b] (g/cm^3)	1
Low rate[c] ($\mu m/y$)	1,740
High rate ($\mu m/y$)	10,910

Sources: [a] DOE 2002 [DIRS 161752], Table 5.
[b] DOE 2002 [DIRS 161752], Section 1.2.1.3.
[c] The low 20°C rate from output
DTN: MO0705GEOMODEL.000, file *LiCon.xls*.
[d] The estimated 40°C rate from output
DTN: MO0705GEOMODEL.000, file *LiCon.xls*.

4.1.6 Waste Package Material Compositions

This report analyzes four waste package design configurations for different fuel types: the 21-PWR CSNF waste package, the 2-MCO/2-DHLW waste package containing N-reactor fuel, the 5-DHLW/DOE SNF long waste package containing FFTF fuel, and the 5-DHLW/DOE SNF long waste package containing TMI fuel. The last three configurations are codisposal waste packages, meaning that fuel is packaged for disposal together with HLWG. However, since most of the codisposal cases were run using the N-reactor waste package, the N-reactor waste package is referred to in tables and file names as the codisposal (CDSP) waste package. For the purposes of this report, the following labels are used to describe the four waste package configurations: CSNF, CDSP, FFTF, and TMI. Using these labels, Table 4-16 lists the metal alloys and their shorthand references, as they are used in this model for each waste package type.

In SNL 2007 ([DIRS 179394], Tables A-1 and A-2), two potential design cases for the transportation, aging, and disposal (TAD) canister are presented. For Case 1, the following materials are identified: Alloy 22 for the outer corrosion barrier; Stainless Steel Type 316 for the inner vessel; Stainless Steel Type 316L for the basket guides, stiffeners, and fuel basket tubes; and Aluminum Alloy 6061 and borated stainless steel for the fuel basket plates (SNL 2007 [DIRS 179394], Table A-1). For Case 2, all materials are the same except the fuel basket tubes are constructed of borated stainless steel and the fuel basket plates are constructed of Stainless Steel Type 316L.

Table 4-16. Materials Nomenclature and Waste Package Breakdown

Material Nomenclature	Shorthand	Waste Package Type			
		CSNF	CDSP	FFTF	TMI
Alloy 22 (UNS N06022)	Alloy 22	X	X	X	X
SA-240 (UNS S31600) Stainless Steel	Stainless Steel Type 316	X	X	X	X
SA-240 (UNS S31603) Stainless Steel	Stainless Steel Type 316L	X	X	X	X
SA-240 S30403 Stainless Steel	Stainless Steel Type 304L		X	X	X
SA-516 Grade 70 Carbon Steel	Carbon Steel Type A516		X	X	X
SB-209 (UNS A96061 T4)	Aluminum Alloy Type 6061	X			
Aluminum Alloy-1100	Aluminum Alloy Type 1100		X		
Alloy (UNS N06464)	Nickel-Gadolinium alloy			X	
Aluminum Alloy with gadolinium	Aluminum-Gadolinium alloy			X	
304B4 (UNS S30464)	Borated stainless steel	X			

Source: See Table 4-1 for sources for each waste package type.

NOTE: CSNF = commercial spent nuclear fuel; CDSP = codisposal; FFTF = Fast Flux Test Facility; TMI = Three Mile Island.

The main codisposal (N-reactor) waste package components use the following materials: Alloy 22 for the outer corrosion barrier, Stainless Steel Type 316 for the inner vessel, Carbon Steel Type A516 for the divider plate fuel support assemblies (SNL 2007 [DIRS 179567], Table 4-10), Stainless Steel Type 304L for the MCO (DOE 2000 [DIRS 150095], Section 4) and glass pour canisters (DOE 1992 [DIRS 102812]), and Aluminum Alloy 1100 for the MCO spacer (DOE 2000 [DIRS 150095], Section 4).

Table 4-17 summarizes the composition of the steel and aluminum alloys present in the CSNF and DOE SNF waste packages. The material compositions from Table 4-17 are converted to EQ6 format in *Steel and Alloys REV02.xls*.

Table 4-17. Composition of Steel and Aluminum Alloys

Element	Carbon Steel Type A516 (wt %)	Borated Stainless Steel (wt %)	Aluminum Alloy 6061 (wt %)	Stainless Steel Type 316[a] and 316L (wt %)	Aluminum Alloy 1100 (wt %)	Stainless Steel Type 304L (wt %)	Ni–Gd Alloy (wt %)
Carbon	0.28[b]	0.08	–	0.08 (316L: 0.03)	–	0.03	0.01
Manganese	0.79 to 1.30 (1.045)[c, b]	2.00	0.15	2.00	0.05	2.00	0.5
Phosphorus	0.035	0.045	–	0.045	–	0.045	0.005
Sulfur	0.035	0.030	–	0.03	–	0.03	0.005
Silicon	0.13 to 0.45 (0.29)[c]	0.75	0.40 to 0.8 (0.60)[c]	0.75	0.95 (Si+Fe) 0.45	0.75	0.08
Chromium	–	18.00-20.00 (19.00)	0.04 to 0.35 (0.195)[c]	16.0 to 18.0 (17.00)[c]	–	18.0 to 20.0 (19.00)[c]	14.5- to 17.1 (15.8)[c]
Nickel	–	12.00-15.00 (13.5)[c]	–	10.0 to 14.0 (12.00)[c]	–	8.0 to 12.0 (10.00)[c]	Balance: 64.035[d]
Cobalt	–	–	–	–	–	–	2
Molybdenum	–	–	–	2.00 to 3.00 (2.50)[c]	–	–	13.1 to 16.0 (14.55)[c]
Nitrogen	–	0.1	–	0.1	–	0.1	0.01
Iron	Balance: 98.3[d]	Balance: 63.295[d]	0.7	Balance: 65.495 (316L: 65.545)[d]	0.95 (Si+Fe) 0.50	Balance: 68.045[d]	1
Boron	–	1.00 to 1.24 (1.2)[e]	–	–	–	–	–
Zinc	–	–	0.25	–	0.10	–	–
Copper	–	–	0.15 to 0.40 (0.275)[c]	–	0.05 to 0.20 (0.125)[c]	–	–
Magnesium	–	–	0.8 to 1.2 (1.0)[c]	–	–	–	–
Titanium	–	–	0.15	–	–	–	–

Table 4-17. Composition of Steel and Aluminum Alloys (Continued)

Element	Carbon Steel Type A516 (wt %)	Borated Stainless Steel (wt %)	Aluminum Alloy 6061 (wt %)	Stainless Steel Type 316[a] and 316L (wt %)	Aluminum Alloy 1100 (wt %)	Stainless Steel Type 304L (wt %)	Ni–Gd Alloy (wt %)
Aluminum	–	–	Balance: 96.68[d]	–	Balance: 98.78[d]	–	–
Gadolinium	–	–	–	–	–	–	1.9 to 2.1 (2.0)[c]
Oxygen	–	–	–	–	–	–	0.005
Total	100.0	100.0	100.0	100.0	100.0	100.0	100.0

Source: See Table 4-1.

NOTES: [a] Composition applies to Stainless Steel Types 316 and 316L, unless otherwise specified.
[b] Value is for Grade 70 thicknesses between ½ in to 2 in.
[c] Represents the average of the range specified in source.
[d] Balance values calculated based on the averaged values.
[e] Indicates value used in calculations, based on upper limit (SNL 2007 [DIRS 179394], Section 4.1.1.5).

4.1.7 Waste Package Materials Density

Table 4-18 provides the densities and corrosion rates for the waste package metal alloys described in Table 4-17.

Table 4-18. Steel and Alloy Densities and Corrosion Rates

Metal	Density (g/cm^3)
Carbon Steel Type A516	7.85
Aluminum Alloy 6061	2.70
Aluminum Alloy 1100	2.71
Stainless Steel Type 316 and 316L	7.98
Stainless Steel Type 304L	7.94
Borated Stainless Steel	7.81
Ni–Gd Alloy	8.76
Zircaloy-4	6.56
Inconel 718	8.19

Source: Table 4-1.

4.1.8 Waste Package Materials Corrosion Rates

Tables 4-19 and 4-20 contain the corrosion rates used in this model, which come from DTN: MO0409SPAACRWP.000 [DIRS 172059], *Interim Report on the Corrosion Performance of a Neutron Absorbing Ni-Cr-Mo-Gd Alloy* (DOE 2004 [DIRS 168434]), and DTN: MO0706ECTBSSAR.000 [DIRS 181380] for temperatures from 25°C to 90°C. The corrosion rates used are justified because they consider the range of degradation rates for the materials that make up the waste package as documented by *Aqueous Corrosion Rates for Waste Package Materials* (BSC 2004 [DIRS 169982], Section 1).

Table 4-19. Corrosion Rates for Steels and Alloys

Metal	Conditions	Corrosion Rate (µm/yr)			Source
		10%[a]	90%	50%	
Stainless Steel Type 304L	Freshwater (25°C to 100°C)	0.0113	0.47	0.127	DTN: MO0409SPAACRWP.000 [DIRS 172059], spreadsheet *ECDF_metals2.xls*, "304-ecdf-low," "304-ecdf-max" Used in file: *Steels and Alloys REV02.xls*
Stainless Steel Type 316	Freshwater (29.5°C)	0.0007	0.0113	0.003	DTN: MO0409SPAACRWP.000 [DIRS 172059], spreadsheet *ECDF_metals2.xls*, "316-ecdf-fresh" Used in file: *Steels and Alloys REV02.xls*
	Freshwater (50°C to 100°C)	0.1016	0.51	0.229	
Carbon Steel Type A516	SDW (60°C) (simulated dilute well, 10x J-13 well water)	70	85.68	74.6	DTN: MO0409SPAACRWP.000 [DIRS 172059], spreadsheet *ECDF_metals2.xls*, "A-516-ecdf" Used in file: *Steels and Alloys REV02.xls*
	SDW (90°C)	36.38	65.88	48.3	
Aluminum alloy	Freshwater	1.52	27.56	9.5	DTN: MO0409SPAACRWP.000 [DIRS 172059], spreadsheet "ECDF_metals2.xls," aluminum-ecdf-0-100% Used in file: *Steels and Alloys REV02.xls*

Table 4-19. Corrosion Rates for Steels and Alloys (Continued)

Metal	Conditions	Corrosion Rate (µm/yr)			Source
		Min	Max	Median	
Nickel-gadolinium-alloy	Freshwater (30°C immersion)	0.0201	0.0774	0.0557	DTN: MO0409SPAACRWP.000 [DIRS 172059], Spreadsheet: *ECDF_metals2.xls*, tab "Ni-Cr-Mo-Gd-Alloy ecdf" Used in file: *Steels and Alloys REV02.xls*
	Freshwater (30°C potentiometric, J-13 Solution)	0.039	0.067	0.0595	DOE 2004 [DIRS 168434], p. 53 Used in file: *NiCrMoGdalloy.xls*
	Freshwater (60°C potentiometric, J-13 Solution)	0.172	0.525	0.2655	DOE 2004 [DIRS 168434], p. 53 Used in file: *NiCrMoGdalloy.xls*

NOTE: [a] The column headings 10%, 90% and 50% in the first part of the table refer to the percentiles in the ECDF (empirical cumulative distribution function), where the ECDF records the proportion of observations less than or equal to a particular corrosion rate, as shown in the cited source documents.

Table 4-20. Corrosion Rates for Borated Stainless Steel

LPR Measurements, Average Corrosion Rate (µm/yr)		Gravimetric Analysis, Corrosion Rate (µm/yr)	
Type 304B4	Type 304B5	Type 304B4	Type 304B5
3.61×10^{-2}	3.80×10^{-2}	0.0641	0.074
4.44×10^{-2}	3.74×10^{-2}	0.0956	0.0528
3.09×10^{-2}	3.51×10^{-2}	0.0428	0.0423
1.39×10^{-2}	7.29×10^{-3}		
1.93×10^{-2}	2.87×10^{-2}		
1.96×10^{-2}	2.25×10^{-2}		
3.61×10^{-2}	2.53×10^{-1}		
2.90×10^{-2}	1.51×10^{-2}		
1.63×10^{-2}	1.28×10^{-2}		
2.53×10^{-2}	2.63×10^{-2}		
2.34×10^{-2}	1.58×10^{-2}		
3.03×10^{-2}	1.18×10^{-2}		

Source: DTN: MO0706ECTBSSAR.000 [DIRS 181380], Tables 5, 6, and 7. Used in *304B4 INL results.xls.*

NOTE: LPR = linear polarization resistance.

4.1.9 Atomic Weights

Atomic weights of the elements and radionuclides used were taken from *Atomic Mass Adjustment, Mass List for Analysis* (Audi and Wapstra 1995 [DIRS 149625]) and *Nuclides and Isotopes, Chart of the Nuclides* (Parrington et al. 1996 [DIRS 103896], p. 50). The atomic weights of the elements are used to convert the weight percent of the elements in the metal alloys to moles of elements in the metal alloys used as input in the EQ6 files.

4.1.10 Thermodynamic Values at Elevated Temperatures

As discussed in Section 4.1.1, for some species, *data0.ymp.R5* (DTN: SN0612T0502404.014 [DIRS 178850]) contains data for 25°C only. Several of these species are potentially important for control of actinide or rare earth solubilities, so the thermodynamic data for these species are calculated at elevated temperature and applied in sensitivity studies via the EQ6 "AugmentLogK" option, as discussed in Appendix D. The sources for these up-temperature calculations are thermodynamic data reported by Cantrell and Byrne (1987 [DIRS 181066], p. 555) and Pankratz (1982 [DIRS 181065]).

4.1.11 Established Fact References

The following references provide direct inputs that are classified as "Established Fact" as described in SCI-PRO-004, *Managing Technical Product Inputs:*

- *Properties and Selection: Nonferrous Alloys and Special-Purpose Materials*. Volume 2 of *ASM Handbook* (ASM International 1990 [DIRS 141615]) is considered established fact because it is a professional society/industry code, criteria, and/or standard.

- *Standard Specification for General Requirements for Steel Plates for Pressure Vessels* (ASTM A 20/A20M-99a 1999 [DIRS 147578]) is considered established fact because it is a professional society/industry code, criteria, and/or standard.

- *Standard Specification for Chromium and Chromium-Nickel Stainless Steel Plate, Sheet, and Strip for Pressure Vessels and for General Applications* (ASTM A 240/A 240M-03b 2003 [DIRS 165003]) is considered established fact because it is a professional society/industry code, criteria, and/or standard.

- *Standard Specification for Pressure Vessel Plates, Carbon Steel, for Moderate- and Lower-Temperature Service* (ASTM A 516/A 516M-01 2001 [DIRS 162723]) is considered established fact because it is a professional society/industry code, criteria, and/or standard.

- *Standard Specification for Borated Stainless Steel Plate, Sheet, and Strip for Nuclear Application*. (ASTM A 887-89 2000 [DIRS 154062]) is considered established fact because it is a professional society/industry code, criteria, and/or standard.

- *Standard Specification for Aluminum and Aluminum-Alloy Sheet and Plate [Metric]* (ASTM B 209M-02 2002 [DIRS 162727]) is considered established fact because it is a professional society/industry code, criteria, and/or standard.

- *Standard Specification for Low-Carbon Nickel-Chromium-Molybdenum-Gadolinium Alloy Plate, Sheet, and Strip*. (ASTM B 932-04 2004 [DIRS 168403]) is considered established fact because it is a professional society/industry code, criteria, and/or standard.

- *Standard Practice for Preparing, Cleaning, and Evaluating Corrosion Test Specimens*. (ASTM G 1-90 1999 [DIRS 103515]) is considered established fact because it is a professional society/industry code, criteria, and/or standard.

- *Atomic Mass Adjustment, Mass List for Analysis* (Audi and Wapstra 1995 [DIRS 149625]), containing tables of the atomic mass for radioisotopes of the chemical elements, is considered established fact because it is a source scientists would use in their normal work practices.

- "Micro-Melt NeutroSorb PLUS Alloys" *Alloy Data* (Carpenter Technology 2003 [DIRS 179642]) is considered established fact because it contains numerical data from a supplier of proprietary materials.

- *CRC Handbook of Chemistry and Physics* (Lide 2006 [DIRS 178081]), containing tables of mineral/solid densities and chemical equilibrium constants (log K data), is considered established fact because it is a source chemists would use in their normal work practices.

- *Practical Handbook of Materials Science* (Lynch 1989 [DIRS 154076]), containing tables of mineral/solid densities, is considered established fact because it is a source scientists would use in their normal work practices.

- *Nuclides and Isotopes, Chart of the Nuclides* (Parrington et al. 1996 [DIRS 103896]), containing tables of the atomic weights and the half-lives of radioisotopes of the chemical elements, is considered established fact because it is a source scientists would use in their normal work practices.

4.2 CRITICALITY CRITERIA

4.2.1 Key Technical Issue Agreements

The Key Technical Issue agreements that will be addressed in this report are CLST 5.04, ENFE 5.03, and RT 4.03 (Reamer and Williams 2000 [DIRS 155464], Attachment 1). Each of these agreements commits the DOE to submitting *Geochemistry Model Validation Report: Material Degradation and Release Model* to the U.S. Nuclear Regulatory Commission (NRC). The validation for the model is covered in Section 7.

4.2.2 Safety Evaluation Report Open Item

The Safety Evaluation Report (Reamer 2000 [DIRS 150765], Section 2.3.2) contains acceptance criteria on how the conditions inside the waste package could influence the occurrence of criticality. The applicable acceptance criteria (Acceptance Criteria 1, 2, 4, and 5) and open item 3 (Reamer 2000 [DIRS 150765], Section 4) are addressed by this report.

Section 8.2.1 quotes the full text of the applicable acceptance criteria and open items and provides pointers to the information within this report that pertains to the item of interest.

4.2.3 Disposal Criticality Analysis Methodology Topical Report

The following sections of *Disposal Criticality Analysis Methodology Topical Report* (YMP 2003 [DIRS 165505]) are addressed in this report:

- Section 3.3, Figures 3-2a and 3-2b, Internal Criticality Master Scenarios
- Section 3.3.1, Internal Scenarios
- Section 3.3.3, Effect of Seismic Events
- Section 3.3.4, Effect of Volcanic Events
- Section 3.4.1, Configurations with the Potential for Internal Criticality.

Section 8.2.2 provides pointers to the information within this report that pertain to the items of interest.

4.2.4 Yucca Mountain Review

As identified in the TWP (SNL 2006 [DIRS 179452], Section 3.2), the acceptance criteria from *Yucca Mountain Review Plan, Final Report* (NRC 2003 [DIRS 163274]) that will be addressed in this report are as follows:

- Section 2.2.1.3.1.3, Degradation of Engineered Barriers (Acceptance Criteria 1 through 5)

- Section 2.2.1.3.3.3, Quantity and Chemistry of Water Contacting Waste Packages and Waste Forms (Acceptance Criteria 1 through 5)

- Section 2.2.1.3.4.3, Radionuclide Release Rates and Solubility Limits (Acceptance Criteria 1 through 5).

Section 8.2.3 quotes the full text of the applicable acceptance criteria and provides pointers to the information within this report that pertain to the items of interest.

4.3 CODES, STANDARDS, AND REGULATIONS

This model documentation was prepared to comply with the NRC high-level waste regulation (10 CFR Part 63 [DIRS 180319]). Subparts of this rule applicable to data include Subpart B, Section 15 (Site Characterization), and Subpart E, Section 114 (Requirements for Performance Assessment). Subpart E, Section 114 is also the subpart applicable to models. The sections applicable to feature, events, and processes are 10 CFR 63.114(d), (e), and (f) [DIRS 180319].

No additional codes, standards, or regulations are applicable to this report.

INTENTIONALLY LEFT BLANK

5. ASSUMPTIONS

5.1 WASTE PACKAGE SATURATION

Assumption: The void space within a waste package is assumed to be 30% filled with water—referred to as 30% waste package saturation. The waste package saturation (via the ratio of water to solid reactants) is a necessary input for the EQ6 simulations.

Rationale: In a fully flooded waste package, the saturation would initially be 100%, assuming ingress were through a breach through the top of an otherwise unbreached package. However the exact range of possible saturation is difficult to define. In the fault-displacement seismic scenario, the waste package may experience disruption, from simple crimping to shearing (SNL 2007 [DIRS 176828], Section 6.11), and may not be fully flooded. For the igneous case, the possible intrusion of magma into the package may significantly reduce void space (SNL 2007 [DIRS 177430], Section 6.4.8.3). The igneous-affected waste package is expected to be even more damaged than the seismic-affected package. In the igneous case, water near the degrading waste may be held only by capillary retention and may not accumulate on the bottom of the package. For all cases, even when no water accumulates on the bottom of the package, a certain quantity of water coats the surfaces of the fuel, basket materials, and corrosion products within the waste package.

Since the saturation level is uncertain, a sensitivity study was conducted to determine the effect of varying the assumed saturation; the results are given in Appendix C. It was found that variation from 3 to 100% has little effect on the peak aqueous concentrations, on the timing of the peaks (after breach), or on the width of the concentration peaks. The variation in saturation also had no impact on the combined plutonium and uranium release from the waste package, but did show a small impact on the gadolinium retention. The base case value of 30% saturation had gadolinium retention about 4% higher than the lowest saturation and 10% lower than the highest retention. Thus 30% saturation was chosen as the base case for the present report. The 30% value results in dissolved concentrations midway between the 3% and 100% saturation values on the concentration versus time plots (Figures C-2 through C-4, Appendix C). In addition, when high saturation is likely, the 30% saturation value results in underestimating gadolinium retention (i.e., a criticality event is more likely); and results in slightly overestimating (up to 4%) gadolinium retention (i.e., a criticality event is less likely) when saturation below 30% is likely.

The range examined in the sensitivity study is appropriate, for the following reasons. First, the corrosion products that form on the surfaces of degrading materials, and fall off and collect in parts of the package, will be porous materials. The corrosion products overwhelmingly have larger molar volumes (per cation) than the uncorroded materials from which they originate, and the added volume more than offsets the loss of reactant (uncorroded) material volume. Thus, the initial void space will decline as the package degrades, so the maximum saturation will be below 100%. Second, even in the drip-through scenario (Section 6.6.1), some water will be retained inside the package by capillarity, particularly on corroded surfaces or in the corrosion products. In *EBS Radionuclide Abstraction* (SNL 2007 [DIRS 177407], Section 6.5.3.1.1.2), it is argued that the corrosion products will be similar to unconsolidated geologic materials with approximately 42% porosity. Bear (1972 [DIRS 101379], Figure 9.2.6) shows that the residual saturation of wetted, unconsolidated sands reaches a lower value of approximately 10% of the

porosity, even at high capillary pressures; the upper limit of residual saturation for a variety of other synthetic and natural sedimentary materials is approximately 40%. The wettability characteristics of the corrosion products and unconsolidated soils are expected to be similar. The EQ6 calculations predict goethite (FeOOH) as a dominant corrosion product, while sands are predominantly quartz. However, quartz and goethite-rich iron ore powders have similar water-air-mineral contact angles. Iveson et al. (2000 [DIRS 181337], Table 1) reports a contact angle of approximately 29° for FeOOH-rich powders, whereas Janczuk and Zdziennicka (1994 [DIRS 181338], Table 1) report approximately 27° for water on quartz. Hence quartz sand and goethite-rich aggregates are expected to have similar wetting properties, and, in a scenario that admits ingress of liquid water, some water can be retained with fine-grained corrosion products.

No further confirmation of the assumption is required at this time. This conclusion is based on the insensitivity of peak aqueous plutonium, uranium and gadolinium concentrations to the saturation in the range studied and on the expectation that a breached package will be able to retain some water due to capillarity.

Use in the Model: The amount of saturation is used in each EQ6 input file (output DTN: MO0705GEOMODEL.000), via the choice of aqueous solution mass relative to mass of solids. Typically the saturation is set via the "SETMWTMAX" keystring (e.g., a value of 300 indicates 30% saturation).

5.2 WALL THICKNESS AND FILL VOLUME OF HLWG POUR CANISTER

Assumption: The wall thickness of the glass pour canisters is 1.05 cm and the fill volume of HLWG in the glass pour canisters is 87%.

Rationale: *Characteristics of Potential Repository Wastes* (DOE 1992 [DIRS 102812] Figure 3.4.1) depicts a 3-m-long Hanford glass pour canister with a wall thickness of 0.95 cm. However, Taylor (1997 [DIRS 126175], p. 2), when proposing use of a 4.5-m-long Hanford canister, assumes that a 10% increase in wall thickness (1.05 cm) is needed to accommodate a greater canister mass {(0.95 x 0.1) + 0.95 = 1.045 or 1.05}. Since the 4.5-m-long canisters are used for this model report, a glass pour canister wall thickness of 1.05 cm is justified. This wall thickness has also been used by other criticality evaluations and calculations (CRWMS M&O 2001 [DIRS 154194], Table 2-2; BSC 2002 [DIRS 164418], Section 5.1.3; Radulescu et al. 2004 [DIRS 165482], Table 2-4).

Taylor (1997 [DIRS 126175], p. 2) assumes a HLWG fill-volume of 87% in a Hanford 4.5-m-long glass pour canister. As the rationale for this assumption, Taylor says that the fill height in an 87%-full 4.5-m-long canister is equivalent to the fill height in an 80%-full 3-m-long canister if all other canister dimensions are equal. Moreover, the effect of heat generation per unit length on centerline temperature in an 87%-full 4.5-m-long canister is also equivalent to heat generation per unit length in an 80%-full 3-m-long canister. This 87% fill volume is close to the 85% fill volume shown in Table 3.4.2 (footnote b) of *Characteristics of Potential Repository Wastes* (DOE 1992 [DIRS 102812]), which lists characteristics of the Hanford site high-level waste form and canister. Section 3.4.3 of *Characteristics of Potential Repository Wastes* (DOE 1992 [DIRS 102812]) also states that a 15% void volume minimizes the potential of canister overfill. The 87% fill volume has also been used by other criticality evaluations and

calculations (CRWMS M&O 2001 [DIRS 154194], Table 2-2; BSC 2002 [DIRS 164418], Section 5.1.3; Radulescu et al. 2004 [DIRS 165482], Table 2-4).

Use in the Model: The wall thickness and the fill volume of the glass pour canisters are used to calculate the volumes and surfaces areas of the glass pour canisters and the HLWG in *CDSP WP_REV02.xls* (output DTN: MO0705GEOMODEL.000).

5.3 GADOLINIUM CONTENT, DIAMETER AND POROSITY OF ALUMINUM-GADOLINIUM SHOT FILL MATERIAL

Assumption: The gadolinium content of the aluminum-gadolinium shot is 15 wt %. The diameter of the aluminum-gadolinium shot surrounding the FFTF driver fuel assemblies and the IDENT 69 inside the DOE Canister is 3 mm, and the porosity of the shot in place is 30%.

Rationale: Radulescu et al. 2004 ([DIRS 165482] Table 10-2) states that the most reactive FFTF configuration includes four driver fuel assemblies with an IDENT-69 fuel pin container in the center compartment and one empty radial compartment. This configuration would require the addition of at least 30.8 kg of gadolinium, probably as an aluminum-gadolinium shot material, in the voids outside of the DFAs and IDENT-69 containers. An aluminum-gadolinium filler with 4 wt % gadolinium in the void space, as calculated in *CDSP_Long WP_FFTF_REV02.xls* (sheet "Al-Gd shot," output DTN: MO0705GEOMODEL.000), would be sufficient to contain this mass of gadolinium; however, since there is uncertainty in that calculation and the measurements used, and losses of gadolinium may occur during waste package degradation, an aluminum-gadolinium filler with 15 wt % gadolinium is considered reasonable for this model.

A 3-mm shot diameter is the same as that assumed for the aluminum-gadolinium phosphate shot proposed for placement inside the DOE canister for Shippingport LWBR SNF waste packages (Radulescu et al. 2004 [DIRS 165482], Table 10-14). Therefore, a diameter of 3 mm for the aluminum-gadolinium shot used for this model is reasonable.

In a previous report, a 25% porosity was assumed for the aluminum-gadolinium phosphate shot proposed for placement inside the DOE canister for Shippinport LWBR SNF waste packages (CRWMS M&O 2000 [DIRS 151243], Section 3.2.1). Such a low porosity would require a larger shot particle-size distribution than what can be observed by visual inspection of aluminum shot (CRWMS M&O 1999 [DIRS 111447], Section 3.1.8). Measured bulk density of carbon steel shot indicated a porosity of 38% to 40% (CRWMS M&O 1996 [DIRS 104115], Section 7.3.1). Therefore, a porosity of 30% for the aluminum-gadolinium shot used in this model is reasonable.

Use in the Model: A gadolinium concentration of 15 wt % is used to calculate the chemical composition, density, and molar volume of the aluminum-gadolinium shot in *CDSP_Long WP_FFTF_REV02.xls* (sheet "Al-Gd shot," output DTN: MO0705GEOMODEL.000). The 3-mm aluminum-gadolinium shot diameter is used to estimate the surface area and volume of the aluminum-gadolinium shot fill material in *CDSP_Long WP_FFTF_REV02.xls* (sheet "Al-Gd shot," output DTN: MO0705GEOMODEL.000). A porosity of 30% is used to estimate the bulk density of the aluminum-gadolinium shot fill material and the number of individual aluminum-gadolinium shot pieces that would fit in the available void space inside the FFTF

DOE canister in *CDSP_Long WP_FFTF_REV02.xls*, sheet "Al-Gd shot" (from output DTN: MO0705GEOMODEL.000).

5.4 THICKNESS OF RADIAL DIVIDER PLATES IN THE IDENT69

Assumption: The thickness of the radial divider plates inside of the compartmented version of the IDENT-69 fuel pin container is the same as the thickness of the central compartment of the IDENT-69 fuel pin container, or 1.524 mm.

Rationale: The inside and outside radius of the central compartment of the IDENT-69 container are given by the Idaho National Engineering and Environmental Laboratory in *FFTF (MOX) Fuel Characteristics for Disposal Criticality Analysis* (2000 [DIRS 158820], Section 3) as 20.701 mm and 22.225 mm, respectively. Thus the thickness of this central tube is $22.225 - 20.701 = 1.524$ mm. An assumption that the radial divider plates in the central compartment have the same thickness of 1.524 mm has been used by several previous criticality calculations, evaluations and reports (CRWMS M&O 1999 [DIRS 125206], Figure 2-9; BSC 2002 [DIRS 164418], Section 5.1.1; Radulescu et al. 2004 [DIRS 165482], Figure 3-4; BSC 2006 [DIRS 177193], Table 45). Since the thickness of the radial divider plates would probably be close to the same value as the thickness of the central tube and since a small change in this dimension does not affect the outcome of the model, it seems reasonable to use a thickness of 1.524 mm.

Use in the Model: The thickness of the radial divider plates inside of the compartmented version of the IDENT-69 fuel pin container is used to calculate the volume of Stainless Steel Type 304L in the IDENT-69 fuel pin container in *CDSP_Long WP_FFTF_REV02.xls* (sheet "FFTF-assemb," output DTN: MO0705GEOMODEL.000).

6. MODEL DISCUSSION

6.1 OBJECTIVE

The objective of the MDR model is to determine the extent to which separation of neutron absorbers and fissile material can occur within a degrading waste package containing spent nuclear fuel. The separation can occur when neutron absorbers are released from the waste package, leaving fissile material inside, and when fissile material is released from the waste package, causing an external criticality concern. The elements uranium and plutonium are of interest because of their potential to cause a criticality event. Boron, gadolinium, and certain other elements are important because they are thermal neutron absorbers (poisons) that prevent criticality. The simplified results of this model report are summarized in terms of loss and retention of the elements gadolinium, uranium, and plutonium in the waste package. Based on the results of this report, the potential for either an internal or external criticality event is analyzed in other reports. The output from this document will be used in the exclusion argument for features, events, and processes related to in-package criticality (DTN: MO0706SPAFEPLA.001 [DIRS 181613], FEPs 2.1.14.16.0A, 2.1.14.19.0A, 2.1.14.22.0A, and 2.1.14.25.0A).

This report analyzes four waste package configurations with different fuel types: the 21-PWR CSNF waste package, the 2-MCO/2-DHLW containing N-reactor fuel, the 5-DHLW/DOE SNF long waste package containing FFTF fuel, and the 5-DHLW/DOE SNF long waste package containing TMI fuel. As explained in Section 4.1.6, the four types of waste packages are referred to throughout this document as CSNF, CDSP, FFTF, and TMI.

6.2 CONCEPTUAL MODEL

If a waste package is breached due to a seismic or igneous event, water and solutes might enter and leave the waste package by several mechanisms, including diffusion, condensation of vapor, and advection of liquid water. The quantity of material released by diffusion would be small due to the tortuosity of the path, and therefore the diffusion-only scenario is not considered in this model. Condensation on the waste package is considered unlikely in the first 10^4 years (SNL 2007 [DIRS 181648], Section 6.1.2[a]), as the package will generally be the hottest point in the system. Thus only advection of liquid water is considered in this report.

Advection of liquid water through the package is possible only if the drip shield is displaced and the package is breached. In TSPA for the license application (TSPA-LA), only two scenarios give rise to liquid water advection through the waste package: (1) seismic fault displacement; and (2) igneous intrusion. This section describes how these two scenarios are implemented in the MDR model. Specific inputs for the two scenarios (seepage flux, degradation rates) are discussed in Sections 6.3 and 6.4.

The default MDR model is a single-cell well-mixed flow-through system, in which the package materials (fuel, steels, HLWG, aluminum) react with water at specified corrosion rates. The calculation is performed with the EQ3/6 V. 8.1 (STN: 10813-8.1-00 [DIRS 176889]) speciation and reaction path codes, in solid-centered flow-through mode. Seepage water enters the package at a constant rate and is removed at the same rate, along with any components dissolved in the

water. Corrosion rates are based on experimental measurements. In a single calculation, O_2 and CO_2 fugacities are assumed fixed and apply to the entire contents of the package; sensitivity studies examine the effect of different fixed fugacities (Section 6.3.14). The minerals that form during the reaction of seepage water with the waste package components are based on the code predictions; minerals may be suppressed (not allowed to form) if they are not consistent with literature and experimental results. Adsorption on iron-oxide corrosion products is not included in the modeling, but is presented as an alternative model in Section 6.6.3. The three important outputs of the model are (1) the percent of neutron absorbers (boron, gadolinium) and fissile material (plutonium, uranium) remaining within the waste package at 10,000 years, (2) the corrosion products mass and composition as a function of time, and (3) quantity of intact waste package components (basket, fuel) as a function of time.

Basis for Single-Cell Model

In the single-cell model, the water in the waste package system is well mixed. That is, at any moment, all nonreactant components are in instantaneous equilibrium, across the extent of the waste package, and there is one homogeneous aqueous composition. The calculations use the EQ6 solid-centered flow-through mode (CRWMS M&O 1998 [DIRS 106278], Section 1.2.1; BSC 2005 [DIRS 180678], Section 2.2). In the solid-centered flow-through mode, an incremental amount of water drips into the package, is instantly mixed, and the same volume of water exits the package. This mode simulates the leakage of the package and possible removal of both actinides and neutron control materials to the invert and surrounding rock.

The "well-mixed" system is a basic limitation of the EQ6 code. A well-mixed system is most reasonable when the reactions are slow and diffusion is fast, compared to the advective flux of water (e.g., when the degradation of stainless steel is the primary composition-controlling reaction). The well-mixed system is also reasonable when the package is relatively uniform, with close proximity of all major components (e.g., the CSNF and steel fuel containers). A "bathtub" configuration, with a wholly or partially flooded package in convective overturn (perhaps from residual heat or gas generation) could promote mixing. (A bathtub might exist if there are no open breaches in the bottom of the package, so that in-dripping water accumulates until an overflow condition is reached.) However, in some codisposal packages, with carbon steel and segregation of components into glass and fuel, "close proximity" is clearly questionable. In addition, the igneous scenario calls for dripping of water through an extensively damaged waste package and might never produce a bathtub configuration.

The suitability of the single-cell model is examined in Section 6.6.1, Multiple-Cell Drip-Through Model. An alternative multiple-cell model is developed, which does not require equilibrium among the cells or compositional uniformity of the cells. As shown in Section 6.6.1, this alternative model produces results that differ little from the single-cell.

6.2.1 Seismic Scenario Conceptual Model

The only seismic event that is likely to expose the waste to significant water is the "Fault Displacement" scenario, outlined in *Seismic Consequence Abstraction* (SNL 2007 [DIRS 176828]). In a large fault displacement, the drip shield is displaced, and the fault shear zone may intersect a waste package near its lid, in which case the welds may fracture and the

entire lid might be separated from the package (SNL 2007 [DIRS 176828], Section 6.11.5). In addition, even if the lid is not displaced, the top of the package may suffer sufficient damage to allow seepage to enter the package, creating a bathtub situation.

The EQ6 model for the seismic scenario implements a single-cell model, in which the package is partly filled with seepage water (Assumption 5.1, Section 5). Several compositions of seepage waters are considered (Tables 4-2 and 4-3). The rate of water addition is determined by the amount of seepage available to flow through the openings in a breached waste package. Upon entry into the waste package, water interacts with the internal components per the single-cell model. Consistent with TSPA-LA, all the fuel cladding is assumed to have been breached, and the total fuel surface area is available for reaction.

The descriptions of the seismic and igneous scenarios presented here differ from the TWP, because the TWP incorrectly reversed the descriptions of the seismic and igneous scenarios (SNL 2006 [DIRS 179452], Section 2.1, p. 1).

6.2.2 Igneous Scenario Conceptual Model

In this scenario, magma enters the repository drift. The magma encapsulates and possibly enters the waste packages. The high-temperature magma so disrupts the individual packages that multiple breaches are likely and a bathtub configuration is considered unlikely. However, water may drip through the package, remove radionuclides, and affect the likelihood of criticality by removing neutron absorbers and hydrating the remaining components. Section 6.3 describes how these changes are incorporated in the reaction-path calculations of waste package degradation.

The possible thermal effects caused by the intrusion of magma are documented in *Dike/Drift Interactions* (SNL 2007 [DIRS 177430], Section 6.4.8.3.1). The waste package will deform and weaken due to the high temperatures. There will be differential pressure of several MPa between the inside and outside, and this difference may cause a rupture. The first failures are predicted to occur at the weakest points of the waste package, which are the unannealed welds at the shield plug or vessel lids.

The elevated temperatures will also have a chemical effect on the waste package components. N-reactor fuel is composed of uranium metal; CSNF is composed of UO_2. Uranium metal- and UO_2-based fuels will rapidly react with air to produce fine-grained UO_x solids (i.e., $x > 2$) (DOE 2000 [DIRS 152658], Section 2; McEachern and Taylor 1997 [DIRS 101726], 1998 [DIRS 113270]).

Dike/Drift Interactions (SNL 2007 [DIRS 177430], Section 6.4.8.3.3) also considers interactions that may occur between the waste package components and the magma, particularly in the event that magma enters the waste package. However, the probability that magma will enter a package is not quantified and is best regarded as highly uncertain. It is beyond the scope of the current report to elaborate on those considerations.

Other materials will be altered by the high temperatures of the inundating magma. According to *Dike/Drift Interactions* (SNL 2007 [DIRS 177430], Section 6.4.8.3), the waste package internal temperatures may be up to 1,100°C. The HLWG will likely melt and may flow to the bottom of

the package. In addition, eutectics among zirconium in Zircaloy and components of stainless steel (iron and nickel) may cause limited local melting (SNL 2007 [DIRS 177430], Section 6.4.8.3.3). The effect of these processes on the final package geometry is not specified; most likely, the result will be a reduction in the effective surface area of the components. However, to ensure that the impacts are not minimized (e.g., by overestimation for rates of glass degradation and stainless steel corrosion rates), the initial, undisturbed surface areas are used in the EQ6 reaction path calculations for the igneous scenario. In addition, sensitivity cases are performed using medium and high corrosion rates of steels and alloys to determine the impact of a possible increase in corrosion rates due to melting and subsequent solidification of materials (*CSIGHi.6i, CSIGMed.6i, CD_I_SH2.6i, CD_ISM2.6i*). *Dike/Drift Interactions* (SNL 2007 [DIRS 177430], Section 6.4.8.3.3) allows for the possibility that intruding magma may react with the package internals.

In principle, heating of the stainless steel to magmatic temperatures might cause sensitization and a reduction in corrosion resistance. During sensitization, chemical composition in the vicinity of the grain boundaries can be altered by the precipitation of chromium-containing carbides. The precipitation of the carbides depletes chromium at the edges of the adjacent alloy grains (typically austenite) and increases potential for intergranular corrosion, since the chromium-depleted regions fail to produce a chromium-oxide passivating layer (Tekin and Martin 1991 [DIRS 182347]; Boeuf et al. 1981 [DIRS 180828]; Shimada et al. 2002 [DIRS 180823]; Moreno et al. 2004 [DIRS 179295]). Subsequent slow cooling at 500°C to 750°C may desensitize the steel, as chromium diffuses back into the depleted zones (Tekin and Martin 1991 [DIRS 182347]; Mayo 1997 [DIRS 180824], Figure 11). However, the fate at still lower temperatures is less clear, as the solubility of the carbide phase decreases. Fox and McCright 1983 [DIRS 159344] argue that heating in the repository for years, at temperatures of 350°C and below, may cause sensitization, especially in Stainless Steel Type 304 alloys.

The increase in general corrosion rates due to sensitization is not well-quantified. Most literature is concerned with intergranular corrosion and cracking. However, the greater concern for EQ6 calculation is the general corrosion rate; no credit is taken for the structural integrity of the steel parts after an igneous event, so intergranular corrosion is of limited importance. Kain et al. (1995 [DIRS 182348]; Table 2) show that the corrosion rate of sensitized Stainless Steel Type 304L is no more than a factor of 3.7 times the corrosion rate of the "as-received" Stainless Steel Type 304L, under the same extreme conditions (boiling acid). In the MDR, there is a factor of 42 between the low (default) Stainless Steel Type 304L corrosion rate and the high rate (Section 6.3.6), so that the MDR model seems to encompass the effects of sensitization in Stainless Steel Type 304L.

The Stainless Steel Type 304B does not suffer sensitization in the same way that Stainless Steel Type 304L is affected (Moreno et al. 2004 [DIRS 179295]). The metal borides are actually boro-carbides of the form $(Cr,Fe)_2(B,C)$ or $(Cr,Fe)_{23}(B,C)_6$ and effectively soak up most excess carbon. The borides precipitate at rather high temperatures and are stable down to fairly low temperatures, so there is no formation of chromium carbide. For heat-treated Stainless Steel Type 304B, Moreno et al. (2004 [DIRS 179295]) conclude, "it is not possible to talk about a common sensitized state as no carbides are found at the grain boundaries." The pitting potential for heat-treated Stainless Steel Type 304B was approximately the same as for the as-received material, which is not the case for non-borated Stainless Steel Type 304. However, in these

relatively short tests, a chromium-depleted region may have formed around the boride particles, enhancing the chance that the boride grains might break free from a corroding surface, under conditions where a concomitant oxide corrosion product is slow to form. As with Stainless Steel Type 304L, the Stainless Steel Type 304B rates are varied over a factor of 42 for sensitivity studies (Section 6.3.6), which should accommodate any igneous-related increase in corrosion rate.

Eventually, the drift temperature will drop below the boiling temperature of water, and seepage water may enter the drift. Water will move through fractures in the solidified magma and will enter the package through ruptures. The water will enter at a rate determined by the amount of seepage available to flow into the drift. The composition of the water will be equilibrated with the overlying host rocks and solidified magma in and outside the package. Water entry into the waste package will cause additional corrosion of the steels, glass, fuel, and other internals.

The corrosion products are expected to stay in or near the remnants of the package. Metal corrosion products form a coating on the surface of the components, and these oxides (trevorite, $NiFe_2O_4$) and oxyhydroxides (goethite, FeOOH) will incorporate the borocarbide crystals into this layer. As calculated in Section 6.7.4, colloidal removal of the corrosion products should be insignificant. Advective transport of larger particles (above colloidal size) will be very limited. The first solids that cascade through the package are expected to form a filter pack on the downstream end of the package, preventing further removal; and the maximum seepage rates—1000 L/yr, corresponding to less than a drop per second, over the entire footprint of the package—are not expected to provide significant flushing action.

The igneous scenario is implemented in EQ6 simulations via two stages. In the first stage, using the titration mode in EQ6 with water as a special reactant, the fuel alone is oxidized and hydrated to the equilibrium assemblage predicted by EQ6 (mostly schoepite). This stage is meant to represent the reactions that would invariably take place as the disrupted, oxidized, and fragmented fuel cooled down though the boiling point of water. The normal rates for degradation of spent UO_2 fuel would certainly be inapplicable, because the fuel form, composition, and surface area would be altered by the high-temperature reactions. This first stage is really a simple initialization of the system and spans less than 100 years. The second stage represents the time after water seepage has entered the disrupted waste package and begins to react with the steels, glass, and other components; this stage spans approximately 10^4 yr. The fuel components are still available for reaction, but they are not constrained by kinetics; in EQ6 parlance, the reacted fuel is allowed to enter the equilibrium system in the first stage. The second stage is implemented with a single-cell, solid-centered flow-through model.

6.3 INPUT CALCULATIONS

This section describes calculations that were required to convert the inputs in Section 4 to a form suitable for use with the EQ6 software. In addition, this section describes the range of values used for all inputs in the calculations.

6.3.1 Waste Package Components

The waste package components have to be converted for input to EQ6 as described below. The detailed calculations are found in output DTN: MO0705GEOMODEL.000, folders: CDSP (N-reactor), FFTF, TMI, files: *CSNF WP and TAD.xls*, *CDSP WP REV02.xls*, *CDSP_Long WP_FFTF_REV02.xls*, *CDSP_Long_WP_TMI_REV02.xls,* and *CDSP_HLWGlass_2004_hws5.xls*.

Normalized Moles of Components—For convenience in modeling, the EQ6 simulations are based on 1 L of void volume. To accomplish this, the mass of each waste package component is converted to normalized moles. The normalization factor is the void volume of the waste package, in liters. As an example, the normalized moles for the Stainless Steel Type 316 inner vessel in the CSNF waste package is calculated as follows (*CSNF WP and TAD.xls,* tab: "EQ6 inputs"):

$$1.44 \times 10^4 \text{ kg } 316 \div 100 \text{ g/mole} \div 7{,}664 \text{ L} \times 1000 \text{ g/kg} = 20 \text{ normalized moles } 316$$

where 100 g/mole is the molecular weight of each component and 7,664 L is the void volume of the CSNF waste package. The normalized moles are reduced to one significant figure due to the uncertainty in the values. (Calculations are found in output DTN: MO0705GEOMODEL.000, folders: CDSP (N-reactor), FFTF, TMI, Glass, *CSNF WP and TAD.xls*, *CDSP WP REV02.xls*, *CDSP_Long WP_FFTF_REV02.xls*, *CDSP_Long_WP_TMI_REV02.xls,* and *CDSP_HLWGlass_2004_hws5.xls*.)

Normalized Surface Area of Components—The surface area of each waste package component is divided by the normalization factor to get the normalized surface area.

Composition of Components—The composition of each component, in wt %, is converted to moles of elements in 100 grams. As an example, for Stainless Steel Type 316 (*Steels and Alloys REV02.xls*, tab: "Materials"):

$$0.08 \text{ wt \% C} \div \text{molecular weight of C (12.0107 g/mole)} = 6.66 \times 10^{-3} \text{ moles C per 100 g of 316}$$

The normalized values of moles and surface area are provided in Table 6.3-1.

HLWG Adjustments—The initial HLWG composition contains lithium. However, there are very few lithium compounds in the thermodynamic database, even though the lithium readily substitutes into many clays and other silicates in nature (Borchardt 1995 [DIRS 156639], pp. 703 and 704). As a consequence, EQ6 simulations with degrading HLWG will allow Li^+ to build in the aqueous phase to unrealistic concentrations. Hence the glass composition is reformulated by substituting an equal amount of sodium for lithium (output DTN: MO0705GEOMODEL.000, file *CDSP_HLWGlass_2004_hws5.xls*). This substitution

causes the HLWG to have a formal molecular weight of 104 in the thermodynamic database; however, the effective molecular weight for determining the moles of HLWG is still 100 g/mole.

Aluminum-Gadolinium Fill Material Composition—The composition of the aluminum-gadolinium fill material was calculated in *CSNF_LONG WP_FFTF_REV02.xls* and is presented in Table 6.3-2.

Table 6.3-1. EQ6 Scaled Inputs for Seismic and Igneous Scenarios

Waste Package Type	Material	Initial Normalized Moles	Normalized Surface Area (cm^2)
CSNF Normalization factor = 7,664 liters	Stainless Steel Type 316 inner vessel	20	50
	Stainless Steel Type 304B4	8	200
	Aluminum Alloy 6061	0.8	80
	Stainless Steel Type 316L TAD canister	20	400
	Stainless Steel Type 316L shield plug	7	7
	CSNF	10	3,000 (60,000 for sensitivity)
CDSP (normalization factor = 5698 liters)	Carbon Steel Type A516	3	60
	Stainless Steel Type 304L	10	100
	Stainless Steel Type 316	30	60 (including plug)
	Aluminum Alloy 1100	0.3	20
	N-Reactor	20	1,700
	HLWG (most probable $f_{exposure}$)	20	100
	HLWG (maximum $f_{exposure}$)	20	500
FFTF (normalization factor = 6430 liters)	Carbon Steel Type A516	9	100
	Stainless Steel Type 316	30[b]	300
	Stainless Steel Type 304L	6	100
	Mixed oxide (MOX) fuel	0.3	30[a]
	UO_X fuel	0.01	1[a]
	HLWG	20	300 (1,000 for maximum $f_{exposure}$)
	Nickel–gadolinium alloy	0.7	20
	Aluminum-gadolinium alloy	2	900 (1000 with IDENT 69)
TMI (normalization factor = 6,430 liters)	Carbon Steel Type A516	10 (9 with 316 sleeve)	100
	Stainless Steel Type 304L	6	200
	Stainless Steel Type 316	30	60 (70 with Stainless Steel Type 316 sleeve)
	LiCon[b]	0.2	10
	TMI fuel	0.8	50[a]
	HLWG	20	300 (1,000 for maximum $f_{exposure}$)

Source: Output DTN: MO0705GEOMODEL.000, folders: CSNF, CDSP (N-reactor), FFTF, TMI, files: *CSNF WP and TAD.xls*, *CDSP WP REV02.xls*, *CDSP_Long WP_FFTF_REV02.xls*, *CDSP_Long_WP_TMI_REV02.xls*

NOTES: [a] The CSNF-specific surface area was used to calculate the degradation rate of the MOX, UO_X and TMI fuels. In the EQ6 input files the surface area of MOX and UO_X was entered as "1" and for TMI as "100."

[b] The moles of Stainless Steel Type 316 in FFTF were modeled as 4 instead of 30 moles; however there is no impact since the amount of Stainless Steel Type 316 was never exhausted during the EQ6 simulations, as shown in output DTN: MO0705GEOMODEL.000, folder FFTF, files **.6o*.

Table 6.3-2. Composition and Density of Aluminum-Gadolinium Fill Material

Element	Moles of Element per 100-gram mole of Reactant[a]
Silicon	1.513×10^{-2}
Iron	7.610×10^{-3}
Copper	5.819×10^{-2}
Manganese	9.283×10^{-3}
Magnesium	5.246×10^{-2}
Chromium	1.635×10^{-3}
Zinc	3.250×10^{-3}
Titanium	2.664×10^{-3}
Gadolinium	9.539×10^{-2}
Aluminum	2.900×10^{0}
Density[a]	3.5 (g/cm^3)
Molecular weight[b]	100 (g/mole)
Molar volume[c]	28 (cm^3/mole)

Source: [a] Output DTN: MO0705GEOMODEL.000, file *CDSP_Long WP_FFTF_REV02.xls*, tab "Al-Gd shot."

NOTES: [b] The molecular weight of each waste package component was set to 100 grams to simplify inputs to EQ6.

[c] Molar volume = molecular weight / density.

The aluminum-gadolinium shot material will be added to FFTF waste packages inside the DOE canister around the DFAs and in the void basket position. A shot diameter of 3 mm was chosen (see Assumption 5.3, Section 5) to be consistent with the aluminum-gadolinium shot modeled for the Shippingport LWBR SNF waste packages (Radulescu et al. 2004 [DIRS 165482], Table 10-14). For geochemical modeling of the Shippingport LWBR SNF waste packages, the voids in the packed aluminum-gadolinium shot were set at 25% (CRWMS M&O 2000 [DIRS 151243], Section 3.1.8). However, voids closer to 38% to 40% would be expected (CRWMS M&O 1999 [DIRS 111447], Section 3.1.8), so the void space in the packed aluminum-gadolinium shot was set at 30% (see Assumption 5.3, Section 5) for calculations of volume, surface area, and mass of the fill material in *CDSP_Long WP_FFTF_REV02.xls,* tab *"Al-Gd shot"* (output DTN: MO0705GEOMODEL.000).

Composition of LiCon Fill in the TMI Canister—Table 6.3-3 presents the composition, density, and degradation rates used in EQ6 input files to represent the LiCon fill material inside the TMI canister and outside of the center box structure from *SNF Canister Characteristics for Criticality Analysis of a Dual Canister/Waste Package Disposal Strategy* (DOE 2002 [DIRS 161752], Section 1.2.1.3 and Table 5).

Codisposal (N-Reactor) Fuel—N-reactor fuel is considered to be pure uranium metal. No credit is taken for the cladding due to its poor condition (DOE 2000 [DIRS 150095], Section 3.1.5 and Appendix C, Section 3). The details of parameters used to prepare EQ6 input files are in *CDSP WP_REV02.xls* (output DTN: MO0705GEOMODEL.000).

Waste Package Materials Not Included in the EQ6 Input File—The waste package outer barrier is constructed of Alloy 22, and the CSNF cladding is made of Zircaloy, both of which degrade slowly compared to the other materials in the waste package. These two materials are not included in the EQ6 input file because they would react so slowly that the effect on the results would be negligible. The corrosion rate for Zircaloy is low, 25.4 μm in a million years (BSC 2004 [DIRS 169982], Section 6.2.5); similarly, both the corrosion rate of Alloy 22, which ranges from 0 to 15 nm/year (SNL 2007 [DIRS 178519], Figure 6-10) and the probability of corroding quickly is low (SNL 2007 [DIRS 178519], Section 8.1).

Table 6.3-3. Elemental Composition, Degradation Rate Constants, and Density of LiCon Fill in TMI SNF Waste Package

Element	LiCon Weight%[a]	Moles of Element per 100-gram mole of Reactant[a]
Hydrogen	3.7329	3.7035
Oxygen	65.929	4.1207
Sodium	0.63271	2.7521×10^{-2}
Aluminum	14.658	5.4325×10^{-1}
Silicon	4.6869	1.6688×10^{-1}
Magnesium	0.16680	6.8629×10^{-3}
Calcium	10.049	2.5073×10^{-1}
Iron	0.14510	2.5982×10^{-3}
Total	100	—
Molecular weight[b]	100	(g/mole)
Molar volume[c]	100	(cm^3/mole)
Low rate constant[d]	1.6×10^{-15}	(mole/cm^2 s)
High rate constant[d]	1.7×10^{-12}	(mole/cm^2 s)

Sources: [a] Output DTN: MO0705GEOMODEL.000, *CDSP_Long_WP_TMI_REV02.xls*, tab "Fuel & LiCon."

NOTES: [b] The molecular weight of each waste package component was set to 100 grams to simplify inputs to EQ6.
[c] Molar volume = molecular weight / density.
[d] The degradation rates in units of μm/y are multiplied by the density divided by 10^4 μm/cm, divided by 100 g/mole, divided by 365.25 days/yr, and divided by 86,400 s/day to convert to units of moles/(cm^2 s). This rate constant must be multiplied by the normalized surface area (*sk* in the EQ6 input file) in cm^2 of each waste package component to calculate the actual degradation rate in 100-g moles/s of that component.

6.3.2 CSNF Fuel Composition

The simplified CSNF composition was presented in Table 4-8. The percent of each isotope in the simplified composition was calculated (output DTN: MO0705GEOMODEL.000, file *CSNF Fuel REV02.xls*, tab: "for Tables in Document") and is presented in Table 6.3-4. The simplified fuel composition was used as the base-case composition. For a sensitivity case (*CSIGPI.6i*), the principal isotopes that were not included in the simplified composition were combined into a separate phase called "Principal_Isotopes" (output DTN: MO0705GEOMODEL.000, file *CSNF Fuel REV02.xls*, tab: "Principal Isotopes for EQ6"). The quantity of "Principal_Isotopes" was calculated to be 0.004 moles of "Principal_Isotopes" per mole of CSNF (*CSNF WP and TAD.xls*,

tab: "EQ6 inputs"). Though the quantity of the principal isotopes is small, the sensitivity cases were performed to see which minerals are likely to form from all the principal isotopes. The composition of principal isotopes is presented in Table 6.3-5.

Table 6.3-4. CSNF Simplified Composition

Element Modeled in EQ6	Moles/100g	Isotope	Isotope Percent
Uranium	0.3617	^{234}U	0.04
		^{235}U	1.11
		^{236}U	0.69
		^{238}U	98.16
Neptunium	0.0009	^{237}Np	100.00
Plutonium	0.0027	^{239}Pu	76.66
		^{240}Pu	13.78
		^{242}Pu	9.56
Zirconium	0.0005	^{93}Zr	100.00
Molybdenum	0.0009	^{95}Mo	100.00
Technetium	0.0008	^{99}Tc	100.00
Ruthenium	0.0020	^{101}Ru	41.07
		^{103}Rh	25.83
		^{105}Pd	20.37
		^{108}Pd	7.99
		^{107}Ag	0.01
		^{109}Ag	4.73
Cesium	0.0013	^{133}Cs	79.57
		^{135}Cs	20.43
Barium	0.0010	^{138}Ba	100.00
Gadolinium	0.0035	^{89}Y	15.51
		^{141}Pr	24.63
		^{143}Nd	17.79
		^{145}Nd	14.06
		^{148}Nd	7.81
		^{147}Sm	4.78
		^{149}Sm	0.11
		^{150}Sm	6.83
		^{152}Sm	2.58
		^{151}Eu	0.39
		^{153}Eu	2.54
		^{154}Gd	0.62
		^{155}Gd	0.13
		^{156}Gd	1.72
		^{158}Gd	0.47
		^{160}Gd	0.02
Oxygen	0.7385	^{16}O	100.00

Source: Output DTN: MO0705GEOMODEL.000, *CSNF Fuel REV02.xls*.

Table 6.3-5. Principal Isotopes Not Included in the Simplified CSNF Composition

Element Modeled in EQ6	Moles/100g	Isotope	Isotope Percent
Americium	0.0065	^{243}Am	100.00
Rhodium	0.1274	^{103}Rh	100.00
Silver	0.0234	^{107}Ag	0.28
		^{109}Ag	99.72
Neodymium	0.3383	^{143}Nd	44.85
		^{145}Nd	35.45
		^{148}Nd	19.70
Samarium	0.1220	^{147}Sm	33.44
		^{149}Sm	0.78
		^{150}Sm	47.76
		^{152}Sm	18.01
Europium	0.0250	^{151}Eu	13.29
		^{153}Eu	86.71
Oxygen	0.7409	^{16}O	100.00

Source: Output DTN: MO0705GEOMODEL.000, *CSNF Fuel REV02.xls*.

6.3.3 Modified Composition of Borated Stainless Steel

Table 4-17 provides the composition of the borated stainless steel present in the CSNF waste package. The material composition was converted to EQ6 format in *Steel and Alloys REV02.xls* (Output DTN: MO0705GEOMODEL.000). The composition in EQ6 format includes only the elements that are released into the aqueous solution during degradation. Evidence shows that the boron in borated stainless steel has a very low solubility within the iron matrix of the steel (He et al. 2000 [DIRS 181597], p. 218; Goldschmidt 1971 [DIRS 181593], p. 911; Sourmail et al. 2004 [DIRS 181595], p. 1275). Instead of a solid solution, the boron is present as separate chromium boride particles, with a composition of $(Cr_2Fe)_{7.66}(B,C)_6$ (Moreno et al. 2004 [DIRS 179295], p. 577). These particles do not dissolve into the aqueous solution during degradation of the steel but are left behind as insoluble products during corrosion (Fix et al. 2004 [DIRS 171745], p. 126; Lister et al. 2007 [DIRS 182177], pp 39 to 43). To correctly model this corrosion behavior in EQ6, the borated stainless steel composition was altered in output DTN: MO0705GEOMODEL.000, file *Steel and Alloys REV02.xls* (tab "Borated Stainless Steel") by removing the quantity of iron, chromium, boron, and carbon that are present in the boride particles, such that the remaining composition represents those elements that dissolve into the aqueous solution upon degradation. The modified composition for the borated stainless steel is given in output DTN: MO0705GEOMODEL.000, file *Steel and Alloys REV02.xls* (tab "Materials").

6.3.4 Seepage Flux

Figures 4-1 and 4-2 show the seepage flux per waste package. The values represent all the water entering the drift. Since it is likely that some of the water would be diverted by waste package or drift shield remains, a value of 1 L/yr was chosen as the base-case flux. A set of sensitivity simulations was performed to evaluate the effects of the seepage rate ranging from 1 L/yr to

1,000 L/yr (Figures 4-1 and 4-2). The results are presented in Appendix F. The sensitivity simulations revealed that, at lower seepage rates, more of the fissile material remains in the waste package, creating conditions more favorable for criticality occurrences. For external criticality considerations, sensitivity cases using the highest flux of 1,000 L/yr were implemented for each fuel type (*CS_S_F9.6i, CSNFIG2.6i, CSIGAdEh.6i, CD_I_f9.6i, FFTFIG_2.6i,* and *TMI_IG_2.6i*).

6.3.5 Incoming Water Composition

Incoming water composition (Section 4.1.2) is varied to account for the different types of water compositions that would be available to seep into a waste package over the regulatory time frame. For the seismic case, J-13 well-water composition was used as the base case. Since the future seepage water composition is uncertain,, three additional pore water compositions were used as sensitivity cases (*CS_S_W1.6i, CS_S_W2.6i, CS_S_W3.6i, CD_S_W1.6i, CD_S_W2.6i,* and *CD_S_W3.6i*). For the igneous scenario, three different basalt-equilibrated basalt waters are used as the seepage water composition, as described in Section 4.1.2. The sensitivity cases using different basalt water compositions were as follows: *CSIG_IB.6i, CSIG_CB2.6i, CD_I_C2.6i,* and *CD_I_IB.6i)*.

6.3.6 Corrosion Rates

The rates from Table 4-19 were converted to EQ6 format in *Steel and Alloys REV02.xls* (output DTN: MO0705GEOMODEL.000). For Stainless Steel Type 304L and the aluminum alloy, the 10%, median, and 90% confidence values were chosen to represent low, medium, and high rates in Table 6.3-6. For those alloys with more than one value listed for each confidence level (Stainless Steel Type 316, Carbon Steel Type A-516, and the nickel-gadolinium alloy) in Table 4-19, an average was taken of each confidence level and averaged to arrive at the low, medium, and high values. For the nickel-gadolinium alloy, the minimum, median, and maximum from Table 4-19 were used to represent the low, medium, and high values in Table 6.3-6.

The Stainless Steel Type 304B rates in Table 6.3-6 were obtained by multiplying the Stainless Steel Type 304L corrosion rates by a factor of 6. This process gives high, medium, and low Stainless Steel Type 304B corrosion rates that trace to qualified data and is justified below.

The Stainless Steel Type 304B rates in Table 4-20 average 0.040 μm/y for linear polar resistance analyses, and 0.062 μm/y for gravimetric analyses. These Stainless Steel Type 304B rates were collected under relatively benign conditions (starting pH 5.5 to 7, low ionic strength, 60°C; output DTN: MO0706ECTBSSAR.000) and are analogous to the low, base-case rates for Stainless Steel Type 304L in Table 6.3-6. These low Stainless Steel Type 304B rates are 3.5 to 5.5 times greater than the low corrosion rate for Stainless Steel Type 304L. There are no qualified data that give a medium rate and high rate under more corrosive conditions, analogous to the medium and high rates listed for Stainless Steel Types 304L and 316L in Table 6.3-6. However, it is expected that corrosion rates for Stainless Steel Types 304L and 304B should have parallel behavior; that is, most conditions that cause a higher rate for Stainless Steel Type 304L should also cause a higher rate for Stainless Steel Type 304B. Thus, if only these low Stainless Steel Type 304B corrosion rates were used in EQ6 calculations, a logical

inconsistency would develop: in calculations with high Stainless Steel Type 304L rates, Stainless Steel Type 304L would be predicted to corrode much faster than Stainless Steel Type 304B. This last result would be contrary to observation.

Hence the low, medium, and high Stainless Steel Type 304B rates in Table 6.3-6 were obtained by multiplying the qualified low, medium, and high Stainless Steel Type 304L corrosion rates by a factor of 6. This factor of 6 is justified because: (1) it is consistent with the 3.5 to 5.5 derived by comparing the average rates in Table 4-20, with the low Stainless Steel Type 304L rate in Table 6.3-6; and (2) it is consistent with the factors of 6.28 and 6±2 derived in spreadsheet *304B_vs_304_witness_hws031907.xls* (output DTN: MO0705GEOMODEL.000, folder: corrosion rates). The last two factors were obtained from tests that subjected witness coupons of Stainless Steel Type 304L to the same conditions as coupons of Stainless Steel Type 304B, allowing direct determination of the ratio of corrosion rates (Van Konynenburg et al. 1998 [DIRS 100948], Table 3; Fix et al. 2004 [DIRS 171745], Table 3). Use of the factor 6 multiplier assures that the Stainless Steel Type 304B rates will be higher than the Stainless Steel Type 304L rates in all calculations and allows for greater loss of neutron moderator if more-aggressive conditions (lower pH, higher ionic strength, and higher temperature) develop in the package.

Table 6.3-6. Steel and Alloy Corrosion Rates

	Units	Carbon Steel Type A516	Aluminum Alloys	Stainless Steel Types 316 and 316L	Stainless Steel Type 304L	Borated Stainless Steel	Ni–Gd Alloy
Base-case (low) corrosion rate	μm/yr	53.2	1.52	0.0512	0.0113	0.0678	0.0770
Medium corrosion rate		61.5	9.50	0.116	0.127	0.760	0.127
High corrosion rate		75.8	27.6	0.261	0.470	2.82	0.223
Base-case (low) corrosion rate	$Mol/cm^2/sec$	1×10^{-11}	1×10^{-13}	1×10^{-14}	3×10^{-15}	2×10^{-14}	2×10^{-14}
Medium corrosion rate		2×10^{-11}	8×10^{-13}	3×10^{-14}	3×10^{-14}	2×10^{-13}	4×10^{-14}
High corrosion rate		2×10^{-11}	2×10^{-12}	7×10^{-14}	1×10^{-13}	1×10^{-12}	6×10^{-14}

Source: DTN: Output MO0705GEOMODEL.000, file *Steels and Alloys REV02.xls.*

The corrosion rates in Table 6.3-6 represent short-term corrosion rates (from less than one year to several years) compared to the modeling period of 10,000 years. Corrosion rates tend to decrease with time due to a build-up of corrosion products that limits the availability of oxygen to the uncorroded material, as discussed in Section 6.6.2. Therefore, to account for the lowering of corrosion rates with time, the "low" corrosion rates in Table 6.3-6 were chosen as the base-case corrosion rates. However, sensitivity cases were performed with medium and high corrosion rates to evaluate their effects (*TMI_MxAL.6i, CSIGHi.6i, CSIGMed.6i, CD_I_SH2.6i,* and *CD_I_SM2.6i*).

The corrosion rates in Table 6.3-6 are applicable to both the seismic and igneous scenarios, even though the materials are subjected to high temperatures during the igneous scenario, as discussed in Section 6.2.2.

The EQ6 rate constants in Table 6.3-7 used for FFTF and TMI DSNF are calculated using Equations 4-1 and 4-2 (Section 4.1.5.1) evaluated at 50°C with a negative log of O_2 fugacity (pO_2) equal to 0.7, in output DTN: MO0705GEOMODEL.000, files *CDSP_Long_WP_FFTF_REV02.xls* and *CDSP_Long_ WP_TMI_REV02.xls* with the effective specific surface area for CSNF (see Table 4-10). For TMI, the rate is multiplied 100× by using a factor of 100 for the surface area in the fuel reactant block of TMI EQ6 input files, as per Section 4.1.5.5.

Table 6.3-7. Waste Form Corrosion Rates

Waste Form	Conditions	Corrosion Rates for EQ6 input (moles/cm^2/sec)	Calculated in
CSNF	50°C	rk1 × $[H+]^{0.34}$ +rk2 × $[HCO3-]^{0.102}$ rk1=1.1E-11, rk2=1.4E-13	*CSNF WP and TAD.xls*, tab "SNF Rate"
	90°C	rk1 × $[H+]^{0.34}$ +rk2 × $[HCO3-]^{0.102}$ rk1=2.6 × 10^{-11}, rk2=3.3 × 10^{-13}	
N-Reactor	50°C	1.29 × 10^{-09}	*CDSP WP_REV02.xls*
	90°C	1.97 × 10^{-08}	
FFTF MOX	50°C	rk1 × $[H+]^{0.34}$ +rk2 × $[HCO3-]^{0.102}$ rk1=6.4 × 10^{-10}, rk2=8.1 × 10^{-12}	*CDSP_Long_WP_FFTF_REV02.xls*, tab "CSNF Rate"
TMI	50°C (most likely)	rk1 × $[H+]^{0.34}$ +rk2 × $[HCO3-]^{0.102}$ rk1=1.8 × 10^{-09}, rk2=2.3 × 10^{-11}	*CDSP_Long_WP_TMI_REV02.xls,* tab Rates
	50°C (maximum)	rk1 × $[H+]^{0.34}$ +rk2 × $[HCO3-]^{0.102}$ rk1=3.6 ×10^{-08}, rk2=4.6 ×10^{-10}	*CDSP_Long_WP_TMI_REV02.xls,* tab Rates
HLWG	50°C (most likely)	rk1 × $[H+]^{0.49}$ +rk2 × $[H+]^{-0.49}$ rk1=9.5 ×10^{-13}, rk2=2.3 × 10^{-21}	*CDSP WP_REV02.xls*
	50°C (maximum)	rk1 × $[H+]^{0.49}$ +rk2 × $[H+]^{-0.49}$ rk1=1.3 × 10^{-9}, rk2=2.8 × 10^{-18}	
	90°C	rk1 × $[H+]^{0.49}$ +rk2 × $[H+]^{-0.49}$ rk1=3.4 × 10^{-12}, rk2=3.9 × 10^{-20}	

Source: Output DTN: MO0705GEOMODEL.000.

NOTE: CSNF = commercial spent nuclear fuel; FFTF = Fast Flux Test Facility; MOX = mixed oxide; TMI = Three Mile Island; HLWG = high-level waste glass.

6.3.7 Sequence of Corrosion

For the seismic scenario, all materials in the waste package begin corrosion at the same time. For the igneous scenario, the high temperatures are expected to cause rapid oxidation of the SNF (SNL 2007 [DIRS 177430], Section 6.4.8.3, Chemical Considerations). Therefore, for the igneous cases, the first step of each EQ6 simulation is to oxidize the fuel completely. Then, in step two, oxidation of the rest of the contents of the waste package occurs at the rates specified in Section 6.3.6.

6.3.8 Waste Package Saturation

Waste package saturation is defined as the quantity of water in a waste package divided by the void space in the waste package. The base case model uses 30% waste package saturation (Assumption 5.1, Section 5), with sensitivities ranging from 3% to 100%, as presented in Appendix C. The amount of saturation is varied in the EQ6 input file (V. 8.1) by setting the special keystring named "SETMWTMAX" equal to 300 for 30%, where "300" refers to the maximum grams of water in a waste package scaled to 1,000 g or 1 L.

6.3.9 Waste Package Temperature

The temperature of the waste package during the first 10,000 years after emplacement was not used directly but instead was calculated by adding the average temperature difference between the drift wall temperature and the waste package surface (ΔT) to the hottest and coolest temperatures estimated for the drift wall. The first step was to calculate the average ΔT values based on the individual temperatures of the drift wall and the waste package surface as calculated by the in-drift natural convection and condensation model, as presented in DTN: SN0408T05093.007 [DIRS 171547], file *2DComparison.mcd*. The ΔT was calculated in *DeltaT.xmcd* (Output DTN: MO0705GEOMODEL.000, folder: temperature). The results are presented in *Mathcad-Calculation of DeltaT.pdf* and in *Waste package temperature.xls*, tab "WP DeltT Data" (output DTN: MO0705GEOMODEL.000). Next, the ΔT was fitted to a curve using the EXCEL built-in function "Solver" (output DTN: MO0705GEOMODEL.000, file: *waste package temperature.xls*). The resulting ΔT was added to the hottest drift wall temperature, the coolest drift wall temperature, and the average of the hottest and coolest drift wall temperatures, as they vary with time. The hottest drift wall temperature represents the temperature calculated using the 10th percentile thermal conductivity value, in the middle of Drift 5, which is centrally located in the repository (SNL 2007 [DIRS 181648], Figure 6.3.5-11). The coolest drift wall temperature represents the temperature calculated using the 90th percentile thermal conductivity value, at the edge of Drift 3, at the edge of the repository footprint (SNL 2007 [DIRS 181648], Figure 6.3.5-9.)

The waste package surface temperature is calculated in output DTN: MO0705GEOMODEL.000, file *waste package temperature.xls*. Figure 6.3-1 shows the time history for the waste package surface temperature during the first 10,000 years after emplacement. The time-weighted average temperature was calculated to be 54°C in output DTN: MO0705GEOMODEL.000, file *waste package temperature.xls*. The temperature calculations are for intact waste packages; however a breached waste package, with in-dripping water, may be cooler. Hence the time-weighted average was rounded down to 50°C for the base-case temperature, with sensitivity cases set at 90°C for CSNF and N-reactor seismic scenarios (*CS_S_90.6i, CS_S_90K.6i,* and *CD_S_9.6i*).

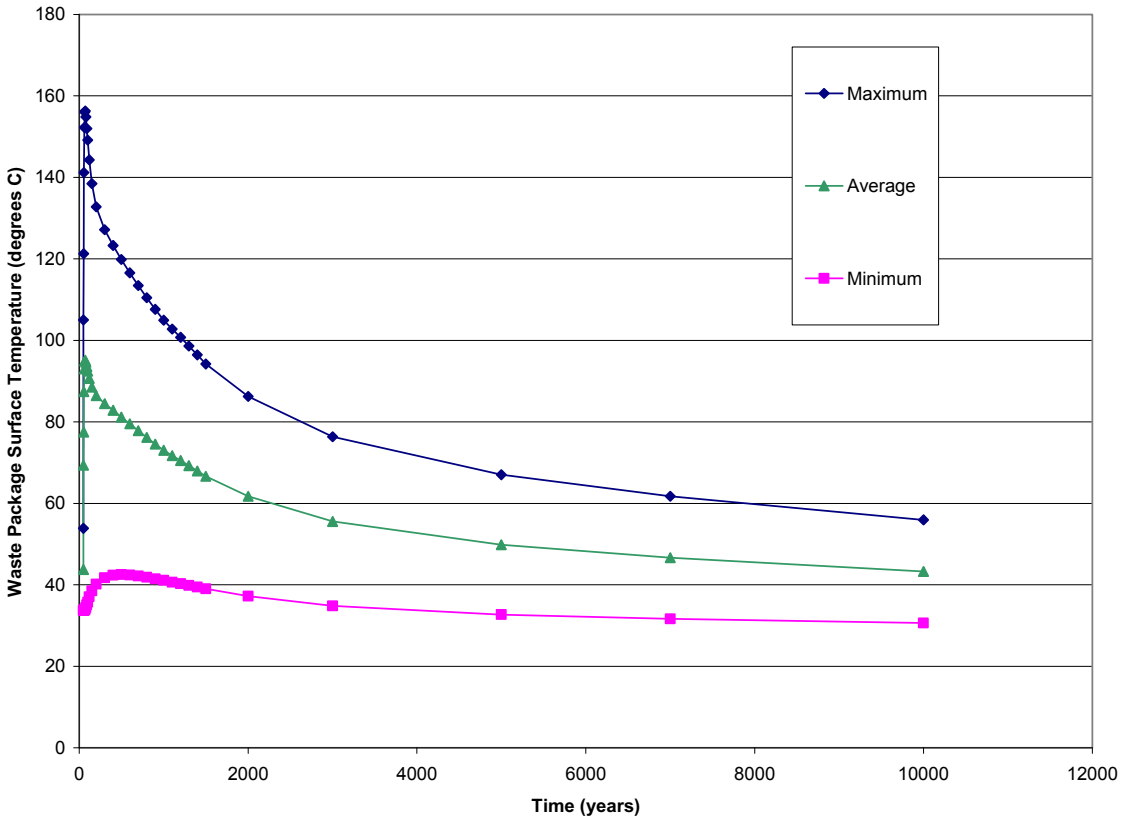

Source: Output DTN: MO0705GEOMODEL.000, file *waste package temperature.xls.*

Figure 6.3-1. Waste Package Surface Temperature

6.3.10 CSNF Cladding Failure

The condition of the CSNF cladding in a seismic or igneous event is predicted to be highly damaged; therefore, base-case cladding failure is set at 100%. As a sensitivity case, the cladding failure is reduced to 1% (*CS_S_1c.6i*).

6.3.11 Uncertainty in TAD Canister Design

CSNF TAD Canister Case 2—As discussed in Section 4.1.6, there are two potential design cases for the CSNF TAD canister. For the base case, Case 1, the fuel basket tubes are constructed of Stainless Steel Type 316L and the fuel basket plates are constructed of borated stainless steel. A sensitivity case (*CS_S_TC2.6i*) is performed using Case 2 materials, in which all materials are the same except the fuel basket tubes are constructed of borated stainless steel and the fuel basket plates are constructed of Stainless Steel Type 316L.

TMI A-516 Sleeve—There is uncertainty regarding the material used for the sleeve or basket holding the TMI fuel canister in position inside the DOE canister. The sleeve may be made of Carbon Steel Type A516 or Stainless Steel Type 316 (Radulescu et al. 2004 [DIRS 165482], Section 3.2.1; Taylor 2005 [DIRS 180657], Appendix C). For the base-case FFTF EQ6

simulations, Carbon Steel Type A516 will be used for the sleeve material, and a sensitivity case (*TMI_316s.6i*) considers the sleeve made of Stainless Steel Type 316.

FFTF Waste Package—The base case for the FFTF waste package contains four DFAs and one IDENT 69 in the DOE canister. A sensitivity case (*FFTF5DFA.6i*) considers an alternate configuration of five DFAs with no IDENT 69.

6.3.12 Plutonium Decay

When possible, ^{239}Pu decay is included in the EQ6 calculations. The limitation imposed by EQ6 V. 8.1 is that the plutonium decay can be included only for special reactants (constant degradation rate). For the CSNF igneous scenario, the fuel is oxidized in one step. For the following step, when the rest of the waste package is corroded, plutonium decay is included. For the DOE codisposal waste packages, plutonium is a component of the HLWG; therefore the decay option is not available for any of the simulations. The impact is small because the calculations run for 10,000 years and the half-life of ^{239}Pu is 24,100 years (Parrington et al. [DIRS 103896], p. 48).

6.3.13 Thermodynamic Database

The thermodynamic database *data0.ymp.R5* (DTN: SN0612T0502404.014 [DIRS 178850]), was revised and renamed *data0.ymp.R5.criticality* (output DTN: MO0705GEOMODEL.000) for use in the EQ6 simulations. The changes are discussed below:

Waste Form Compositions—The compositions of several waste forms were added to the database as solid phases, as shown in Table 6.3-8. This was necessary in order to allow the use of pH-dependent and bicarbonate-dependent corrosion rates. As indicated under "Source" in Table 6.3-8, some of the waste form compositions were taken directly from an input source, but in other cases, the composition had to be calculated in a spreadsheet.

Solid-Solution Formation—For the sensitivity case in which the CSNF composition contains all the principal isotopes identified in *Disposal Criticality Analysis Methodology Topical Report* (YMP 2003 [DIRS 165505], Table 3-1), two ideal solid solutions were added to the database to model the solid solution formation of lanthanide phosphates (Rhabdophane-ss) and lanthanide carbonates (La-carbonate-ss). Ideality is justified because the lanthanides are chemically very similar and preferentially form solid solutions in nature. Table 6.3-9 contains the additional solids added to *data0.ymp.R5.criticality.ss* besides the solids listed in Table 6.3-8. Lanthanides are often found in solid solutions, which tend to lower the solubility of the individual elements. Therefore, to include solid solutions is more realistic; whereas not including them tends to increase the loss of lanthanides, which increases the likelihood of in-package criticality. The database with the solid solutions were used for two sensitivity cases (*CSIGPI_R.6i* and *CSIGPIss.6i*) in which the individual lanthanides (gadolinium, neodymium, europium, and samarium) in the CSNF fuel were modeled as separate elements rather than being lumped together and modeled as gadolinium.

Table 6.3-8. Solids Added to Model Database

Name of Solid Entered into Database	Description	Source
CSNF_35at40_10K	Simplified SNF composition	Calculated in *CSNF Fuel REV02*.xl, tab "Simplified Fuel Composition"
Principal_Isotopes	An additional waste form composed of all principal isotopes not included in the simplified composition	Calculated in *CSNF Fuel REV02.xls,* tab "Principal Isotopes for EQ6"
UOX Mixed oxide (MOX)	FFTF SNF composition	Calculated in *CDSP_Long_WP_FFTF_REV02*.xl, tab FFTF Comp
Three Mile Island (TMI)	TMI SNF composition	Calculated in *CDSP_Long_WP_TM_REV02*.xls, tab: Fuel & LiCon
High-level waste glass (HLWG)	HLWG composition	Calculated in *CDSP_HLWGlass_2004.xls*
GlassSRL	Glass composition used in previous calculations	CRWMS M&O 2001 [DIRS 153263], Table 3

NOTE: Solids listed above were entered into output DTN: MO0705GEOMODEL.000, file *data0.ymp.R5.criticality*.

Table 6.3-9. Additional Solids Added to the Thermodynamic Database

Name of Solid Entered into Database	Description
Rhabdophane-ss	A solid solution of lanthanide phosphates with the following composition: (Nd,Eu,Sm,Gd)PO4:H2O
La-carbonate-ss	A solid solution of lanthanide carbonates with the following composition: (Nd,Eu,Sm,Gd)2(CO3)3

NOTE: Solids listed above were entered into output DTN: MO0705GEOMODEL.000, file *data0.ymp.R5.criticality.ss.*

High Temperature LogK—Some aqueous species for gadolinium and plutonium in the thermodynamic database have values only for 25°C. Thus, when the EQ6 simulations are performed at higher temperatures, such as 50°C or 90°C, the 25°C data are used. To assess the impact of using 25°C data, the log K of important gadolinium and plutonium aqueous species were calculated at 50°C and 90°C in spreadsheet *Gd-CO3-complex-augmentk.xls* (output DTN: MO0705GEOMODEL.000), using the sources presented in Table 4-1. The details of the calculations are presented in Appendix D. For a CSNF seismic sensitivity case at 90°C (*CS_S_90K.6i*), the log K was adjusted in the EQ6 input file as follows:

```
|GdCO3+                                  |AugmentLogK     |-0.76539    |
|Gd(CO3)2-                               |AugmentLogK     |-1.337473   |
|GdHCO3++                                |AugmentLogK     |-1.306291   |
|Gd2(CO3)3                               |AugmentLogK     |-3.49621    |
|PuO2CO3(aq)                             |AugmentLogK     |-0.574025   |
```

For a CSNF igneous sensitivity case at 50°C (*CSIGMedK.6i*) and for all the FFTF cases at 50°C, the log K was adjusted in the EQ6 input file as follows:

```
|GdCO3+                                  |AugmentLogK     |-0.29949   |
|Gd(CO3)2-                               |AugmentLogK     |-0.51542   |
|GdHCO3++                                |AugmentLogK     |-0.53328   |
|Gd2(CO3)3                               |AugmentLogK     |-1.37366   |
|PuO2CO3(aq)                             |AugmentLogK     |-0.24979   |
```

Other Corrections and Ferrimolybdate [$Fe_2(MoO_4)_3$]—Section 6.8 of *Qualification of Thermodynamic Data for Geochemical Modeling of Mineral–Water Interactions in Dilute Systems* (SNL 2007 [DIRS 177409]) identifies numerous corrections that were not incorporated in the *data0.ymp.R5* database (DTN: SN0612T0502404.014 [DIRS 178850]). For the MDR model, all these unincorporated corrections were examined for potential impact. The examination process involved determining if (1) the affected aqueous species were important in any simulations; (2) the affected solids formed in any simulations; and (3) the potential corrections would affect the releases of elements important to criticality in the calculations. Two potentially significant solids were identified: $NiMoO_4$ and ferrimolybdate ($Fe_2(MoO_4)_3$). For $NiMoO_4$, a correction was provided in Section 6.8 of the qualification document (SNL 2007 [DIRS 177409]), and it was shown that use of the uncorrected data caused mild overestimation of the solubility of the phase at temperatures greater than 25°C. This overestimation is not significant for criticality concerns, because the effect, if any, would be to increase the releases of actinides or lanthanides, as $NiMoO_4$ precipitation reduces acidity and ionic strength in the EQ6 simulations in the MDR model, providing a sink for both nickel and molybdenum.

For ferrimolybdate, *Qualification of Thermodynamic Data for Geochemical Modeling of Mineral–Water Interactions in Dilute Systems* (SNL 2007 [DIRS 177409], Section 6.8) simply determined that the thermodynamic data for this phase were not trustworthy, and no correction was offered. None of the CSNF simulations formed ferrimolybdate, so there is no impact. However, in a few of the N-reactor (CDSP) simulations, ferrimolybdate did form. To assess the impact of suppressing ferrimolybdate, sensitivity cases were performed (*CD_S_b2A.6i* and *CD_I_b2A.6i*).

6.3.14 Fugacity of CO_2 and O_2

During the model calculations, the waste package solutions are maintained in equilibrium with the oxygen and carbon dioxide levels in the ambient atmosphere outside of the waste package. The fugacity of carbon dioxide is set equal to 10^{-3} bar which is higher than the atmospheric value ($10^{-3.5}$ bar) because ambient fluids drawn from boreholes near the repository horizon appear to be in equilibrium with above-atmospheric carbon dioxide levels (Yang et al. 1996 [DIRS 100194], Table 8). Sensitivity calculations using higher CO_2 fugacity ($10^{-1.5}$ bar) are performed for each fuel type for either the seismic or igneous scenario (*CSIGCH.6i*, *CD_IHFC.6i, FFTF_1_5.6i,* and *TMI_1_5*). In addition, a case using a lower CO_2 fugacity (10^{-5} bar) is also performed (*CSIGCL.6i* and *CD_ILFC.6i*). This range of CO2 fugacity values is consistent with those used in TSPA-LA modeling (SNL 2007 [DIRS 177418], Section 1).

For most cases, the partial pressure of O_2 for the ambient repository atmosphere is set to atmospheric value, 0.2 bar (Weast 1977 [DIRS 106266], p. F-210). For a few cases that showed high plutonium releases from the waste package, the EQ6 cases were rerun using the adjusted-Eh

model from the *Dissolved Concentration Limits of Radioactive Isotopes* (SNL 2007 [DIRS 177418], Section 6.5.3). The adjusted-Eh model was developed because the results of the plutonium-solubility modeling using a redox potential calculated from the atmospheric values of oxygen did not represent plutonium-solubility behavior in laboratory experiments (SNL 2007 [DIRS 177418], Figure V-2). The differences are caused by the oxidation state of plutonium, which has a large impact on the geochemical behavior of plutonium in aqueous environments. The model using atmospheric levels of oxygen predicted the formation of Pu(VI) as the dominant dissolved species, whereas measurements in experiments and natural waters observed Pu(V) as the dominant dissolved species (SNL 2007 [DIRS 177418], Section V.2.3). The adjusted-Eh model, which results in a lower oxygen fugacity, generates a plutonium concentration that closely matches concentrations measured in equilibrium laboratory experiments (SNL 2007 [DIRS 177418], Figure 6.5-6). Based on the adjusted-Eh model, the fugacity of oxygen was calculated to be $10^{-8.7514}$ bar (output DTN: MO0705GEOMODEL.000, file *Adjusted_Eh.xls*) using:

$pE = 20.78 - pH + ¼ \log(pO_2)$	Stumm and Morgan 1996 [DIRS 125332], Equation 58, p. 456
$pE = [nF]Eh \div 2.303\ RT$	Langmuir 1997 [DIRS 100051], Equation 11.12
$Eh = 1.1 - 0.0592\ pH$	SNL 2007 [DIRS 177418], Equation V-5.

When implementing the adjusted-Eh cases, $N_2(aq)$ was suppressed in the EQ6 input files, as it is not expected to form.

6.3.15 Activity Coefficient Model

Applicability of the B-dot Equation—The thermodynamic database used in this report, DTN: SN0612T0502404.014 [DIRS 178850], is for dilute solutions and is used with the B-dot equation within the EQ3/6 software. The B-dot equation is defined and carefully examined in *Dissolved Concentration Limits of Radioactive Isotopes* (SNL 2007 [DIRS 177418], Section 6.3.3.4). CR 7763 indicates that there is a low level of confidence in the ability of YMP geochemical models to predict the solubilities of plutonium, neptunium, uranium, thorium, and americium for solutions with a pH of 9 or higher in the presence of CO_2. To address CR 7763, the study described below shows that for the purposes of the MDR model, EQ3/6 results generated using the B-dot activity coefficient equation for solutions with ionic strength greater than 1 molal and up to 4 molal are sufficiently accurate for the intent of the model.

Appendix VII in *Dissolved Concentration Limits of Radioactive Isotopes* (SNL 2007 [DIRS 177418]) derives correction ratios for the EQ3/6-predicted concentrations of many aqueous actinide species, in equilibrium with the predicted most-likely solubility-controlling solids. The derivation is based on comparison with the semi-empirical specific-ion interaction theory (SIT) approach. In fact, SIT was used to derive most of the actinide data in the current *data0.ymp.R5* database (DTN: SN0612T0502404.014 [DIRS 178850]) by extrapolation from higher ionic strengths, so it is consistent to use SIT for a comparison. For most uranium species, it was found that the correction factor was near or below 1 for ionic strengths up to 4 molal, meaning that B-dot gave insignificantly different results or slightly overpredicted the

concentration of dissolved uranium in these species. For plutonium, the deviation was somewhat greater. While B-dot tended to overpredict the concentration of PuO_2^{++} in equilibrium with PuO_2 (hydrated and aged), it underpredicted the concentrations of some charged plutonium carbonate complexes. However, the underprediction was modest (by a factor of 0.3 to <1) for ionic strengths up to 2 molal. Therefore B-dot calculations for uranium are reasonable up to 4 molal, whereas those for plutonium are reasonable up to 2 molal ionic strength, when the dominant aqueous species are charged carbonate complexes. When the dominant plutonium species is PuO_2^{++}, the corrections are adequate to 4 molal. Since neutral aqueous species such as PuO_2CO_3 (aq) generally suffer a much lower ionic strength effect (Guillaumont et al. 2003 [DIRS 168382]), it is likely that the B-dot correction for such species are adequate for higher ionic strengths.

6.3.16 Minerals Formed and Suppressed

EQ6 calculates the thermodynamically most stable mineral assemblage, given the simulation conditions (pH, gas fugacity, temperature, pressure and solution concentrations). A phase or aqueous species must be in the thermodynamic database to be considered. Sometimes, however, the most thermodynamically stable mineral is not what is observed to form or control the aqueous activity of a particular species, either in nature or in experiments. For example, the dissolved silica activity in Yucca Mountain area waters is typically more indicative of equilibrium with cristobalite, than with quartz, so the later may be suppressed (prevented from forming) in some simulations. Similarly, anhydrous PuO_2 is predicted to be the stable phase, but the thermodynamic properties were derived by high-temperature calorimetry. In low-temperature aqueous studies, a much-more-soluble hydrated PuO_2 is observed, possibly because of unannealed radiation damage. Thus the hydrous equivalent may be allowed to form and the anhydrous phase suppressed, depending on which criticality location—internal or external to the waste package—is being addressed.

Table 6.3-10 contains a list of the minerals that were allowed to form in the waste package. The minerals that were suppressed are documented in Table 6.3-11. The rationale for inclusion or exclusion from the EQ6 simulations is included in each of the tables. A solid phase is allowed to precipitate if one or more of these criteria are met: (1) the solid forms in nature at 0°C to 100°C, moderate pH (generally 4 to 9), and atmospheric pressure; (2) the solid forms in experiments consistent with the pressure, temperature, and pH of the EQ6 simulations (this criterion is important for phases that contain elements—such as plutonium and americium—that are extremely sparse in nature but are significant components of the waste); and (3) the solid is normally regarded as "high-temperature," but low-temperature alternatives are not represented in the thermodynamic database and precipitation is deemed to be necessary for maintaining realism in the EQ6 simulation. As an example of the last criterion, all the zirconium minerals in the database are generally regarded as high-temperature minerals. The solid ZrO_2 may be allowed to precipitate, even though the observed experimental low-temperature phase is a zirconium hydroxide. There is no zirconium hydroxide in the database. If no zirconium solid is allowed to form, aqueous zirconium concentrations may climb to unrealistic levels.

Table 6.3-10. Minerals Likely to Form in EQ6 Simulations

Mineral	Chemical Formula [as it appears in data0 , if different]	Justification
Alunite	$KAl_3(OH)_6(SO_4)_2$	Alunite is a low-temperature (i.e., on the order of 100°C) mineral that often forms as a result of the action of sulfuric acid derived from the oxidation of pyrite (Gaines et al. 1997 [DIRS 172360], p. 632). Data also indicates formation at 1 atm and mildly acidic conditions.
Anthophylite	$(Mg,Fe^{2+})_7Si_8O_{22}(OH)_2$	This mineral occurs in metamorphic and metasomatic rocks (Roberts et al. 1990 [DIRS 107105], p. 34). The mass formed in EQ6 simulations is small, typically < 10^{-4} the mass of schoepite.
Amesite-14A	$(Mg_2Al)[SiAl]O_5(OH)_4$ $[Mg_4Al_4Si_2O_{10}(OH)_8]$	Amesite forms during calcium metasomatism of biotite in granite (calcium to magnesium); found with calcite, magnetite, clinochlore, diopside, clinozoisite, sometimes grossular, occasionally margarite (Gaines et al. 1997 [DIRS 172360], pp. 1,422 to 1,423). Amesite's precipitation with calcite and magnetite suggests possible formation under waste package conditions.
AmO_2	AmO_2	Not enough americium in nature to form pure mineral. However, +4 is the principal oxidation state for americium. (Cotton et al. 1999 [DIRS 157545], pp. 1133-1137).
Anatase	TiO_2	Anatase is a low-temperature polymorph of $Ti0_2$ (Deer et al. 1992 [DIRS 163286], p. 553). It is a fairly common detrital mineral in sediments, where it is often of authigenic origin (Deer et al. 1992 [DIRS 163286], p. 553), which indicates low temperature (e.g., on the order of 100°C), standard pressure, and relatively neutral pH.
Anhydrite	$CaSO_4$	Important rock-forming mineral, often associated with gypsum, saltbeds, dolomite, or limestone. Also in cavities in igneous trap rocks (Roberts et al. 1990 [DIRS 107105], p. 30).
Antlerite	$Cu_3(SO_4)(OH)_4$	Antlerite is a secondary mineral formed in the oxidized zones of copper deposits in arid regions, associated with atacamite and other copper sulfates (Gaines et al. 1997 [DIRS 172360], p. 626). As such, it will form in conditions relevant to the waste package (e.g., on the order of 100°C, near-neutral pH, and 1 atm).
Baddeleyite	ZrO_2	Hydrolysis of zirconium salts leads to precipitation of poorly crystalline oxides at low temperatures (Milnes and Fitzpatrick 1995 [DIRS 105911], pp. 1,189 to 1,190) and soluble zirconium may be incorporated in or sorb onto clay mineral surfaces (Milnes and Fitzpatrick 1995 [DIRS 105911], pp. 1,185 to 1,186). However, there are no low-temperature zirconium oxide-hydroxides in the thermodynamic database, nor are there zirconium sorption models, so baddeleyite is allowed to precipitate in simulations, to prevent dissolved zirconium from reaching unrealistic concentrations.
$BaHPO_4$	$BaHPO_4$	$BaHPO_4$ is a solid that forms between 25°C to 50°C (Smith and Martell 1976 [DIRS 127382], p. 56).
Barite	$BaSO_4$	Barite has been found as a secondary precipitate in acid soils in coastal plains and associated river terrace soils (Doner and Lynn 1995 [DIRS 169277] p. 297); this indicates formation at temperatures at or below 100°C, near-neutral pH, and 1 atm.

Table 6.3-10. Minerals Likely to Form in Repository Conditions (Continued)

Mineral	Chemical Formula [as it appears in data0 , if different]	Justification
$BaUO_4$	$BaUO_4$	Precipitation is based on thermodynamic data and the documented formation reaction that is consistent with anticipated waste package conditions: $Ba + UO_2 + 2H_2O = BaUO_4^+$ (CTDP 2004 [DIRS 175057]).
BaU_2O_7	BaU_2O_7	Precipitation of BaU_2O_7 is possible under waste package conditions, based on Cordfunke and Ouweltjes (1988 [DIRS 175093], pp. 235 to 238) in Grenthe et al. (1992 [DIRS 101671], pp. 346 and 673).
Becquerelite	$Ca(UO_2)_6O_4(OH)_6:8H_2O$	Occurs as a secondary uranium mineral usually closely associated with uraninite (Roberts et al. 1990 [DIRS 107105], p. 78).
Boltwoodite-Na	$NaUO_2SiO_3OH:1.5H_2O$	A known low-temperature alteration phase of synthetic or natural UO_2 (Wronkiewicz and Buck 1999 [DIRS 169286], Figure 3).
Carbonate-Calcite	(Ca, Mn, Zn, Mg, Fe)CO_3	Varying degrees of solid solution exist between $CaCO_3$ and the following minerals (Gaines et al. 1997 [DIRS 172360], pp. 426 to 439): $MnCO_3$ (rhodochrosite), $ZnCO_3$ (smithsonite), $MgCO_3$ (magnesite), and $FeCO_3$ (siderite); therefore, formation under the waste package is possible because of ample evidence for $CaCO_3$ precipitation under waste package temperatures and pressures.
$CaUO_4$	$CaUO_4$	Moroni and Glasser (1995 [DIRS 178395]) reported formation of $CaUO_4$ in cement and other high calcium environments.
Chabazite	$K_{0.6}Na_{0.2}Ca_{1.55}Al_{3.8}Si_{8.2}O_{24}:10.0H_2O$	Chabazite is a zeolite commonly found in sedimentary environments. Chabazite is an alteration product of volcanic glass in alkaline and saline lakes (Ming and Mumpton 1995 [DIRS 156843] p. 884). Basaltic glass is generally considered to be an appropriate natural analogue for nuclear waste glass (Ewing and Haaker 1979 [DIRS 161749]).
Chalcedony	SiO_2	A general term for fibrous, microcrystalline varieties of quartz deposited from aqueous solutions (Klein and Hurlbut 1985 [DIRS 105907], p. 442). Chalcedony forms at near-neutral pH and at 100°C, which is consistent with waste package conditions. It is slightly more soluble than well-crystallized quartz, and may be kinetically favored for precipitation in sediments.
Chlorargyrite	AgCl	Chlorargyrite occurs naturally as a secondary mineral in the oxidation zone of silver deposits, often associated with native silver, jarosite, iron, and manganese oxides (Roberts et al. 1990 [DIRS 107105], p. 167). Last two oxides will be present upon corrosion of stainless steel members.

Table 6.3-10. Minerals Likely to Form in Repository Conditions (Continued)

Mineral	Chemical Formula [as it appears in data0 , if different]	Justification
Clinoptilolite-Ca Clinoptilolite-K Clinoptilolite-Na	$Ca_{1.7335}Al_{3.45}Fe_{.017}Si_{14.533036}$:10.922$H_2O$ $K_{3.467}Al_{3.45}Fe_{.017}Si_{14.533036}$:10.922$H_2O$ $Na_{3.467}Al_{3.45}Fe_{.017}Si_{14.533036}$:10.922$H_2O$	Often present in saline, alkaline lake sedimentary deposits derived from volcanic material (Gaines et al. 1997 [DIRS 172360], p. 1,673). As such, precipitation in the waste package is possible. Clinoptilolite is a major low-temperature alteration mineral in the tuffs of Yucca Mountain (Wilkin and Barnes 1998 [DIRS 172351]).
Compreignacite	$K_2(UO_2)_6O_4(OH)_6$:8H_2O	This phase was one of the uranium phases formed during laboratory degradation of UO2 (Wronkiewicz et al. 1996 [DIRS 102047], Table 5). Also, found as a rare oxidation product of "pitchblende" in uranium deposits, along with other uranium minerals favorable to forming in the waste package, such as schoepite and uranophane.
$CsTcO_4$	$CsTcO_4$	Crystalline $CsTcO_4$ exists at temperatures (on the order of 100°C), pH (near neutral) and pressure (1 atm) compatible with waste package conditions (Rard et al. 1999 [DIRS 157912], pp. 211 to 217).
Eskolaite	Cr_2O_3	As discussed in Section 6.3.16, Cr_2O_3 is thought to form on stainless steels at low temperature, Chromium-substituted goethite can be synthesized by aging a chromium-ferrihydrite [$Fe_4(CrO_4)(OH)_{10}$] precipitate (Schwertmann and Cornell 1991 [DIRS 144629], Chapter 5). It is likely that chromium-substituted ferrihydrite or $Fe(OH)_3$ minerals which form during waste package degradation will eventually transform to chromium-substituted goethite or hematite. Eskolaite was allowed to form as a discrete mineral, since the EQ6 database does not contain a solid-solution for substitution of eskolaite in hematite (e.g. $(Fe,Cr)_2O_3$).
$EuOHCO_3$	$EuOHCO_3$	Spahiu and Bruno provided thermodynamic data for formation of $EuOHCO_3$ at 25 °C. $EuOHCO_3$ is allowed to form as most stable carbonate form of europium in the thermodynamic database (1995 [DIRS 103804]).
$EuPO_4$:H_2O	$EuPO_4$:H_2O	Formation and solubility of the rare earth element phosphates, including europium, were reported at the temperature range of 23°C to 150°C by Cetiner et al. (2005 [DIRS 181082]).
Ferrite-Zn	$ZnFe_2O_4$	Experimental evidence shows this mineral forming from ferrihydrite coprecipitated with zinc at pH 12 and 70°C; these temperatures and pH were employed to accelerate the formation of crystalline products, and the mechanisms for a zinc-substituted magnetite/spinel-type phase forming may be influenced more by the presence and amount of zinc than the experimental conditions (Cornell 1988 [DIRS 175065], pp. 329 to 332).
Ferrimolybdate	$Fe_2(MoO_4)_3$	The adsorption of Mo(VI) on iron oxides, aluminum oxides, and smectites (like nontronites) is pH-dependent, reaching a maximum between pH values of 4 and 5 and then decreasing with increasing pH with very little adsorption above pH 8 (Goldberg et al. 1996 [DIRS 158382]). The adsorption process cannot be modeled with EQ6 at this time, but ferrimolybdate, $Fe_2(MoO_4)_3$, may also be the product of the reaction of iron oxides with Mo(VI) (Lindsay 2001 [DIRS 153210], Chapter 22; Titley 1963 [DIRS 153213]).

Table 6.3-10. Minerals Likely to Form in Repository Conditions (Continued)

Mineral	Chemical Formula [as it appears in data0 , if different]	Justification
Fluorapatite	$Ca_5(PO_4)_3F$	May be formed from reaction of phosphate fertilizers with soils or soil constituents (Lindsay et al. 1995 [DIRS 169289], Table 22-3), which indicates formation at or below 100°C, 1 atm, under mildly basic conditions.
Fluorite	CaF_2	Fluorite occurs as an authigenic mineral (Sheppard and Gude 1969 [DIRS 175105], pp. D69 to D74) and will precipitate at temperatures on the order of 100°C, near-neutral pH, and 1 atm.
$Gd_2(CO_3)_3$	$Gd_2(CO_3)_3$	Precipitation at 25°C of $Gd_2(CO_3)_3$ in the waste package is supported by Hull et al. (2000 [DIRS 175241], pp. 40 to 44). Experimental evidence indicates this species is stable between 25°C to 100°C (Spahiu and Bruno 1995 [DIRS 103804], p. 18).
$GdPO_4:2H_20$*	$GdPO_4:2H_20$	Gadolinium phosphates have been formed at temperatures of 21°C and 70°C (Table D-1).
Gibbsite	$Al(OH)_3$	Most common low temperature $Al(OH)_3$ polymorph (Hsu 1995 [DIRS 105875]).
Glauberite	$Na_2Ca(SO_4)_2$	Glauberite is a low-temperature mineral (Gaines et al. 1997 [DIRS 172360], pp. 579 to 580), which will form at temperatures on the order of 100°C, near-neutral pH, and 1 atm.
Goethite	α-FeOOH [FeOOH]	Goethite (α-FeOOH) and hematite (α-Fe_2O_3) are the two most thermodynamically stable and most widespread iron minerals occurring under oxidizing conditions (Schwertmann and Taylor 1995 [DIRS 105959]). FeOOH polymorphs are the most common iron-rich phases in the weathering of steels at low temperature, under oxidizing conditions (Section 6.3.16). Sensitivity runs were performed allowing hematite to form in lieu of goethite.
Hydroboracite	$CaMg[B_3O_4(OH)_3]_23H_20$ [$MgCaB_6O_{11}:6H_2O$]	This mineral forms in arid environments (such as in the Furnace Creek, California area) at temperatures on the order of 100°C, near-neutral pH, and 1 atm (Gaines et al. 1997 [DIRS 172360], p. 554).
Hydroxylapatite	$Ca_5(OH)(PO_4)_3$	Hydroxylapatite is in complete solid solution with fluorapatite [$Ca_5(PO_4)_3F$] and incomplete solid solution with chlorapatite [$Ca_5(PO_4)_3Cl$] (Gaines et al. 1997 [DIRS 172360], pp. 854 to 861, especially p. 858). Precipitation as disseminated nodules in nearshore marine environments (Gaines et al. 1997 [DIRS 172360], p. 859) or as primary deposits in sedimentary rocks (Deer et al. 1992 [DIRS 163286], p. 668) indicates similarities to waste package conditions.
Kaolinite	$Al_2Si_2O_5(OH)_4$	Most common kaolin, formation at 25°C is usually slow; however it can crystallize easily from the alteration of smectites (Dixon 1995 [DIRS 159374]).
Laumontite	$Ca_4[Al_8Si_{16}O_{48}]16H_20$ [$K_{0.2}Na_{0.2}Ca_{1.8}Al_4Si_{8.0}O_{24}:8.0H_2O$]	Laumontite forms as an authigenic mineral in sedimentary rocks, which indicates that it precipitates at or below 100°C and standard pressure and pH at or near neutral (Deer et al. 1992 [DIRS 163286], p. 521).
Mesolite	$Na_{.676}Ca_{.657}Al_{1.99}Si_{3.01}O_{10}:2.647H_2O$	Mesolite is a zeolite that can precipitate as a hydrothermal mineral with (for example) calcite; it is isostructural with and forms incomplete solid solution with the zeolites, natrolite and scolecite (Gaines et al. 1997 [DIRS 172360], p. 1,688). Formation of these zeolites is consistent with waste package conditions.

Table 6.3-10. Minerals Likely to Form in Repository Conditions (Continued)

Mineral	Chemical Formula [as it appears in data0 , if different]	Justification
Natrolite	$Na_2Al_2Si_3O_{10}:2H_2O$	Natrolite is a zeolite that can precipitate as a hydrothermal mineral with (for example) calcite; it is isostructural with and forms incomplete solid solution with mesolite and scolecite (Gaines et al. 1997 [DIRS 172360], pp. 1,677 to 1,679, and 1,688). Formation of these zeolites is consistent with waste package conditions.
$Na_4UO_2(CO_3)_3$	$Na_4UO_2(CO_3)_3$	This carbonate may form as an oxidation product of uranium-fuel degradation, as discussed in *Dissolved Concentration Limits of Elements with Radioactive Isotopes* (SNL 2007 [DIRS 177418], p. 6-12).
$NdPO_4:H_2O$	$NdPO_4:H_2O$	This mineral is reported at 100°C (Spahiu and Bruno 1995 [DIRS 103804], pp. 22 and 36), which suggests that waste package formation is possible.
$NdOHCO_3$	$NdOHCO_3$	In a study by Carroll (1993 [DIRS 181429]), orthorhombic $NdOHCO_3$ (s) was determined to be the stable neodymium-carbonate phase in the Nd-CO_2-H_2O system at pCO_2 0.1 and 1.0 atm at 25°C.
NiMoO4	NiMoO4	Found in thin corrosion films on nickel/molybdenum alloys (Delichere et al. 1988 [DIRS 181430]).
Nontronite-Ca	$Ca(Fe,Al)_2(Si,Al)_4O_{10}(OH)_2\ nH_2O$ $[Ca_{.165}Fe_2Al_{.33}Si_{3.67}H_2O_{12}]$	One of the three most common smectite minerals, produced by the degradation of aluminosilicate minerals and glasses (Section 6.3.16). Smectites are common in temperate and cold climates (Allen and Hajek 1995 [DIRS 159372]).
Nontronite-H	$H_2(Fe,Al)_2(Si,Al)_4O_{10}(OH)_2\ nH_2O$ $[H_{.33}Fe_2Al_{.33}Si_{3.67}H_2O_{12}]$	See Nontronite-Ca.
Nontronite-Mg	$Mg(Fe,Al)_2(Si,Al)_4O_{10}(OH)_2\ nH_2O$ $[Mg_{.165}Fe_2Al_{.33}Si_{3.67}H_2O_{12}]$	See Nontronite-Ca.
Nontronite-Na	$Na_2(Fe,Al)_2(Si,Al)_4O_{10}(OH)_2\ nH_2O$ $[Na_{.33}Fe_2Al_{.33}Si_{3.67}H_2O_{12}]$	See Nontronite-Ca.
NpO_2	NpO_2	NpO_2 formation is justified in *Dissolved Concentration Limits of Elements with Radioactive Isotopes* (SNL 2007 [DIRS 177418]), where it is predicted to be the solubility controlling phase in the waste package. In addition, the study by Roberts et al. (2003 [DIRS 162536]) supports the formation of NpO_2.
Powellite	$Ca(Mo,W)O_4$ $[CaMoO_4]$	Occurs as a secondary mineral in the oxidation zones of ore deposits (Roberts et al. 1990 [DIRS 107105], p. 692). It is often formed by the alteration of molybdenite, in copper deposits (Palache et al. 1951 [DIRS 162280], p. 1,080). As such, formation under waste package conditions is possible.
PuO_2 (hyd,aged)	PuO_2 (hyd,aged)	Studies of PuO_2 or PWR (pressurized water reactor) spent nuclear fuel degradation have shown that aqueous concentrations of plutonium are between the solubility of PuO_2 and that of a more soluble phase ($Pu(OH)_4$ or $PuO_2{\cdot}$(hyd,aged)) (Rai and Ryan 1982 [DIRS 112060]; Wilson and Bruton 1989 [DIRS 137607], Section 3.1 and Table 3). PuO_2(hyd, aged) has been allowed to form and PuO_2 has been suppressed.

Table 6.3-10. Minerals Likely to Form in Repository Conditions (Continued)

Mineral	Chemical Formula [as it appears in data0 , if different]	Justification
PuO_2CO_3	PuO_2CO_3	Thermodynamic data at standard temperature and pressure indicate formation under waste package conditions is possible (OECD 2001 [DIRS 159027], pp. 338 and 339).
Pyrolusite	MnO_2	Pyrolusite is very common in high pH, oxidizing conditions; in bogs, lacustrine, or shallow marine deposits; as deep sea-floor nodules; and as deposits formed by circulating meteoric waters (Gaines et al. 1997 [DIRS 172360], p. 239). Formation under waste package conditions is possible.
Rh_2O_3	Rh_2O_3	Mahan discusses chemistry of rare earth elements including rhodium, a member of platinum family. Mahan list Rh_2O_3 as one of the principal oxides of rhodium. (Mahan 1975 [DIRS 125331], Table 16.9, p. 708).
RuO_2	RuO_2	RuO_2 is synthesized in industry, and is used as a coating on titanium to form dimensionally stable electrodes used in the chlor-alkali process (Rard 1985 [DIRS 151313], p. 2). RuO_2 is typically synthesized at 150°C, pH 7 to 9.5 (Zhang et al. 2001 [DIRS 175107]). Based on the temperature of synthesis, it is possible that RuO_2 will form in the waste package.
Saponite Saponite-Ca Saponite-H Saponite-K Saponite-Mg Saponite-Na	$(Ca_{0.5},H,K,Mg_{0.5},Na)_{0.33}Mg_3(Si,Al)_4O_{10}(OH)_2$ $[Ca_{.165}Mg_3Al_{.33}Si_{3.67}O_{10}(OH)_2]$ $[H_{.33}Mg_3Al_{.33}Si_{3.67}O_{10}(OH)_2]$ $[K_{.33}Mg_3Al_{.33}Si_{3.67}O_{10}(OH)_2]$ $[Mg_{3.165}Al_{.33}Si_{3.67}O_{10}(OH)_2]$ $[Na_{.33}Mg_3Al_{.33}Si_{3.67}O_{10}(OH)_2]$	Trioctahedral magnesium-rich smectites (saponite or stevensite) can precipitate in saline and alkaline lakes and lake margins (Hover and Ashley 2003 [DIRS 169212]; Akbulut and Kadir 2003 [DIRS 169213]).
Schoepite	$UO_3{:}2H_2O$	Alteration product of uraninite (UO_2); associated with bequerelite, curite and other secondary minerals of uranium (Palache et al. 1944 [DIRS 163604], p. 628).
Schoepite (dehyd,0.9)	$UO_3{:}0.9H_2O$	This phase was one of the uranium phases formed during laboratory degradation of UO2 (Wronkiewicz et al. 1996 [DIRS 102047], Table 5).
Sepiolite	$Mg_4Si_6O_{15}(OH)_2{:}6H_2O$	Sepiolite may form in lacustrine environments characterized by alkaline solutions with high activities of silicon and magnesium (Singer 1995 [DIRS 169280], pp. 856 to 857). Precipitation in lacustrine environments is on the order of 100°C, slightly alkaline pH, and 1 atm. As such, formation is possible in the waste package.
$Sm_2(CO_3)_3$	$Sm_2(CO_3)_3$	Spahiu and Bruno (1995 [DIRS 103804]) provided thermodynamic data for selected rare earth elements. The most common oxidation state of samarium is +3 and $Sm_2(CO_3)_3$ is presented as most stable carbonate of samarium.
SmPO4:H2O	SmPO4:H2O	Formation and solubility of the rare earth element phosphates, including samarium, was reported at the temperature range of 23°C to 150°C by Cetiner et al. (2005 [DIRS 181082]).
Soddyite	$(UO_2)_2SiO_4{:}2H_2O$	A known alteration phase of synthetic or natural UO_2 (Wronkiewicz and Buck 1999 [DIRS 169286], Figure 3). Soddyite is an oxidation product of uranium ores (Gaines et al. 1997 [DIRS 172360], p. 1,115).

Table 6.3-10. Minerals Likely to Form in Repository Conditions (Continued)

Mineral	Chemical Formula [as it appears in data0 , if different]	Justification
Spinel-Co	Co_3O_4	Cornell and Giovanoli (1989 [DIRS 181442]) reported formation of Spinel-Co (CoCo2O4), at pH 12 and 70°C, in a Co2+ solution and its structure was confirmed by XRD analysis of the resulting precipitate.
Stellerite	$CaAl_2Si_7O_{18}$ $7H_20$ [$Ca_{2.0}Al_{4.0}Si_{14.0}O_{36}$:$14.0H_2O$]	A zeolite; occurs in low-temperature settings (on the order of 100°C) such as geothermal fields or in veins and geodes in basalts and other basic volcanic rocks, and on their fracture surfaces (Gaines et al. 1997 [DIRS 172360], p. 1,676).
Tenorite	CuO	Tenorite is a low-temperature mineral that forms in the upper enriched zone of copper deposits, forming as an oxidation product of primary copper minerals such as chalcopyrite and often associated with other low-temperature secondary minerals such as limonite (Roberts et al. 1990 [DIRS 107105], p. 856). Experimental evidence suggests formation temperatures below 100°C; for example, tenorite may precipitate at 25°C, 1 atm. total pressure, and near-neutral pH (Zemann 1969 [DIRS 175094], p. 29-D-10).
Trevorite	$NiFe_2O_4$	Although spinels are typically high pressure/temperature minerals (Roberts et al. 1990 [DIRS 107105], p. 881), there are low temperature spinel corrosion products (Fe_3O_4) that form on iron in oxygen-poor environments. Thus, trevorite was allowed to form since nickel-substituted goethite, hematite, and $NiFe_2O_4$ can be synthesized at 70°C (Cornell et al. 1992 [DIRS 164025], p. 78]), and nickel-substituted iron oxides are not in the EQ6 database.
$(UO_2)_3(PO_4)_2$:$4H_2O$	$(UO_2)_3(PO_4)_2$:$4H_20$	$(UO_2)_3(PO_4)_2$:$4H_2O$ is reported as a solubility controlling phase in groundwater at low temperature and pH values (Sandino 1991 [DIRS 113307], pp. 16 to 17).
Uranophane (alpha)	$Ca(UO_2SiO_3OH)2$:$5H_2O$	A known alteration phase of synthetic or natural UO_2 (Wronkiewicz and Buck 1999 [DIRS 169286], Figure 3).
Zn_2SiO_4 (Willemite)	Zn_2SiO_4	Zn_2SiO_4 precipitates in the oxidized zone of zinc deposits (Gaines et al. 1997 [DIRS 172360], p. 1,022). At Franklin, Sussex County, New Jersey, Zn_2SiO_4 is associated with secondary minerals zincite and calcite (Barthelmy 2005 [DIRS 175137]), which suggests formation under waste package conditions.

Table 6.3-11. Minerals Suppressed in EQ3/6 Simulations

Mineral	Formula	Justification
Andradite	$Ca_3Fe_2(SiO_4)_3$	Andradite is a high pressure/temperature mineral found in metamorphic and igneous rocks (Deer et al. 1966 [DIRS 102773], p. 30).
Annite	$KFe^{+2}{}_3AlSi_3O_{10}(OH)_2$ [$KFe_3AlSi_3O_{10}(OH)_2$]	Annite is an end member of biotite; a mica found only in igneous and metamorphic rocks (Deer et al. 1966 [DIRS 102773], pp. 211, 212, and 216).

Table 6.3-11. Minerals Suppressed in EQ3/6 Simulations (Continued)

Mineral	Formula	Justification
Antigorite	$Mg_3Si_2O_5(OH)_4$	Antigorite is stable at temperatures above typical waste package conditions (i.e., commonly associated with other serpentines, magnetite, magnetite-magnesiochromite, talc, magnesite, dolomite, amphiboles, and pyroxenes) (Winkler 1979 [DIRS 182040], pp 154 to 167).
Chrysotile	$Mg_3Si_2O_5(OH)_4$	Chrysotile is an ultramafic rock that is stable at temperatures above typical waste package conditions. At higher temperatures chrysotile converts to antigorite (Winkler 1979 [DIRS 182040], pp 154 to 167).
Chromium dioxide	CrO_2	Chromium dioxide is most commonly a synthesized film on recording tape; formation will not occur in the waste package. Rutile (TiO_2) displays a minor amount of chromium substitution for titanium; however, rutile is confined to igneous and metamorphic environments (Gaines et al. 1997 [DIRS 172360], pp. 235 to 237), which are inconsistent with waste package conditions.
Diopside	$Ca(Mg,Fe)[Si_2O_6]$	Diopside is a typical metamorphic mineral formed of alkaline olivine basalt parentage and in ultramafic nodules found in alkali olivine basalts and kimberlites. Its formation at 90°C is unlikely (Klein and Hurlbut 1999 [DIRS 124293], pp. 170 to 176).
Dolomite	$CaMg(CO_3)_2$	Dolomite is usually derived by secondary mineralization, from the replacement of calcium for magnesium in the calcite crystal structure in magnesium-rich waters (Klein and Hurlbut 1985 [DIRS 105907], p. 340). Because it rarely occurs as a primary mineral, it was also suppressed.
Ferrite-Ca Ferrite-Mg	$CaFe_2O_4$ $MgFe_2O_4$	Magnesioferrite has been found in sintered magnesite of furnace linings and other refractories (Palache et al. 1944 [DIRS 163604], p. 705) and is not expected to form at low temperatures.
Hematite	α-Fe_2O_3 [Fe_2O_3]	Goethite (α-FeOOH) and hematite (α-Fe_2O_3) are the two most thermodynamically stable and most widespread iron minerals occurring under oxidizing conditions (Schwertmann and Taylor 1995 [DIRS 105959]). Total suppression of the formation of hematite and goethite is not realistic considering the duration of the time frame of this analysis, 10,000 years after waste-package breach. Considering the temperature, solution and pH conditions in the waste package, a mixture of goethite and hematite would, eventually, be the most abundant iron oxides in the corrosion products (Schwertmann and Cornell 1991 [DIRS 144629], Chapters 4, 5, and 10). It is not possible to simulate the formation of such a mixture of iron oxides with EQ6 since only the most thermodynamically stable solid is allowed to form. If hematite is not suppressed, it will be the only iron oxide formed in a simulation. If hematite is suppressed and goethite is not, then goethite will be the only iron oxide that forms during an EQ6 simulation. However, during waste package degradation, mixed Fe(II)-Fe(III) minerals, such as magnetite (Fe_3O_4) and green rusts (iron hydroxy salts of chloride, sulfate or carbonate) as well as Fe(III) oxides such as maghemite (γ-Fe_2O_3) and lepidocrocite (γ-FeOOH) may also be the products of steel corrosion in the waste package (Schwertmann and Cornell 1991 [DIRS 144629], Introduction and Chapter 1; Furet et al. 1990 [DIRS 143296]). Of these minerals, only magnetite is in the EQ6 database, and magnetite will not form during most of the simulations because the assumption about O_2 fugacity (see Section 6.2) has the effect of completely oxidizing Fe(0) to Fe(III), as well as Cr(0) to Cr(VI) and Mo(0) to Mo(VI). In conclusion, hematite is currently being suppressed and goethite is the only iron oxide that is forming now.

Table 6.3-11. Minerals Suppressed in EQ3/6 Simulations (Continued)

Mineral	Formula	Justification
MnO_2(gamma)	MnO_2(gamma)	MnO_2(gamma) is suppressed because there are no high-temperature thermodynamic data for it and it is an alteration product of primary manganese minerals. The mineral did not form at 25°C. MnO_2 (gamma), known as Nsutite (Bricker 1965 [DIRS 157873], pp. 1,296 to 1,354), is a widespread alteration mineral in most of the world's major manganese deposits. Manganoan nsutite (MnO_2) is typically derived from the oxidation of manganese carbonate minerals such as rhodochrosite ($MnCO_3$) (Gaines et al. 1997 [DIRS 172360], p. 248).
Muscovite	$KAl_2(Si_3Al)O_{10}(OH,F)$ $[KAl_3Si_3O_{10}(OH)_2]$	Occurs in high temperature (>300°C) and pressure (above 1 atm) mineral assemblages (Roberts et al. 1990 [DIRS 107105], p. 586).
Phlogopite	$KMg_3AlSi_3O_{10}(OH)_2$	Occurs chiefly in metamorphic limestones and ultrabasic rocks at high temperature and pressure (Roberts et al. 1990 [DIRS 107105], p. 671).
PuO_2	PuO_2	The solubilities of solid Pu(IV) oxide/hydroxide scatter within several orders of magnitude because of the difficulties of establishing equilibrium of Pu(IV), polymerization and disproportionation reactions and the strong sorption capacities of Pu_4^+ (Runde 1999 [DIRS 144800], p. 8). Experimental plutonium solution concentrations during PuO_2 or PWR SNF degradation have been shown to be between the solubility of PuO_2 and that of a more-soluble phase, $Pu(OH)_4$ (or PuO_2·hyd,aged) (Rai and Ryan 1982 [DIRS 112060]; Wilson and Bruton 1989 [DIRS 137607], Section 3.1 and Table 3).
PuO2(OH)2:H2O	PuO2(OH)2:H2O	EQ6 simulations at 50 °C and 0.2 bars fO_2 showed $PuO_2(OH)_2$:$2H_2O$ to be marginally more stable than PuO_2(hyd,aged). Neither PuO_2(hyd, aged) nor $PuO_2(OH)_2$:$2H_2O$ have temperature coefficients in the *data0.ymp.R5* database (DTN: SN0612T0502404.014 [DIRS 178850]) However, the identity of $PuO_2(OH)_2$:$2H_2O$ has never been confirmed, and the logK (25°C) is given an uncertainty of 1 logK unit (Section 17.2.2.1 of *Chemical Thermodynamics of Neptunium and Plutonium* (OECD 2001 [DIRS 159027])). Furthermore, PuO_2(hyd, aged) is thought to become more stable (less soluble) with temperature (Efurd et al. 1998 [DIRS 108015]). Therefore, $PuO_2(OH)_2$:$2H_2O$ is suppressed.
Quartz	SiO_2	Quartz is suppressed to favor cristobalite stability. Local Yucca Mountain waters are often nearer to cristobalite saturation than quartz saturation, and abundant clinoptilolite has a stability incompatible with quartz saturation (Wilkin and Barnes 1998 [DIRS 172351]).
Talc	$Mg_3Si_4O_{10}(OH)_2$	Talc is characteristically associated with low-grade metamorphic rock and hydrothermal alteration of ultrabasic rocks (Kerr 1977 [DIRS 161606], p. 450), which is unlike waste package conditions.
Tremolite	$Ca_2Mg_5Si_8O_{22}(OH)_2$	The amphiboles are high-pressure/high-temperature minerals (i.e., >>300°C and 1 atm) that occur in igneous rocks (Huang 1995 [DIRS 169305], p. 1,013).
Tridymite	SiO_2	Tridymite is suppressed to favor chalcedony formation. There are no up-temperature data for tridymite in the current database, and the mineral appears to have an unrealistically high estimated stability at 25°C, relative to other SiO_2 polymorphs.
$(UO_2)_3(PO_4)_2$:$6H_2O$	$(UO_2)_3(PO_4)_2$:$6H_2O$	$(UO_2)_3(PO_4)_2$:$6H_2O$ has been suppressed in favor of $(UO_2)_3(PO_4)_2$:$4H_2O$, which has been allowed to form since uranyl phosphates are associated with a wide range of weathered uranium deposits (Finch and Murakami 1999 [DIRS 145442]). Few uranyl phosphates are included in the EQ6 database.

Table 6.3-11. Minerals Suppressed in EQ3/6 Simulations (Continued)

Mineral	Formula	Justification
Zircon	$ZrSiO_4$	Zircon is a high-pressure/high-temperature mineral (i.e., >>300°C and 1 atm) found in sedimentary deposits as a detrital mineral. (Roberts et al. 1990 [DIRS 107105], p. 975).
$ZnCr_2O_4$	$ZnCr_2O_4$	$ZnCr_2O_4$, known as zincochromite, occurs with quartz and amorphous Cr-V-Fe oxides and hydroxides (Gaines et al. 1997 [DIRS 172360], p. 303). Like chromite, its temperature of formation (>500°C) is typically well above waste package conditions.

In general, the lower-temperature hydrated form of a mineral will form in preference to the high-temperature form. However, often the database contains only the high-temperature form. The higher-temperature unstable forms are most confidently suppressed in the model when the database is seen to contain the equivalent lower temperature assemblage. In many simulations a silicate of calcium, magnesium, and sodium will form; the exact identity of the silicate is relatively unimportant when its mass is very small compared to the mass of the major uranium phases.

In natural systems, minor and trace components are usually incorporated into solid solutions of major element alteration phases. For example, goethite (α-FeOOH) can contain several weight percent of such transition metals as chromium, nickel, and manganese (Schwertmann and Cornell 1991 [DIRS 144629]). However, there are few thermodynamic data for solid solutions. Thus, the minor and trace elements are modeled as individual minerals (e.g., Cr_2O_3, $NiFe_2O_4$, and MnO_2).

The primary corrosion products predicted to form in the waste package are discussed below.

Corrosion Products of Stainless Steel—In the TAD-canister design (SNL 2007 [DIRS 179394]), much of the support material is stainless steel containing nickel, chromium, and perhaps molybdenum and boron. The alteration phases for stainless steel may be significantly different from those that form on carbon steels. This section reviews the evidence for identity of the solids that might form on corroding stainless steel.

There are few studies of stainless steel corrosion products at low temperature, in aqueous matrices. A significant problem is that the oxide coating grown on stainless steel near room temperature is typically very thin. For example, the summed thickness of the chromium, nickel, and iron oxides grown on the (100) faces of Fe-18Cr-13Ni (close to the composition of Stainless Steel Type 304), via potentiostatic polarization, was ≈2.2—2.4 nm (Maurice et al. 1998 [DIRS 181409], p. 913). Thus, special means are required for phase characterization.

The low-temperature studies use a wide variety of aqueous phase compositions but generally agree that a Cr(III)-rich oxide-hydroxide is a major passivating phase. For example, Lin et al. (2006 [DIRS 181428]) studied the corrosion products that formed on stainless orthodontic brackets at 37.6°C in artificial saliva. The passive coating was determined to be Cr_2O_3 and Fe_2O_3 with a small amount of NiO. Wang et al. (2001 [DIRS 178973]) characterized the passive film that formed on Stainless Steel Type 316L after immersion of the sample in 35% HNO_3 at 35°C for six hours. Even though this solution may be regarded as highly oxidizing (in fact, Cr(IV), Mo(IV) and Mo(VI) were detected), the solid phases that formed still contained Cr(III). The methodology was not sensitive to specific phases but gave an indication of the molecular environment of the metal atoms. The outer layer of the film was found to contain CrOOH, FeOOH, $Cr(OH)_3$, and $Fe(OH)_3$, while the inner layer was thought to contain oxides of chromium, iron, and nickel. Bastidas et al. (1998 [DIRS 181411]) used X-ray absorption spectroscopy to characterize the passive surface formed on Stainless Steel Type 304 subjected to anodic polarization at room temperature in a 5% NaCl solution (pH 8). The authors report Cr_2O_3 in the outside layer, possibly with FeO and metallic iron, and nickel in the layer below, with some hint of hydroxides. The exact identity of the Cr_2O_3 phase in the passivating layer is uncertain. The *data0.ymp.R5* database (DTN: SN0612T0502404.014 [DIRS 178850]) predicts

that Cr_2O_3 is stable relative to $Cr(OH)_3$; however, the thermodynamics of such small crystals carries some uncertainty, regardless of the phase identification. Probably this layer is partly hydrated at lower temperatures, in the presence of liquid water, as are most oxide surfaces. Ziemniak et al. (1998 [DIRS 181408]) apparently produced equilibrium between $FeCr_2O_4$ and aqueous solutions down to 25°C. However, $FeCr_2O_4$-rich phases will exist at relatively low fO_2, and would probably never occur in the current EQ6 simulations with $fO_2 = 0.2$ bar.

Even fewer studies address the fate of molybdenum during weathering of Stainless Steel Type 316. Delichere et al. (1988 [DIRS 181430]) found $NiMoO_4$ formed on the surface of nickel-molybdenum alloy films subject to anodic polarization in 0.5 sulfuric acid solutions, apparently at room temperature. The solid was poorly crystallized and may have been hydrated.

Studies at higher temperatures produce thicker coatings that are more amenable to phase identification. For example, Da Cunha Belo et al. (1998 [DIRS 178971]) characterized the coatings that formed on Stainless Steel Type 316L in a simulated pressurized water reactor (PWR) environment, with liquid water at 350°C. The corrosion products were multi-layered. The outermost, coarse layer was $Ni_{0.75}Fe_{2.25}O_4$ (analogous to trevorite); the intermediate region contained a mix of $Ni_{0.75}Fe_{2.25}O_4$ and Fe_3O_4; and the innermost fine-grained region contained a mix of Cr_2O_3 and $FeCr_2O_4$. Kim (1999 [DIRS 105168]) analyzed the oxide film formed on Stainless Steel Type 304 at 288°C in pressurized water containing O_2, H_2 and H_2O_2. After two weeks exposure, the oxide layer was 0.9 to 1.3 μm thick, and consisted of submicron, euhedral crystals on the exposed surface. Direct X-ray diffraction of the surface typically showed an iron spinel structure, but this technique could not distinguish between γ-Fe_2O_3 (maghemite) and Fe_3O_4 (magnetite). The definitive surface analyses were examined via Auger spectroscopy, scanning and transmission electron microscopy with electron diffraction. From the electron diffraction patterns, all samples had an outer "thick" layer with the structures of Fe oxides, on a fine inner layer containing spinel-structure $FeCr_2O_4$. In the oxygenated samples, the outer oxides had the structure of α-Fe_2O_3 (hematite); in the H_2O_2 samples, the oxide was γ-Fe_2O_3; and in the H_2 samples, the outer layer appears to be Fe_3O_4. In the outer oxide, significant chromium (25 wt % of metals) was present only in the H_2 sample; significant nickel (20 wt %) was present only in the H_2O_2 sample. In all samples, the inner layer contained significant chromium (25-40 wt %) and nickel (5-10 wt %). This study did not identify a separate nickel oxide. For scales formed at high temperatures (e.g., 600°C; Ziemniak and Hanson 2006 [DIRS 181413]), $(Ni,Fe)(Cr,Fe)_2O_4$ may form. However, $NiCr_2O_4$-rich phases are apparently not observed at lower temperatures.

Thermodynamic studies (Cubicciotti 1993 [DIRS 181416]; Beverskog and Puigdomenech 1999 [DIRS 181627]) predict corrosion products that are very similar to those observed in laboratory experiments. In particular, Beverskog and Puigdomenech (1999 [DIRS 181627]) predict Cr_2O_3, $NiFe_2O_4$, and Fe_2O_3 in oxic conditions, while $FeCr_2O_4$ is predicted to form at lower oxygen potentials. The phase $NiCr_2O_4$ has a narrow stability field relative to the other mixed spinels, and is predicted to form only at temperatures well above 100°C. With that exception, the thermodynamic studies indicate that the stable alteration phases should not change significantly between 25°C and 300°C. Thus the higher temperature, which produces more rapid corrosion, may substitute for greater time in the experiments to determine corrosion products of stainless steel.

Physical and Chemical Environment (SNL 2007 [DIRS 177412], Section 6.8) suppresses Cr_2O_3 but allows $NiCr_2O_4$ to form. Either phase serves the same purpose in EQ6 simulations: it acts as a sink for chromium and prevents unrealistically high (and experimentally unobserved) levels of Cr(III) species in aqueous solution. Both phases can be regarded as higher temperature solids, and a hydrous form may precipitate in preference.

Especially at low temperatures, the initial passivating layer on stainless steel is iron-poor compared to the bulk steel composition. However, corrosion of the alloys is modeled in EQ6 as a stoichiometric process, with a constant rate; therefore substantial iron-rich phases must form in EQ6 simulations purely to satisfy mass balance, as iron is not that soluble. There are no precise long-term analogs for stainless steel, either in nature or in historic human use, so there are no thick corrosion products to help predict the identity of the long-term phases. Weathering steels, with up to 5% nickel or chromium, serve as partial analogs for greater corrosion—suggesting the fate of nickel and chromium when a thicker crust forms, with a greater contribution from iron oxides. High-nickel meteorites may develop weathering crusts that are tens of thousands of years old; meteorites lack the chromium contents of stainless steel, but an analogy with the long-term behavior of weathering steels suggests the fate of at least part of the nickel and chromium.

Cook (2005 [DIRS 181406]) reviewed the corrosion products that form on "weathering" steels in marine environments at close to room temperatures. As expected, a host of iron hydroxides and oxides made up the bulk of the corrosion products. However, from various spectroscopic analyses, it was inferred that chromium substituted in FeOOH. It was speculated that passivation was achieved because chromium terminated growth of the FeOOH crystals, producing a very fine, compact coating that was adherent to the steel surface. Zhang et al. (2002 [DIRS 178975]) also studied weathering steels (containing more than 2 wt. % chromium) exposed to a marine environment for two years and found the protective layer consisted of (Fe,Cr)OOH. Sudakar et al. (2004 [DIRS 181407]) confirm that the substitution of chromium in goethite (FeOOH polymorph) reduces the particle size (to less than 0.05 μm in that study). Kimura et al. (2005 [DIRS 181414]) examined the products formed on high-nickel (3 wt. %) weathering steels exposed to an alternating wet-and-dry, low-temperature environment (in this case, an ocean-side wharf) for nine years. Characterization, by X-ray absorption fine structure and X-ray diffraction, showed a variety of FeOOH polymorphs, as well as spinel-structure Fe_2NiO_4 (trevorite).

In meteorites, the corrosion products provide constraints on the substitution of nickel in iron oxyhydroxides, and on the coherence of the corrosion crust. Typically the bulk of corrosion products form below the soil line (Johnson and Francis 1980 [DIRS 125291], Section 4.3.2), under high-humidity conditions. The Hoba meteorite, which fell approximately 8×10^4 years ago in what is now Namibia, has weathered to form maghemite, magnetite, goethite, and lepidocrocite. Initially, the meteorite metal was approximately 16% nickel by weight; in the corrosion crust, the nickel is distributed in all of the oxide minerals, with more in the spinel-structure phases (maghemite and magnetite; Golden et al. 1995 [DIRS 181412]). The last finding supports the assumption that spinel-structure trevorite will be a major nickel-containing phase or part of a solid solution with iron-rich spinel in the weathering of stainless steel. Post and Buchwald (1991 [DIRS 181415]) characterized akaganéite from the corrosion crust of the Campo del Cielo meteorite in Argentina. Nominally, akaganéite is a polymorph of FeOOH, but it typically contains other elements, either trapped in the tunnels of the structure, or substituting

for iron; this phase is also found in the corrosion film of "weathering" steels (Cook 2005 [DIRS 181406]). In the Camp del Cielo meteorite, nickel substitutes for approximately 5 atom % of the iron sites in the akaganéite. A meteorite from Roosevelt County, New Mexico, dated at 16,500 ± 1,300 years, contains maghemite (spinel-structure γ-Fe_2O_3) in the corrosion products, but no nickel analysis is given (Berry et al. 1994 [DIRS 181433]). Bland et al. (1998 [DIRS 181410]) found the weathering minerals were "magnetite, maghemite, ferrihydrite, lepidocrocite, goethite, and, principally, akaganéite." Most analyzed samples were old (>10^4 y), and the authors noted a tendency toward minerals with magnetically ordered iron (maghemite and magnetite) for meteorites that weathered in more humid climates. Initial weathering was rapid and then, once the passivation layer formed, proceeded slowly. Remarkably, the coating remained coherent even up to 45% to 50% oxidation of the sample (based on the molar conversion of Fe(0) and Fe(II) to Fe(III), determined by Mössbauer spectroscopy). The alteration crust was described as "well indurated", and is firmly attached to the underlying metal. The meteorite alteration crusts, though tough, have porosity up to 14%, with the majority of samples between 0 and 8% (Bland et al. 1998 [DIRS 181410], Figure 12). Thus it is reasonable that the long-term corrosion products of the stainless steel will remain in place, near the uncorroded alloy.

In summary, the characterization of corrosion products from steel, nickel-chromium weathering steel, and meteorites suggests that Cr_2O_3 (possibly hydrous), $NiFe_2O_4$, $NiMoO_4$, and various nickel- and chromium-substituted polymorphs of FeOOH will form during short- and long-term aqueous corrosion. Currently, the EQ6 thermodynamic data (DTN: SN0612T0502404.014 [DIRS 178850], file *data0.ymp.R5*) contains no model for trace substitution in FeOOH, so Cr_2O_3 and $NiFe_2O_4$ are allowed to form instead.

Carbon Steel Corrosion Products—The discussion of steel corrosion products in this paragraph is taken mainly from *The Iron Oxides, Structure, Properties, Reactions, Occurrences and Uses* (Cornell and Schwertmann 2003 [DIRS 173037], Chapter 18), and others as indicated. Steel is observed in nature and in experiments to corrode to metal oxides whose specific identities depend upon the particular conditions of corrosion and the composition of the steel. All the major iron oxides have been reported as the products of iron and steel corrosion. The occurrence of green rust, magnetite (Fe_3O_4), and lepidocrocite (γ-FeOOH) in rust indicates high availability of Fe^{2+} ions. Magnetite formation occurs near the steel surface where oxygen may be limited and requires neutral pH values, while lepidocrocite and goethite form an outer layer under oxidizing conditions. Green rusts, Fe(II)/Fe(III) hydroxides containing CO_3^{2-}, SO_4^{2-}, or Cl^- ions for charge balance, are unstable and transform to lepidocrocite or goethite (α-FeOOH). Lepidocrocite transforms to goethite, which is more thermodynamically stable, under both temperate and tropical conditions (Furet et al. 1990 [DIRS 143296]). So, it is appropriate to represent the steel corrosion products with goethite in the seismic model (and the single-cell modeling in general). Hematite (α-Fe_2O_3) is a product of aqueous steel corrosion at high temperatures (Pednekar 1987 [DIRS 159329]). However, goethite and hematite are the most stable iron oxides at earth surface conditions; for example, they are the most abundant iron oxides in soils. So iron oxyhydroxide transformations after all steels are corroded may eventually yield a mixture of these two minerals.

Recent experimental work was conducted on the corrosion of miniature waste packages (Zarrabi et al. 2003 [DIRS 171238]) in bathtub and flow-through configurations. The miniature waste packages were fabricated from carbon steel with similar interior geometry as codisposal waste packages. The X-ray diffraction analysis of the corrosion products revealed that a variety of iron oxyhydroxide minerals formed, regardless of the chemical conditions of the water flowing into the miniature waste packages. The corrosion products were mainly goethite (α-FeOOH), lepidiocrocite (γ-FeOOH), magnetite ($FeFe_2O_4$), and maghemite-C (γ-Fe_2O_3). Hematite was not observed, likely due to the short duration of the experiment. But these minerals are consistent with other experimental work that did see the formation of hematite (Pednekar 1987 [DIRS 159329]). In dynamic systems (bathtub and flow-through configurations), formation of goethite is favored over hematite (Zarrabi et al. 2003 [DIRS 171238]).

In the study of miniature waste packages (Zarrabi et al. 2003 [DIRS 171238]), changes in pH and conductivity of several inflow solutions with different compositions were monitored. In one case, the pH of the inflow was adjusted to 2.1, and the outflow pH increased for the first week to 4.9 and then stabilized at a pH of 4.2. In the same experiment, conductivity of the effluent decreased from its original value of about 4,030 (μS/cm) to about 1,950 (μS/cm) and remained low for the duration of the experiment. This indicates the steady-state buffering and sorption capacity of carbon steel corrosion products.

HLWG Corrosion Products—The HLWG is expected to alter to clays, phosphates, manganese oxides, carbonates, and perhaps a silica-rich phase. These conclusions come from studies of both nuclear waste glasses, and archeological samples.

Buck and Bates (1999 [DIRS 109494]) performed leaching tests at 90°C with radioactive and non-radioactive borosilicate nuclear waste glass. The major colloidal phase in the leachates was partially crystalline dioctahedral smectite clay. Carbonates (calcite and dolomite) also formed, along with transitional metal oxides including layered hydrous manganese oxides. Rhabdophane-like phosphates formed ($LnPO_4$:H_2O, where Ln represents several lanthanides) and accounted for much of the lanthanide content of the original glass. Menard et al. (1998 [DIRS 171053]) leached radioactive and non-radioactive simulants of nuclear waste glass, and found 98.5% of the lanthanides and thorium were apparently associated with phosphates and retained in a siliceous leached layer. The outer alteration layer was composed of smectitic phyllosilicates (clays). Thus both studies revealed similar alteration phases.

Cooper and Cox (1994 [DIRS 155741]; 1996 [DIRS 156251]) studied corrosion products of archeological alkali glasses and synthetic analogues. They used both MCC-4 lab experiments (Strachan et al. 1980 [DIRS 155740]) and examination of 450 year-old glass exhumed from soils near the River Ouse, in York, England. The glasses have low corrosion resistance and high alkali and alkaline-earth content; they are therefore more similar to waste glass than are natural analogues involving rhyolitic or basaltic glasses. For MCC-4 leach tests at 85.5°C, Cooper and Cox (1996 [DIRS 156251], p. 513) found smectite clay and apatite formed as alteration products. They characterize the smectite as $Mg_{(2-x)}Mn_x[(Si_{(4-y)}Al_y)O_{10}](OH)_2 \cdot nH_2O$, where x varies from 0 to 0.4 and y from 0.1 to 0.4; this formula requires the manganese to be in the (IV) state for charge balance. Since Mn(IV)-smectites are not well-known, it seems possible that the clay observed by Cooper and Cox is actually an intergrowth of smectite and amorphous MnO_2.

Indeed, Cox and Ford (1993 [DIRS 155742], Figure 2) examined microscopically the corrosion crusts on similar archeological glasses and found MnO_2 dendrites intergrown with leached, silica-rich glass. For the archeological corrosion crusts, the observed phases were a porous silica "gel," calcium-phosphate, $CaCO_3$, and MnO_2. The silica gel may be associated with either SiO_2(am) or chalcedony in the *data0.ymp.R5* database (DTN: SN0612T0502404.014 [DIRS 178850]). Presumably, silica gel is thermodynamically less stable than chalcedony; however, the "gel" may be stabilized, relative to chalcedony, by residual alkali (Deer et al. 1966 [DIRS 102773], pp. 345 to 346). However, it must be recognized that the codisposal waste packages will contain abundant iron degradation products (from corrosion of carbon steel). A highly reactive silica gel might combine with excess iron (not present in MCC-4 leach tests or the English soils) and other glass components to form iron-rich clays. Similarly, the high uranium content of the waste packages might cause much of the phosphate to be associated with uranium, rather than calcium or lanthanide phosphates.

Gadolinium—For the CSNF igneous scenario, the first stage involves rapid oxidation of the fuel. During this stage there is an absence of phosphorous in the system; therefore, gadolinium forms a carbonate ($Gd_2(CO_3)_3$), rather than a more stable phosphate ($GdPO_4{:}2H_2O$). During the second stage EQ6 simulation, when degradation of steel occurs, releasing phosphorus into the system, the model predicts that all the $Gd_2(CO_3)_3$ converts to the more thermodynamically favored $GdPO_4{:}2H_2O$. Sometimes in nature, even though it is thermodynamically favored, once a mineral is formed (in this case $Gd_2(CO_3)_3$), the mineral does not readily change to another mineral (in this case $GdPO_4{:}2H_2O$). To measure the impact of this, the $GdPO_4{:}2H_2O$ is suppressed in a sensitivity case (*CSIGnoP.6i*).

Plutonium—In most simulations the mineral PuO_2 is suppressed in favor of the less thermodynamically stable mineral PuO_2(hyd, aged) (Table 6.3-10), to be consistent with TSPA-LA modeling. For in-package criticality, however, it would be more appropriate to allow the PuO_2 to form, since it has a lower solubility and is less likely to be transported out of the waste package. A sensitivity case was performed in which the mineral PuO2 was not suppressed and was therefore allowed to form (*CSIGPuO2.6i*).

Schoepite—Schoepite is here defined as $UO_3{:}2H_2O$; this is the stoichiometry used by Grenthe et al. (1992 [DIRS 101671], p. 116) to derive thermodynamic data, and was retained in the update of that work (Guillaumont et al. 2003 [DIRS 168382], p. 164). The latter reports that $UO_3{:}2H_2O$ is stable in water below 40°C (p 434). In other documents, $UO_3{:}2H_2O$ is also referred to as meta-schoepite (BSC 2004 [DIRS 169987], Section 6.2.2.3, p. 6-11).

The hydrous uranyl solid that forms from 0°C to 50°C will likely be schoepite, especially if the system is thermodynamically saturated with liquid water. However, the result is less certain for higher temperatures. Some sources indicate that schoepite still forms to 90°C and above, and others indicate dehydrated schoepite ($UO_3 \cdot xH_2O$, $x < 1$) forms instead.

According to Guillaumont et al. (2003 [DIRS 168382], p. 588), formation of dehydrated schoepite does not occur until system temperatures are above 120°C. This result is consistent with the findings of O'Hare et al. (1988 [DIRS 113277], pp. 1292 and 1293), who show the vapor pressure for the reaction, given by Equation 6-1:

$$UO_3 \cdot 2H_2O = UO_3 \cdot 0.9H_2O + 1.1H_2O(g) \quad \text{(Eq. 6-1)}$$

is just 0.9 atm at 100°C.

Wronkiewicz et al. (1996 [DIRS 102047]) found both schoepite and dehydrated schoepite in samples taken from drip tests performed at just 90°C. However, identification was carried out via conventional electron microscopy (e.g., the samples were essentially in vacuum, and one would expect some dehydration of schoepite to occur purely as an analytical artifact).

The EQ6 database and supporting spreadsheets (DTNs: SN0612T0502404.014 [DIRS 178850] and SN0702T0502404.015 [DIRS 181228]) contain logK(T) data for both schoepite and dehydrated schoepite. The logK for dissolution of the phases, as given in the database, is shown in Table 6.3-12.

Table 6.3-12. Variation of logK(T) from the EQ6 Database

For reaction: $UO_3 \cdot zH_2O + 2H^+ = UO_2^{2+} + (1+z)H_2O$				
Temperature	**0°C**	**25°C**	**60°C**	**100°C**
logK schoepite (z = 2)	5.6756	4.8443	3.9389	3.1556
logK dehydrated schoepite (z = 0.9)	6.1471	5.0904	3.9109	2.8634

Source: DTN: SN0612T0502404.014 [DIRS 178850].

These data indicate that, at 25°C, schoepite is the stable phase (smaller logK for dissolution), but at 60°C, dehydrated schoepite is very marginally more stable. However, the uncertainty in the schoepite logK at 25°C is estimated to be 0.43 to 0.5 logK units (Guillaumont et al. 2003 [DIRS 168382], pp. 408 and 409). In addition, the temperature variation in logK for the two phases was estimated (not measured) via estimated heat capacities (DTN: SN0702T0502404.015 [DIRS 181228], spreadsheet *Minerals_cal_KBH_Usilicates.xls*), for the logK(T≠25°C). Hence the database values of the logKs for the two phases are essentially the same at 60°C and 100°C, within the uncertainty estimates. Due to the uncertainty in the logKs, the schoepite with the highest water content is the most appropriate for criticality calculations. Therefore the formation of dehydrated schoepite is suppressed in calculations above 50°C.

Cr (III) Minerals—Cr(III) model is described and justified in Section 6.8.1.2 of *Engineered Barrier System: Physical and Chemical* Environment (SNL 2007 [DIRS 177412]). Cr(VI) is readily reduced to Cr(III) in the presence of electron donors, such as uncorroded or partially corroded steels; even small amounts of Fe(II) in hematite are sufficient to reduce Cr(VI). Observed corrosion products of steels invariably contain Cr(III) and not Cr(VI).

6.4 MODEL IMPLEMENTATION

Tables 6.4-1 and 6.4-2 list the input filenames for the seismic cases and the description of each case for CSNF and DOE waste packages, respectively. Tables 6.4-3 and 6.4-4 provide the filenames and descriptions for the igneous cases. In the tables, the description of the base case applies to all cases, except for the differences described next to each filename. For the seismic and igneous cases, the greater numbers of sensitivity cases were performed for the CSNF and CDSP waste packages. Since the FFTF and TMI waste packages are similar to the CDSP waste package, in that the fuel is codisposed with HLWG, a smaller subset of FFTF and TMI sensitivity cases was performed.

Table 6.4-1. CSNF Seismic Case Descriptions

Filename	Description	Associated Section or Table
CSNF Waste Package		
CS_S_b	**Base case**: average fuel corrosion rate, low steel and alloy corrosion rate, 1 L/yr seepage rate, J-13 well water seepage composition, 50°C ambient temperature, log O_2 fugacity = -0.7, log CO_2 fugacity = −3, waste package 30% saturation, 100% cladding failure, Case 1 TAD canister design, plutonium decay not included, Cr(III) rather than Cr(VI) is dominant, goethite is iron-oxide formed, PuO_2 (hyd, aged) formed, simplified CSNF fuel composition	All subsections in Section 6.3
CS_S_1c	1% cladding failure	Section 6.3.10
CS_S_90	Temperature of 90°C	Section 6.3.9
CS_S_90K	Temperature of 90°C and high temperature logK for gadolinium and plutonium aqueous species	Section 6.3.13, Appendix D
CS_S_F9	Seepage flux of 1,000 L/yr	Section 6.3.4
CSS_F9Eh	Seepage flux of 1,000 L/yr and adjusted-Eh model	Section 6.3.14
CS_S_Max	Maximum surface area of CSNF degradation rate	Table 6.3-1
CS_S_TC2	TAD-canister Case 2 design	Section 6.3.11
CS_S_W1	W1 seepage water	Section 6.3.5
CS_S_W2	W2 seepage water	Section 6.3.5
CS_S_W3	W3 seepage water	Section 6.3.5

Table 6.4-2. DOE Codisposal Seismic Case Descriptions

Filename	Description	Associated Section or Table
CDSP (N Reactor) Waste Package		
CD_S_b	**Base case**: average fuel rate, low steel and alloy corrosion rates, most probable glass corrosion rate, most likely glass exposure factor, 2004 HLWG composition, 1 L/yr seepage rate, J-13 well water seepage composition, 50°C ambient temperature, log O_2 fugacity = -0.7, log CO_2 fugacity = −3, waste package 30% saturation, Cr(III) rather than Cr(VI) is dominant, goethite formed	All subsections in Section 6.3
CD_S_9	Base case at 90°C	Section 6.3.9
CD_S_GM	Maximum HLWG corrosion rate	Section 6.3.6
CD_S_GX	Glass maximum exposure factor	Section 4.1.5.3
CD_S_GS	Historical HLWG Composition (GlassSRL)	Table-12
CD_S_W1	W1 seepage water	Section 6.3.5
CD_S_W2	W2 seepage water	Section 6.3.5
CD_S_W3	W3 seepage water	Section 6.3.5
CD_S_b2A	Sensitivity for suppression of ferrimolybdate	Section 6.3.13
FFTF Codisposal Waste Package		
FFTF_S_b	**Base case**: average fuel rate, low steel and alloy corrosion rates, most probable glass corrosion rate, most likely glass exposure factor, 2004 HLWG composition, 1 L/yr seepage rate, J-13 well water seepage composition, 50°C ambient temperature, log O_2 fugacity = −0.7, log CO_2 fugacity = −3, waste package 30% saturation, Cr(III) rather than Cr(VI) is dominant, goethite formed, most reactive FFTF waste package configuration (four DFAs and one IDENT 69 fuel pin container), high-temperature log K for gadolinium and plutonium aqueous species	All subsections in Section 6.3
FFTF5DFA	Less reactive FFTF waste package configuration (five DFAs, no IDENT 69)	Section 6.3.11
FFTF_1_5	log(fCO2)= −1.5	Section 6.3.14
FFTF_hem	Hematite forms (rather than goethite)	Table 6.3-10
FFTF_MxG	Maximum HLWG corrosion rate	Section 6.3.6
FFTFMxGE	Maximum HLWG corrosion rate and adjusted-Eh model	Section 6.3.14
TMI Codisposal Waste Package		
TMI_S_b	**Base case**: average fuel rate, low steel and alloy corrosion rates, most probable glass corrosion rate, most likely glass exposure factor, 2004 HLWG composition, 1 L/yr seepage rate, J-13 well water seepage composition, 50°C ambient temperature, log O_2 fugacity = -0.7, log CO_2 fugacity = −3, waste package 30% saturation, Cr(III) rather than Cr(VI) is dominant, goethite formed, sleeve/basket structure constructed of Carbon Steel Type A516, high LiCon corrosion rate	All subsections in Section 6.3

Table 6.4-2. DOE Codisposal Seismic Case Descriptions (Continued)

Filename	Description	Associated Section or Table
TMI Codisposal Waste Package (Continued)		
TMI_MxAL	High steels and alloys corrosion rate	Section 6.3.6
TMI_MxG	Maximum HLWG corrosion rate	Section 6.3.6
TMI_MxFu	Maximum TMI fuel rate	Table 6.3-7
TMI_1_5	log(fCO2)= −1.5	Section 6.3.14
TMI_hem	Hematite forms (rather than goethite)	Table 6.3-10
TMI_316s	Stainless Steel Type 316 sleeve, not Carbon Steel Type A516	Section 6.3.11
TMI_LiCL	Low LiCon rate	Table 4-15

Table 6.4-3. CSNF Igneous Case Descriptions

Filename	Description	Associated Section or Table
CSNF Waste Package		
CSNFIG1	**Base case**: two-stage simulation with oxidation of fuel in first stage and oxidation of the remaining components in second stage, maximum fuel corrosion rate (i.e., maximum CSNF surface area), low steel and alloy corrosion rate, 1 L/year seepage rate, basalt seepage water composition 1 (Columbia Basin), 50°C temperature, log O_2 fugacity = −0.7, log CO_2 fugacity = −3, 30% saturation, 100% cladding failure, Case 1 TAD canister design, plutonium decay included, Cr(III) rather than Cr(VI) is dominant, goethite is iron-oxide formed, PuO_2 (hyd, aged) formed, simplified CSNF fuel composition	All subsections in Section 6.3
CSIGPI	Principal isotopes Included	Section 6.3.2
CSIGPI_R	Principal isotopes included, solid solution of lanthanide phosphates allowed to form	Table 6.3-9
CSIGPIss	Principal isotopes included, solid solutions of lanthanide phosphates and lanthanide carbonates allowed to form	Table 6.3-9
CSIGCH	log(fCO2)= −1.5	Section 6.3.14
CSIGCL	log(fCO2)= −5	Section 6.3.14
CSNFIG2	Seepage 1,000 L/yr	Section 6.3.4
CSIGAdEh	Seepage 1,000 L/yr; adjusted-Eh	Section 6.3.14
CSIGHi	High steel and alloy corrosion rate	Section 6.3.6
CSIGMed	Medium steel and alloy corrosion rate	Section 6.3.6
CSIGMedK	Medium steel and alloy corrosion rate, high-temperature log K	Section 6.3.13, Appendix D
CSIGnoP	No gadolinium phosphates allowed to form	Section 6.3.16
CSIGPuO2	PuO2 formed	Section 6.3.16
CSIG_IB	Icelandic basalt water	Section 6.3.5
CSIG_CB2	Columbia Basin Water 2	Section 6.3.5

Table 6.4-4 DOE Codisposal Igneous Case Descriptions

Filename	Description	Associated Section or Table
CDSP (N Reactor) Waste Package		
CD_I_B	**Base case**: two-stage simulation with oxidation of fuel in first stage and oxidation of the remaining components in second stage, average fuel rate, low steel and alloy corrosion rates, most probable glass corrosion rate, most likely glass exposure factor, 2004 HLWG composition, 1 L/yr seepage rate, seepage water composition 1 (Columbia Basin), 50°C ambient temperature, log O_2 fugacity = −0.7, log CO_2 fugacity = −3, waste package 30% saturation, Cr(III) rather than Cr(VI) is dominant, goethite formed	All subsections in Section 6.3
CD_IHFC	log(fCO2)= −1.5	Section 6.3.14
CD_ILFC	log(fCO2)= −5	Section 6.3.14
CD_I_f9	Seepage 1,000 L/yr	Section 6.3.4
CD_I_W2	Columbia Basin Water 2	Section 6.3.5
CD_I_WI	Icelandic basalt water	Section 6.3.5
CD_I_SH2	High steel and alloy corrosion rate	Section 6.3.6
CD_I_SM2	Medium steel and alloy corrosion rate	Section 6.3.6
CD_I_b2A	Sensitivity for suppression of ferrimolybdate	Section 6.3.13
FFTF Codisposal Waste Package		
FFTF1_IG	**Base case**: two-stage simulation with oxidation of fuel in first stage and oxidation of the remaining components in second stage, average fuel rate, low steel and alloy corrosion rates, most probable glass corrosion rate, most likely glass exposure factor, 2004 HLWG composition, 1 L/yr seepage rate, seepage water composition 1 (Columbia Basin), 50°C ambient temperature, log O_2 fugacity = −0.7, log CO_2 fugacity = −3, waste package 30% saturation, Cr(III) rather than Cr(VI) is dominant, goethite formed, most reactive FFTF waste package configuration (four DFAs and one IDENT 69 fuel pin container), high-temperature log K for gadolinium and plutonium aqueous species	All subsections in Section 6.3
FFTFIG_2	Seepage 1,000 L/yr	Section 6.3.4
TMI Codisposal Waste Package		
TMI_IG_1	**Base case**: two-stage simulation with oxidation of fuel in first stage and oxidation of the remaining components in second stage, average fuel rate, low steel and alloy corrosion rates, most probable glass corrosion rate, most likely glass exposure factor, 2004 HLWG composition, 1 L/yr seepage rate, seepage water composition 1 (Columbia Basin), 50°C ambient temperature, log O_2 fugacity = −0.7, log CO_2 fugacity = −3, waste package 30% saturation, Cr(III) rather than Cr(VI) is dominant, goethite formed, sleeve/basket structure constructed of Carbon Steel Type A516, high LiCon corrosion rate	All subsections in Section 6.3
TMI_IG_2	Seepage 1,000 L/yr	Section 6.3.4

6.5 MODELING RESULTS

6.5.1 Gadolinium, Plutonium, and Uranium Percent Remaining Within Waste Package

An important measure for criticality is the percent remaining within the waste package of neutron absorbers and radionuclides. The cases with significant neutron absorber loss are of most interest for in-package criticality, whereas the cases with significant plutonium or uranium loss are of most interest for external criticality. The results for the seismic cases are provided in Tables 6.5-1 and 6.5-2, and the results for the igneous cases are provided in Tables 6.5-3 through 6.5-5. A discussion of the results is provided in Section 6.5.3.

Table 6.5-1. CSNF Seismic Results: Gadolinium, Plutonium, and Uranium Percent Remaining

Filename	Conditions	pH Max	pH Min	Percent Remaining at 10,000 Years		
				Gadolinium	Plutonium	Uranium
CS_S_b	Base Case	8.15	5.91	93.5	99.0	100.0
CS_S_1c	1% cladding	8.15	5.21	100.0	99.1	100.0
CS_S_90	90°C	8.30	6.05	60.7	96.6	100.0
CS_S_90K	90°C, high-temperature log K	8.30	5.45	87.7	91.9	100.0
CS_S_F9	1,000 L/yr flux	8.15	8.02	99.0	0.0	99.0
CSS_F9Eh	1,000 L/yr and adjusted-Eh	8.15	8.02	99.0	99.8	99.0
CS_S_Max	Max CSNF surface area	8.15	5.91	93.5	99.1	100.0
CS_S_TC2	TAD-canister Case 2	8.15	5.94	96.0	99.1	100.0
CS_S_W1	W1 seepage water	8.16	5.91	93.5	99.1	100.0
CS_S_W2	W2 seepage water	7.84	5.92	93.1	99.1	100.0
CS_S_W3	W3 seepage water	7.71	5.91	93.4	99.1	100.0

Source: Output DTN: MO0705GEOMODEL.000, CSNF/ *CSNF Seismic Summary.xls.*

Table 6.5-2. DOE SNF Codisposal Seismic Results: Gadolinium, Plutonium, and Uranium Percent Remaining

Filename	Conditions	pH Max	pH Min	Percent Remaining at 10,000 Years		
				Gadolinium	Plutonium	Uranium
CDSP (N Reactor) Waste Package						
CD_S_b	Base case	8.15	4.13	N/A	99.8	100.0
CD_S_9	Temperature at 90°C	8.30	4.12	N/A	99.7	100.0
CD_S_GM	Glass maximum corrosion rate	8.15	7.22	N/A	70.6	100.0
CD_S_GX	Glass maximum exposure factor	8.15	4.83	N/A	99.6	100.0
CD_S_GS	Historical HLWG composition (GlassSRL)	8.15	4.25	N/A	NA	100.0
CD_S_W1	W1 seepage water	8.16	4.18	N/A	99.8	100.0
CD_S_W2	W2 seepage water	7.82	4.05	N/A	99.8	100.0
CD_S_W3	W3 seepage water	8.16	4.17	N/A	99.8	100.0
CD_S_b2A	Sensitivity for suppression of ferrimolybdate	8.15	4.13	N/A	99.8	100.0

Table 6.5-2. DOE SNF Codisposal Seismic Results: Gadolinium, Plutonium, and Uranium Percent Remaining (Continued)

Filename	Conditions	pH Max	pH Min	Percent Remaining at 10,000 Years		
				Gadolinium	Plutonium	Uranium
FFTF Codisposal Waste Package						
FFTF_S_b	Base case	8.16	6.72	100.0	98.6	100.0
FFTF5DFA	Less reactive FFTF waste package configuration (five DFAs, no IDENT 69)	8.16	6.73	100.0	98.6	100.0
FFTF_1_5	log(fCO2)= −1.5	6.98	6.45	100.0	82.0	100.0
FFTF_hem	Hematite forms (rather than goethite)	8.16	6.70	100.0	98.4	100.0
FFTF_MxG	Maximum HLWG corrosion rate	9.03	8.15	100.0	5.3	83.0
FFTFMxGE	Maximum HLWG corrosion rate and adjusted-Eh-model	9.14	8.15	100.0	99.9	79.7
TMI Codisposal Waste Package						
TMI_S_b	Base case	8.16	6.11	N/A	99.8	100.0
TMI_MxAL	High steel and alloy corrosion rate	8.16	5.39	N/A	99.6	100.0
TMI_MxG	Maximum HLWG corrosion rate	9.96	7.64	N/A	57.5	79.5
TMI_MxFu	Maximum TMI fuel rate	8.15	6.11	N/A	99.8	100.0
TMI_1_5	log(fCO2)= −1.5	7.36	6.10	N/A	99.8	99.9
TMI_hem	Hematite forms (rather than goethite)	8.16	5.95	N/A	99.8	100.0
TMI_316s	Stainless Steel Type 316 sleeve not Carbon Steel Type A516	8.16	6.11	N/A	99.8	100.0
TMI_LiCL	low LiCon rate	8.16	6.11	N/A	99.8	100.0

Source: Output DTN: MO0705GEOMODEL.000, CDSP/*CDSP Seismic Summary.xls;* FFTF/*FFTF Seismic Summary.xls*; TMI/*TMI Seismic Summary.xls.*

Table 6.5-3. CSNF Igneous Results: Gadolinium, Plutonium, and Uranium Percent Remaining

Filename	Conditions	pH Max	pH Min	Percent Remaining at 10,000 Years			
				Gadolinium	Plutonium	Uranium[a]	Pu/U Combined[a]
CSNFIG1	Base case	7.17	5.92	94.0	74.1	100.2	100.0
CSIGPI	Principal isotopes included	7.20	5.97	95.4	74.1	100.2	100.0
CSIGPI_R	Solid solution formation	7.20	6.00	95.4	74.2	100.2	100.0
CSIGPIss	Solid solution formation	7.20	5.96	95.2	74.1	100.2	100.0
CSIGCH	log(fCO2)= −1.5	6.67	5.60	99.9	65.9	100.2	99.9
CSIGCL	log(fCO2)= −5	7.18	6.17	85.5	74.8	100.2	100.0
CSNFIG2	Seepage 1,000 L/yr	8.17	7.12	99.0	0.0	98.6	97.9
CSIGAdEh	Seepage 1,000 L/yr; adjusted-Eh	8.17	7.12	99.0	74.8	98.8	98.6
CSIGHi	High steel and alloy corrosion rate	7.16	4.71	70.4	60.2	100.2	99.9

Table 6.5-3. CSNF Igneous Results: Gadolinium, Plutonium, and Uranium Percent Remaining (Continued)

Filename	Conditions	pH Max	pH Min	Percent Remaining at 10,000 Years			
				Gadolinium	Plutonium	Uranium[a]	Pu/U Combined[a]
CSIGMed	Medium steel and alloy corrosion rate	7.17	4.78	61.3	66.8	100.2	99.9
CSIGMedK	Medium steel and alloy corrosion rate, high-temperature log K	7.17	4.78	62.5	67.3	100.2	99.9
CSIGnoP	No phosphates allowed to form	7.17	5.92	93.6	74.1	100.2	100.0
CSIGPuO2	PuO2 formed	7.17	5.92	93.7	75.0	100.2	100.0
CSIG_IB	Icelandic basalt water	7.16	5.91	93.1	74.1	100.2	100.0
CSIG_CB2	Columbia Basin Water 2	7.18	5.92	93.9	74.1	100.2	100.0

Source: Output DTN: MO0705GEOMODEL.000, CSNF/ *CSNF Igneous Summary.xls.*

NOTE: [a]Decay of ^{239}Pu is included in CSNF igneous EQ6 simulations; therefore uranium retention is greater than 100% for some cases. Due to decay, the retention of combined uranium/plutonium is reported.

Table 6.5-4. CSNF Igneous Results: Selected Elements Remaining

Filename	Conditions	Percent Remaining at 10,000 years												
		Gd	Pu	U	Ag	Am	Eu	Mo	Nd	Np	Rh	Ru	Sm	Tc
CSIGPI	Principal isotopes included	95	74	100	32	95	92	97	99	100	100	100	76	3
CSIGPI_R	Lanthanide phosphate solid solution formation	95	74	100	32	95	92	97	99	100	100	100	73	3
CSIGPIss	Lanthanide phosphate and lanthanide darbonate solid solution formation	94	74	100	32	94	90	97	99	100	100	100	89	3

Source: Output DTN: MO0705GEOMODEL.000, CSNF/*CSNF Igneous Summary.xls.*

NOTE: Gd = gadolinium; Pu = plutonium; U = uranium; Ag = silver; AM = americium; Eu = europium; Mo = molybdenum; Nd = neodymium; Np = neptunium; Rh = rhodium; Ru = ruthenium; Sm = samarium; Tc = technetium.

Table 6.5-5. DOE SNF Codisposal Igneous Results: Gadolinium, Plutonium, and Uranium Percent Remaining

Filename	Conditions	pH Max	pH Min	Percent Remaining at 10,000 years		
				Gadolinium	Plutonium	Uranium
CDSP (N Reactor) Waste Package						
CD_I_B	Base case	8.37	4.15	N/A	100.0	100.0
CD_IHFC	log(fCO2)= −1.5	7.10	4.15	N/A	100.0	100.0
CD_ILFC	log(fCO2)= −5	9.78	3.95	N/A	100.0	100.0
CD_I_f9	Seepage 1,000 liter/yr	8.36	7.97	N/A	100.0	99.0
CD_I_W2	Columbia Basin water 2	8.37	4.97	N/A	99.0	100.0
CD_I_WI	Icelandic basalt water	8.37	4.79	N/A	100.0	100.0

Table 6.5-5. DOE SNF Codisposal Igneous Results: Gadolinium, Plutonium, and Uranium Percent Remaining (Continued)

Filename	Conditions	pH Max	pH Min	Percent Remaining at 10,000 years		
				Gadolinium	Plutonium	Uranium
CDSP (N Reactor) Waste Package (Continued)						
CD_I_SH2	High steel and alloy corrosion rate	8.03	4.05	N/A	100.0	100.0
CD_I_SM2	Medium steel and alloy corrosion rate	7.94	4.07	N/A	100.0	100.0
CD_I_b2A	Sensitivity for suppression of ferrimolybdate	8.36	4.14	N/A	100.0	100.0
FFTF Codisposal Waste Package						
FFTF1_IG	Base case	8.11	6.72	100.0	98.6	100.0
FFTFIG_2	Seepage 1,000 L/yr	8.32	7.80	99.8	6.6	63.7
TMI Codisposal Waste Package						
TMI_IG_1	Base case	8.15	6.11	N/A	99.8	100.0
TMI_IG_2	Seepage 1,000 L/yr	8.48	7.94	N/A	99.9	88.9

Source: Output DTN: MO0705GEOMODEL.000, CDSP/ *CDSP Igneous Summary.xls;* FFTF/*FFTF Igneous Summary.xls*; TMI/ *TMI Igneous Summary.xls.*

The gadolinium in the CSNF tables (Tables 6.5-1, 6.5-3, 6.5-4) represents all the lanthanide fission products (gadolinium, neodymium, samarium, europium) that act as neutron absorbers in the spent fuel (Table 6.3-4) and are therefore of interest. The other significant neutron absorber in the CSNF waste package, boron, is not listed in the CSNF tables, because the retention of boron from degradation of the absorber plates is 100%. As discussed in Sections 6.3.3 and 6.3.16, as the borated stainless steel plates degrade, the insoluble boron-carbide grains originating in the steel remain in place near the uncorroded alloy within the waste package. The plutonium in the N-reactor cases represents the plutonium in the HLWG. The gadolinium in the FFTF represents the gadolinium in the basket material and the aluminum-gadolinium shot material in the DOE canister (Section 6.3.1).

In waste packages with Type A516 carbon steel, the simulations may predict a minimum pH $\approx$ 4, caused by rapid steel degradation and oxidation of sulfur, nitrogen, and other trace components. The period of A516 degradation is brief and occurs at early time. EQ6 may predict too low a pH in this time period, for the reasons outlined in *In-Package Chemistry Abstraction* (SNL 2007 [DIRS 180506], Section 6.7.1). Abundant iron oxyhydroxides may buffer pH via surface sorption.

6.5.2 Minerals Formed, Mineral Quantities, Unreacted Component Quantities, and Aqueous Concentrations

The minerals formed within the waste package, the quantity of unreacted components, and the aqueous concentrations versus time are outputs from the MDR model and are used for in-package criticality calculations. All of the minerals that were formed in each case are tabulated in output DTN: MO0705GEOMODEL.000 (folders: CSNF, CDSP (N-reactor), FFTF, and TMI). (The formulas for all minerals are provided in Table 6.3-10.) The base-case minerals formed and the unreacted components remaining in the waste package are plotted versus time in Appendix E. The plots in Appendix E are useful in that they provide a quick assessment of the

major minerals that are formed. Schoepite is the major uranium-bearing mineral, with minor amounts of boltwoodite-Na, uranophane, and compreignacite in the first stage of the igneous case. The solid PuO_2(hyd, aged) is the plutonium-bearing mineral. The gadolinium-bearing minerals are $Gd_2(CO_3)_3$ and $GdPO_4$: $2H_2O$. Other major minerals formed and their major elements in parentheses are goethite (iron), gibbsite (aluminum), and trevorite (Ni, Fe).

Table 6.5-6 gives instructions on how to extract information from the EQ6 output files (output DTN: MO0705GEOMODEL.000, *Output Extraction/Output Extraction.xls*), such as quantity of minerals, unreacted components, and aqueous concentration versus time.

Table 6.5-6. Directions for Extracting Information from Output Files

Information Desired	Steps for Extraction of Information Using Igneous Scenario CSIGMed as an Example[a]	Location of Example Results in File: *Output Extraction.xls* (Output DTN: MO0705GEOMODEL.000
Moles of minerals formed (corrosion products) versus time.	Step 1a: Copy normalized moles of minerals in waste package from EQ6 output file CSIGMed.min_info.txt (Output DTN: MO0705GEOMODEL.000, folder: CSNF\CSNF Igneous\Medium Corrosion Rates).	Spreadsheet Tab Title: "Step 1a, Norm. Moles Mins"
	Step 1b: Multiply the moles in Step 1a by the normalization factor (Table 6.3-1) to calculate total moles in waste package.	Spreadsheet Tab Title: "Step 1b, Tot Moles Mins"
Volume of minerals formed (corrosion products) versus time.	Step 2a: Create a table that contains the molar volumes of all minerals. Most are available in the *data0.ymp.R5* database (DTN: SN0612T0502404.014 [DIRS 178850]), but some must be obtained from outside sources, such as Lide (1991 [DIRS 131202]) and *External Accumulation of Fissile Material from DOE Co-Disposal Waste Packages* (BSC 2002 [DIRS 159913]), as shown in tab "Step 2a, Molar volumes."	Spreadsheet Tab Title: "Step 2a, Molar volumes"
	Step 2b: Calculate the total volume of minerals in the waste package; multiply the total moles of each mineral in Step 1b by the molar volume in Step 2a.	Spreadsheet Tab Title: "Step 2b, Total Volume"
Mass of unreacted waste package components versus time.	Step 3a. Extract normalized moles of unreacted components from EQ6 output file *CSIGMed.bin* (output DTN: MO0705GEOMODEL.000, folder: CSNF\CSNF Igneous\Medium Corrosion Rates) using ASPRIN software as follows: 1. Run ASPRIN, with the file CSIGMed.bin in the same directory as the executable. Use the following command: `asprin.exe CSIGMed.bin` [Note: If the file is larger than 100 MB, use the command `asprin.exe filename.bin X`, where X indicates that ASPRIN will read every Xth point in the file. ASPRIN can handle about 100 MB, so if file is 200 MB, use X=2] 2. Once ASPRIN opens, type "N" for Read_Plt alone. 3. Select items of interest. For reactants, choose K, then the items of interest (including time). 4. Esc to go back to menu. Esc to leave menu system and write output file.	Spreadsheet Tab Title: "Step 3a, Norm. Moles Unreacted"
	Step 3b: Calculate Mass (g) of unreacted components. Multiply normalized moles of reactants from Step 3a by normalization factor (Table 6.3-1). Multiply by 100 grams per mole.	Spreadsheet Tab Title: "Step 3b, Tot Mass Unreacted"

Table 6.5-6. Directions for Extracting Information from Output Files (Continued)

Information Desired	Steps for Extraction of Information Using Igneous Scenario CSIGMed as an Example[a]	Location of Example Results in File: *Output Extraction.xls* (Output DTN: MO0705GEOMODEL.000
Aqueous concentration (moles/kg) of elements in waste package versus time.	Step 4a: Copy moles in aqueous phase in waste package from EQ6 output file *CSIGMed.elem_aqu.txt* (output DTN: MO0705GEOMODEL.000, folder: CSNF\CSNF Igneous\Medium Corrosion Rates).	Spreadsheet Tab Title: Step 4a, Norm. Aqueous moles
	Step 4b: Calculate molality (moles/kg water) by dividing the normalized moles aqueous by the normalized kg of water in waste package (0.3 kg, Assumption 5.1, Section 5).	Spreadsheet Tab Title: Step 4b, Aqueous Concentration

Source: Output DTN: MO0705GEOMODEL.000, Output Extraction*Output Extraction.xls.*

NOTE: [a] All EQ6 and ASPRIN output files ending in *.txt are tab-delimited and easily opened in Excel.

6.5.3 Discussion of Results

The results are discussed in the context of the end use—either in-package or external criticality. The cases with the highest loss of neutron absorbers and highest retention of radionuclides will be used for in-package criticality analyses. The cases with the highest loss of radionuclides will be used in the external accumulation model. The external accumulation model results will then be used for external criticality analyses.

6.5.3.1 In-Package Criticality

The cases with the greatest interest for in-package criticality are those cases with the highest loss of neutron absorbers. These are discussed below.

CSNF Waste Packages—For the CSNF seismic scenario (Table 6.5-1), only one case had significant Gd release from the waste package. That was the high temperature case (*CS_S_90.6i*), with 61% retention. However that calculation is uncertain, because the thermodynamic database lacks temperature coefficients for many important gadolinium species. As shown by the high-temperature log K sensitivity case (*CS_S_90K.6i*), when the database was adjusted using the "augmentLogK" option (Section 6.3.13) to correct for the high-temperature effects on the log K of the gadolinium aqueous species, the retention of gadolinium was much higher at 90% (the justification for the high-temperature log K corrections is given in Appendix D). None of the rest of the seismic scenario cases showed significant releases of gadolinium. Table 6.5-1 indicates that the retention of plutonium ranged from 0 to 99%. However, due to the more realistic plutonium solubilities predicted using the adjusted-Eh model, when any of the cases are used for internal criticality calculations, all of the plutonium should be assumed to be retained in the waste package. As shown in Section 6.5.3.2, when cases with significant plutonium releases from the waste package are rerun using the more likely adjusted-Eh conditions, the plutonium release is negligible.

For the CSNF igneous scenario (Tables 6.5-3 and 6.5-4), two cases with significant release of gadolinium were the cases using medium and high corrosion rates (*CSIGMed.6i* and *CSIGHi.6i*), with 61% and 70% retention of gadolinium, respectively. Using the high-temperature logK

corrections (*CSIGMedK.6i*), the gadolinium retention increased slightly to 62%. As discussed in Section 6.3.6, the medium and high corrosion rates are based on the 50% and 90% confidence values from experiments measured over mostly short time periods (from less than one year to several years) (Table 4-19). Since corrosion rates tend to decrease with time, the medium and high corrosion rates are not likely to occur for long time periods, such as 10,000 years.

Another CSNF igneous scenario of interest for criticality is the low CO_2 fugacity case (*CSIGCL.6i*), with 85% retention of gadolinium. As shown in the list of minerals, one reason is that, in the low CO_2 case, no $Gd_2(CO_3)_3$ formed (output DTN: MO0705GEOMODEL.000, *CSNF_minerals.xls*).

Other CSNF cases with interesting results for in-package criticality are the cases that used the complete fuel composition, including all the principal isotopes. In those cases, the neutron absorbers (neodymium, samarium, and europium) were modeled as separate elements, rather than being modeled as gadolinium. For those cases, the results showed that a slightly higher loss (24%) occurred for samarium when the elements were modeled independently (*CSIGPI.6i*) compared to the loss (11%) when solid solutions of lanthanides were employed (*CSIGPI_R.6i* and *CSIGPIss.6i*). This is expected, since the solubility of each separate lanthanide is proportional to the solubility of the pure phase times the mole fraction in the solid solution. Since the mole fraction is typically much less than 1, the solubility must be reduced below the pure end-member value. The results using the solid solutions are thought to be the most likely outcomes, since the lanthanides are all similar and tend strongly to form solid solutions.

The waste package saturation sensitivity (Appendix C) showed that varying the saturation from 3% to 100% had little effect on the modeled pH and the peak concentrations of aqueous uranium, plutonium, and gadolinium. The main effect of reducing saturation is to sharpen the transitions in pH and aqueous concentration, since the residence time in the package is reduced for the same drip rate. However, the timing of the peak concentrations differed only slightly for this wide range of saturations, and the widths of the peaks were similar. The saturation study also showed that the range of saturation had a small impact on the gadolinium retention (Table C-1). When low saturation (below 30%) in the waste package is likely, the 30% saturation values result in slightly overestimating (up to 4%) gadolinium retention.

N-Reactor and TMI Waste Packages—For the N-reactor and TMI seismic and igneous scenario (Tables 6.5-2 and 6.5-5), no neutron absorbers are added to the waste package, so the removal of neutron absorbers from the waste package is not a concern.

FFTF Waste Packages—For the FFTF seismic and igneous case, none of the cases resulted in significant loss of gadolinium. Only the high seepage flux igneous case showed a measurable loss, with retention of 99.8% of the gadolinium.

6.5.3.2 External Criticality

The cases with the greatest interest for external criticality are those cases with the highest loss of fissile material.

CSNF Waste Packages—For the CSNF seismic and igneous scenarios (Tables 6.5-1, 6.5-3, and 6.5-4), the cases with the highest plutonium and uranium losses were the high-flux cases

(*CS_S_F9.6i* and *CSNFIG2.6i*). Both cases used an oxygen fugacity of 0.2 bar, which overestimates the solubility of plutonium, as discussed in Section 6.3.14, and unrealistically predicted all of the plutonium would be released from the waste package. When the cases were rerun using the adjusted-Eh model (*CSS_F9Eh.6i* and *CSIGAdEh.6i*), the retention was increased to nearly 100%. (For the igneous scenario, a combined plutonium/uranium retention is calculated because the Pu-239 decay to U-235 was included in the simulations.) These results show that very little plutonium or uranium is released from the waste package in the seismic or igneous scenarios.

Another case of interest for the CSNF igneous scenario is the sensitivity in which all the principal isotopes were included. The elements of interest for external criticality were retained at 94% for americium and 100% for neptunium. None of the rest of the CSNF igneous scenario cases showed significant losses of plutonium/uranium combined.

The waste package saturation sensitivity (Appendix C) showed that variation of the saturation from 3% to 100% had little effect on the modeled pH and the peak concentrations of aqueous uranium and plutonium. The timing of the peak concentrations differed only slightly, and the widths of the peaks were about the same. In addition, the percent remaining of the plutonium and uranium was not impacted by the range in saturation (Appendix C, Table C-1). Thus the aqueous concentrations and waste package retention of fissionable materials, as passed to the external criticality models, is affected little by the choice of waste package saturation.

N-Reactor Waste Packages—For the N-reactor seismic and igneous scenarios (Tables 6.5-2 and 6.5-5), none of the cases released significant amounts of uranium from the waste package. The only case that released a small amount of uranium (1%) was the high-seepage flux case (*CD_I_f9*). The high glass corrosion rate case (*CD_S_GM*) for the seismic scenario retained only 70% of the plutonium; however that plutonium is only present in the HLWG. The total plutonium in the HLWG in the CDSP waste package is less than 1 kg (output DTN: MO0705GEOMODEL.000, glass/*HLWG_Isotopic_Composition.xls*); therefore, the release is insignificant for external criticality.

FFTF and TMI Waste Packages—For the seismic scenario (Table 6.5-2), the cases with the most-significant releases of uranium and plutonium are the cases with maximum HLWG corrosion rates (*FFTF_MxG.6i, FFTFMxGE.6i,* and *TMI_MxG.6i*). In those cases, the pH values reach above 9 due to the leaching of alkali metals from the HLWG which leads to higher solubility of uranium and plutonium. The maximum pH is higher in the TMI and FFTF waste packages than the CDSP (N-reactor) waste packages (Table 6.5-2) due to the number of HLWG canisters in each waste package type—five for FFTF and TMI versus two for CDSP. For the igneous scenario (Table 6.5-5), the cases with the high-seepage flux resulted in 64% and 89% uranium retention for the FFTF and TMI cases, respectively. The high releases for the high-seepage case are due to the flushing of 1,000 times more water through the waste package than the base case, which, over 10,000 years, leads to significant uranium release.

6.6 ALTERNATIVE MODELS

6.6.1 Multiple-Cell Drip-Through Model

As outlined in Section 6.2, most calculations implement a single-cell, well-mixed, flow-through model in which the package fills partly or wholly with in-dripping water. Water drips in through a breach in the package, eventually reaching an overflow condition, after which water leaks to the invert. In this single-cell model (often referred to as a bathtub model), all the components react with the same aqueous solution, and there is complete interchange among all parts of the equilibrium system.

The needs of criticality in-package modeling and in-package chemistry modeling for use in TSPA-LA may be quite different. The bathtub configuration is often the most reactive for in-package criticality, since water is a good neutron moderator, and the overflow condition may maximize the dissolution of neutron control material. In-package criticality analyses are generally concerned with conditions that cause actinides to be retained in the package, whereas TSPA-LA models are inherently more concerned with conditions that cause actinides to leave the package. The current criticality analysis includes scenarios wherein the top of the package is punctured, leading to a bathtub configuration in the seismic fault-displacement scenario.

However, the applicability of the bathtub model—and hence of the single-cell model—becomes less obvious when the saturation of the void space is substantially less than 100% and the aqueous solutions are presumed to drip down through the corroding materials without pooling. In the current igneous intrusion scenarios, the package is assumed to be so disrupted that water drips through it and may never reach bathtub conditions. Hence there is a need to examine how the single-cell model compares with more detailed analyses that do not involve continuous mixing of all dissolved components.

This section compares single-cell calculations with multi-cell calculations that involve liquid drips through the package at relatively low saturation. The package is broken into ten separate cells. As a volume of water moves down through the package, it may react with local materials in a cell; but once it leaves a particular cell and enters a lower cell of the package, it cannot back-react with the materials in the cell above. Water is constantly supplied at the top of the package, and constantly drips through; the fluid in each cell changes with time and continuously drips through into the cell below. These cells are not intended in any way to match the cells assumed in TPSA; rather the intent is to determine how much the "well-mixed" single-cell model deviates from drip-through (multi-cell) calculations. Hence the calculations use as many cells as are practical to study the behavior of the waste package.

This "drip-through" capability is built with the EQ6 V. 8.1 "variable displacer" option (BSC 2002 [DIRS 173170], Section10.2; BSC 2005 [DIRS 180678], Section 2.2). For a system composed of n cells, there are n separate, sequential EQ6 simulations, each with a fraction of the total mass of the system (the fraction is $1/n$ for a simple system of initially identical cells). The first cell (0) is a normal EQ6 simulation ranging over the full time t of the simulation (typically, $t = 10{,}000$ yr). This cell 0 has a constant-composition fluid displacer, which represents the in-dripping water. The composition of the water leaving the cell is stored, as a function of time, in the file *elem_aqu.bin*. The next simulation represents cell 1, conceptually below cell 0; this

simulation picks up the time-varying composition stored in *elem_aqu.bin* and uses this composition as a time-varying displacer, also over the full time t of the simulation. Each subsequent ith cell picks up the time-varying water composition output by the previous $(i-1)$th cell, is run for time t, and passes the water composition on to the $(i+1)$th cell, down to the $(n-1)$th cell at the bottom. Thus all cells run for the same model time, and have constantly varying water compositions that are continuously dripping into and modifying the cells below.

Two packages are considered; a CSNF package, and a codisposal package. Calculations for both packages assume fixed $fO_2 = 0.2$ bars and $fCO2 = 10^{-3}$ bars, at 50°C. In the drip-through models, the contents of each cell are scaled so the volume occupied by aqueous fluid is approximately 1 L and corresponds (on average) to a saturation of 10%. That is, the ratio of total volume of fluid in the aggregate of cells to the total mass of solid reactants in the aggregate is 1/10 the ratio of void space to reactant mass in the intact package. The 10% value is chosen over the default of 30% saturation because a drip-through system is inherently expected to have lower saturation than a flooded or bathtub system. The input files for the calculations are in directory "drip-thru vs single-cell" of output DTN: MO0705GEOMODEL.000. (The subdirectories in this folder have "readme" files that describe the running of the calculations in detail.) The CSNF system is used mainly to explore the possible separation of reaction fronts, for stacked, similar composition cells; the codisposal package investigates a system where local compositional inhomogeneities are inevitable and an inherent part of the modeling.

Note that with the drip-through model, the value of $fO_2 = 0.2$ bars is more reasonable than in the fully flooded models. This is because, in the drip-through model, the water-saturated portion of the corrosion products might be just centimeters thick, allowing much faster O_2 access by diffusion.

6.6.1.1 CSNF Drip-Through Model

In the CSNF drip-through case, the mass is divided into ten cells that are stacked on top of each other, from cell 0 (top) to cell 9 (bottom). Initially the fuel in each cell is pre-reacted with "Basalt Composition 1" water (Table 4-3), and all cells start with the same water composition at time 0. This starting condition is consistent with the scenario developed for the igneous case (Section 6.2.2), in which fuel reacts with gaseous and liquid water as the package cools down to ambient temperatures after the igneous event. Since the simulation begins when the fuel has all reacted to uranium minerals, the TSPA-LA estimates of pore space in the reacted fuel (5% to 30%, from DTN: LL010902212241.026 [DIRS 163089]) are reasonably consistent with 10% saturation. After the basalt has cooled to the ambient state, water begins to drip through the package from top to bottom.

Compared to codisposal packages, the distribution of materials in a CSNF package is fairly homogenous. There are no masses of potentially fast-reacting carbon steel, which might sustain a local inhomogeneity; all the steel is a form of stainless. Hence all the cells are initially identical; that is, each cell contains 1/10th the total steel, 1/10th the total reacted fuel, and so on. Basalt 1 water drips onto the top-most cell, 0; this cell reacts with the water, changing its composition with time. The time-varying effluent from cell 0 drips into cell 1. Then the time-varying effluent from cell 1 drips into cell 2, and so on, until effluent comes out the bottom of cell 9, thence to the invert. Even though all cells start with the same water composition at

time 0, the water compositions in the cells diverge with time. Thus each cell changes the composition of the water on its path downward through the package. A parallel calculation, with the same scaled masses of materials in a single cell, is run for comparison.

Two multi-cell models were run for the CSNF case. The first model used the base-case metal corrosion rates and the basalt water seepage rate (the same values were used in the single-cell CSNF igneous calculation *CSNFIG1.6i*, Table 6.5-3). This multi-cell model produced results that were very similar to the equivalent single-cell model with 10% saturation (the results are in subdirectory \csnf0, and are summarized in file *csnf0-drip-GdPuUpH-cell9&bat.xls*); since all the rates were low, this first multi-cell model did not produce significant pH excursions and provided few features—such as concentration spikes—to stress the system. Therefore, a second multi-cell model was run with ten times the base-case corrosion rates and ten times the seepage (drip-through) rate for the basalt water aqueous phase. These relatively aggressive conditions were chosen to stress the system, particularly to drive the pH relatively low and remove gadolinium and plutonium. (In the CSNF calculations, gadolinium is representative of all lanthanides, which are chemically similar in behavior and are important neutron absorbers in the spent fuel.) The higher drip rate also ensures that the individual cells retain approximately 10% saturation. With the combination of low drip rate (1 L/yr) and high corrosion rates, the water may be totally consumed in some cells or may reach high ionic strengths not amenable to solution by the EQ6 code with the *data0.ymp.R5* thermochemical database (DTN: SN0612T0502404.014 [DIRS 178850]), so the higher drip rate is necessary with the choice of higher corrosion rates. As discussed in Appendix C, a smaller saturation (i.e., 10% versus 30%) leads to sharper fluctuations of the chemistry in the aqueous system, potentially emphasizing differences between the drip-through and single-cell calculations. This second multi-cell system, with ten times higher rates, is the focus for the remainder of Section 6.6.1.1.

Figures 6.6-1 through 6.6-4 compare results for the second CSNF 10-cell drip-through system, and the corresponding single-cell system. In brief, it is obvious that the two systems produce very similar results. Figure 6.6-1 shows the pH results for all cells as well as the result for the single-cell system. While there is some variation for individual cells in the package, the effluent pH (cell 9) tracks closely the single-cell pH (represented as pHb).

There is little variation in the distribution of retained gadolinium and uranium among the cells (here gadolinium represents all lanthanides). Gadolinium retained in the package varies from 27% in cell 5, to 31% in cell 9; there is no uranium variation, within three significant digits. Retained plutonium does vary from 0% in cell 0, to 41% in cell 9; however, this result has no impact on criticality calculations. In-package neutronics calculations assume complete retention of plutonium (Section 6.5.3.1). For external criticality calculations, the results in Section 6.5.3.2 show that when the more realistic adjusted-Eh model is implemented the plutonium retention is nearly 100%. These results are summarized in the spreadsheet *CSNF-dripthru-cell-resolved-GdUPu-retention.xls* (output DTN: MO0705GEOMODEL.000, folder Drip-thru_vs_single-cell\CSNF). Thus the resolution of the batch system into multiple cells does not effect a substantial spatial separation of fissile materials and lanthanide neutron absorbers.

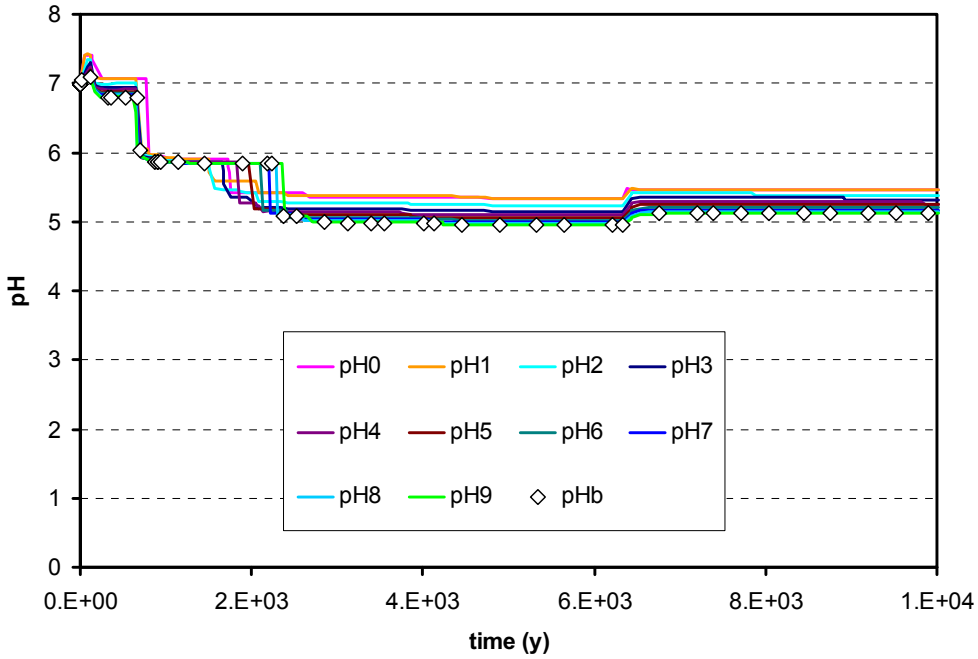

Source: Output DTN: MO0705GEOMODEL.000, file *CSNFnp1d-B.xls*.

NOTE: Plot shows variations for the 10-cell drip-through system (lines pH0 through pH9) and the corresponding single-cell model with the same bulk characteristics (diamonds, pHb). The effluent from the multi-cell package would be equivalent to the pH9 line, which is nearly coincident with the pHb values.

Figure 6.6-1. pH Variation with Time in the CSNF Systems

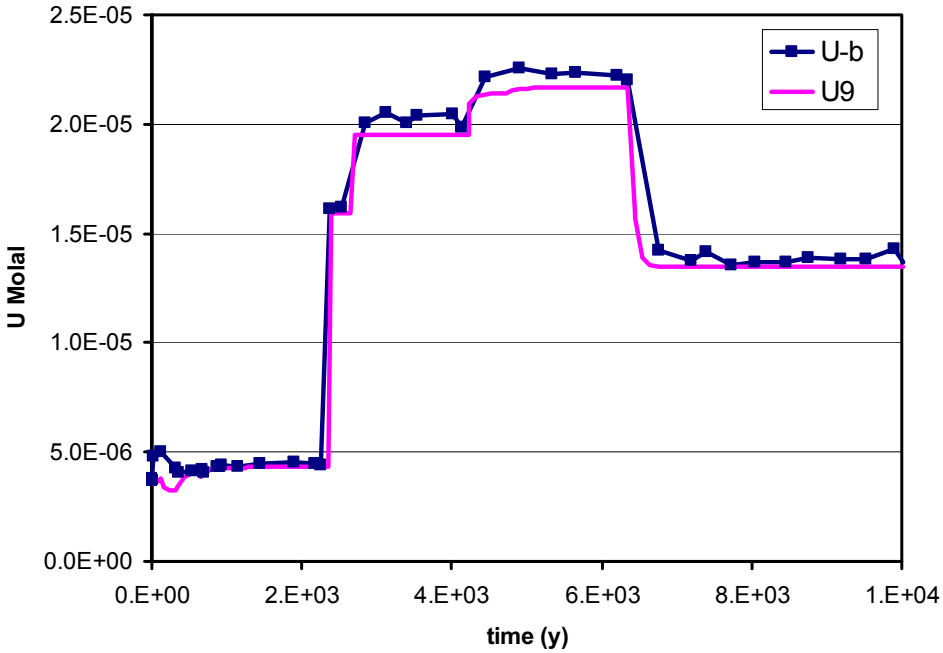

Source: Output DTN: MO0705GEOMODEL.000, file CSNFnp1d-*B.xls*.

NOTE: Plot shows molality of uranium for the 10-cell drip-through system (line U9) and the corresponding single-cell model with the same bulk characteristics (line U-b, with squares).

Figure 6.6-2. Molality of Uranium in the Effluent of the CSNF Systems

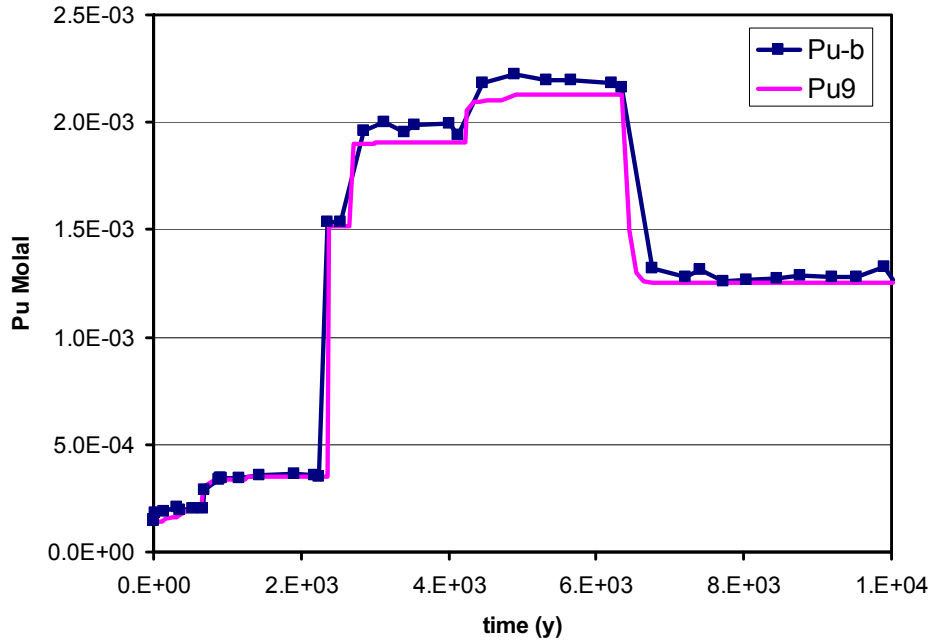

Source: Output DTN: MO0705GEOMODEL.000, file *CSNFnp1d-B.xls.*

NOTE: Plot shows molality of plutonium for the 10-cell drip-through system (line Pu9) and the corresponding single-cell model with the same bulk characteristics (line Pu-b, with squares).

Figure 6.6-3. Molality of Plutonium in the Effluent of the CSNF Systems

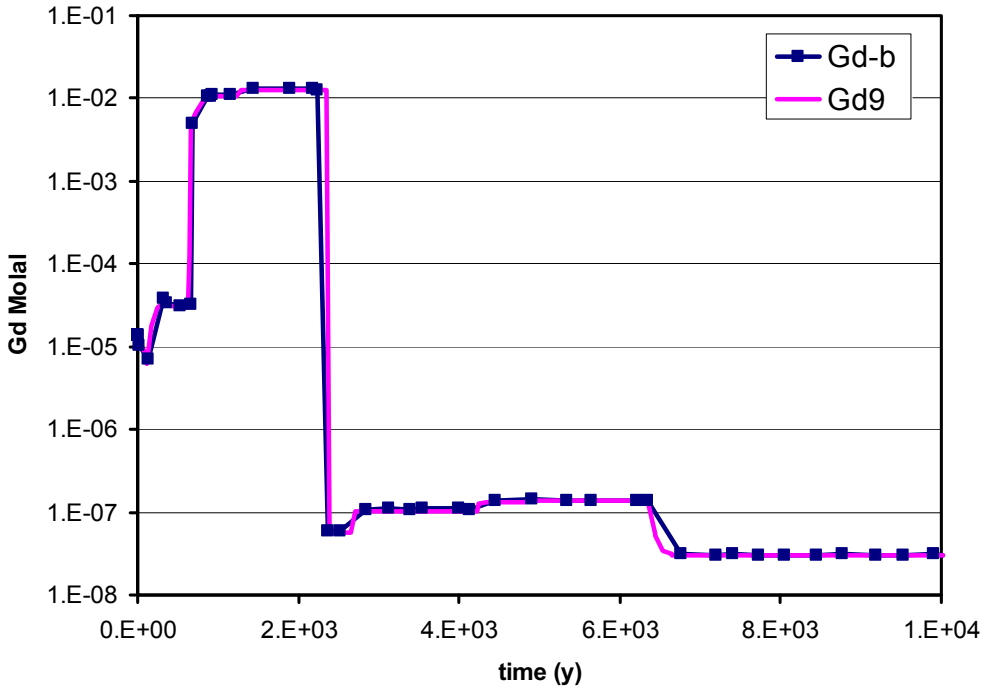

Source: Output DTN: MO0705GEOMODEL.000, file *CSNFnp1d-B.xls*.

NOTE: Plot shows molality of gadolinium for the 10-cell drip-through system (line Gd9) and the corresponding single-cell model with the same bulk characteristics (line Gd-b, with squares).

Figure 6.6-4. Molality of Gadolinium in the Effluent of the CSNF Systems

6.6.1.2 CDSP N-Reactor

The CDSP (N-reactor) packages have a greater capacity for chemical inhomogeneity, when compared to the CSNF. Large regions of the codisposal package contain glass, with a potential to raise pH and also provide silica to precipitate boltwoodite (a uranium silicate). There are also substantial amounts of carbon steel, which may provide an acidic environment upon corrosion. When these components are modeled with a single-cell model, the "well-mixed" system tends to drive the pH to an average value in the waste package as a whole, rather than the extremes that might occur in a locally reacting, inhomogeneous waste package.

This section describes a multi-cell drip-through system for CDSP (N-reactor) packages and contrasts the results with those from an equivalent well-mixed single-cell model. An additional case is examined, where the entire 1 L/yr of in-dripping water goes through a single cell that contains only fuel and the accompanying steel. This last scenario is an intentional extreme case for maximal removal of uranium from the package and reflects the possible channeling of the flow, without any interaction with the glass. The N-reactor package was also chosen as representative of codisposal packages by the in-package report (SNL 2007 [DIRS 180506]); a modified version of this package is used by TSPA. The intent is not to give the most accurate model of the N-reactor package, but rather, to contrast the single-cell and drip-through system under conditions that emphasize chemical inhomogeneity.

The N-reactor package contains two Stainless Steel Type 304L canisters of HLWG and two Stainless Steel Type 304L canisters of N-reactor uranium metal fuel. Both the fuel and the HLWG are enclosed in Stainless Steel Type 304L canisters, and the canisters are held in place with Carbon Steel Type A516 dividers (DOE 2000 [DIRS 150095]; SNL 2007 [DIRS 179567]). The A-1100 aluminum alloy is all contained within the fuel canisters. In the seismic fault-displacement scenario (Section 6.2.1), the canisters are breached and damaged, exposing the canister contents nearly simultaneously to percolating waters, assumed to have an initial J-13-like composition (DTN: MO0006J13WTRCM.000 [DIRS 151029]). The fuel is pre-reacted to schoepite, since the fuel degradation rate is so high that the transformation would occur within a few years. The vast bulk of the uranium is in the fuel (that is, there is relatively little uranium in the HLWG). This EQ6 model places all the plutonium in the HLWG, since the N-reactor fuel is assumed to be fresh fuel.

Table 6.6-1 shows the division of the waste package into calculation units of the "drip-through" configuration, for four different scenarios, called stack1, stack2, stack3, and stack4. The waste package is broken into 10 cells, each with an approximate saturation of 10% of the void space (Section 6.6.1.1 and Appendix C give the motivation for 10% saturation). In the stack1 scenario, J-13 water drips in through a Stainless Steel Type 316 cell (approximately representing the TAD canister), then successively through four cells containing a mix of oxidized fuel, Carbon Steel Type A516, A-1100 aluminum alloy, and Stainless Steel Type 304L representing the fuel canister. The fluid then drips successively through four cells containing HLWG, Carbon Steel Type A516, and Stainless Steel Type 304L. The stack2 scenario is an upside-down version of stack1, so water must first flow over the HLWG, and then drip successively down the oxidized fuel cells. Lastly, the stack3 and stack4 scenarios interleave the fuel and glass cells as indicated in Table 6.6-1. Stack1 and stack2 might represent a waste package configuration in which relatively intact glass canisters are on the bottom and top of the waste package, respectively, while stack3 and stack4 might represent a higher level of disruption after a fault-displacement event.

Table 6.6-1. The Four Drip-Through Configurations for the N-Reactor Fuel

Stack 1	Stack 2	Stack 3	Stack 4
↓ J-13 water in ↓	↓ J-13 water in ↓	↓ J-13 water in ↓	↓ J-13 water in ↓
↓ 316 Stainless ↓	**↓ 316 Stainless ↓**	**↓ 316 Stainless ↓**	**↓ 316 Stainless ↓**
↓ Fuel, Steels, Al↓	↓ HLWG, Steels↓	↓ HLWG, Steels↓	↓ Fuel, Steels, Al↓
↓ Fuel, Steels, Al↓	↓ HLWG, Steels↓	↓ Fuel, Steels, Al↓	↓ HLWG, Steels↓
↓ Fuel, Steels, Al↓	↓ HLWG, Steels↓	↓ HLWG, Steels↓	↓ Fuel, Steels, Al↓
↓ Fuel, Steels, Al↓	↓ HLWG, Steels↓	↓ Fuel, Steels, Al↓	↓ HLWG, Steels↓
↓ HLWG, Steels↓	↓ Fuel, Steels, Al↓	↓ HLWG, Steels↓	↓ Fuel, Steels, Al↓
↓ HLWG, Steels↓	↓ Fuel, Steels, Al↓	↓ Fuel, Steels, Al↓	↓ HLWG, Steels↓
↓ HLWG, Steels↓	↓ Fuel, Steels, Al↓	↓ HLWG, Steels↓	↓ Fuel, Steels, Al↓
↓ HLWG, Steels↓	↓ Fuel, Steels, Al↓	↓ Fuel, Steels, Al↓	↓ HLWG, Steels↓
↓ 316 Stainless ↓	**↓ 316 Stainless ↓**	**↓ 316 Stainless ↓**	**↓ 316 Stainless ↓**
↓ effluent leaves ↓	↓ effluent leaves ↓	↓ effluent leaves ↓	↓ effluent leaves ↓

Figure 6.6-5 shows the calculated evolution of pH with time in the effluent from the four stacks in Table 6.6-1, as well as the two single-cell configurations. It is emphasized that this is the pH of the aqueous fluid that drips out the very bottom cell of each stack or of the composition in the two single-cell calculations. In general, all the multi-cell drip-through configurations produce a more-stable effluent pH than the two single-cell simulations. In the multi-cell simulations, the pH drops after a short transient and generally stays close to 5 or 5.5 for the bulk of the simulation. In the single-cell simulations, the pH of the effluent dips down to 4 or even 3.3 early on, and the final pH is 6.7-7.5. However, the pH for individual cells in the stacks may dip below 3 in the initial transient. The initial transient is principally due to the degradation of the Carbon Steel Type A516, and EQ6 may predict too low a pH in this time period, for the reasons outlined in *In-Package Chemistry Abstraction* (SNL 2007 [DIRS 180506], Section 6.3.2).

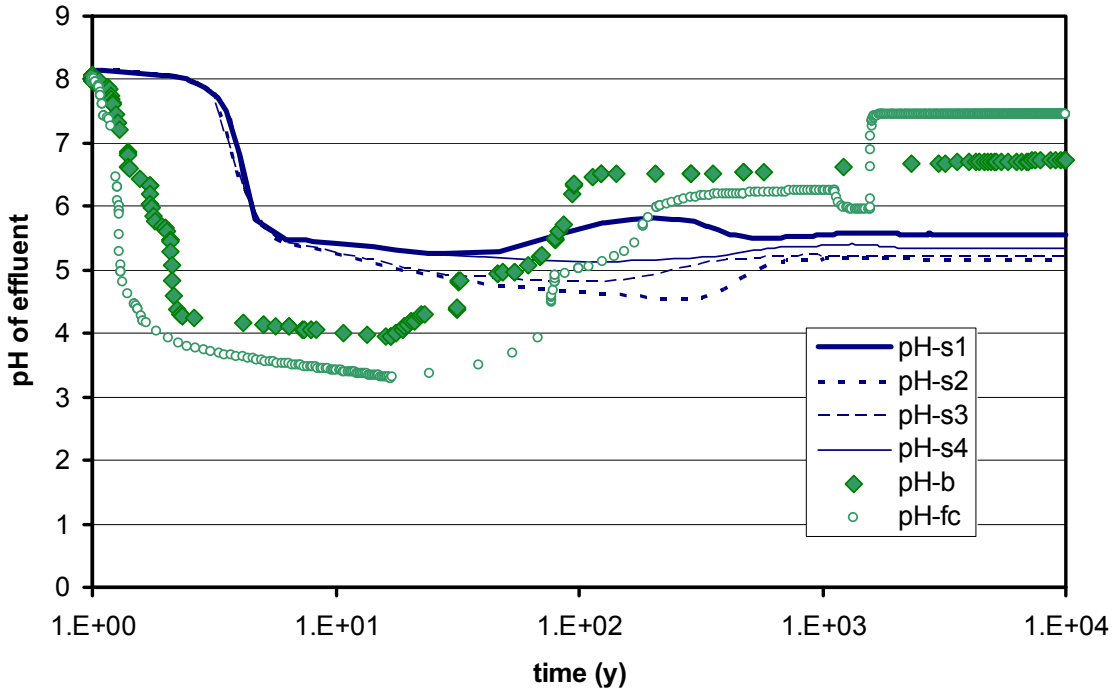

Source: Output DTN: MO0705GEOMODEL.000, file *cmp-bat-stack-1-2-3-4.xls*.

NOTES: pH-s1 through pH-s4 represent stacks 1, 2, 3, and 4, respectively, in Table 6.6-1.
pH-b represents the corresponding single-cell model with the same bulk characteristics.
pH-fc represents flow through a fuel cell but without HLWG interaction.

Figure 6.6-5. pH in the Effluent from the N-Reactor Package, for the Three Configurations in Table 6.6-1

Figures 6.6-6 and 6.6-7 give the calculated aqueous concentrations for uranium and plutonium with time (both figures contain the same information, but Figure 6.6-7 uses a log time scale to emphasize changes in the first 100 years). After 1,000 years, the effluent concentrations are fairly constant for all models, and the single-cell model predicts the highest dissolved uranium and plutonium in the effluent. From Figure 6.6-7, it is apparent that the stack1 and stack4 models give very similar results even in the first 100 years; yet the stack3 and stack4 models diverge in this time period, particularly for uranium. When there is any HLWG near the point of exit for the effluent (as in the stack1 and stack3 scenarios), the higher pH and abundant silica

cause precipitation of boltwoodite, which lowers the uranium concentration. Again, this difference is only significant in the early parts of the simulations, when the chemistry is dominated by Carbon Steel Type A516 degradation, perhaps artificially.

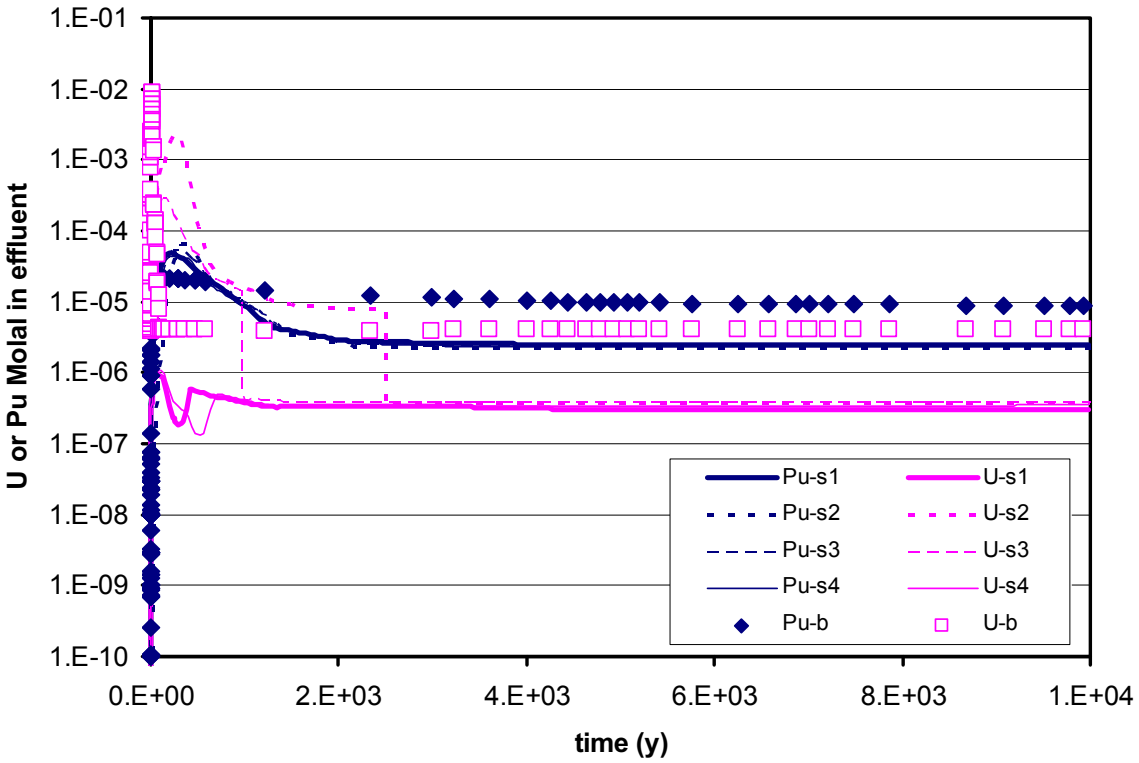

Source: Output DTN: MO0705GEOMODEL.000, file *cmp-bat-stack-1-2-3-4.xls*.

NOTE: Concentrations shown are for the four configurations in Table 6.6-1 (s1, s2, s3, and s4 correspond to stack1, stack2, stack3, and stack4, respectively, from that table). The diamonds and squares correspond to the single-cell model with the same bulk characteristics and are labeled Pu-b and U-b in the figure.

Figure 6.6-6. Uranium and Plutonium Aqueous Concentration in the Effluent from the N-Reactor Package

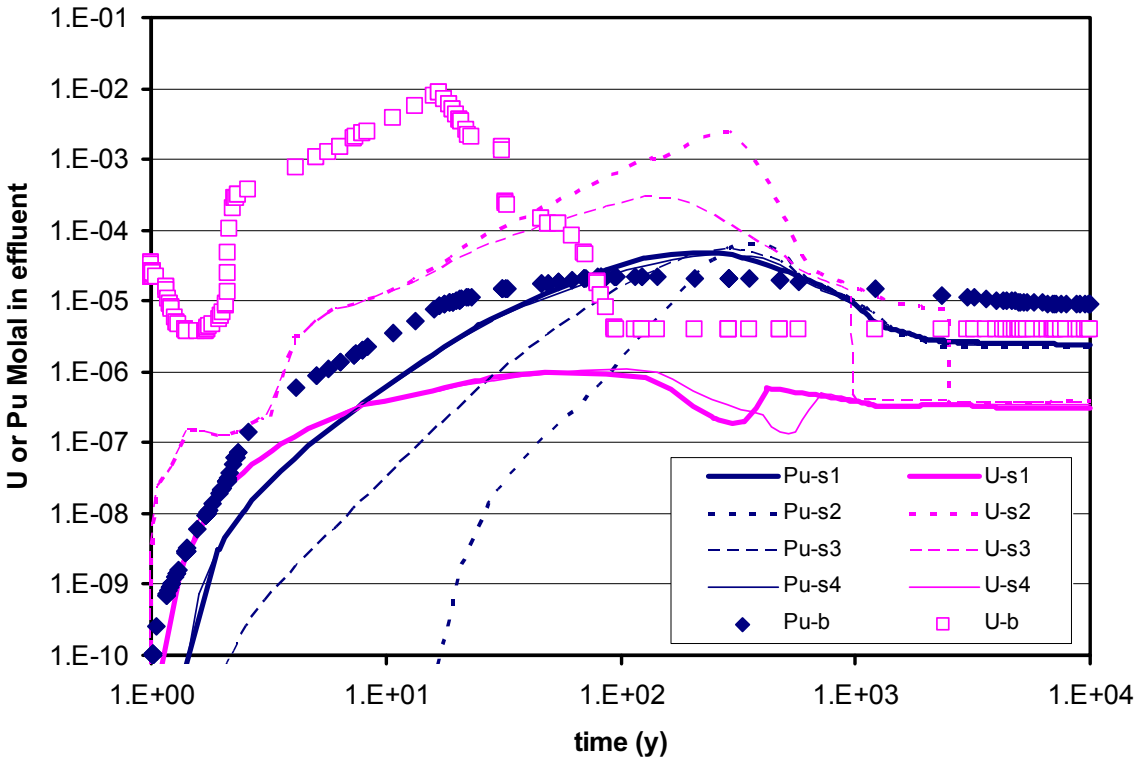

Source: Output DTN: MO0705GEOMODEL.000, file *cmp-bat-stack-1-2-3-4.xls*.

NOTE: Concentrations shown are for the four configurations in Table 6.6-1 (s1, s2, s3, and s4 correspond to stack1, stack2, stack3, and stack4, respectively, from that table). The diamonds and squares correspond to the single-cell model with the same bulk characteristics and are labeled Pu-b and U-b in the figure. This is the same as Figure 6.6-6 but with a log time scale, to emphasize the first 10^2 years of the simulation.

Figure 6.6-7. Uranium and Plutonium Aqueous Concentration in the Effluent from the N-Reactor Package with Log Time Scale

Figures 6.6-8 and 6.6-9 illustrate that the loss of uranium and plutonium from the package is small for all configurations. All models produce very similar plutonium losses after 10^2 years, and the single-cell model generally overpredicts plutonium loss before that time. Since all the plutonium is in the HLWG in these calculations, and there are no plutonium silicates in the thermodynamic database, the main effect of the degrading fuel cells on plutonium loss is through the pH- dependence of the HLGW degradation rate. For both uranium and plutonium loss, stack1 and stack4 produce extremely similar results; in particular, they produce lower long-term losses when compared to the batch reactor. Similarly, stack2 and stack3 produce somewhat similar results. However, stack2 produces somewhat higher uranium losses than the single-cell model (greater by a factor of 3-4). For uranium loss, the difference between stack1 and stack2 is that the first allows the dissolved uranium to pass over silica-rich glass degradation products, trapping the uranium as solid uranium silicates. In stack2, the dissolved silica that leaches from the HLWG is very small, and the only significant effect of the path through the HLWG, when the solutions subsequently hit the fuel area, is on the pH. Similar reasoning applies to the smaller differences between stack3 and stack4. Thus, the drip-through model has different outcomes when the effluent of HLWG drips onto fuel, versus the opposite case, when the effluent of the fuel drips onto HLWG.

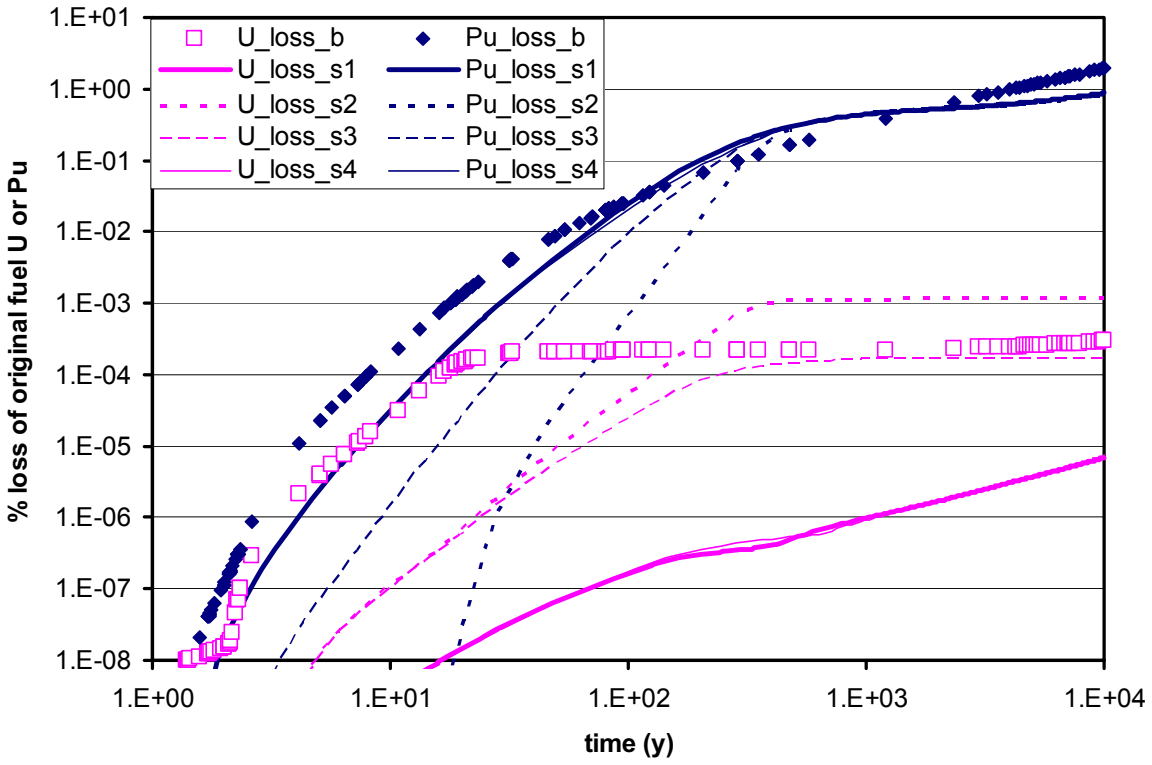

Source: Output DTN: MO0705GEOMODEL.000 file *cmp-bat-stack-1-2-3-4.xls*.

NOTE: Losses shown are for the four configurations in Table 6.6-1 (s1, s2, s3, and s4 correspond to stack1, stack2, stack3, and stack4, respectively, from that table). The diamonds and squares correspond to the single-cell model with the same bulk characteristics and are labeled Pu-b and U-b in the figure.

Figure 6.6-8. Percent Loss of Uranium and Plutonium for the N-Reactor Package

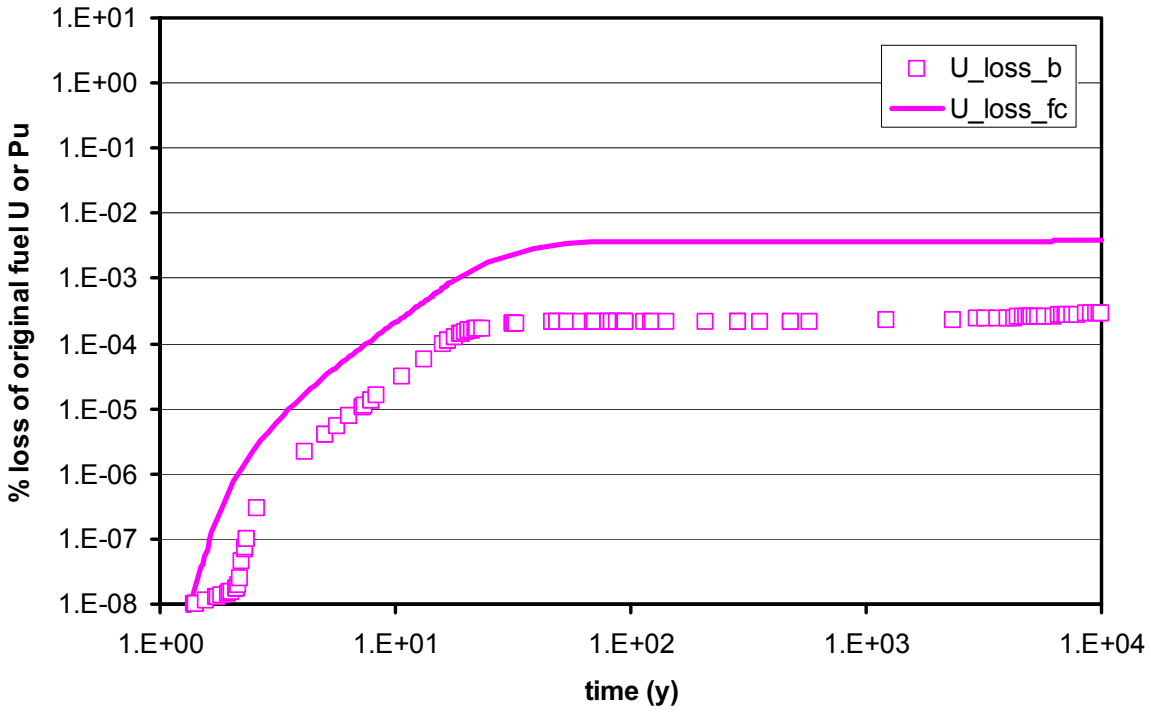

Source: Output DTN: MO0705GEOMODEL.000, file *cmp-bat-stack-1-2-3-4.xls*.

NOTE: U_loss_b represents single-cell model results. Configuration of model directs all flow through the fuel (U_loss_fc), allowing no HLWG contact.

Figure 6.6-9. Percent Loss of Uranium for the Single-cell Model N-Reactor Package

In all the drip-through models, the vast bulk of the uranium does not move from the initial fuel-containing cells. A small amount of the uranium mobilized from the fuel may be reprecipitated as boltwoodite in the HLWG cells, but the boltwoodite still represents a small mass of the total uranium in the system.

6.6.1.3 Channeling

There is an additional uncertainty associated with the acceptance of a drip-through model versus a bathtub model, namely that a drip-through model allows for the possibility that water follows one highly channelized path through the waste package, perhaps wetting just a fraction F of the total material in the package. If the wetted path still samples all the materials in the waste package, then the concentrations of elements in the effluent would be similar to those from a fully-wetted package with a $1/F$ higher drip rate.

6.6.1.4 Summary of Contrast between Single-cell and Drip-through Models

The CSNF comparison (Section 6.6.1.1) shows that, when the waste package internals are relatively uniform, there is very little difference between single-cell model and drip-through models, at least for the conditions studied. The N-reactor comparisons (Section 6.6.1.2) show that the long-term effluent concentrations of uranium and plutonium are overestimated by the single-cell model. Even though the chemistry predicted for the initial pH transient differs between single-cell and multi-cell models, all predict uranium losses well below 0.01% and

plutonium losses below 2%, so the differences among models is relatively insignificant for criticality calculations.

6.6.2 Time-Dependent Corrosion Rates and Protective Layer Formation

Corrosion rates for most waste package materials are constant during the EQ6 calculations (Section 6.3.6). An alternative would allow corrosion rates to decrease with time. For example, the carbonation depth of aluminous concretes (such as LiCon) are often assumed to be proportional to the square root of time (Dunster et al. 2000 [DIRS 181194], Figure 2), which implies the rate of carbonation decreases with time, as might be expected for a diffusion-limited process.

The decrease in corrosion rates may be caused by protective layer formation. Typically the layer would be formed from secondary minerals, such as iron oxides on steels, schoepite on fuel, and clays on HLWG. The presence of the layer retards the migration of reactants (e.g., water, oxygen, CO_2), slowing the reactions and, therefore, lowering the apparent corrosion rate of the material. The expectation of rate reduction with time is discussed below for carbon steels, CSNF, and HLWG. Some specific examples are considered in this discussion.

Carbon Steels—Corrosion rates for Carbon Steel Type A516 were observed to decrease with time, as reported in DTN: MO0409SPAACRWP.000 [DIRS 172059]. The reported corrosion rates were from experiments performed at 60°C and 90°C, with dilute and concentrated waters. The dilute and concentrated waters were J-13 well water modified to represent fresh and saltwater, respectively. The samples were divided into two groups: those reacted for less than 0.53 years and those greater than 1 year. The corrosion rates for all samples were found to decrease with time.

Commercial Spent Nuclear Fuel—Laboratory experiments on the surface structure of spent fuel during dissolution have shown that UO_2 dissolution is accompanied by the formation of a protective layer of secondary phases that retards further corrosion. Johnson and Shoesmith (1988 [DIRS 175705]) summarized the results of these investigations. However, they did not determine the composition or mineralogy of this protective layer.

HLWG—The results of studies concerning the characteristics and behavior of HLWG protective layers has been summarized in *High-Level Waste Borosilicate Glass: A Compendium of Corrosion Characteristics* (Cunnane et al. 1994 [DIRS 130693], Section 2.1), which concludes that the evidence suggests HLWG surface layers can act as a barrier that slows down glass reaction rates. However, the extent of this effect depends on the glass composition, layer structure and composition, temperature, test conditions, and the silicic acid gradient in the surface layers. This report also notes that the physical barrier effects were usually much less than the solution compositional effect. However, the surface barrier effect was found to be important in alkaline solutions, in leachants containing magnesium ions, or under conditions resulting in very low matrix dissolution rates. Further, results from long-term (up to 600 days) tests showed that the dissolution of soluble elements (boron, sodium, and lithium) may be diffusion-controlled.

These studies suggest that the constant corrosion rates used in EQ6 models tend to overestimate the rates of corrosion by ignoring the effect of secondary mineral buildup on corroding surfaces. Since a quantitative time-dependent rate law for the conditions of waste package degradation is not available, constant rates are used for the current MDR model.

6.6.3 Adsorption or Incorporation of Actinide Elements in Waste Package Alteration Phases

The EQ6 thermodynamic modeling results and calculations are based on stoichiometric mineral compositions with limited solid solution and no adsorption. A more realistic model would include solid solutions that are known to form in nature. For example, unstable iron minerals (such as ferrihydrite) tend to recrystallize to more stable phases, such as goethite and hematite; then, the impurities (such as uranium and plutonium) are exsolved and precipitated as discrete microcrystalline phases such as uranyl phosphate or saleeite (Murakami et al. 1992 [DIRS 175703], 2005 [DIRS 175700]). In addition, there is good evidence for the substitution of chromium in FeOOH (Sudakar et al. 2004 [DIRS 181407]). However, the activity coefficients for the CrOOH-FeOOH solid solution have not been measured.

A more realistic model would also include adsorption. Experimental and field data indicate that elements that are important to criticality (uranium, plutonium, and lanthanides) will be adsorbed on or incorporated into alteration products that form in the waste package. For example, iron oxyhydroxides and clays, formed from alteration of steels and HLWG, may strongly sorb actinides and lanthanides (Murakami et al. 2005 [DIRS 175700]; Landstrom and Tullborg 1995 [DIRS 175706], Section 7.2.1; Breck 1984 [DIRS 144977], Chapter 7).

Solid solution formation and adsorption would tend to lower actinide and lanthanide concentrations below those predicted by EQ6 and could delay release from the package. The use of the simpler EQ6 model, however, is sufficient for criticality calculations. Ignoring adsorption and solid solution formation results in higher releases of actinides or neutron absorbers and a greater likelihood of criticality occurring inside the waste package (for those cases with higher neutron absorber releases) and outside the waste package (for those cases with higher actinide releases).

6.7 RELATIONSHIP TO TSPA-LA AND OTHER MODELS

The needs of the MDR and TSPA-LA waste package models are very different, and these different needs are reflected in the implementation of the models. The MDR model is primarily intended to provide inputs for criticality neutronic calculations and is focused on the changes that take place within the waste package. The MDR model attempts to elucidate conditions where the fissile materials might remain in the package, and the neutron absorbers (such as gadolinium) will leave and cease to be effective criticality controls. In contrast, TSPA-LA is concerned with the release of radionuclides as dissolved species or colloidal particles and their contribution to dose; there is no explicit concern with criticality control materials. Thus conditions that are conducive for internal criticality (such as retention of fissile materials in the package) might tend to underestimate releases for TSPA-LA. TSPA-LA puts emphasis on the transport of colloids away from the waste package, and these colloids may be formed by adsorption of radionuclides onto corrosion products; the emphasis is reflected in the discretization of the TSPA-LA models.

The mass of the transported colloids is small and generally insignificant to criticality, as shown in Section 6.7.4; however, the colloids may affect the far-field dose calculated by TSPA-LA.

This section discusses some of the differences in the implementation of the TSPA-LA and MDR models. Despite these differences, many modeling assumptions and inputs are very similar between the TSPA-LA and MDR models; both use similar corrosion rates, seepage water compositions, thermodynamic databases, fugacities of O_2 and CO_2, and the choice of minerals formed and suppressed.

6.7.1 Discretization

The TSPA-LA models of in-package degradation and transport are generally similar to those used in the MDR model, but there are differences in the division of the packages into "domains." *EBS Radionuclide Transport Abstraction* (RTA) (SNL 2007 [DIRS 177407], Section 6) details the TSPA-LA division of the waste package into domains; this document is the basis of the discussion below.

In the RTA report (SNL 2007 [DIRS 177407]), either "domains" or "subdomains" may be analogous to the cells in the MDR model. When there are no subdomains within a domain, the RTA domain is analogous to a cell; but when there are subdomains, each subdomain is analogous to a cell. The RTA domains and subdomains also map into computational cells as defined for the modeling software. In the RTA report, the CSNF package is discretized into a cel1 1, containing the fuel, steel basket tubes, and the borated steel neutron absorber plates; and a cell 2, containing corrosion degradation products from the fuel basket guides, the TAD canister, and the inner vessel. In the codisposal waste package, the RTA report defines a cell 1a that contains the HLWG and its steel canister; a cell 1b that contains the fuel and the immediately associated steels (canisters, sleeves and other components); and a cell 2 that contains corrosion products from the Carbon Steel Type A516 support tube, the Carbon Steel Type A516 divider plates, and the inner Stainless Steel Type 316 vessel. Roughly speaking, the codisposal model in the RTA report is somewhat like stack 2 described in Section 6.6.1 of the present document. For the CSNF model, the RTA report takes flow from cell 1 into cell 2 (where adsorption takes place), then out into the invert; in the codisposal model, flow enters cell 1a, then goes through cell 1b, then through 2 (where adsorption takes place), and out into the invert. There is no separate cell 2 in the MDR model, because there is no explicit accommodation for sorption and, particularly, no concern with eventual transport of small colloid masses.

In the MDR model, the tie between chemistry and transport is relatively simple, as both are carried out implicitly in EQ6 simulations. In single-cell MDR models, the influx of water is through a displacer reactant and solid-centered flow-through mode; the time-varying effluent may then be passed on external criticality calculations. In the MDR multi-cell models (Section 6.6.1), multiple cells are linked by sequential EQ6 simulations and the variable-displacer mode. However, in the RTA, the tie between transport and EQ6 simulations from *In-Package Chemistry Abstraction* (IPC) (SNL 2007 [DIRS 180506]) is more complex. The IPC EQ6 simulations are designed to feed separate pH and ionic strength to RTA; short simulations are used to define mineral assemblages and pH for each cell, and much longer (in terms of model time) simulations are used to define ionic strength. Some simulations are used to define the buffering of the system under externally imposed pH, via titrations. The codisposal

cells 1a and 1b are run separately and not allowed to interact via EQ6; the RTA allows the cells to interact for radionuclide transport.

A significant difference between the models in the RTA report and the multi-cell MDR model described in Section 6.6.1 of this document is that the models in the RTA report may allow diffusion among cells. Since the multi-cell MDR model is intended to examine a drip-though environment with relatively low water contents, back-diffusion is not modeled between cells. However, both the RTA report and the MDR model treat each cell as a well-mixed reactor.

6.7.2 Saturation

The MDR model uses the term "saturation" to describe the fraction of initial package void space that is filled by aqueous fluid. For the MDR model, the default "saturation" is 30%, but, as shown in Appendix C, the influence of waste package saturation is relatively minor, in the tested range of 3 to 100%. For purposes of neutronic calculations, the exact saturation is not explicitly used. The IPC model uses waste package saturation of 50% for TSPA-LA inputs, and addresses the sensitivity of that value in Section 6.6.1[a] (SNL 2007 [DIRS 180506]); however, the RTA defines its own water saturation, independently of the IPC. The RTA saturations are not directly related to the package void volume and involve assumptions about the fraction of volume in corrosion-product pore space and a presumed alteration "rind" surrounding the fuel and HLWG.

6.7.3 Temperature

Another difference is the modeling temperature of 25°C for IPC and 50°C for the MDR model. The use of 50°C in this report is based on the time-weighted average of temperature over the first 10,000 years after emplacement, as discussed in Section 6.3.9. Based on the temperature versus time plot in Figure 6.3-1, it is evident that the waste package temperature continues to decrease as time increases. So, if temperatures out to 1,000,000 years are a concern, which is the case for the IPC, the time-weighted average would be lower. Therefore, the fact that the temperatures used in IPC are different from those used in this report is due to the fact that IPC is concerned with modeling out to 1,000,000 years, whereas, the MDR model is concerned with the first 10,000 years only.

6.7.4 Absorption and Colloids

The MDR model does not account for sorption on colloids or corrosion products (Section 6.6.3). This does not impact internal criticality considerations; because this report recommends that no credit be taken for releases of plutonium from the waste package when internal criticality calculations are performed (Section 6.5.3.1). For external criticality, the lack of colloids in the model does not underestimate the chances of a criticality event because, if adsorption were included, a large portion of the plutonium would adsorb to the stationary corrosion products in the waste package and only a small amount would adsorb to iron-oxide colloids and be released from the waste package as plutonium-adsorbed colloids. In the MDR, all of the dissolved plutonium is in the aqueous solution and subject to flow out of the waste package. To get a rough estimate of the quantity of plutonium that could be released from the waste package if a model consistent with TSPA-LA were applied, a sample calculation was made. For simplicity, the following discussion focuses on plutonium and CSNF packages (the latter is the most

abundant package type). The TSPA-LA RTA report (SNL 2007 [DIRS 177407], Appendix B) details the basic model and assumptions for estimating plutonium loss as colloids and dissolved species.

For CSNF, the transportable colloid species are (1) the iron oxyhydroxide particles (such as ferrihydrite or FeOOH), designated as "FeO" in the RTA (SNL 2007 [DIRS 177407], Appendix B) and as "FeOx" in DTN: MO0701PAIRONCO.000 [DIRS 180440]; and (2) "spent fuel" colloids derived from corrosion of CSNF, as quantified in DTN: MO0701PACSNFCP.000 [DIRS 180439]. In the package, the FeOx colloids exist with chemically similar FeOx corrosion products. Within the limits of differing kinetic absorption models for the two forms of FeOx, plutonium is partitioned between the immobile corrosion products and colloids according to the relative masses of the two forms of FeOx. The fraction of the plutonium removed by FeOx colloids is best judged by comparison with the fraction of FeOx that remains in the CSNF package. In the RTA (SNL 2007 [DIRS 177407], Section 6.3.4.4), the concentration of colloids is determined to be dependent on the ionic strength and pH only.

The amount of plutonium lost to colloids is estimated in spreadsheet *FeOx_coll_vs_CP.xls* (output DTN: MO0705GEOMODEL.000) for four cases in the igneous scenario: (1) the base case (*CSNFIG1.6i*), with 1 L/yr seepage and the default (low) metal corrosion rates; (2) a case with the same seepage but high metal corrosion rates (*CSIGHi.6i*); (3) a case with default corrosion rates but high seepage rates (*CSNFIG2.6i*); and (4) a case with default corrosion rates, high seepage, and the adjusted-Eh conditions. (The conditions for these cases are outlined in Table 6.4-3.) In cases (1) and (2), the pH and ionic strength are such that FeOx colloid suspensions are always unstable and the calculated loss of plutonium as FeOx colloids is trivial ($< 10^{-9}$%). In cases (3) and (4), the loss is < 1% of the plutonium that would be associated with the immobile corrosion products via absorption. The loss via plutonium "embedded" in CSNF colloids is also estimated in spreadsheet *FeOx_coll_vs_CP.xls* (output DTN: MO0705GEOMODEL.000) for the same four cases. In all the cases, the threshold ionic strength is calculated to be below the ionic strength in the package at the same time. Thus, suspensions of CSNF colloids are never stable, and losses of plutonium on CSNF colloids are always insignificant for these four cases. In summary, projected losses on FeOx and CSNF colloids are small and can largely be ignored for the cases examined.

INTENTIONALLY LEFT BLANK

7. VALIDATION

The purpose of the MDR model is to predict the fate of the waste package materials, specifically the retention or mobilization of the radionuclides and the neutron-absorbing material as a function of time after the breach of a waste package. The output of this model is used directly to assess the potential for a criticality event inside the waste package due to the retention of the radionuclides combined with a loss of the neutron-absorbing material. The output of this model is also used by the external accumulation model to assess the potential for accumulation of radionuclides outside the waste package. The model validation consists of one confidence building exercise during model development (Section 7.1.1, Corroboration of EQ3/6 and PHREEQC Model Outputs) and one postdevelopment validation activity (Section 7.2, Critical Review Conducted by a Technical Specialist).

7.1 DOCUMENTED DECISIONS AND ACTIVITIES IMPLEMENTED DURING MODEL DEVELOPMENT PROCESS

The TWP (SNL 2006 [DIRS 179452], Section 2.3) specifies that the MDR model requires a Level I validation.

Achieving Level I validation, specified by SCI-PRO-002, *Planning for Science Activities* (Attachment 3), requires at a minimum, discussion of documented decisions and activities that are implemented during the model development process that build confidence and verify and justify that an adequate technical approach using scientific and engineering principles was taken to:

(1) *Evaluate and select input parameters and/or data that are adequate for the model's intended use*: Section 4.1 provides the inputs used in the MDR model, which include waste package design information, material compositions, atomic weights, densities, water compositions, waste form compositions, corrosion or reaction rates, and thermodynamic data. These inputs were chosen to best represent the phenomena expected to exist during waste package degradation scenarios. Therefore, this criterion has been met for all of the salient features.

(2) *Formulate defensible assumptions and simplifications that are adequate for the model's intended use*: Sections 5, 6.2, and 6.3 provide the assumptions (Section 5) and simplifications (Sections 6.2 and 6.3) used in the MDR model. All model assumptions and simplifications have been discussed in the context of criticality applications, so that none of the assumptions or simplifications lead to conditions that decrease the likelihood of a criticality event either internal or external to the waste package. Therefore, this criterion has been met for all of the salient features of the model.

(3) *Ensure consistency with physical principles, such as conservation of mass, energy, and momentum, to an appropriate degree commensurate with the model's intended use*: EQ6 conserves mass, both of solids and water; therefore, the MDR model also conserves these properties. The physical changes in the system due to seismic and igneous events are incorporated into the conceptual models, taking into account the

changes in water seepage compositions, cladding conditions, and temperature effects of corrosion rates (Sections 6.2.1 and 6.2.2). For each EQ6 simulation, the output files (filename: **.elem_tot.txt*) give the number of moles of each element in the aqueous phase, corrosion products, and unreacted special reactants, as a function of time (output DTN: MO0705GEOMODEL.000, folders: CSNF, CDSP (N-reactor), FFTF, and TMI.

(4) *Represent important future state (aleatoric), parameter, and alternative model uncertainties to an appropriate degree commensurate with the model's intended use*: The inputs to the MDR model (including sensitivity studies) were selected to span wide ranges of temperature, flux, and seepage composition. Alternative conceptual models were discussed in Section 6.6 and the robustness of the current MDR model eliminates the need to use these alternative conceptual models for generating output. Therefore, this criterion has been met for all of the salient features.

(5) *Ensure simulation conditions have been designed to span the range of intended use and avoid inconsistent outputs or that those inconsistencies can be adequately explained and demonstrated to have little impact on results*: Sections 6.2 and 6.3 outline the wide range of inputs (flux, fuel exposure, temperature, reactant combinations) that were used in the MDR model. These inputs span the range of conditions expected to occur during the seismic and igneous scenarios modeled by the MDR. Therefore, this criterion has been met for all of the salient features.

(6) *Ensure that model predictions (performance parameters) adequately represent the range of possible outcomes, consistent with important uncertainties and modeling assumptions, conceptualizations, and implementation*: Sections 6.2 and 6.3 provide the inputs to the model that span the range of the waste package conditions expected during degradation; thus, the outputs also represent the range of possible outcomes. Additionally, sensitivity analyses have been performed to expand the performance parameters to values consistent with important conditional uncertainties. Therefore, this criterion has been met for all of the salient features.

7.1.1 Corroboration of EQ3/6 and PHREEQC Model Outputs

According to the TWP (SNL 2006 [DIRS 179452], Section 2.3, Model Validation Activities), a validation exercise to build confidence in the ability of EQ6 to execute the mathematical model is required. A seismic base case and igneous intrusion base case were executed using a separate code, PHREEQC V. 2.11. PHREEQC is a U.S. Geological Survey code that has many of the same features as EQ6. It can be used to perform a variety of aqueous geochemical calculations and has capabilities for kinetic processes, mixing reactions, and one-dimensional transport. Each of the processes simulated by EQ6 in the waste package degradation model can be simulated using PHREEQC.

Section 7.1.1.1 gives the inputs for the validation exercise. Sections 7.1.1.2 and 7.1.1.3 document the development of the PHREEQC seismic and igneous simulations. The resulting PHREEQC calculations are compared to EQ6 calculations in Section 7.1.1.4. The EQ6 and PHREEQC validation files are documented in validation DTN: MO0705MODELVAL.000.

7.1.1.1 Inputs

The EQ6 and PHREEQC input and output files and other inputs used in the comparison come from the previous version of this report, REV01 (BSC 2006 [DIRS 176911]). The files listed in Table 7-1 were brought forward unchanged from the DTN: MO0608MWDGEOMA.001 [DIRS 177332] and included in the validation DTN: MO0705MODELVAL.000. The main differences between the EQ6 files used in this validation exercise and the EQ6 files used in Section 6 of this report are that the files for the validation exercise are based on the previous CSNF waste package configuration that contained carbon steel basket material and nickel-gadolinium neutron absorber plates, rather than the current TAD design of stainless steel basket material and borated stainless steel neutron absorber plates. The design difference is not important for this confidence-building validation exercise, because, the validation test is more rigorous due to the addition of carbon steel with a fast corrosion rate that could cause greater changes in the chemistry of the system. Another difference is that the input files used in the validation comparison are based on a fully-flooded, or bathtub, scenario. A sensitivity study presented in Appendix C shows that the results are not significantly impacted by the quantity of water in the waste package. Therefore, a match between the EQ6 and PHREEQC results for the validation case is sufficient confirmation that EQ6 executes the mathematical model correctly.

Table 7-1. PHREEQC Validation Files

Input Description	Name or Value	Source
CSNF seismic base-case EQ6 input and output files	*CS-S-b-C5.6i* *CS-S-b-C5.6o* *CS-S-b-C5.elem_aqu.txt* *CS-S-b-C5.min_info.txt*	Validation DTN: MO0705MODELVAL.000, folder: EQ6 files/Seismic
CSNF igneous base-case EQ6 input and output files	*oxidized1_CSNF.6i* *oxidized1_CSNF.6p* *CSNFIG1.6i* *CSNFIG1.6o* *CSNFIG1.elem_aqu.txt* *CSNFIG1.min_info.txt*	Validation DTN: MO0705MODELVAL.000, folder: EQ6 files/Igneous
PHREEQC database	*phreeqcDATA025bdot Cr3az.dat*	Validation DTN: MO0705MODELVAL.000, folder: PHREEQC files
CSNF scaling factor	5,528	BSC 2006 [DIRS 176911], Table 6-10, Bathtub Scenario

7.1.1.2 PHREEQC Implementation of Seismic Base Case

The MDR model uses the solid-centered flow-through mode of the EQ6 code. This mode simulates the flow of source water into and through a constant-volume single-cell model. At the beginning of each equilibration step, a small amount of source water displaces an equal amount of water already equilibrated with the phases in the cell. The water in the cell then mixes completely, and the water, solids, and gases within the cell re-equilibrate. If specified, kinetically controlled reactants are added to the cell prior to each equilibration.

PHREEQC V. 2.11 can be used to mimic the EQ6 flow-through mode. A “cell” in PHREEQC can represent the single cell used in EQ6, but cells in PHREEQC are generally fully flushed with

water at each equilibration step in single-cell model and transport problems. To simulate partial displacements of water in a cell using PHREEQC, a set of mixing reactions must be defined.

In the seismic base case, the flow rate is 1 L/yr per waste package. Thus, in the scaled waste package, in which the single-cell model is scaled down to the size needed to simulate a control volume containing one liter of water, a much-lower flow rate is used. For this validation exercise, the scaling factor for a waste package is 5,528, which implies a 0.000181-L/yr flow rate through the scaled waste package (1 L/yr ÷ 5,528). For equilibration steps of 0.2 years, the amount of water displaced before each equilibration in the CSNF waste package is 0.0000362 L, or 0.00362%. To accomplish this in PHREEQC, source water from one cell (cell 4 in this example) is mixed with water from the reactor cell (cell 1) in a ratio of 0.0000362:0.9999638 to produce the new combined liter in the reactor cell. This mixing is defined using the *MIX* subroutine in PHREEQC as follows:

```
MIX 1
    1    0.9999638
    4    0.0000362
END
```

The mixing approach is straightforward for simulating displacement of small portions of water in the reactor. However, it is impractical to use by itself for a system in which hundreds or thousands of incremental displacements are simulated. To mimic EQ6's solid-center flow-through mode using PHREEQC, however, the subroutine *TRANSPORT* can be used in conjunction with the *MIX* subroutine to execute the repeated fractional displacements and provide user-friendly, tabulated output.

Two transport cells had to be defined so that "no flow" boundaries could be defined for the first and last transport cell. Specifying "no flow" boundaries prevents displacement of the full water volume of each cell at each equilibration step and allows implementation of the "diffusion only" mode for transport between the transport cells. In this case, cells 1 and 2 were defined as the first and final cells. In addition, one stagnant cell was defined for each transport cell; cell 4 for transport cell 1 and cell 5 for transport cell 2. These stagnant cells were defined to represent the source water for the displacement via mixing and were prevented from exchanging with their associated transport cells except via the *MIX* option. Thus, cells 4 and 5 are identical and contain the source water (e.g., simulated J-13 well water), and cells 1 and 2 are identical and contain the degrading waste package materials, CSNF, and the evolving aqueous solution.

The following excerpt from the PHREEQC file *SBC* (validation DTN: MO0705MODELVAL.000, folder: PHREEQC files\Seismic) applies to the first time period modeled and is an example of the mixing and transport sections of the PHREEQC input files:

```
MIX 1
    1    0.9999638
    4    0.0000362
END
MIX 2
    2    0.9999638
    5    0.0000362
END
```

```
TRANSPORT
    cells                2
    shifts               25     # 5 years
    time_step            6311500 # seconds = 0.2 years
    flow_direction       diffusion_only
    boundary_conditions  closed closed
    stagnant             1  0  0  0
    print_cells          1
    print_frequency      40
    punch_cells          1
    punch_frequency      1
    warnings             true
END
```

Mixing between cells 1 and 4 and between cells 2 and 5 is identical. As a result, diffusion between transport cells 1 and 2 has no effect. The evolving compositions in cell 1 can be considered the evolving aqueous and mineral compositions in the waste package reactor. Further information on the inputs specified above can be found in the PHREEQC user's manual (Parkhurst and Appelo 1999 [DIRS 159511]).

Overall, the PHREEQC simulations perform the same calculations as the EQ6 simulations. However, there are minor differences. One is the step frequency. Instead of EQ6's dynamically changing time intervals, the time intervals in the PHREEQC simulations must be constant. There is also a minor difference in how potential minerals are specified in the input files. In EQ6, all minerals in the database are allowed to precipitate if supersaturated with the exception of those minerals suppressed in the input file. In PHREEQC, the convention is the opposite: all minerals in the database are suppressed except those specified in the input file. Including a potential mineral in the PHREEQC input file with a starting value of 0 moles has no effect on the calculations unless the mineral reaches saturation, whereupon it will precipitate.

The thermodynamic database for the PHREEQC simulation was *phreeqcDATA025bdot Cr3az.dat*, a translation of the 25°C thermodynamic data from the EQ3/6 *data0.ymp.R4* database (DTN: SN0410T0510404.002 [DIRS 172712]). The PHREEQC database was modified in three ways that are particularly important to the simulation. First, Cr(VI) species are completely removed from the database. Second, the PHREEQC database contains a correction to an erroneous log K for eskolaite (Cr_2O_3) contained in *data0.ymp.R4*. Third, "−gamma 0.00 0.0410" was replaced with "−gamma 4.00 0.0410" to correct the database, as explained in CR 8766.

One additional modification involved the mineral anatase. Anatase is a highly insoluble form of TiO_2. In the EQ6 simulation, anatase precipitation keeps aqueous titanium at concentrations less than 1×10^{-46} molal. Such a low concentration is unreasonable and can be considered zero. PHREEQC apparently cannot handle such low calculated concentrations, and as a result computations do not converge when anatase is allowed to precipitate. Thus, in the PHREEQC simulation, a more soluble phase of TiO_2, rutile, was allowed to precipitate in its place. The only difference this difference makes between the EQ6 and PHREEQC simulations is that the aqueous titanium concentrations in the PHREEQC simulation are higher, though still extremely low.

The ion-activity model used in each simulation follows the B-dot expression developed by Helgeson (Wolery 1992 [DIRS 100835]). PHREEQC uses the identical B-dot expression, but refers to the expression by a different name—the extended Debye-Hückel expression. The A and B parameters in the Debye-Huckel expression are used to calculate activity coefficients. In the EQ3/6 database, the A and B parameters at 25°C are 0.5114 and 0.3288 (DTN: SN0410T0510404.002 [DIRS 172712]). The PHREEQC values for A and B are calculated in the subroutine "model.c" of the PHREEQC code as a function of temperature. At 25°C, the calculated values for A and B are 0.5093 and 0.3283. These differences have a small impact on the results, as discussed in Section 7.1.1.4.

The complete set of PHREEQC input and output files for this simulation are documented in validation DTN: MO0705MODELVAL.000. The file names and descriptions are:

- Input file: *sbc*
- Output file: *sbc.out*
- Tabulated output, 0 to 5 years: *sbc1.xls*
- Tabulated output, 5 to 50 years: *sbc1b.xls*
- Tabulated output, 50 to 450 years: *sbc2.xls*
- Tabulated output, 450 to 10,050 years: *sbc2b.xls*
- Tabulated output, 10,050 to 120,050 years: *sbc3.xls.*

7.1.1.3 PHREEQC Implementation of Igneous Base Case

The PHREEQC input file for the CSNF igneous base case is much like the input file for the seismic case in the way the flow-through reactor is simulated. As for the inputs, however, there are several important differences. First, the initial water in the reactor contains oxidized CSNF such that all of the CSNF is degraded to mineral and/or aqueous phases within the reactor. In addition, the incoming water in the model is basalt water. Finally, rates and amounts of material degradation were also adjusted to match the EQ6 simulation.

The EQ6 pickup file, *oxidized1_CSNF.6p*, provided the water composition for the PHREEQC simulation and the starting point for the EQ6 flow-through reactor simulation *CSNFig1.6i*. The input file *CSNFig1.6i* produced *CSNFig1.6o*, which provided the initial mineral assemblage for the PHREEQC simulation.

The igneous base-case PHREEQC input and output files are included in validation DTN: MO0705MODELVAL.000. The file names and descriptions are:

- Input file: *CSig1*
- Output file: *CSig1.out*
- Tabulated output, 0 to 5 years: *CSig1-1.xls*
- Tabulated output, 5 to 50 years: *CSig1-1b.xls*
- Tabulated output, 50 to 450 years: *CSig1-2.xls*
- Tabulated output, 450 to 10,050 years: *CSig1-2b.xls.*
- Tabulated output, 10,050 to 120,050 years: *CSig1-3.xls.*

7.1.1.4 Comparison of PHREEQC and EQ6 Results

To evaluate corroboration of the PHREEQC and EQ6 results, spreadsheets *PHRQC Val CSNF Seismic bc 4.xls* and *PHRQC Val CSNFig1 4.xls* (validation DTN: MO0705MODELVAL.000) were generated for graphical comparison of the respective output. The first workbook compares results of the CSNF seismic base case, and the second compares the results of the CSNF igneous base case. Relevant graphs from this spreadsheet are reproduced and discussed in this section. As mentioned in Section 7.1.1.1, both EQ6 and PHREEQC cases are based on a fully-flooded scenario.

Each of the graphs contains one or more chemical output parameters plotted as a function of time. Because EQ6 dynamically adjusts the time interval as needed, EQ6 results have data that are irregularly spaced and far fewer in number. In contrast, the PHREEQC data points are spaced at fairly regular intervals, as specified in the input file.

For plotting purposes, three additional calculations were added to the first three columns in the "PHR calcs" worksheet of *PHRQC Val Seismic bc 4.xls*. In the first column, time in years was calculated from the output time in seconds by applying by the following conversion factors: 60 s/min, 60 min/hr, 24 hr/day, and 365.24 days/yr. In the second column, the number of cumulative reactor flushes was calculated by multiplying the flush rate (0.000181 L/yr) by the total years in the first column. Eh (volts) was calculated in the third column by dividing the output pe (defined as the negative log of the electron activity) in column G by 16.9, which is the appropriate conversion factor at 25°C (Drever 1988 [DIRS 100725], p. 285).

Figure 7-1, compares pH and Eh trajectories for the seismic base case. Qualitatively, the curves are essentially identical, easily satisfying the validation criterion.

Ionic strength and the total dissolved concentrations of the J-13 well water seepage components in the seismic base case are compared over time in Figure 7-2, which shows PHREEQC predictions are identical or nearly identical to the EQ6 predictions.

Figures 7-3 through 7-5 compare predicted concentrations of waste package and fuel components. Figure 7-3 compares the predicted aqueous concentrations of the modeled components of Carbon Steel Type A516 and Stainless Steel Type 316. Aqueous concentrations of additional waste package components are compared in Figure 7-4. These additional components originate from the nickel–gadolinium alloy and/or aluminum alloys. Aqueous titanium is not plotted. Finally, the total dissolved concentrations of the components of the degrading CSNF are plotted in Figure 7-5.

The predictions for the CSNF igneous base case are presented in Figures 7-6 through 7-10. As in the seismic base case, there is agreement between the code calculations.

The differences in PHREEQC and EQ6 calculations are largest for barium (Figure 7-10) and sulfur (Figure 7-8) in the igneous simulation between 1,000 and 2,000 years. There is a brief time during this period when the calculations for barium or sulfur differ by a factor of approximately 100. The difference is due to the timing of a sudden and large change in the concentrations of barium and sulfur predicted by each code. The PHREEQC simulation predicts this change to occur approximately 300 years after the time predicted in the EQ6 simulation.

An explanation for the difference in the timing during this period is likely related to the difference in water masses predicted by each code. The PHREEQC water mass drops from 1 kg to about 0.76 kg after the first 50 years. It remains at approximately 0.76 kg for about 3,000 years until it slowly starts rising, returning to 1 kg around 20,000 years. The water mass in the EQ6 simulation follows the same pattern except that it falls to around 0.65 kg between 50 and 3,000 years. The general decrease in water mass is explained by the oxidation and precipitation of degradation products, which consume water in the process. The difference in calculated water masses suggests there might be an important difference in how water is effectively advected in the simulations. That is, the fluid mixing approach in PHREEQC might not perfectly simulate the displacement mode of EQ6 when the mass of water within the reactor considerably departs from 1 kg. This change in water mass affects the nondimensional flush rate (i.e., the time required to fully replace the water in the cell), which in turn could affect the timing of sudden concentration changes, such as those observed for barium and sulfur around 1,500 years. The timing of a sudden concentration change, however, is not important to criticality, since short term differences in concentration would not result in a significant difference in the calculated retention of material inside the waste package.

Predictions of the concentrations of uranium, plutonium, and gadolinium are the most important outputs of the MDR model. All three are plotted in Figure 7-5 for the seismic simulation. An analysis of the differences in predictions was performed for the seismic simulation to quantify the differences in predictions by the two codes. The analysis was complicated by the fact that the two data sets cannot be compared at common times because the time intervals are different for the two codes. To allow comparisons at common times, a linear interpolation was performed on the EQ6 predictions.

The results are plotted in Figure 7-11. Some of the scatter in the differences is due simply to linear interpolation of the EQ6 results. To screen out some of the comparisons that likely have considerable linear interpolation error, the only interpolations used in the analysis were ones for which the time interval was not more than 20% of the total time to that point.

Figure 7-11 shows that the predictions in the seismic simulations for gadolinium, plutonium, and uranium are generally within 10% of each other except when ionic strength exceeds approximately 0.07 molal between 1,000 years and 10,000 years. At the conditions with the maximum difference (54%), the PHREEQC concentrations for gadolinium (the highest concentration of the three elements) would result in an increase release of gadolinium from the waste package of about 4% (as compared to the release from the waste package using EQ6 gadolinium concentrations), calculated as follows:

$(4.70 \times 10^{-3} - 3.07 \times 10^{-3})$ moles/kg	PHREEQC gadolinium concentration minus EQ6 concentration (validation DTN: MO0705MODELVAL.000, folder: PHREEQC files\Seismic, file: *PHRQC Val CSNF Seismic bc4.xls*, tab "Stats," row 49)
× 1 kg/L	Unit conversion for density of water
× 1 L/year	Seepage rate into the waste package

$\times$ (10,000 – 1,000) years	Number of years
$\div$ (0.0035 $\times$ (1.10×10^5))	Total moles of gadolinium in CSNF (moles of gadolinium per mole CSNF (Table 6.3-4) times moles of CSNF (output DTN: MO0705GEOMODEL.000, folder: CSNF, file: *CSNF WP and TAD.xls*, tab: "EQ6 Inputs," row 10))
= 3.8%	Increase in gadolinium release due to higher PHREEQC concentrations between 1,000 and 10,000 years.

A difference of 4% is low compared to the variability in the results presented in Section 6.5. Much of the difference at high ionic strength is likely due to EQ3/6 pH rescaling. EQ3/6 adjusts activity coefficients to conform to the National Bureau of Standards pH scale, and PHREEQC does not. A secondary factor that likely contributes to a lesser degree is the small difference in the Debye-Huckel A and B parameters used by each code to calculate activity coefficients as discussed in Section 7.1.1.2.

In summary, although differences are observed between the EQ6 and PHREEQC simulations, the differences observed are small compared to model uncertainties and compared to the ranges of concentrations predicted for each of these components over the time period modeled. Therefore, the comparison of PHREEQC and EQ6 model simulations support the argument that the EQ6 execution of the seismic and igneous scenarios of the MDR model is valid.

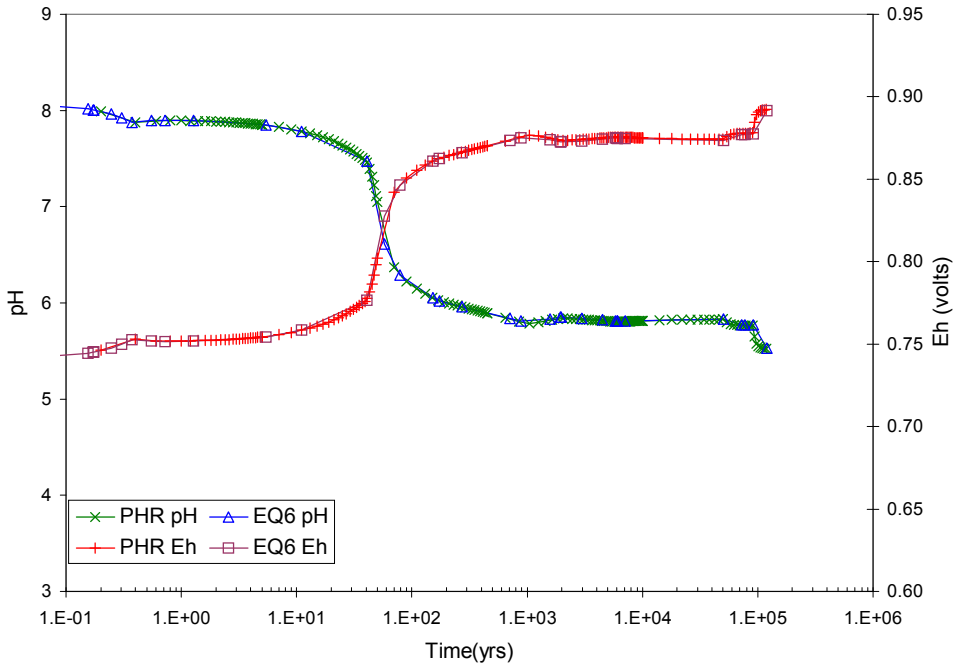

Source: Validation DTN: MO0705MODELVAL.000, folder: PHREEQC Files, *PHRQC Val CSNF Seismic bc4.xls*.

Figure 7-1. Comparison of Predicted pH and Eh in PHREEQC and EQ6 Simulations of the CSNF Seismic Base Case

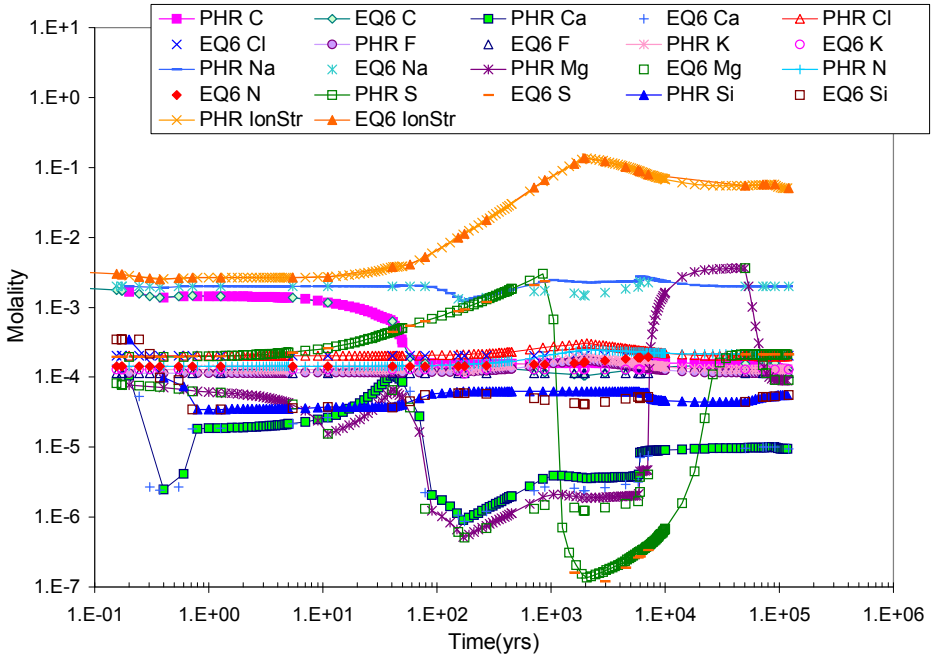

Source: Validation DTN: MO0705MODELVAL.000, folder: PHREEQC Files, *PHRQC Val CSNF Seismic bc4.xls*.

Figure 7-2. Comparison of Predicted Aqueous Concentrations of Seepage Components in PHREEQC and EQ6 Simulations of the CSNF Seismic Base Case

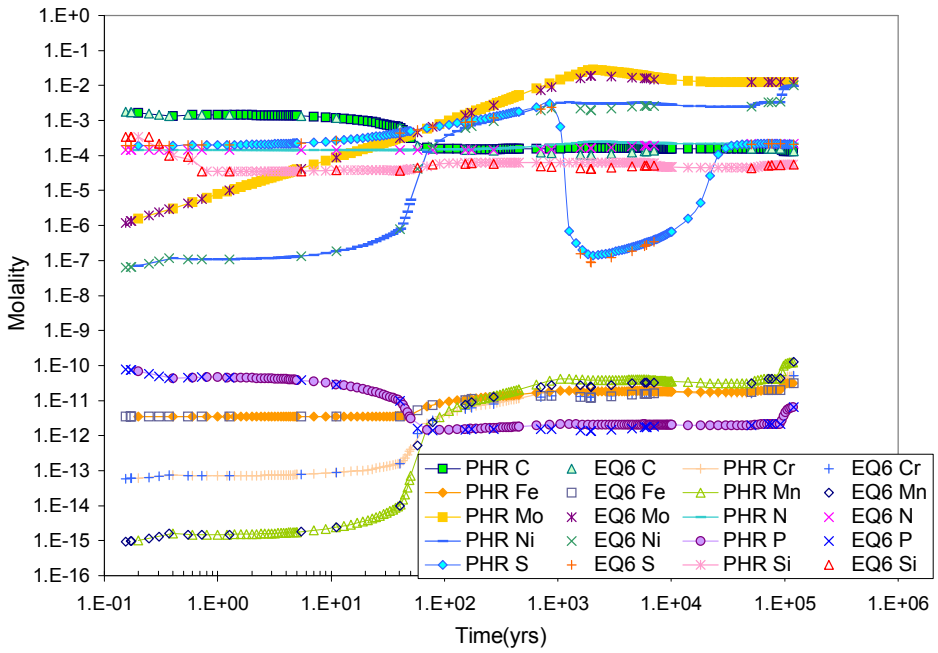

Source: Validation DTN: MO0705MODELVAL.000, folder: PHREEQC Files, *PHRQC Val CSNF Seismic bc4.xls*.

Figure 7-3. Comparison of Predicted Aqueous Concentrations of Steel Components in PHREEQC and EQ6 Simulations of the CSNF Seismic Base Case

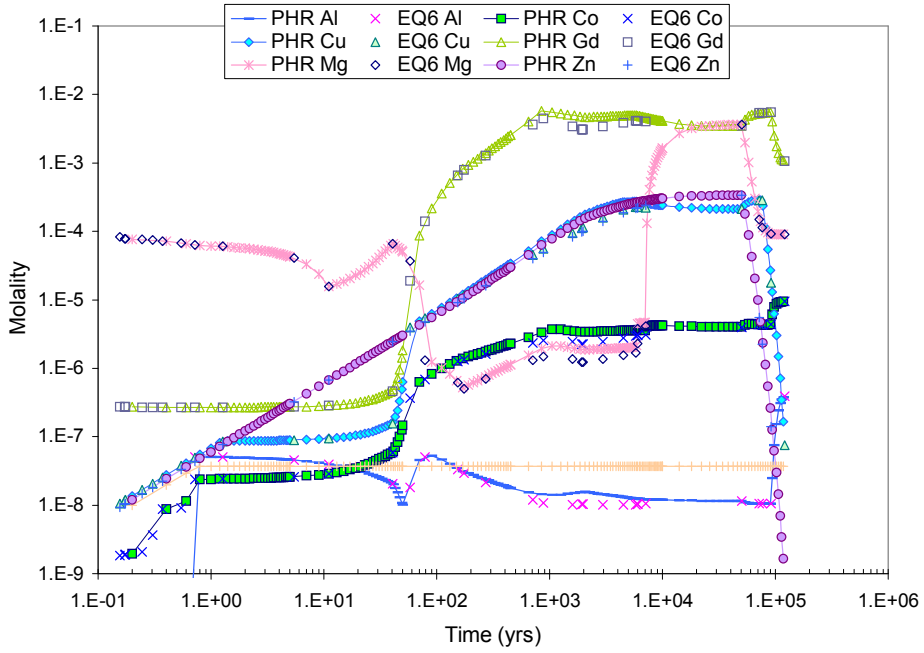

Source: Validation DTN: MO0705MODELVAL.000, folder: PHREEQC Files, *PHRQC Val CSNF Seismic bc4.xls*.

Figure 7-4. Comparison of Predicted Aqueous Concentrations of Additional Structural Components in PHREEQC and EQ6 Simulations of the CSNF Seismic Base Case

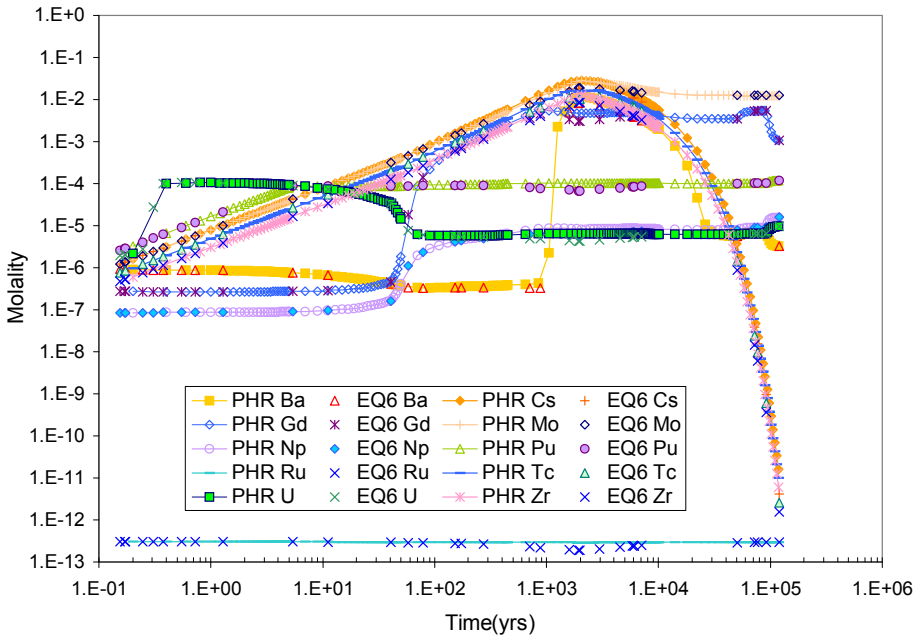

Source: Validation DTN: MO0705MODELVAL.000, folder: PHREEQC Files, *PHRQC Val CSNF Seismic bc4.xls*.

Figure 7-5. Comparison of Predicted Aqueous Concentrations of CSNF Components in PHREEQC and EQ6 Simulations of the CSNF Seismic Base Case

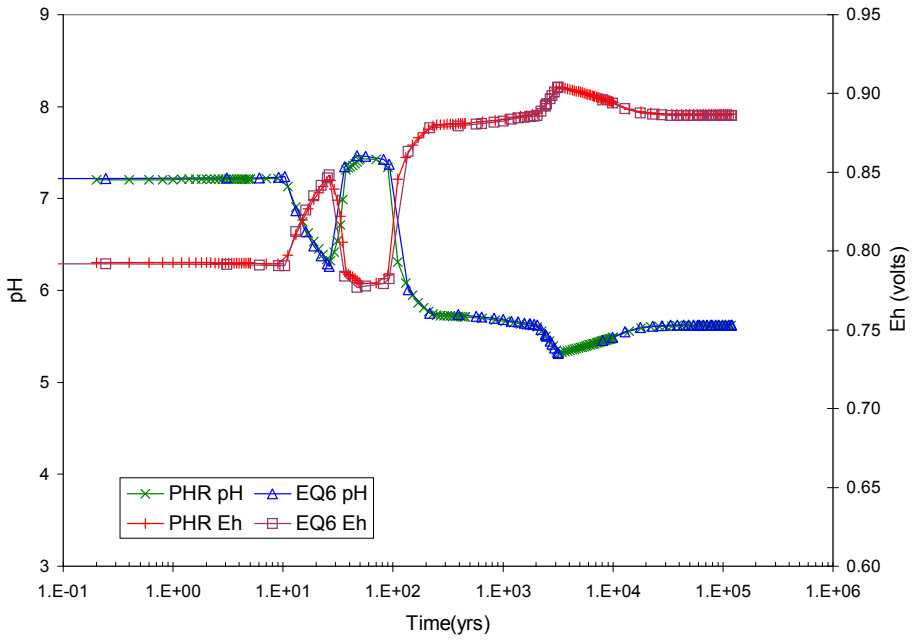

Source: Validation DTN: MO0705MODELVAL.000, folder: PHREEQC Files, *PHRQC Val CSNF Seismic bc4.xls*.

Figure 7-6. Comparison of Predicted pH and Eh in PHREEQC and EQ6 Simulations of the CSNF Igneous Base Case

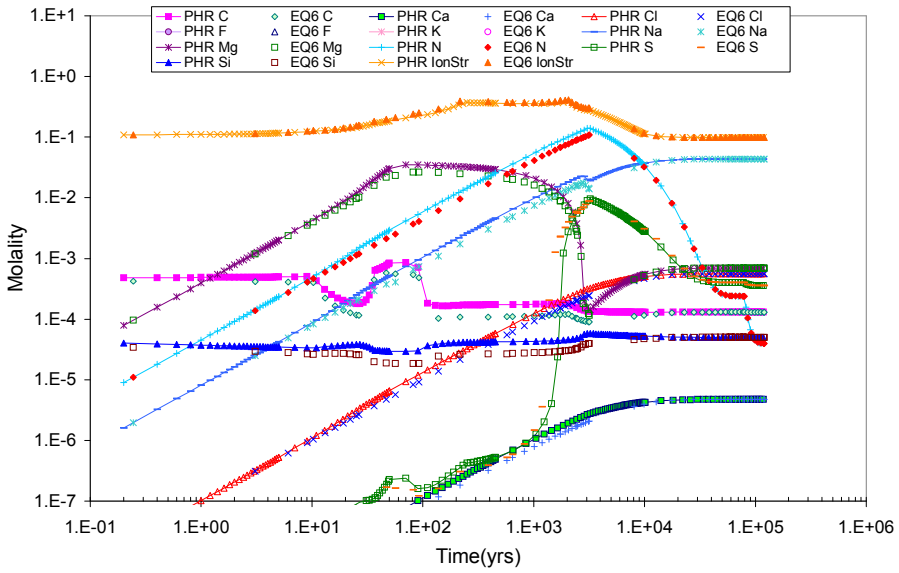

Source: Validation DTN: MO0705MODELVAL.000, folder: PHREEQC Files, *PHRQC Val CSNF Seismic bc4.xls*.

Figure 7-7. Comparison of Predicted Aqueous Concentrations of Seepage Components in PHREEQC and EQ6 Simulations of the CSNF Igneous Base Case

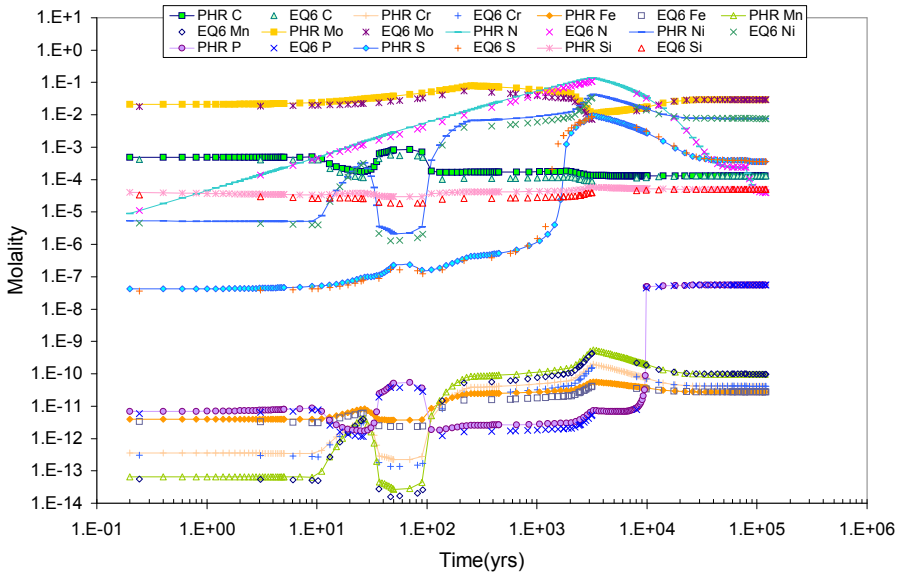

Source: Validation DTN: MO0705MODELVAL.000, folder: PHREEQC Files, *PHRQC Val CSNF Seismic bc4.xls*.

Figure 7-8. Comparison of Predicted Aqueous Concentrations of Steel Components in PHREEQC and EQ6 Simulations of the CSNF Igneous Base Case

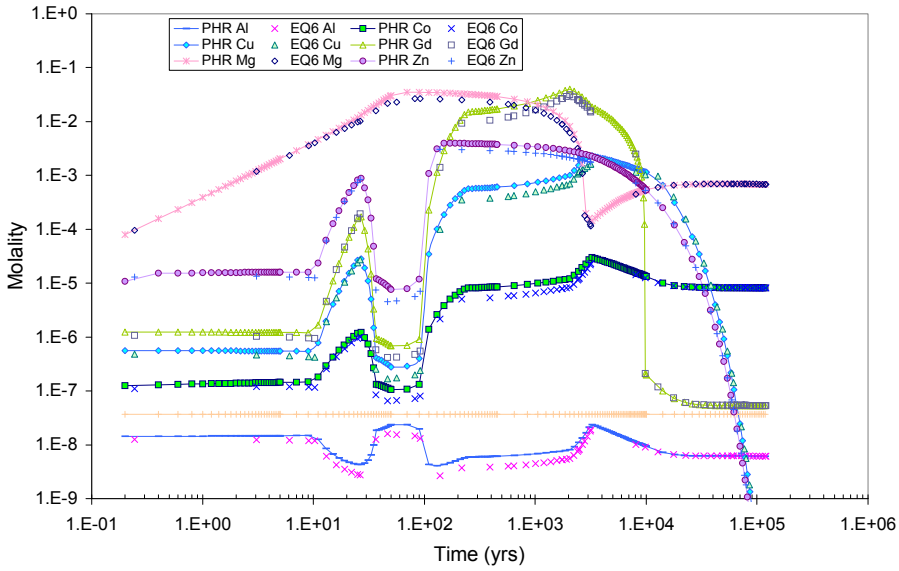

Source: Validation DTN: MO0705MODELVAL.000, folder: PHREEQC Files, *PHRQC Val CSNF Seismic bc4.xls*.

Figure 7-9. Comparison of Predicted Aqueous Concentrations of Additional Steel Components in PHREEQC and EQ6 Simulations of the CSNF Igneous Base Case

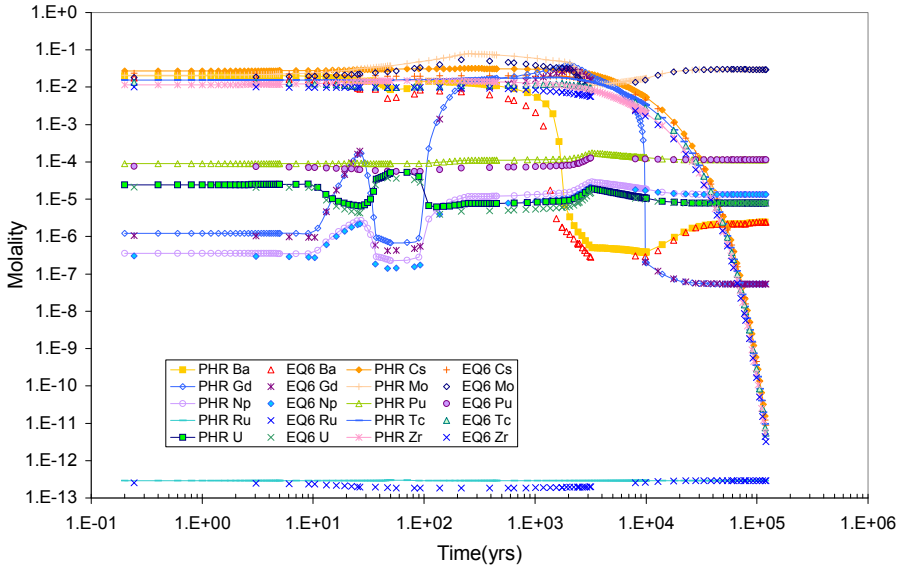

Source: Validation DTN: MO0705MODELVAL.000, folder: PHREEQC Files, *PHRQC Val CSNF Seismic bc4.xls*.

Figure 7-10. Comparison of Predicted Aqueous Concentrations of CSNF Components in PHREEQC and EQ6 Simulations of the Igneous CSNF Base Case

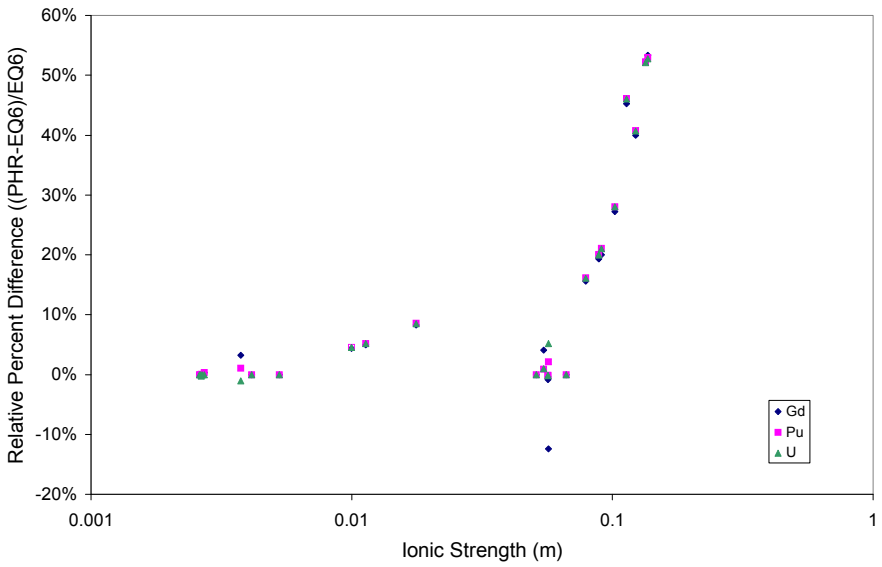

Source: Validation DTN: MO0705MODELVAL.000, folder: PHREEQC Files, *PHRQC Val CSNF Seismic bc4.xls*.

Figure 7-11. Differences in Predicted Aqueous Concentrations of Uranium, Plutonium, and Gadolinium versus Ionic Strength for the Seismic CSNF Base Case

7.2 CRITICAL REVIEW CONDUCTED BY A TECHNICAL SPECIALIST

Level I validation includes one method of postdevelopment model validation consistent with a model of lower relative importance. As specified in the TWP (SNL 2006 [DIRS 179452], Section 2.3), the validation was performed by critical review conducted by a technical specialist in accordance with SCI-PRO-006, Section 6.3.2, 5th dash. The TWP specifies that the validation technical reviewer shall:

1. Review the validation criteria in the TWP to determine if they are adequate for intended use of the model
2. Review the material degradation and release model in draft
3. Assess whether or not the model as documented in the report meets the validation criteria
4. Assess whether or not the model is adequate for its intended use. Meet with the author to resolve comments, and recommend actions, as appropriate, to resolve any inadequacies found as part of the review
5. Document the final conclusion as to whether the model is valid for its intended use, as a memo to be included as an appendix in the report.

The technical specialist shall evaluate the extent to which the following criteria are met:

1. The use of the thermodynamic database in the EQ3/6 modeling and the choice of mineral suppressions and formations are sufficiently justified and appropriate for the intended use of the model.

2. Modeling assumptions are clearly defined, discussed, and justified as appropriate for the intended use of the model.
3. Uncertainties in parameters, processes, and assumptions are appropriately described, and impacts of these uncertainties on the intended use of the model are discussed.
4. The overall technical credibility of the approach, including assumptions, parameters, and equations, is appropriate for the model's intended use.

Appendix A documents the selection of Dr. Florie A. Caporuscio as the critical reviewer for validation purposes. Appendix B contains a memo from Dr. Caporuscio which indicates that the MDR model is valid for its intended use.

8. CONCLUSIONS

The MDR model predicts the extent to which separation of neutron absorbers and fissile material can occur within a degrading waste package containing spent nuclear fuel; these predictions are then inputs for criticality calculations documented elsewhere. The separation can occur when neutron absorbers are released from the waste package, leaving fissile material inside, and when fissile material is released from the waste package, causing an external criticality concern. The simplified results of this model report are summarized in terms of retention of the elements gadolinium, uranium, and plutonium in the waste package. Based on the results of this report, the potential for either an internal or external criticality event is analyzed in other reports.

The model is based on the EQ3/6 computational code and simulates the degradation of waste package components once aqueous solutions have entered the waste package. As a function of time, the model calculates: (1) dissolved concentrations, (2) corrosion products mass and composition, and (3) quantity of intact waste package components (basket, fuel, etc.). The model is limited to the scenarios that involve seepage water entering the waste package—the seismic fault displacement and igneous scenarios. In the seismic scenario, the drip shield is displaced; waste package, cladding, and fuel containers fail; and seepage water flows through the waste package. In the igneous scenario, the drip shield is displaced, basalt fills the drift, and basalt-equilibrated water flows through the waste package.

The output of this model is used directly to assess the potential for a criticality event inside the waste package due to the retention of the radionuclides combined with a loss of the neutron-absorbing material. The output of this model is also used by the external accumulation model, to assess the potential for accumulation of radionuclides outside the waste package. This report analyzes four waste package configurations with different fuel types: the 21-PWR CSNF waste package, the 2-MCO/2-DHLW containing N-reactor fuel, the 5-DHLW/DOE SNF long waste package containing FFTF fuel, and the 5-DHLW/DOE SNF long waste package containing TMI fuel. The results of the model are restricted to uses that are consistent with the inputs and assumptions as described in Sections 4.1, 5, 6.2, and 6.3.

The MDR model input and output files and calculations are provided in output DTN: MO0705GEOMODEL.000. The files used in the confidence building exercise in support of validation, documented in Section 7.1.1, are contained in validation DTN: MO0705MODELVAL.000.

8.1 MODEL OUTPUT

8.1.1 Gadolinium, Plutonium, and Uranium Percent Remaining in Waste Package

The percent of neutron absorbers, plutonium, and uranium remaining at 10,000 years after waste package breach was calculated for all seismic and igneous cases described in Section 6.4. Tables 8.1-1 through 8.1-3 include the results from the cases that are most likely to occur (such as high-temperature logK corrections, adjusted-Eh, formation of solid solutions, low steel and alloy corrosion rates). All of the EQ6 input and output files are located in folders CSNF, CDSP (N-reactor), FFTF, and TMI in output DTN: MO0705GEOMODEL.000. The summary of the

results is presented in the following subsections in the context of the end use—either in-package criticality or external criticality.

Table 8.1-1. Seismic Results: Gadolinium, Plutonium, and Uranium Percent Remaining

Filename	Conditions	pH Max	pH Min	Percent Remaining at 10,000 Years		
				Gadolinium[a]	Plutonium	Uranium
CSNF Waste Package						
CS_S_b	Base case	8.15	5.91	93.5	99.0	100.0
CS_S_1c	1% cladding	8.15	5.21	100.0	99.1	100.0
CS_S_90K	90°C high-temperature logK	8.30	5.45	87.7	91.9	100.0
CSS_F9Eh	1,000 L/yr and adjusted-Eh	8.15	8.02	99.0	99.8	99.0
CS_S_TC2	TAD-canister Case 2	8.15	5.94	96.0	99.1	100.0
CDSP (N Reactor) Waste Package						
CD_S_b	Base case	8.15	4.13	N/A	99.8	100.0
CD_S_GM	Glass maximum corrosion rate	8.15	7.22	N/A	70.6[b]	100.0
FFTF Codisposal Waste Package						
FFTF_S_b	Base case	8.16	6.72	100.0	98.6	100.0
FFTF_1_5	log(fCO2)= −1.5	6.98	6.45	100.0	82.0	100.0
FFTFMxGE	Maximum HLWG corrosion rate and adjusted-Eh model	9.14	8.15	100.0	99.9	79.7
TMI Codisposal Waste Package						
TMI_S_b	Base case	8.16	6.11	N/A	99.8	100.0
TMI_MxG	Maximum HLWG corrosion rate	9.96	7.64	N/A	57.5[b]	79.5

Source: Output DTN: MO0705GEOMODEL.000, CDSP/*CDSP Seismic Summary.xls;* FFTF/*FFTF Seismic Summary.xls*; TMI/*TMI Seismic Summary.xls.*

NOTES: [a] Gadolinium in the CSNF EQ6 simulations represents all the lanthanide fission products (Table 6.3-4). For the FFTF simulations, the gadolinium is included in the DOE canister for criticality control.

[b] Plutonium initially in glass is approximately 1 kg.

Table 8.1-2. CSNF Igneous Results: Gadolinium, Plutonium, and Uranium Percent Remaining

Filename	Conditions	pH Max	pH Min	Percent Remaining at 10,000 Years			
				Gadolinium	Plutonium[a]	Uranium[a]	Pu/U Combined[a]
CSNFIG1	Base Case	7.17	5.92	94.0	74.1	100.2	100.0
CSIGCH	log(fCO2)= −1.5	6.67	5.60	99.9	65.9	100.2	99.9
CSIGCL	log(fCO2)= −5	7.24	6.17	85.5	74.8	100.2	100.0
CSIGAdEh	Seepage 1,000 L/yr; adjusted-Eh	8.17	7.12	99.0	74.8	98.8	98.6
CSIG_IB	Icelandic basalt water	7.16	5.91	93.1	74.1	100.2	100.0

Source: Output DTN: MO0705GEOMODEL.000, CSNF/*CSNF Igneous Summary.xls.*

NOTE: [a] Decay of Pu-239 is included in CSNF igneous EQ6 simulations, therefore, uranium retention is greater than 100% for some cases. Due to decay, the retention of combined U/Pu is reported.

Table 8.1-3. CSNF Igneous Results: Selected Elements Remaining

Filename	Conditions	Percent Remaining at 10,000 Years												
		Gd	Pu	U	Ag	Am	Eu	Mo	Nd	Np	Rh	Ru	Sm	Tc
CSIGPIss	Lanthanide phosphate and Lanthanide carbonate solid solution formation	95	74	100	32	94	90	97	99	100	100	100	89	3

Source: Output DTN: MO0705GEOMODEL.000, CSNF/*CSNF Igneous Summary.xls.*

NOTE: Gd = gadolinium; Pu = plutonium; U = uranium; Ag = silver; Am = americium; Eu = europium; Mo = molybdenum; Nd = neodymium; Np = neptunium; Rh = rhodium; Ru = ruthenium; Sm = samarium; Tc = technetium.

Table 8.1-4. DOE SNF Codisposal Igneous Results: Gadolinium, Plutonium, and Uranium Percent Remaining

Filename	Conditions	pH Max	pH Min	Percent Remaining at 10,000 Years		
				Gadolinium	Plutonium	Uranium
CDSP (N Reactor) Waste Package						
CD_I_B	Base case	8.37	4.15	N/A	100.0	100.0
CD_I_f9	Seepage 1,000 liter/yr	8.36	7.97	N/A	100.0	99.0
FFTF Codisposal Waste Package						
FFTF1_IG	Base case	8.11	6.72	100.0	98.6	100.0
FFTFIG_2	Seepage 1,000 liter/yr	8.32	7.80	99.8	6.6	63.7
TMI Codisposal Waste Package						
TMI_IG_1	Base case	8.15	6.11	N/A	99.8	100.0
TMI_IG_2	Seepage 1,000 liter/yr	8.48	7.94	N/A	99.9	88.9

Source: Output DTN: MO0705GEOMODEL.000, CDSP/*CDSP Igneous Summary.xls;* FFTF/*FFTF Igneous Summary.xls*; TMI/*TMI Igneous Summary.xls.*

Uncertainty Due to Waste Package Saturation—The waste package saturation sensitivity (Appendix C) showed that for values of saturation less than the base case 30%, the gadolinium retention could be overestimated. Since the waste package saturation is unknown (Assumption 5.1, Section 5), the gadolinium retention could be as much as four percentage points lower than the values listed in Tables 8.1-1 through 8.1-3.

8.1.1.1 In-Package Criticality

The cases with the greatest interest for in-package criticality are those cases with the highest loss of neutron absorbers. These are discussed below.

CSNF—The gadolinium in the CSNF EQ6 simulations represents all the lanthanide fission products (gadolinium, neodymium, samarium, europium) that act as neutron absorbers in the spent fuel (Table 6.3-4). The quantity of gadolinium remaining in the waste package for all the cases ranged from 85% to 100% (Tables 8.1-1 and 8.1-2). The boron remaining in the CSNF waste package is 100% for all cases, because, as discussed in Section 6.3.3, as the borated stainless steel plates degrade, the insoluble boron-carbide grains remain within the waste

package. The plutonium retention for all cases used for internal criticality should be considered to be 100%, as discussed in Section 6.5.3.1.

CDSP, FFTF, TMI—The CDSP and TMI waste packages do not contain any gadolinium. The gadolinium in the FFTF waste package is contained in the basket material and the aluminum-gadolinium shot material. For the FFTF, there was no significant release of gadolinium (< 1%) for all of the simulations.

8.1.1.2 External Criticality

The cases with the greatest interest for external criticality are those cases with the highest loss of uranium or plutonium. These are discussed below.

CSNF—The quantity of uranium remaining in the waste package in the CSNF EQ6 simulations for seismic and igneous cases ranged from 99% to 100% (Tables 8.1-1 and 8.1-2). The quantity of plutonium remaining in the waste package ranged from 0% to 100%. As discussed in Sections 6.5.3.2 and 6.3.14, the cases with the high plutonium releases were due to the base-case oxygen fugacity level (0.2 bar), which results in much-higher plutonium solubility than is observed in experiments. When corrected using the adjusted-Eh model, all of the plutonium was predicted to remain in the waste package.

CDSP—The CDSP waste packages do not contain any plutonium in the fuel—only a small amount in the HLWG (< 1 kg). The CDSP (N-reactor) waste packages results (Tables 8.1-1 and 8.1-4) showed no significant uranium releases from the waste package (< 1%) for the seismic and igneous cases.

FFTF—For FFTF, the quantity of uranium remaining in the waste package ranged from 64% to 100% (Tables 8.1-1 and 8.1-4). The cases with the highest uranium release were the cases with the maximum HLWG corrosion rate and the high seepage flux. Essentially all of the plutonium was retained in the waste package for all likely cases.

TMI—The TMI waste packages do not contain any plutonium in the fuel—only a small amount in the HLWG. The quantity of uranium remaining in the waste package ranged from 80% to 100% (Tables 8.1-1 and 8.1-4). The cases with the highest uranium release were the cases with the maximum HLWG corrosion rate and the high seepage flux.

8.1.2 Minerals Formed, Mineral Quantities, Unreacted Component Quantities, and Aqueous Concentrations

All of the minerals that were formed in each EQ6 simulation are tabulated in output DTN: MO0705GEOMODEL.000 (folders: CSNF, CDSP (N-reactor), FFTF, and TMI). (The formulas for the minerals are provided in Table 6.3-10.) The base case minerals formed and the unreacted components remaining in the waste package are plotted versus time in Appendix E. The plots in Appendix E provide a quick assessment of the major minerals that are formed. Schoepite is the major uranium-bearing mineral, with minor amounts of boltwoodite-Na, uranophane, and compreignacite in the first stage of the igneous case. The solid PuO2(hyd, aged) is the major plutonium-bearing mineral. The gadolinium-bearing minerals are $Gd_2(CO_3)_3$

and $GdPO_4:2H_2O$. Other major minerals formed (with their major elements in parentheses) are goethite (iron), gibbsite (aluminum), and trevorite (nickel, iron).

Instructions on how to extract information from the EQ6 output files, such as quantity of minerals, unreacted components, and aqueous concentration versus time are provided in Section 6.5.2 (Table 6.5-6). An example extraction is provided in output DTN: MO0705GEOMODEL.000, *Output Extraction/Output Extraction.xls.*

8.2 CRITERIA

Section 4.2 lists the acceptance criteria and other requirements for this report. The subsections to follow indicate how the criteria and requirements were met.

8.2.1 Safety Evaluation Report

The Safety Evaluation Report contains acceptance criteria concerning how the conditions inside the waste package could influence the occurrence of criticality (Reamer 2000 [DIRS 150765], Section 2.3.2). The applicable acceptance criteria (acceptance criteria 1, 2, 4, and 5) and open item 3 (Reamer 2000 [DIRS 150765], Section 4) and how they are addressed by this report are provided below:

Mathematical model limitations and uncertainties in modeling were defined and documented.

The model limitations and modeling uncertainties are documented and discussed in Sections 6.1, 6.2, and 6.3.

Primary and alternative modeling approaches consistent with available data and current scientific understanding were investigated and their results and limitations considered in evaluating the subissue.

The primary modeling and approaches consistent with available data and current scientific understanding were investigated and their results and limitations considered in evaluating the subissue are documented in Sections 6.1 through 6.5. The alternative modeling approaches are documented in Section 6.6.

DOE has identified all the features, events, and processes that may increase the reactivity of the system inside the WP.

The features, events, and processes that may increase the reactivity of the system inside the waste package have been identified and listed in Section 6.3.

DOE has identified the configuration classes and configurations that have potential for nuclear criticality. If models are used to develop the configuration, approach and accuracy in modeling verification and validation will be evaluated.

The verification and validation of the models used are documented in Section 7.

The Safety Evaluation Report open item (Reamer 2000 [DIRS 150765], Section 4) addressed in this report is:

> *Open item 3—The DOE needs to provide a modeling approach for igneous-activity-induced criticality.*
>
> The modeling approach of igneous-activity-induced criticality is provided in Section 6.2.2, and the results are documented in Section 6.5.

8.2.2 Disposal Criticality Analysis Methodology Topical Report

Disposal Criticality Analysis Methodology Topical Report (YMP 2003 [DIRS 165505]) contains sections applicable to the MDR model.

Section 3.3, Figure 3-2a and Figure 3-2b, and Section 3.3.1, Internal Criticality Master Scenarios, and Section 3.31, Internal Scenarios

The internal criticality configuration classes are shown in Figure 3-2a and Figure 3-2b and described in Section 3.3.1 of *Disposal Criticality Analysis Methodology Topical Report* (YMP 2003 [DIRS 165505]). The configuration class groups are described as follows:

1. *The basket containing the neutron absorber is degraded, but the waste form is either intact or degraded. For criticality to occur, several additional conditions are required: sufficient moderator is present, neutron absorber is flushed from the waste package, and most of the fissionable material remains in the package (configuration classes IP-3b, IP-3c, and IP-3d). These configuration classes arise from the scenarios in which the basket containing the neutron absorber degrades before the waste form. They result from scenario group IP-3, which involves the waste form degrading at a much lower rate than the non-SNF components in the waste package.*

   Group 1 is described as having the following characteristics: (1) the waste package is flooded, (2) the waste package internal structures degrade faster than the waste form, and (3) soluble neutron absorbers are flushed from the waste package (YMP 2003 [DIRS 165505], Figure 3-2a, Scenario IP-3). The waste form is retained in the waste package in either an intact or degraded state. For CSNF, this configuration for intact fuel is accounted for by setting cladding failure to 1% (Section 6.3.10), which prevents the degradation of most of the shielded fuel and permits the waste package components to corrode. For the degraded scenario for the seismic EQ6 cases, the configuration is achieved by varying the following parameters that increase the neutron-absorber releases from the waste package and retain nearly all of the degraded waste form in the waste package: high steel-degradation rates (Table 6.3-6), high temperature (Section 6.3.9), low fugacity of CO_2 (Section 6.3.14), and low seepage flux (Section 6.3.4). None of the igneous EQ6 simulations fit this group because the waste package is expected to be too damaged to accumulate water.

2. *Both basket and waste form are degraded simultaneously with the same three additional conditions (water, absorber removal, and fissionable material remaining) as configuration group #1 above (configuration class IP-2a). In general, this configuration will result in the fissionable material accumulating at the bottom of the waste package. Since both waste*

form and non-SNF components in the waste package are fully degraded, with all the soluble degradation products removed, the only residual effect of a difference in degradation rates is the nature of any separation between the degradation products of the waste form and other internal components. The parameters of these configuration classes are determined either by the geochemistry analysis or by the evaluation of conservative alternative configurations. Therefore, this configuration class can arise directly from scenario group IP-2, or from scenario groups IP-1 or IP-3 looping to IP-2 through the D entry point fed by D1 and D2 respectively. Intermediate configuration in which only basket or the waste form is degraded first are covered by configuration group #1 (above) or #3 (below).

Group 2 is described as having the following characteristics: (1) the waste package is flooded, (2) the waste package internal structures degrade at the same rate as the waste form, (3) degraded waste form and components collect at bottom of waste package, and (4) soluble neutron absorbers are flushed from the waste package (YMP 2003 [DIRS 165505], Figure 3-2a, Scenario IP-2). This scenario is not likely since the corrosion products of stainless steel are expected to remain in their initial location, as explained in Section 6.3.16.

3. *The fissionable material from the waste form is mobilized and moved away from the neutron absorber, which remains in the partially degraded basket structure. As with configuration group #2, the fissionable material will most likely accumulate at the bottom of the waste package, but unlike configuration group #2, the opportunities for transport and accumulation are limited because the basket is only partially degraded. This configuration class results from scenario group IP-1, which involves the waste form degrading faster than the basket (non-SNF internal component in the waste package). An alternative configuration class having these relative degradation rates is IP-1a, in which the fissionable component of the waste form does not move significantly after degradation.*

   Group 3 is described as having the following characteristics: (1) the waste package is flooded, (2) the waste package internal structures degrade slower than the waste form, and (3) the waste form is mobilized and separated from the neutron absorbers. (YMP 2003 [DIRS 165505], Figure 3-2a, Scenario IP-1b). This configuration is addressed by setting cladding exposure to 100% (Section 6.3.10, for CSNF) and setting the alloy corrosion rates as low for the base case (Section 6.3.6, for CSNF and DOE spent nuclear fuel). All of the seismic EQ6 cases fit this group, except the following sensitivities: 1% cladding sensitivity (Section 6.3.10), the high corrosion rate (Table 6.3-6), and medium corrosion rate (Table 6.3-6). None of the igneous EQ6 simulations fit this group because the waste package is expected to be too damaged to accumulate water.

4. *Fissionable material accumulates at the bottom of the waste package, together with moderator provided either by water trapped in clay or by hydration of metal corrosion products, so that criticality can occur without water pooling in the waste package (configuration classes IP-4b, IP-5a, and IP-6a). The complete analysis of this configuration group will include the identification of the minimum moderator requirement for physically achievable concentration of fissionable material, and will identify any possible fast (non-moderated) criticality as part of this process. The scenarios leading to this configuration group differ in that class IP-4b does not require the neutron absorber to be flushed from the waste package, but only that a relative displacement occurs between the*

fissionable material at the bottom of the waste package and neutron absorber distributed throughout the container. These configuration classes can result from scenario groups IP-4 though IP-6, all of which have penetrations in the bottom of the waste package, thus preventing water from pooling in the waste package. This flow-through geometry permits removal of soluble corrosion products, but allows the waste package bottom precedes, or directly follows, the penetration of the top, scenario groups IP-4 though IP-6 are said to be directly invoked. If there is significant degradation of waste form or non-NSF components in the waste package, then these scenarios are indirectly invoked after scenario groups IP-1, IP-2, or IP-3. In all of these scenarios, a sequence representing removable of fissionable material form the waste package thought breaches in the bottom of the waste package provides a source term for the external criticality scenarios in Figures 3-3a and 3-3b.

Group 4 is described as having the following characteristics: (1) the waste package is flow-through without water accumulation, (2) waste package internal structures degrade either faster or slower than the waste form, and (3) flow-through flushing removes soluble fissile material or neutron absorbers from the waste package (YMP 2003 [DIRS 165505], Figure 3-2a, Scenarios IP-4b, IP-5a, and IP-6a). The cases that result in the most-significant fissile material loss from the waste package are described in Section 6.5.3.2. The cases with significant neutron-absorber releases are discussed in Section 6.5.3.1. The impact of the flooded waste package versus a flow-through waste package (i.e., water saturation level) is addressed in Section 5.1 and Appendix C.

5. *As with configuration #4, the moderator is provided by water trapped in clay, but in this case, the fissionable material is distributed throughout a major fraction of the waste package's volume (IP-4a). This configurations class can only be reached if the waste form degrades faster than the non-SNF components in the waste package, so that the fissionable material remains in place to be lock in by its own hydration or the hydration of the other internal components. Therefore, it is only reached by scenario group IP-4 (direct) or indirectly after IP-1.*

   Group 5 is described as having the following characteristics: (1) the waste package is flow-through without water accumulation, (2) waste package internal structures degrade slower than the waste form, and (3) waste form degradation products hydrate in initial location (YMP 2003 [DIRS 165505], Figure 3-2a, Scenario IP-4a). This configuration is addressed by setting cladding exposure to 100% (Section 6.3.10, for CSNF) and setting the alloy corrosion rates as low for the base case (Section 6.3.6, for CSNF and DOE spent nuclear fuel). All of the scenarios fit this group, except the following sensitivities: 1% cladding sensitivity (Section 6.3.10), the high corrosion rate (Table 6.3-6), and medium corrosion rate (Table 6.3-6).

6. *Waste form has degraded in place with non-SNF components in the waste package partially degraded (IP-1a). This configuration class is of interest if the degradation of the waste form can distribute the fissionable material into a more reactive geometry than the intact waste form.*

Group 6 is described as having the following characteristics: (1) the waste package is flooded, (2) waste package internal structures degrade slower than the waste form, and (3) the waste form degrades in place (YMP 2003 [DIRS 165505], Figure 3-2a, Scenario IP-1a). This is similar to group 5 except that the waste package is flooded. This configuration is addressed by setting cladding exposure to 100% (Section 6.3.10, for CSNF) and setting the alloy corrosion rates as low for the base case (Section 6.3.6, for CSNF and DOE spent nuclear fuel). All of the seismic EQ6 cases fit this group, except the following sensitivities: 1% cladding sensitivity (Section 6.3.10), the high corrosion rate (Table 6.3-6), and medium corrosion rate (Table 6.3-6). None of the igneous scenarios fit this group because the waste package is expected to be too damaged to accumulate water.

Section 3.3.3, Effect of Seismic Events

The effects of a seismic event are documented in Section 6.5.

Section 3.3.4, Effect of Volcanic Events

The effects of an igneous event are documented in Section 6.5.

Section 3.4.1, Configurations with the Potential for Internal Criticality

Section 3.4.1.1 of the *Disposal Criticality Analysis Methodology Topical Report* (YMP 2003 [DIRS 165505]) lists ten essential steps of geochemical modeling that ensure all configurations with potential for internal criticality are addressed. The first three steps include the specification of corrosion rates, water flux rate, and water composition. These inputs to the model are described in Section 4.1 of this report. The remaining steps are related to the results of the modeling, such as the characterization of the non-degraded materials and corrosion products as a result of chemical degradation. The modeling results are presented in Section 6.5.

8.2.3. Yucca Mountain Review Plan

The acceptance criteria in *Yucca Mountain Review Plan, Final Report* (NRC 2003 [DIRS 163274]) are intended for use by the NRC staff when reviewing the license application submittal. Some of the acceptance criteria listed in the TWP (SNL 2006 [DIRS 179452], Section 3.2) contain subcriteria that are not applicable to this document and therefore are not addressed. The criteria listed below are applicable to the current report and are considered project requirements. All of the criteria have been adequately addressed in the document. The response to each acceptance criteria gives the details as to how each criteria was addressed.

Section 2.2.1.3.1.3, Degradation of Engineered Barriers

- **Acceptance Criterion 1 – System Description and Model Integration Are Adequate**

(6) Adequate technical bases are provided, for selecting the design criteria, that mitigate any potential impact of in-package criticality on repository performance, including considering all features, events, and processes that may increase the reactivity of the system inside the waste package. For example, the technical bases for the abstraction of the degradation of engineered barriers include configuration

classes and configurations that have potential for nuclear criticality, changes in radionuclide inventory, and changes in thermal conditions.

Response: The results of the model focus on factors that could change the reactivity of the system inside the waste package, such as neutron-absorber and radionuclide dissolution and release from the waste package (Sections 6.5 and 8.1).

- **Acceptance Criterion 2 – Data Are Sufficient for Model Justification**

(1) Parameters used to evaluate the degradation of engineered barriers in the license application are adequately justified (e.g., laboratory corrosion tests, site-specific data such as data from drift-scale tests, in-service experience in pertinent industrial applications, and test results not specifically performed for the Yucca Mountain site, etc.). The U.S. Department of Energy describes how the data were used, interpreted, and appropriately synthesized into the parameters.

Response: The corrosion rates are based on laboratory corrosion tests and tests not specifically performed for the Yucca Mountain site (Section 4.1.8). A description of how the base case corrosion rates and the medium and high sensitivity rates were chosen is provided in Section 6.3.6.

(4) Degradation models for the processes that may be significant to the performance of the engineered barriers are adequate. For example, the U.S. Department of Energy models consider the possible degradation of the engineered barriers, as a result of uniform and localized corrosion, stress-corrosion cracking, microbially influenced corrosion, hydrogen embrittlement, and incorporate the effects of fabrication processes, thermal aging, and phase stability.

Response: The degradation rates used are justified in Section 6.3.6. Sensitivity cases are run for medium and high corrosion rates.

Acceptance Criteria 3 through 5 do not apply because this report does not develop a corrosion model abstraction.

Section 2.2.1.3.3.3, Quantity and Chemistry of Water Contacting Waste Packages and Waste Forms

- **Acceptance Criterion 1 – System Description and Model Integration Are Adequate**

(2) The abstraction of the quantity and chemistry of water contacting waste packages and waste forms uses assumptions, technical bases, data, and models that are appropriate and consistent with other related U.S. Department of Energy abstractions.

Response: The seepage rates (Section 6.3.4) are the same values used by TSPA. The chemistry of the seepage water is the same as the IPC model (SNL 2007 [DIRS 180506]). The oxygen and carbon dioxide fugacity values are consistent with the TSPA-LA feeds (Section 6.3.14).

(11) The abstraction of in-package criticality or external-to-package criticality, with in the emplacement drift, provides an adequate technical basis for screening these events. If either event is included in the assessment, then the U.S. Department of Energy uses acceptable technical bases for selecting the design criteria that mitigate the potential impact of in-package criticality on repository performance; identifies the features, events, and processes that may increase the reactivity of the system inside the waste package; identifies the configuration classes and configurations that have potential for nuclear criticality; and includes changes in thermal conditions and degradation of engineered barriers in the abstraction of the quantity and chemistry of water contacting waste packages and waste forms.

Response: All the inputs that could affect the chemistry of the water contacting the waste package and waste form are varied, as described in Section 6.3. The starting seepage water composition (Section 6.3.5), CO_2 fugacity (Section 6.3.14), temperature of the waste package (Section 6.3.9), and corrosion rates (Section 6.3.6) are varied because of their known impacts on water chemistry.

- **Acceptance Criterion 2 – Data Are Sufficient for Model Justification**

(2) Sufficient data were collected on the characteristics of the natural system and engineered materials to establish initial and boundary conditions for conceptual models of thermal-hydrologic-mechanical-chemical coupled processes that affect seepage and flow and the waste package chemical environment.

Response: The seepage water compositions are from pore water composition and ground water compositions measured in the vicinity of Yucca Mountain (Section 4.1.2). The basalt water compositions, for use in the igneous scenario, are natural analog compositions of basalt-equilibrated waters (Section 4.1.2). The water compositions were adjusted in sensitivity calculations to determine the impacts of different boundary conditions, such as high and low CO_2 fugacity (Section 6.3.14), variation in Eh values (Section 6.3.14), and high temperatures (Section 6.3.9).

Acceptance Criteria 3 through 5 do not apply because this report does not develop a model abstraction for the quantity and chemistry of water contacting waste packages and waste forms.

Section 2.2.1.3.4.3, Radionuclide Release Rates and Solubility Limits

- **Acceptance Criterion 1 – System Description and Model Integration Are Adequate**

(2) The abstraction of the radionuclide release rates and solubility limits uses assumptions, technical bases, data, and models, that are appropriate and consistent with other related U.S. Department of Energy abstractions.

Response: The solubility limits are controlled by the thermodynamic database, which is the same database used in *In-Package Chemistry Abstraction* (SNL 2007 [DIRS 180506]) and *Dissolved Concentration Limits of Elements with Radioactive Isotopes* (SNL 2007 [DIRS 177418]), both of which support TSPA-LA (Section 6.3.13). The choices of solubility-controlling phases are consistent with those reports. The use of the reduced Eh

when considering plutonium solubility is consistent with *Dissolved Concentration Limits of Elements with Radioactive Isotopes* (SNL 2007 [DIRS 177418]).

(7) The abstraction of in-package criticality or external-to-package criticality, within the emplacement drift, provides an adequate technical basis for screening these events. If either event is included in the assessment, then the U.S. Department of Energy uses acceptable technical bases for selecting the design criteria that mitigate the potential impact of in-package criticality on repository performance; identifies the features, events, and processes that may increase the reactivity of the system inside the waste package; identifies the configuration classes and configurations that have potential for nuclear criticality; and includes changes in thermal conditions and degradation of engineered barriers in the abstraction of radionuclide release rates and solubility limits.

Response: All the inputs that could affect the radionuclide solubility are varied, as described in Section 6.3. The adjusted-Eh model (Section 6.3.14), variations in CO_2 fugacity (Section 6.3.14), solid solution formation (Section 6.3.13), and mineral suppressions (Section 6.3.16) are varied because of their known impacts on solubility.

- **Acceptance Criterion 2 – Data Are Sufficient for Model Justification**

(3) Where the U.S. Department of Energy uses data supplemented by models to support abstraction of solubility limits, the anticipated range of proportions and compositions of phases under the various physiochemical conditions expected are supported by experimental data.

Response: The reduced Eh conditions that control plutonium concentrations used in *Dissolved Concentration Limits of Radioactive Isotopes* (SNL 2007 [DIRS 177418]) are based on plutonium concentrations observed in experiments (SNL 2007 [DIRS 177418], Figure 6.5-6), as discussed in Section 6.3.14. The uranium minerals predicted to form in the EQ6 simulations are supported by experimental data for schoepite (Wronkiewicz et al. 1996 [DIRS 102047], Table 5) and uranophane and boltwoodite-Na (Wronkiewicz and Buck 1999 [DIRS 169286], Figure 3).

Acceptance Criteria 3 through 5 do not apply because this report does not develop a model abstraction for the radionuclide release rates and solubility limits.

9. INPUTS AND REFERENCES

9.1 DOCUMENTS CITED

169213 Akbulut, A. and Kadir, S. 2003. "The Geology and Origin of Sepiolite, Palygorskite and Saponite in Neogene Lacustrine Sediments of the Serinhisar-Acipayam Basin, Denizli, SW Turkey." *Clays and Clay Minerals, 51,* (3), 279–292. Aurora, Colorado: Clay Minerals Society. TIC: 256064.

159372 Allen, B.L. and Hajek, B.F. 1995. "Mineral Occurrence in Soil Environments." Chapter 5 of *Minerals in Soil Environments.* 2nd Edition. Dixon, J.B. and Weed, S.B., eds. SSSA Book Series, No. 1. Madison, Wisconsin: Soil Science Society of America. TIC: 237222.

168734 Allison, J.M. 2004. "Request for Referenceable Information on High-Level Waste (HLW) Radionuclide Inventories in Support of Preparation of the Yucca Mountain Project License Application (Your Letter, JCP-0445, 1/28/04)." Memorandum from J.M. Allison (DOE/SR) to J. Arthur, III (OCRWM), February 26, 2004, 0303040661, with attachment. ACC: MOL.20040317.0265.

141615 ASM International 1990. *Properties and Selection: Nonferrous Alloys and Special-Purpose Materials.* Volume 2 of *ASM Handbook.* Formerly Tenth Edition, Metals Handbook. 5th Printing 1998. Materials Park, Ohio: ASM International. TIC: 241059.

149625 Audi, G. and Wapstra, A.H. 1995. *Atomic Mass Adjustment, Mass List for Analysis.* Upton, New York: Brookhaven National Laboratory, National Nuclear Data Center. TIC: 242718.

104439 B&W Fuel Company 1991. *Final Design Package Babcock & Wilcox BR-100 100 Ton Rail/Barge Spent Fuel Shipping Cask.* Volume 2. 51-1203400-01. DBABE0000-00272-1000-00014 REV 00. Lynchburg, Virginia: B&W Fuel Company. ACC: MOV.19960802.0083.

175137 Barthelmy, D. 2005. "Willemite." Willemite Mineral Data. Spring, Texas: David Barthelmy. Accessed October 6, 2005. TIC: 257786. URL: http://www.webmineral.com/data/Willemite.shtml.

181411 Bastidas, J.M.; López, M.F.; Gutiérrez, A.; and Torres, C.L. 1998. "Chemical Analysis of Passive Films on Type AISI 304 Stainless Steel Using Soft X-Ray Absorption Spectroscopy." *Corrosion Science, 40,* (2/3), 431-438. New York, New York: Pergamon. TIC: 259504.

101379 Bear, J. 1988. *Dynamics of Fluids in Porous Media.* New York, New York: Dover Publications. TIC: 217568.

181433 Berry, F.J.; Bland, P.A.; Oates, G.; and Pillinger, C.T. 1994. "Iron-57 Mössbauer Spectroscopic Studies of the Weathering of L-Chondrite Meteorites." *Hyperfine Interactions, 91,* 577-581. Basel, Switzerland: J.C. Baltzer AG, Science Publishers. TIC: 259510.

181627 Beverskog, B. and Puigdomenech, I. 1999. "Pourbaix Diagrams for the Ternary System of Iron-Chromium-Nickel." *Corrosion, 55*, (11), 1077-1087. Houston, Texas: NACE International. TIC: 259523.

181410 Bland, P.A.; Sexton, A.S.; Jull, A.J.T.; Bevan, W.R.A.; Berry, F.J.; Thornley, D.M.; Astin, T.R.; Britt, D.T.; and Pillinger, C.T. 1998. "Climate and Rock Weathering: A Study of Terrestrial Age Dated Ordinary Chondritic Meteorites from Hot Desert Regions." *Geochimica et Cosmochimica Acta, 62,* (18), 3169-3184. New York, New York: Pergamon. TIC: 259503.

181193 Blenkinsop, R.D.; Currell, B.R.; Midgley, H.G.; and Parsonage, J.R. 1985. "The Carbonation of High Alumina Cement, Part II." *Cement and Concrete Research, 15,* (3), 385-390. Elmsford, New York: Pergamon Press. TIC: 259450.

182750 Blyth, R.L. 2004. "FY 2003 Quality Assurance Management Assessment (QAMA) for National Spent Nuclear Fuel Quality Assurance Program (NSNFP-QA-04-005." Memorandum from R.L. Blyth (DOE/ID) to R.D. Capshaw (DOE/ORD), February 9, 2004, with attachments. ACC: MOL.20040513.0151.

180828 Boeuf, A.; Coppola, R.; Zambonadi, F.; Morlevat, J.P.; Rustichelli, F.; and Wenger, D. 1981. "Time Dependence at 600 and 650°C of $M_{23}C_6$ Precipitate Composition in AISI 304 Stainless Steel." *Journal of Materials Science, 16,* 1975-1979. New York, New York: Chapman and Hall. TIC: 259186.

156639 Borchardt, G. 1995. "Smectites." Chapter 14 of *Minerals in Soil Environments.* 2nd Edition. Dixon J.B. and Weed, S.B., eds. SSSA Book Series, No. 1. Madison, Wisconsin: Soil Science Society of America. TIC: 237222.

144977 Breck, D.W. 1984. "Ion Exchange Reactions in Zeolites." Chapter 7 of *Zeolite Molecular Sieves, Structure, Chemistry, and Use.* Malabar, Florida: Robert E. Krieger Publishing Company. TIC: 245213.

157873 Bricker, O. 1965. "Some Stability Relations in the System Mn-O_2-H_2O at 25° and One Atmosphere Total Pressure." *American Mineralogist, 50,* 1296-1354. Washington, D.C.: Mineralogical Society of America. TIC: 238855.

182748 Brown, R.D. 2002. "Audit Report EM-ARC-02-10." Memorandum from R.D. Brown (DOE) to M.R. Arenaz (DOE/ID), November 26, 2002, OQA:JB-0307, with enclosure. ACC: MOL.20030303.0016; MOL.20030303.0017.

164418 BSC (Bechtel SAIC Company) 2002. *Criticality Calculation for the Most Reactive Degraded Configurations of the FFTF SNF Codisposal WP Containing an Intact Ident-69 Container.* CAL-DSD-NU-000002 REV A. Las Vegas, Nevada: Bechtel SAIC Company. ACC: MOL.20021028.0128.

159913 BSC 2002. *External Accumulation of Fissile Material from DOE Co-Disposal Waste Packages.* ###-3OR-DSD#-001##-###-#A#. Las Vegas, Nevada: Bechtel SAIC Company. ACC: MOL.20020920.0163.

173170 BSC 2002. *User's Manual for EQ6 V7.2bLV.* SDN: 10075-UM-7.2bLV-01. Las Vegas, Nevada: Bechtel SAIC Company. ACC: MOL.20020819.0126.

169110 BSC 2003. *PWR Assembly End-Effect Reactivity Evaluation.* CAL-UDC-NU-000006 REV 00 Errata 001. Las Vegas, Nevada: Bechtel SAIC Company. ACC: MOL.20010412.0158; DOC.20031014.0007.

172553 BSC 2004. *21-PWR Waste Package with Absorber Plates Loading Curve Evaluation.* CAL-DSU-NU-000006 REV 00C. Las Vegas, Nevada: Bechtel SAIC Company. ACC: DOC.20041220.0002; DOC.20050801.0007.

169982 BSC 2004. *Aqueous Corrosion Rates for Waste Package Materials.* ANL-DSD-MD-000001 REV 01. Las Vegas, Nevada: Bechtel SAIC Company. ACC: DOC.20041012.0003; DOC.20060403.0001.

172201 BSC 2004. *Criticality Potential of Intact DOE SNF Canisters in a Misloaded Dry Waste Package.* CAL-DSD-NU-000008 REV 00A. Las Vegas, Nevada: Bechtel SAIC Company. ACC: DOC.20041004.0008; DOC.20050601.0004; DOC.20050801.0008.

169987 BSC 2004. *CSNF Waste Form Degradation: Summary Abstraction.* ANL-EBS-MD-000015 REV 02. Las Vegas, Nevada: Bechtel SAIC Company. ACC: DOC.20040908.0001; DOC.20050620.0004.

169988 BSC 2004. *Defense HLW Glass Degradation Model.* ANL-EBS-MD-000016 REV 02. Las Vegas, Nevada: Bechtel SAIC Company. ACC: DOC.20041020.0015; DOC.20050922.0002.

172453 BSC 2004. *DSNF and Other Waste Form Degradation Abstraction.* ANL-WIS-MD-000004 REV 04. Las Vegas, Nevada: Bechtel SAIC Company. ACC: DOC.20041201.0007.

177193 BSC 2006. *Dimension and Material Specification Selection for Use in Criticality Analyses.* CAL-DSU-NU-000017 REV 0A. Las Vegas, Nevada: Bechtel SAIC Company. ACC: DOC.20060906.0004.

176911 BSC 2006. *Geochemistry Model Validation Report: Material Degradation and Release Model.* ANL-EBS-GS-000001 REV 01. Las Vegas, Nevada: Bechtel SAIC Company. ACC: DOC.20060901.0009.

109494 Buck, E.C. and Bates, J.K. 1999. "Microanalysis of Colloids and Suspended Particles from Nuclear Waste Glass Alteration." *Applied Geochemistry, 14,* 635-653. New York, New York: Elsevier. TIC: 245946.

181088 Byrne, R.H.; Kump, L.R.; and Cantrell, K.J. 1988. "The Influence of Temperature and pH on Trace Metal Speciation in Seawater." *Marine Chemistry, 25,* 163-181. Amsterdam, The Netherlands: Elsevier. TIC: 259376.

181066 Cantrell, K.J. and Byrne, R.H. 1987. "Temperature Dependence of Europium Carbonate Complexation." *Journal of Solution Chemistry, 16,* (7), 555-566. New York, New York: Plenum Publishing. TIC: 259374.

179642 Carpenter Technology 2003. "Micro-Melt NeutroSorb PLUS Alloys" *Alloy Data.* Wyomissing, Pennsylvania: Carpenter Technology. Accessed August 16, 2006. TIC: 259154. URL: http://cartech.ides.com/datasheet.aspx?&E =232&CK289296&FMT=PRINT.

181429 Carroll, S.A. 1993. "Precipitation of Nd-Ca Carbonate Solid Solution at 25°C." *Geochimica et Cosmochimica Acta, 57,* 3383-3393. New York, New York: Pergamon Press. TIC: 259524.

181082 Cetiner, Z.S.; Wood, S.A.; and Gammons, C.H. 2005. "The Aqueous Geochemistry of the Rare Earth Elements. Part XIV. The Solubility of Rare Earth Element Phosphates from 23 to 150°C." *Chemical Geology, 217,* 147-169. New York, New York: Elsevier. TIC: 259372.

182753 Clark, R.W. 2000. "Office of Civilian Radioactive Waste Management (OCRWM) Quality Assurance (QA) Audit Report EM-ARC-00-17 of the National Spent Nuclear Fuel (NSNF) Program." Letter from R.W. Clark (DOE) to M. Arenaz (DOE/ID), October 5, 2000, OQA:JB:2147, with enclosure. ACC: MOL.20001020.0228; MOL.20001020.0229.

181406 Cook, D.C. 2005. "Spectroscopic Identification of Protective and Non-Protective Corrosion Coatings on Steel Structures in Marine Environments." *Corrosion Science, 47,* 2550-2570. New York, New York: Elsevier. TIC: 259499.

155741 Cooper, G.I. and Cox, G.A. 1994. "A Comparative Study of the Natural and Experimental Corrosion of Poorly Durable Potash-Lime-Silica Glasses." *Scientific Basis for Nuclear Waste Management XVII, Symposium held November 29-December 3, 1993, Boston, Massachusetts.* Barkatt, A. and Van Konynenburg, R.A., eds. *333,* 525-531. Pittsburgh, Pennsylvania: Materials Research Society. TIC: 213541.

156251 Cooper, G.I. and Cox, G.A. 1996. "The Aqueous Corrosion of Potash–Lime–Silica Glass in the Range of 10–250°C." *Applied Geochemistry, 11,* (4), 511-521. Oxford, England: Elsevier. TIC: 250577.

175093 Cordfunke, E.H.P. and Ouweltjes, W. 1988. "Standard Enthalpies of Formation of Uranium Compounds XIV. BaU_2O_7 and $Ba_2U_2O_7$." *Journal of Chemical Thermodynamics, 20,* 236-238. New York, New York: Academic Press. TIC: 257820.

175065 Cornell, R.M. 1988. "The Influence of Some Divalent Cations on the Transformation of Ferrihydrite to More Crystalline Products." *Clay Minerals, 23,* 329-332. London, England: Mineralogical Society. TIC: 257355.

181442 Cornell, R.M. and Giovanoli, R. 1989. "Effect of Cobalt on the Formation of Crystalline Iron Oxides from Ferrihydrite in Alkaline Media." *Clays and Clay Minerals, 37,* (1), 65-70. Bloomington, Indiana: Clay Minerals Society. TIC: 259546.

173037 Cornell, R.M. and Schwertmann, U. 2003. *The Iron Oxides, Structure, Properties, Reactions, Occurrences and Uses.* 2nd Edition. Weinheim, Germany: Wiley-VCH Verlagsgesellschaft. TIC: 257034.

164025 Cornell, R.M.; Giovanoli, R.; and Schneider, W. 1992. "The Effect of Nickel on the Conversion of Amorphous Iron(III) Hydroxide into More Crystalline Iron Oxides in Alkaline Media." *Journal of Chemical Technology and Biotechnology, 53,* (1), 73-79. Oxford, England: Blackwell Scientific Publishing. TIC: 254448.

157545 Cotton, F.A.; Wilkinson, G.; Murillo, C.A.; and Bochmann, M. 1999. *Advanced Inorganic Chemistry.* 6th Edition. New York, New York: John Wiley & Sons. TIC: 245931.

182747 Cowart, C.G. and Notz, K.J. 1992. *Peer Review Report for Revision 1 of DOE/RW-0184, "Characteristics of Potential Repository Wastes."* ORNL/M-2095. Oak Ridge, Tennessee: Oak Ridge National Laboratory. ACC: HQO.19930402.0007.

155742 Cox, G.A. and Ford, B.A. 1993. "The Long-Term Corrosion of Glass by Ground-Water." *Journal of Materials Science, 28,* (20), 5637-5647. London, England: Chapman & Hall. TIC: 245170.

181195 Crammond, N.J. and Currie, R.J. 1993. "Survey of Condition of Precast High-Alumina Cement Concrete Components in Internal Locations in 14 Existing Buildings." *Magazine of Concrete Research, 45,* (165), 275-279. London, England: Thomas Telford. TIC: 259449.

104115 CRWMS M&O (Civilian Radioactive Waste Management System Management & Operating Contractor) 1996. *Waste Package Filler Material Testing Report.* BBA000000-01717-2500-00008 REV 02. Las Vegas, Nevada: CRWMS M&O. ACC: MOL.19970121.0004.

102824 CRWMS M&O 1997. *Criticality Evaluation of Degraded Internal Configurations for the PWR AUCF WP Designs.* BBA000000-01717-0200-00056 REV 00. Las Vegas, Nevada: CRWMS M&O. ACC: MOL.19971231.0251.

106278 CRWMS M&O 1998. *Software Qualification Report (SQR) Addendum to Existing LLNL Document UCRL-MA-110662 PT IV: Implementation of a Solid-Centered Flow-Through Mode for EQ6 Version 7.2B.* CSCI: UCRL-MA-110662 V 7.2b. SCR: LSCR198. Las Vegas, Nevada: CRWMS M&O. ACC: MOL.19990920.0169.

125206 CRWMS M&O 1999. *Evaluation of Codisposal Viability for MOX (FFTF) DOE-Owned Fuel.* BBA000000-01717-5705-00023 REV 00. Las Vegas, Nevada: CRWMS M&O. ACC: MOL.19991014.0235.

111447 CRWMS M&O 1999. *Volumes, Masses, and Surface Areas for Shippingport LWBR Spent Nuclear Fuel in aDOE SNF Canister.* BBA000000-01717-0210-00056 REV 00. Las Vegas, Nevada: CRWMS M&O. ACC: MOL.19991027.0143.

151243 CRWMS M&O 2000. *EQ6 Calculation for Chemical Degradation of Shippingport LWBR (Th/U Oxide) Spent Nuclear Fuel Waste Packages.* CAL-EDC-MD-000008 REV 00. Las Vegas, Nevada: CRWMS M&O. ACC: MOL.20000926.0295.

153263 CRWMS M&O 2001. *EQ6 Calculations for Chemical Degradation of N Reactor (U-metal) Spent Nuclear Fuel Waste Packages.* CAL-EDC-MD-000010 REV 00. Las Vegas, Nevada: CRWMS M&O. ACC: MOL.20010227.0017.

154194 CRWMS M&O 2001. *Evaluation of Codisposal Viability for U-Metal (N Reactor) DOE-Owned Fuel.* TDR-EDC-NU-000004 REV 00. Las Vegas, Nevada: CRWMS M&O. ACC: MOL.20010314.0004.

175057 CTDP (Common Thermodynamic Database Project) 2004. "Barium." *Common Thermodynamic Database Project.* Paris, France: Common Thermodynamic Database Project. Accessed October 7, 2005. ACC: MOL.20051010.0167. URL: http://ctdp.ensmp.fr/.

181416 Cubicciotti, D. 1993. "Potential-pH Diagrams for Alloy-Water Systems Under LWR Conditions." *Journal of Nuclear Materials, 201,* 176-183. New York, New York: Elsevier. TIC: 259509.

130693 Cunnane, J.C.; Bates, J.K.; Bradley, C.R.; Buck, E.C.; Ebert, W.L.; Feng, X.; Mazer, J.J.; Wronkiewicz, D.J.; Sproull, J.; Bourcier, W.L.; McGrail, B.P.; and Altenhofen, M.K. 1994. *High-Level Waste Borosilicate Glass: A Compendium of Corrosion Characteristics, Volume 2.* DOE-EM-0177. Washington, D.C.: U.S. Department of Energy. TIC: 242675.

178971 Da Cunha Belo, M.; Walls, M.; Hakiki, N.E.; Corset, J.; Picquenard, E.; Sagon, G.; and Noel, D. 1998. "Composition, Structure, and Properties of the Oxide Films Formed on the Stainless Steel 316L in a Primary Type PWR Environment." *Corrosion Science*, 40, (2/3), 447-463. New York, New York: Pergamon. TIC: 259108.

102773 Deer, W.A.; Howie, R.A.; and Zussman, J. 1966. *An Introduction to the Rock-Forming Minerals.* New York, New York: John Wiley & Sons. TIC: 245492.

163286 Deer, W.A.; Howie, R.A.; and Zussman, J. 1992. *An Introduction to the Rock-Forming Minerals.* 2nd Edition. New York, New York: Prentice Hall. TIC: 221918.

102773 Deer, W.A.; Howie, R.A.; and Zussman, J. 1966. *An Introduction to the Rock-Forming Minerals.* New York, New York: John Wiley & Sons. TIC: 245492.

181430 Delichere, P.; Hugot-Le Goff, A.; and Joiret, S. 1988. "Study of Thin Corrosion Films by In Situ Raman Spectroscopy Combined with Direct Observation of Nuclear Reactions." *Surface and Interface Analysis, 12,* 419-423. New York, New York: John Wiley & Sons. TIC: 259514.

159374 Dixon, J.B. 1995. "Kaolin and Serpentine Group Minerals." Chapter 10 of *Minerals in Soil Environments.* 2nd Edition. Dixon, J.B. and Weed, S.B., eds. SSSA Book Series, No. 1. Madison, Wisconsin: Soil Science Society of America. TIC: 237222.

102812 DOE (U.S. Department of Energy) 1992. *Characteristics of Potential Repository Wastes.* DOE/RW-0184-R1. Volume 1. Washington, D.C.: U.S. Department of Energy, Office of Civilian Radioactive Waste Management. ACC: HQO.19920827.0001.

150095 DOE 2000. *N Reactor (U-Metal) Fuel Characteristics for Disposal Criticality Analysis.* DOE/SNF/REP-056, Rev. 0. Washington, D.C.: U.S. Department of Energy, Office of Environmental Management. TIC: 247956.

152658 DOE 2000. *Review of Oxidation Rates ofDOE Spent Nuclear Fuel, Part 1: Metallic Fuel.* DOE/SNF/REP-054, Rev. 0. Washington, D.C.: U.S. Department of Energy. TIC: 248978.

158405 DOE 2002. *DOE Spent Nuclear Fuel Information in Support of TSPA-SR.* DOE/SNF/REP-047, Rev. 2. Idaho Falls, Idaho: U.S. Department of Energy, Idaho Operations Office. TIC: 252089.

161752 DOE 2002. *SNF Canister Characteristics for Criticality Analysis of a Dual Canister/Waste Package Disposal Strategy.* DOE/SNF/REP-074, Rev. 0. Idaho Falls, Idaho: U.S. Department of Energy. TIC: 253869.

166027 DOE 2003. *Review of Oxidation Rates ofDOE Spent Nuclear Fuel Part 2. Nonmetallic Fuel.* DOE/SNF/REP-068, Rev. 0. Idaho Falls, Idaho: U.S. Department of Energy, Idaho Operations Office. ACC: DOC.20030905.0009.

164970 DOE 2003. *TMI Fuel Characteristics for Disposal Criticality Analysis.* DOE/SNF/REP-084, Rev. 0. Idaho Falls, Idaho: U.S. Department of Energy, Idaho Operations Office. ACC: MOL.20031013.0388.

168434 DOE 2004. *Interim Report on the Corrosion Performance of a Neutron Absorbing Ni-Cr-Mo-Gd Alloy.* DOE/SNF/REP-086, Rev. 0. Idaho Falls, Idaho: U.S. Department of Energy, Idaho Operations Office. ACC: DOC.20040412.0001.

180678 DOE 2005. *User Information for: EQ3/6 V8.1.* Document ID: 10813-UID-8.1-00. Las Vegas, Nevada: U.S. Department of Energy, Office of Repository Development. ACC: MOL.20050509.0228.

182051 DOE 2007. *Quality Assurance Requirements and Description.* DOE/RW-0333P, Rev. 19. Washington, D.C.: U.S. Department of Energy, Office of Civilian Radioactive Waste Management. ACC: DOC.20070717.0006.

169277 Doner, H.E. and Lynn, W.C. 1995. "Carbonate, Halide, Sulfate, and Sulfide Minerals." Chapter 6 of *Minerals in Soil Environments.* 2nd Edition. Dixon, J.B. and Weed, S.B., eds. SSSA Book Series, No. 1. Madison, Wisconsin: Soil Science Society of America. TIC: 237222.

100725 Drever, J.I. 1982. *The Geochemistry of Natural Waters.* Englewood Cliffs, New Jersey: Prentice Hall. TIC: 240706.

181194 Dunster, A.M.; Bigland, D.J.; and Holton, I.R. 2000. "Rates of Carbonation and Reinforcement Corrosion in High Alumina Cement Concrete." *Magazine of Concrete Research, 52,* (6), 433–441. London, England: Thomas Telford. TIC: 259448.

108015 Efurd, D.W.; Runde, W.; Banar, J.C.; Janecky, D.R.; Kaszuba, J.P.; Palmer, P.D.; Roensch, F.R.; and Tait, C.D. 1998. "Neptunium and Plutonium Solubilities in a Yucca Mountain Groundwater." *Environmental Science & Technology, 32,* (24), 3893-3900. Easton, Pennsylvania: American Chemical Society. TIC: 243857.

161749 Ewing, R.C. and Haaker, R.F. 1979. *Naturally Occurring Glasses: Analogues for Radioactive Waste Forms.* PNL-2776. Richland, Washington: Pacific Northwest Laboratory. ACC: NNA.19900315.0277.

179902 Fellinger, T.L. and Bibler, N.E. 2000. *Technical and QA Plan: Characterization of DWPF Radioactive Glass Pour Stream Samples from Macro Batch 2 (U).* WSRC-RP-99-00832, Rev.0. Aiken, South Carolina: Westinghouse Savannah River Company. TIC: 259654.

145442 Finch, R.J. and Murakami, T. 1999. "Systematics and Paragenesis of Uranium Minerals." Chapter 3 of *Uranium: Mineralogy, Geochemistry and the Environment.* Burns, P.C. and Finch, R.J., eds. Reviews in Mineralogy Volume 38. Washington, D.C.: Mineralogical Society of America. TIC: 247121.

171745 Fix, D.V.; Estill, J.C.; Wong, L.L.; and Rebak, R.B. 2004. "General and Localized Corrosion of Austenitic and Borated Stainless Steels in Simulated Concentrated Ground Waters." *Transportation, Storage, and Disposal of Radioactive Materials, The 2004 ASME/JSME Pressure Vessels and Piping Conference, San Diego, California, USA, July 25-29, 2004.* Smith, A.C. and Hafner, R.S., eds. PVP-Vol. 483. Pages 121-130. New York, New York: American Society of Mechanical Engineers. TIC: 256542.

159344 Fox, M.J. and McCright, R.D. 1983. *An Overview of Low Temperature Sensitization.* UCRL-15619. Livermore, California: Lawrence Livermore National Laboratory. ACC: HQS.19880517.2438.

143296 Furet, N.R.; Haces, C.; Corvo, F.; Diaz, C.; and Gomez, J. 1990. "Corrosion Rate Determination Using Fe-57 Mössbauer Spectra of Corrosion Products of Steel." *Hyperfine Interactions, 57,* 1833-1838. Basel, Switzerland: J.C. Baltzer, A.G. Scientific Publishing Company. TIC: 240940.

172360 Gaines, R.V.; Skinner, H.C.W.; Foord, E.E.; Mason, B.; and Rosenzweig, A. 1997. *Dana's New Mineralogy, The System of Mineralogy of James Dwight Dana and Edward Salisbury Dana.* 8th Edition. New York, New York: John Wiley & Sons. TIC: 256455.

179957 Gislason, S.R. and Eugster, H.P. 1987. "Meteoric Water-Basalt Interactions. II: A Field Study in N.E. Iceland." *Geochimica et Cosmochimica Acta, 51,* 2841-2855. New York, New York: Pergamon. TIC: 259231.

182752 Golan, P.M. 2004. "Issuance of Audit Report No. 04-DOE-AU-004 for the Department of Energy Idaho Operations Office Spent Nuclear Fuel Program." Memorandum from P.M. Golan (DOE) to E.D. Sellers (DOE/ID), September 23, 2004, with attachment. ACC: MOL.20041214.0129; MOL.20041214.0130.

182754 Golan, P.M. 2005. "Issuance of Audit Report No. 05-DOE-AU-001 for the Department of Energy Idaho Operations Office National Spent Nuclear Fuel Program." Memorandum from P.M. Golan (DOE) to E.D. Sellers (DOE/ID), March 29, 2005, with attachment. ACC: MOL.20050502.0186; MOL.20050502.0187.

158382 Goldberg, S.; Forster, H.S.; and Godfrey, C.L. 1996. "Molybdenum Adsorption on Oxides, Clay Minerals, and Soils." *Soil Science Society of America Journal, 60,* 425-432. Madison, Wisconsin: Soil Science Society of America. TIC: 252573.

181412 Golden, D.C.; Ming, D.W.; and Zolensky, M.E. 1995. "Chemistry and Mineralogy of Oxidation Products on the Surface of the Hoba Nickel-Iron Meteorite." *Meteoritics, 30,* 418-422. Fayetteville, Arkansas: Meteoritical Society. TIC: 259505.

181593 Goldschmidt, H.J. 1971. "Effect of Boron Additions to Austenitic Stainless Steels Part II Solubility of Boron in 18%Cr, 15%Ni Austenitic Steel." *Journal of the Iron and Steel Institute,* Pages 910-911. London, England: Iron and Steel Institute. TIC: 259235.

109691 Gray, W.J. and Einziger, R.E. 1998. *Initial Results from Dissolution Rate Testing of N-Reactor Spent Fuel Over a Range of Potential Geologic Repository Aqueous Conditions.* DOE/SNF/REP-022, Rev. 0. Washington, D.C.: U.S. Department of Energy. TIC: 245380.

101671 Grenthe, I.; Fuger, J.; Konings, R.J.M.; Lemire, R.J.; Muller, A.B.; Nguyen-Trung, C.; and Wanner, H. 1992. *Chemical Thermodynamics of Uranium.* Volume 1 of *Chemical Thermodynamics.* Wanner, H. and Forest, I., eds. Amsterdam, The Netherlands: North-Holland Publishing Company. TIC: 224074.

168382 Guillaumont, R.; Fanghänel, T.; Fuger, J.; Grenthe, I.; Neck, V.; Palmer, D.A.; and Rand, M.H. 2003. *Update on the Chemical Thermodynamics of Uranium, Neptunium, Plutonium, Americium and Technetium.* Mompean, F.J.; Illemassene, M.; Domenech-Orti, C.; and Ben Said, K., eds. Chemical Thermodynamics 5. Amsterdam, The Netherlands: Elsevier. TIC: 255230.

181597 He, J.Y.; Soliman, S.E.; Baratta, A.J.; and Balliett, T.A. 2000. "Fracture Mechanism of Borated Stainless Steel." *Nuclear Technology, 130,* (2), 218-225. La Grange Park, Illinois: American Nuclear Society. TIC: 259236.

169212 Hover, V.C. and Ashley, G.M. 2003. "Geochemical Signatures of Paleodepositional and Diagenetic Environments: A STEM/AEM Study of Authigenic Clay Minerals from an Arid Rift Basin, Olduvai Gorge, Tanzania." *Clays and Clay Minerals, 51,* (3), 231-251. Aurora, Colorado: Clay Minerals Society. TIC: 256063.

105875 Hsu, P.H. 1995. "Aluminum Hydroxides and Oxyhydroxides." Chapter 7 of *Minerals in Soil Environments.* 2nd Edition. Dixon, J.B. and Weed, S.B., eds. SSSA Book Series, No. 1. Madison, Wisconsin: Soil Science Society of America. TIC: 237222.

169305 Huang, P.M. 1995. "Feldspars, Olivines, Pyroxenes, and Amphiboles." Chapter 20 of *Minerals in Soil Environments.* 2nd Edition. Dixon, J.B. and Weed, S.B., eds. SSSA Book Series, No. 1. Madison, Wisconsin: Soil Science Society of America. TIC: 237222.

175241 Hull, L.; Pace, M.; Lessing, P.; Rogers, R.; Mizia, R.; Propp, A.; Shaber, E.; and Taylor, L. 2000. *Advanced Neutron Absorbers forDOE SNF Standardized Canister-Feasibility Study.* DOE/SNF/REP-057, Rev. 0. Idaho Falls, Idaho: U.S. Department of Energy, Idaho Operations Office. ACC: MOL.20051021.0173.

158820 INEEL (Idaho National Engineering and Environmental Laboratory) 2002. *FFTF (MOX) Fuel Characteristics for Disposal Criticality Analysis.* DOE/SNF/REP-032, Rev. 1. Idaho Falls, Idaho: U.S. Department of Energy, Idaho National Operations Office. TIC: 252933.

181337 Iveson, S.M.; Holt, S.; and Biggs, S. 2000. "Contact Angle Measurements of Iron Ore Powders." *Colloids and Surfaces A: Physicochemical and Engineering Aspects, 166,* 203-214. New York, New York: Elsevier. TIC: 259487.

181338 Janczuk, B. and Zdziennicka, A. 1994. "A Study on the Components of Surface Free Energy of Quartz from Contact Angle Measurements." *Journal of Materials Science, 29,* 3559-3564. New York, New York: Chapman & Hall. TIC: 259486.

125291 Johnson, A.B., Jr. and Francis, B. 1980. *Durability of Metals from Archaeological Objects, Metal Meteorites, and Native Metals.* PNL-3198. Richland, Washington: Pacific Northwest Laboratory. TIC: 229619.

175705 Johnson, L.H. and Shoesmith, D.W. 1988. "Spent Fuel." Chapter 11 of *Radioactive Waste Forms for the Future.* Lutze, W. and Ewing, R.C., eds. New York, New York: Elsevier. TIC: 103525.

147467 Jonasson, R.G.; Bancroft, G.M.; and Nesbitt, H.W. 1985. "Solubilities of Some Hydrous REE Phosphates with Implications for Diagenesis and Sea Water Concentrations." *Geochimica et Cosmochimica Acta, 49,* 2133-2139. New York, New York: Pergamon Press. TIC: 236998.

182348 Kain, V.; Shinde, S.S.; Gadiyar H.S 1994. "Mechanism of Improved Corrosion Resistance of Type 304L Stainless Steel, Nitric Acid Grade, in Nitric Acid Environments." *Journal of Materials Engineering and Performance, 3,* (6), 699-705. Materials Park, Ohio: ASM International. TIC: 259661.

161606 Kerr, P.F. 1977. *Optical Mineralogy.* 4th Edition. New York, New York: McGraw-Hill. TIC: 252886.

105168 Kim, Y-J. 1999. "Analysis of Oxide Film Formed on Type 304 Stainless Steel in 288°C Water Containing Oxygen, Hydrogen, and Hydrogen Peroxide." *Corrosion*, *55*, (1), 81-88. Houston, Texas: NACE International. TIC: 245184.

181414 Kimura, M.; Kihira, H.; Ohta, N.; Hashimoto, M.; and Senuma, T. 2005. "Control of $Fe(O,OH)_6$ Nano-Network Structures of Rust for High Atmospheric-Corrosion Resistance." *Corrosion Science, 47,* 2499-2509. New York, New York: Elsevier. TIC: 259507.

105907 Klein, C. and Hurlbut, C.S., Jr. 1985. *Manual of Mineralogy.* 20th Edition. New York, New York: John Wiley & Sons. TIC: 242818.

124293 Klein, C. and Hurlbut, C.S., Jr. 1999. *Manual of Mineralogy.* 21st Edition, Revised. New York, New York: John Wiley & Sons. TIC: 246258.

175706 Landström, O. and Tullborg, E.-L. 1995. *Interactions of Trace Elements with Fracture Filling Minerals from the Äspö Hard Rock Laboratory.* SKB TR-95-13. Stockholm, Sweden: Swedish Nuclear Fuel and Waste Management Company. TIC: 221729.

100051 Langmuir, D. 1997. *Aqueous Environmental Geochemistry.* Upper Saddle River, New Jersey: Prentice Hall. TIC: 237107.

131202 Lide, D.R., ed. 1991. *CRC Handbook of Chemistry and Physics.* 72nd Edition. Boca Raton, Florida: CRC Press. TIC: 3595.

178081 Lide, D.R., ed. 2006. *CRC Handbook of Chemistry and Physics.* 87th Edition. Boca Raton, Florida: CRC Press. TIC: 258634.

181428 Lin, M.-C.; Lin, S-C.; Lee, T-H.; and Huang, H-H. 2006. "Surface Analysis and Corrosion Resistance of Different Stainless Steel Orthodontic Brackets in Artificial Saliva." *Angle Orthodontist, 76,* (2), 322-329. Appleton, Wisconsin: Edward H. Angle Society of Orthodontists. TIC: 259511.

153210 Lindsay, W.L. 2001. *Chemical Equilibria in Soils.* 1st Edition. Caldwell, New Jersey: Blackburn Press. TIC: 5873.

169289 Lindsay, W.L.; Vlek, P.L.G.; and Chien, S.H. 1995. "Phosphate Minerals." Chapter 22 of *Minerals in Soil Environments.* 2nd Edition. Dixon, J.B. and Weed, S.B., eds. SSSA Book Series, No. 1. Madison, Wisconsin: Soil Science Society of America. TIC: 237222.

182177 Lister, T.; Mizia, R.; Erickson, A.; and Trowbridge, T. 2007. *Electrochemical Corrosion Testing of Neutron Absorber Materials.* INL/EXT-06-11772, Rev. 1. Idaho Falls, Idaho: Idaho National Laboratory. ACC: LLR.20070731.0149.

168999 Loo, H.H.; MacKay, N.S.; and Wheatley, P.D. 2004. *AdditionalDOE Spent Nuclear Fuel Information in Support of TSPA-LA Analysis.* DOE/SNF/REP-081, Rev. 0. Idaho Falls, Idaho: U.S. Department of Energy,DOE Idaho Operations Office. ACC: DOC.20040202.0007.

154076 Lynch, C.T., ed. 1989. *Practical Handbook of Materials Science.* Boca Raton, Florida: CRC Press. TIC: 240577.

125331 Mahan, B.H. 1975. *University Chemistry.* 3rd Edition. Reading, Massachusetts: Addison-Wesley Publishing. TIC: 240721.

181409 Maurice, V.; Yang, W.P.; and Marcus, P. 1998. "X-Ray Photoelectron Spectroscopy and Scanning Tunneling Microscopy Study of Passive Films Formed on (100) Fe-18Cr-13Ni Single-Crystal Surfaces." *Journal of the Electrochemical Society, 145,* (3), 909-920. Pennington, New Jersey: Electrochemical Society. TIC: 259502.

180824 Mayo, W.E. 1997. "Predicting IGSCC/IGA Susceptibility of Ni-Cr-Fe Alloys by Modeling of Grain Boundary Chromium Depletion." *Materials Science and Engineering, A232,* 129-139. New York, New York: Elsevier. TIC: 259188.

101726 McEachern, R.J. and Taylor, P. 1997. *A Review of the Oxidation of Uranium Dioxide at Temperatures Below 400°C.* AECL-11335. Pinawa, Manitoba, Canada: Atomic Energy of Canada Limited. TIC: 232575.

113270 McEachern, R.J. and Taylor, P. 1998. "A Review of the Oxidation of Uranium Dioxide at Temperatures Below 400°C." *Journal of Nuclear Material, 254,* 87-121. Amsterdam, The Netherlands: Elsevier. TIC: 246427.

171053 Menard, O.; Advocat, T.; Ambrosi, J.P.; and Michard, A. 1998. "Behavior of Actinides (Th, U, Np and Pu) and Rare Earths (La, Ce and Nd) During Aqueous Leaching of a Nuclear Waste Glass Under Geological Disposal Conditions." *Applied Geochemistry, 13,* 105-126. New York, New York: Pergamon. TIC: 256470.

105911 Milnes, A.R. and Fitzpatrick, R.W. 1995. "Titanium and Zirconium Minerals." Chapter 23 of *Minerals in Soil Environments.* 2nd Edition. Dixon, J.B. and Weed, S.B., eds. SSSA Book Series, No. 1. Madison, Wisconsin: Soil Science Society of America. TIC: 237222.

156843 Ming, D.W. and Mumpton, F.A. 1995. "Zeolites in Soils." Chapter 18 of *Minerals in Soil Environments.* 2nd Edition. Dixon, J.B. and Weed, S.B., eds. SSSA Book Series, No. 1. Madison, Wisconsin: Soil Science Society of America. TIC: 237222.

179295 Moreno, D.A.; Molina, B.; Ranninger, C.; Montero, F.; and Izquierdo, J. 2004. "Microstructural Characterization and Pitting Corrosion Behavior of UNS S30466 Borated Stainless Steel." *Corrosion, 60,* (6), 573-583. Houston, Texas: NACE International. TIC: 258529.

178395 Moroni, L.P. and Glasser, F.P. 1995. "Reactions Between Cement Components and U(VI) Oxide." *Waste Management, 15,* (3), 243-254. New York, New York: Pergamon. TIC: 258804.

175703 Murakami, T.; Isobe, H.; Nagano, T.; and Nakashima, S. 1992. "Uranium Redistribution and Fixation During Chlorite Weathering at Koongarra, Australia." *Scientific Basis for Nuclear Waste Management XV, Symposium held November 4-7, 1991, Strasbourg, France.* Sombret, C.G., ed. *257,* 473-480. Pittsburgh, Pennsylvania: Materials Research Society. TIC: 204618.

175700 Murakami, T.; Sato, T.; Ohnuki, T.; and Isobe, H. 2005. "Field Evidence for Uranium Nanocrystallization and its Implications for Uranium Transport." *Chemical Geology, 221,* 117-126. New York, New York: Elsevier. TIC: 257883.

163274 NRC (U.S. Nuclear Regulatory Commission) 2003. *Yucca Mountain Review Plan, Final Report.* NUREG-1804, Rev. 2. Washington, D.C.: U.S. Nuclear Regulatory Commission, Office of Nuclear Material Safety and Safeguards. TIC: 254568.

159027 OECD (Organisation for Economic Co-operation and Development, Nuclear Energy Agency) 2001. *Chemical Thermodynamics of Neptunium and Plutonium.* Volume 4 of *Chemical Thermodynamics.* New York, New York: Elsevier. TIC: 209037.

113277 O'Hare, P.A.G.; Lewis, B.M.; and Nguyen, S.N. 1988. "Thermochemistry of Uranium Compounds, XVII. Standard Molar Enthalpy of Formation at 298.15 K of Dehydrated Schoepite U03.0.9H2O. Thermodynamics of (Schoepite + Dehydrated Schoepite + Water)." *Journal of Chemical Thermodynamics, 20,* 1287-1296. New York, New York: Academic Press. TIC: 246154.

163604 Palache, C.; Berman, H.; and Frondel, C. 1944. *Elements, Sulfides, Sulfosalts, Oxides.* Volume I of *The System of Mineralogy of James Dwight Dana and Edward Salisbury Dana, Yale University 1837–1892.* 7th Edition. New York, New York: John Wiley & Sons. TIC: 209331.

162280 Palache, C.; Berman, H.; and Frondel, C. 1951. *Halides, Nitrates, Borates, Carbonates, Sulfates, Phosphates, Arsenates, Tungstates, Molybdates, Etc.* Volume II of *The System of Mineralogy of James Dwight Dana and Edward Salisbury Dana, Yale University 1837–1892.* 7th Edition. New York, New York: John Wiley & Sons. TIC: 209332.

181065 Pankratz, L.B. 1982. "Gd, Gadolinium." *Thermodynamic Properties of Elements and Oxides.* Bulletin 672. Pages 165-168. Washington, D. C.: U.S. Government Printing Office. ACC: LLR.20070522.0016.

159511 Parkhurst, D.L. and Appelo, C.A.J. 1999. *User's Guide to PHREEQC (Version 2)—A Computer Program for Speciation, Batch-Reaction, One-Dimensional Transport, and Inverse Geochemical Calculations.* Water-Resources Investigations Report 99-4259. Denver, Colorado: U.S. Geological Survey. TIC: 253046.

103896 Parrington, J.R.; Knox, H.D.; Breneman, S.L.; Baum, E.M.; and Feiner, F. 1996. *Nuclides and Isotopes, Chart of the Nuclides.* 15th Edition. San Jose, California: General Electric Company and KAPL, Inc. TIC: 233705.

100486 Pearcy, E.C.; Prikryl, J.D.; Murphy, W.M.; and Leslie, B.W. 1994. "Alteration of Uraninite from the Nopal I Deposit, Pena Blanca District, Chihuahua, Mexico, Compared to Degradation of Spent Nuclear Fuel in the Proposed U.S. High-Level Nuclear Waste Repository at Yucca Mountain, Nevada." *Applied Geochemistry, 9,* 713-732. New York, New York: Elsevier. TIC: 236934.

159329 Pednekar, S.P. 1987. *Final Report on Corrosion of Carbon Steel in Aqueous Environments at Temperatures Below Boiling - A Literature Review to Electric Power Research Institute, February 24, 1987.* Columbus, Ohio: Battelle, Columbus Division. TIC: 224492.

181083 Poitrasson, F.; Oelkers, E.; Schott, J.; and Montel, J. 2004. "Experimental Determination of Synthetic $NdPO_4$ Monazite End-Member Solubility in Water from 21°C to 300°C: Implications for Rare Earth Element Mobility in Crustal Fluids." *Geochimica et Cosmochimica Acta, 68,* (10), 2207-2221. New York, New York: Pergamon. TIC: 259373.

181415 Post, J.E. and Buchwald, V.F. 1991. "Crystal Structure Refinement of Akaganéite." *American Mineralogist, 76,* 272-277. Washington, D.C.: Mineralogical Society of America. TIC: 259508.

172869 Praga, A.N. 1998. *MCO Loading and Cask Loadout Technical Manual.* HNF-2169, Rev. 0. Richland, Washington: Duke Engineering and Services Hanford. TIC: 253692.

155635 Punatar, M.K. 2001. *Summary Report of Commercial Reactor Criticality Data for Crystal River Unit 3.* TDR-UDC-NU-000001 REV 02. Las Vegas, Nevada: Bechtel SAIC Company. ACC: MOL.20010702.0087.

165482 Radulescu, H.; Moscalu, D.; and Saglam, M. 2004.DOE *SNF Phase I and II Summary Report.* TDR-DSD-MD-000001 REV 00. Las Vegas, Nevada: Bechtel SAIC Company. ACC: DOC.20040303.0005.

112060 Rai, D. and Ryan, J.L. 1982. "Crystallinity and Solubility of Pu(IV) Oxide and Hydrous Oxide in Aged Aqueous Suspensions." *Radiochimica Acta, 30,* 213-216. Munchen, Germany: R. Oldenbourg Verlag. TIC: 219107.

151313 Rard, J.A. 1985. "Chemistry and Thermodynamics of Ruthenium and Some of Its Inorganic Compounds and Aqueous Species." *Chemical Reviews, 85,* (1), 1-39. Washington, D.C.: American Chemical Society. TIC: 248565.

157912 Rard, J.A.; Rand, M.H.; Anderegg, G.; and Wanner, H. 1999. *Chemical Thermodynamics of Technetium.* Sandino, M.C.A., and Östhols, E., eds. Chemical Thermodynamics 3. Amsterdam, The Netherlands: Elsevier. TIC: 247228.

150765 Reamer, C.W. 2000. "Safety Evaluation Report for Disposal Criticality Analysis Methodology Topical Report, Revision 0." Letter from C.W. Reamer (NRC) to S.J. Brocoum (DOE/YMSCO), June 26, 2000, with enclosure. ACC: MOL.20000919.0157.

155464 Reamer, C.W. and Williams, D.R. 2000. Summary Highlights of NRC/DOE Technical Exchange and Management Meeting on Subissues Related to Criticality. Meeting held October 23-24, 2000, Las Vegas, Nevada. Washington, D.C.: U.S. Nuclear Regulatory Commission. ACC: MOL.20001208.0097; MOL.20001208.0098; MOL.20001208.0099; MOL.20001208.0100; MOL.20001208.0101; MOL.20001208.0102; MOL.20001208.0103; MOL.20001208.0104; MOL.20001208.0105; MOL.20001208.0106; MOL.20001208.0107; MOL.20001208.0108; MOL.20001208.0109; MOL.20001208.0110.

162536 Roberts, K.E.; Wolery, T.J.; Atkins-Duffin, C.E.; Prussin, T.G.; Allen, P.G.; Bucher, J.J.; Shuh, D.K.; Finch, R.J.; and Prussin, S.G. 2003. "Precipitation of Crystalline Neptunium Dioxide from Near-Neutral Aqueous Solution." *Radiochimica Acta, 91,* (2), 87-92. München, Germany: Oldenbourg Wissenschaftsverlag. TIC: 254035.

107105 Roberts, W.L.; Campbell, T.J.; and Rapp, G.R., Jr. 1990. *Encyclopedia of Minerals.* 2nd Edition. New York, New York: Van Nostrand Reinhold. TIC: 242976.

182751 Roberson, J.H. 2004. "Issuance of Audit Report No. 04-DOE-AU-001 for the Department of Energy Idaho Operations Office National Spent Nuclear Fuel Program." Memorandum from J.H. Roberson (DOE) to E. Sellers (DOE/ID), May 21, 2004, with attachment. ACC: HQO.20040630.0014; HQO.20040630.0015.

144800 Runde, W. 1999. "Letter Report on Plutonium Thermodynamic Database." Letter from W. Runde (LANL) to P. Dixon (LANL), August 1, 1999, with attachments. ACC: MOL.19991214.0624.

113307 Sandino, A. 1991. *Processes Affecting the Mobility of Uranium in Natural Waters.* Ph.D. thesis. Stockholm, Sweden: Royal Institute of Technology. TIC: 246941.

144629 Schwertmann, U. and Cornell, R.M. 1991. *Iron Oxides in the Laboratory: Preparation and Characterization.* New York, New York: VCH Publishers. TIC: 237942.

105959 Schwertmann, U. and Taylor, R.M. 1995. "Iron Oxides." Chapter 8 of *Minerals in Soil Environments.* 2nd Edition. Dixon, J.B. and Weed, S.B., eds. SSSA Book Series, No. 1. Madison, Wisconsin: Soil Science Society of America. TIC: 237222.

175105 Sheppard, R.A. and Gude, A.J. 1969. "Authigenic Fluorite in Pliocene Lacustrine Rocks Near Rome, Malheur County, Oregon." *Geological Survey Research 1969, Chapter D.* Geological Survey Professional Paper 650-D. Pages D69-D74. Washington, D.C.: U.S. Government Printing Office. ACC: MOL.20060306.0106.

180823 Shimada, M.; Kokawa, H.; Wang, Z.J.; Sato, Y.S.; and Karibe, I. 2002. "Optimization of Grain Boundary Character Distribution for Intergranular Corrosion Resistant 304 Stainless Steel by Twin-Induced Grain Boundary Engineering." *Acta Materialia, 50,* 2331-2341. New York, New York: Pergamon. TIC: 259187.

169280 Singer, A. 1995. "Palygorskite and Sepiolite Group Minerals." Chapter 17 of *Minerals in Soil Environments.* 2nd Edition. Dixon, J.B. and Weed, S.B., eds. SSSA Book Series, No. 1. Madison, Wisconsin: Soil Science Society of America. TIC: 237222.

127382 Smith, R.M. and Martell, A.E. 1976. *Inorganic Complexes.* Volume 4 of *Critical Stability Constants.* New York, New York: Plenum Press. TIC: 224070.

179452 SNL (Sandia National Laboratories) 2006. *Technical Work Plan for: In-Package Geochemistry for Criticality Evaluations.* TWP-EBS-MD-000014 REV 05. Las Vegas, Nevada: Sandia National Laboratories. ACC: DOC.20070102.0001.

177430 SNL 2007. *Dike/Drift Interactions.* MDL-MGR-GS-000005 REV 02. Las Vegas, Nevada: Sandia National Laboratories.

177418 SNL 2007. *Dissolved Concentration Limits of Elements with Radioactive Isotopes.* ANL-WIS-MD-000010 REV 06. Las Vegas, Nevada: Sandia National Laboratory.

177407 SNL 2007. *EBS Radionuclide Transport Abstraction.* ANL-WIS-PA-000001 REV 03. Las Vegas, Nevada: Sandia National Laboratories.

177412 SNL 2007. *Engineered Barrier System: Physical and Chemical Environment.* ANL-EBS-MD-000033 REV 06. Las Vegas, Nevada: Sandia National Laboratories. ACC: DOC.20070907.0003.

178519 SNL 2007. *General Corrosion and Localized Corrosion of Waste Package Outer Barrier.* ANL-EBS-MD-000003 REV 03. Las Vegas, Nevada: Sandia National Laboratories. ACC: DOC.20070730.0003; DOC.20070807.0007.

181395 SNL 2007. *Geochemistry Model Validation Report: External Accumulation Model.* ANL-EBS-GS-000001 REV 01 AD 01. Las Vegas, Nevada: Sandia National Laboratories.

181648 SNL 2007. *In-Drift Natural Convection and Condensation.* MDL-EBS-MD-000001 REV 00, AD 01. Las Vegas, Nevada: Sandia National Laboratories. ACC: DOC.20041025.0006; DOC.20050330.0001; DOC.20051122.0005.

180506 SNL 2007. *In-Package Chemistry Abstraction.* ANL-EBS-MD-000037 REV 04 ADD 01. Las Vegas, Nevada: Sandia National Laboratories. ACC: DOC.20050714.0003; DOC.20051130.0007.

177409 SNL 2007. *Qualification of Thermodynamic Data for Geochemical Modeling of Mineral-Water Interactions in Dilute Systems.* ANL-WIS-GS-000003 REV 01. Las Vegas, Nevada: Sandia National Laboratories. ACC: DOC.20070619.0007.

176828 SNL 2007. *Seismic Consequence Abstraction.* MDL-WIS-PA-000003 REV 03. Las Vegas, Nevada: Sandia National Laboratories.

179394 SNL 2007. *Total System Performance Assessment Data Input Package for Requirements Analysis for TAD Canister and Related Waste Package Overpack Physical Attributes Basis for Performance Assessment.* TDR-TDIP-ES-000006 REV 00. Las Vegas, Nevada: Sandia National Laboratories. ACC: DOC.20070918.0005.

179567 SNL 2007. *Total System Performance Assessment Data Input Package for Requirements Analysis forDOE SNF/HLW and Navy SNF Waste Package Overpack Physical Attributes Basis for Performance Assessment.* TDR-TDIP-ES-000009 REV 00. Las Vegas, Nevada: Sandia National Laboratories.

181595 Sourmail, T.; Okuda, T.; and Taylor, J.E. 2004. "Formation of Chromium Borides in Quenched Modified 310 Austenitic Stainless Steel." *Scripta Materialia, 50,* 1271-1276. New York, New York: Elsevier. TIC: 259239.

103804 Spahiu, K. and Bruno, J. 1995. *A Selected Thermodynamic Database for REE to be Used in HLNW Performance Assessment Exercises.* SKB TR-95-35. Stockholm, Sweden: Svensk Kärnbränsleförsörjning A.B. TIC: 225493.

155740 Strachan, D.M.; Barnes, B.O.; and Turcotte, R.P 1981. "Standard Leach Tests for Nuclear Waste Materials." *Scientific Basis for Nuclear Waste Management, Proceedings of the Third International Symposium, Boston, Massachusetts, November 17-20, 1980.* Moore, J.G., ed. *3,* 347-354. New York, New York: Plenum Press. TIC: 204407.

125332 Stumm, W. and Morgan, J.J. 1996. *Aquatic Chemistry, Chemical Equilibria and Rates in Natural Waters.* 3rd Edition. New York, New York: John Wiley & Sons. TIC: 246296.

181407 Sudakar, C.; Subbana, G.N.; and Kutty, T.R.N. 2004. "Effect of Cationic Substituents on Particle Morphology of Goethite and the Magnetic Properties of Maghemite Derived from Substituted Goethite." *Journal of Materials Science, 39,* 4271-4286. Boston, Massachusetts: Kluwer Academic Publishers. TIC: 259500.

180657 Taylor, L.L. 2005. *Using Fuel Parameters to Predict DOE SNF Canister Loadings.* EDF-NSNF-046, Rev. 0. Washington, D.C.: U.S. Department of Energy, National Spent Nuclear Fuel Program. ACC: LLR.20070515.0108.

126175 Taylor, W.J. 1997. "Incorporating Hanford 15 Foot (4.5 Meter) Canister into Civilian Radioactive Waste Management System (CRWMS) Baseline." Memorandum from W.J. Taylor (DOE) to J. Williams (Office of Waste Acceptance Storage and Transportation), April 2, 1997. ACC: HQP.19970609.0014.

182347 Tekin, A.; Martin, J.W.; Senior, B.A. 1991. "Grain Boundry Sensitization and Desensitization During the Ageing 0f 316(N) Austenitic Stainless Steels." *Journal of Materials Science, 26,* 2458-2466. London, England: Chapman and Hall. TIC: 259656.

153213 Titley, S.R. 1963. "Some Behavioral Aspects of Molybdenum in the Supergene Environment." *Transactions of the Society of Mining Engineers, 226,* 199-204. New York, New York: Society of Mining Engineers of AIME. TIC: 249114.

179852 Turney, G.L. 1986. *Quality of Ground Water in the Columbia Basin, Washington, 1983.* Water-Resources Investigations Report 85-4320. Tacoma, Washington: U.S. Geological Survey. ACC: LLR.20070321.0001.

100948 Van Konynenburg, R.A.; Curtis, P.G.; and Summers, T.S.E. 1998. *Scoping Corrosion Tests on Candidate Waste Package Basket Materials for the Yucca Mountain Project.* UCRL-ID-130386. Livermore, California: Lawrence Livermore National Laboratory. ACC: MOL.19980727.0385.

178973 Wang, X.Y.; Wu, Y.S.; Zhang, L.; and Yu, Z.Y. 2001. "Atomic Force Microscopy and X-Ray Photoelectron Spectroscopy Study on the Passive Film for Type 316L Stainless Steel." *Corrosion Science, 57,* (6), 540-546. Houston, Texas: NACE International. TIC: 2591099.

106266 Weast, R.C., ed. 1977. *CRC Handbook of Chemistry and Physics.* 58th Edition. Cleveland, Ohio: CRC Press. TIC: 242376.

172351 Wilkin, R.T. and Barnes, H.L. 1998. "Solubility and Stability of Zeolites in Aqueous Solutions: I. Analcime, Na-, and K-Clinoptilolite." *American Mineralogist, 83*, (7-8), 746-761. Washington, D.C.: Mineralogical Society of America. TIC: 256734.

137607 Wilson, C.N. and Bruton, C.J. 1989. *Studies on Spent Fuel Dissolution Behavior Under Yucca Mountain Repository Conditions.* PNL-SA-16832. Richland, Washington: Pacific Northwest Laboratory. ACC: HQX.19890918.0047.

158013 Wimmer, L.B. 2001. *Summary Report of Commercial Reactor Criticality Data for Three Mile Island Unit 1.* TDR-UDC-NU-000004 REV 01. Las Vegas, Nevada: Bechtel SAIC Company. ACC: MOL.20010921.0047.

182040 Winkler, H.G.F. 1979. *Petrogenesis of Metamorphic Rocks.* 5th Edition. New York, New York: Springer-Verlag. TIC: 206676.

100835 Wolery, T.J. 1992. *EQ3/6, A Software Package for Geochemical Modeling of Aqueous Systems: Package Overview and Installation Guide (Version 7.0).* UCRL-MA-110662 PT I. Livermore, California: Lawrence Livermore National Laboratory. TIC: 205087.

181086 Wood, S.A. 1990. "The Aqueous Geochemistry of the Rare-Earth Elements and Yttrium. 2. Theoretical Predictions of Speciation in Hydrothermal Solutions to 350°C at Saturation Water Vapor Pressure." *Chemical Geology, 88,* 99-125. Amsterdam, The Netherlands: Elsevier. TIC: 259375.

169286 Wronkiewicz, D.J. and Buck, E.C. 1999. "Uranium Mineralogy and the Geologic Disposal of Spent Nuclear Fuel." Chapter 10 of *Uranium: Mineralogy, Geochemistry and the Environment.* Burns, P.C. and Finch, R., eds. Reviews in Mineralogy Volume 38. Washington, D.C.: Mineralogical Society of America. TIC: 247121.

102047 Wronkiewicz, D.J.; Bates, J.K.; Wolf, S.F.; and Buck, E.C. 1996. "Ten-Year Results from Unsaturated Drip Tests with UO_2 at 90°C: Implications for the Corrosion of Spent Nuclear Fuel." *Journal of Nuclear Materials, 238,* (1), 78-95. Amsterdam, The Netherlands: North-Holland. TIC: 243361.

100194 Yang, I.C.; Rattray, G.W.; and Yu, P. 1996. *Interpretation of Chemical and Isotopic Data from Boreholes in the Unsaturated Zone at Yucca Mountain, Nevada.* Water-Resources Investigations Report 96-4058. Denver, Colorado: U.S. Geological Survey. ACC: MOL.19980528.0216.

165505 YMP (Yucca Mountain Site Characterization Project) 2003. *Disposal Criticality Analysis Methodology Topical Report.* YMP/TR-004Q, Rev. 02. Las Vegas, Nevada: Yucca Mountain Site Characterization Office. ACC: DOC.20031110.0005.

171238 Zarrabi, K.; McMillan, S.; Elkonz, S.; and Cizdziel, J. 2003. *Corrosion and Mass Transport Processes in Carbon Steel Miniature Waste Packages.* Document TR-03-003, Rev. 0. Task 34. Las Vegas, Nevada: University of Nevada, Las Vegas. ACC: MOL.20040202.0079.

175094 Zemann, J. 1969. "Crystal Chemistry." Chapter 2 of *Handbook of Geochemistry.* Wedepohl, K.H., ed. Volume 1. New York, New York: Springer-Verlag. TIC: 229493.

175107 Zhang, J.; Jiang, D.; Chen, B.; Zhu, J.; Jiang, L.; and Fang, H. 2001. "Preparation and Electrochemistry of Hydrous Ruthenium Oxide/Active Carbon Electrode Materials for Supercapacitor." *Journal of the Electrochemical Society, 148,* (12), A1362-A1367. Pennington, New Jersey: Electrochemical Society. TIC: 257717.

178975 Zhang, Q.C.; Wu, J.S.; Zheng, W.L.; Chen, J.G.; and Li, A.B. 2002. "The Protective Mechanism of the Native Rust Layer on Cr-Containing Steels Exposed to Marine Atmosphere." *Zeitschrift für Metallkunde*, 93, (6), 590-594. München, Germany: Carl Hanser Verlag. TIC: 259110.

181413 Ziemniak, S.E. and Hanson, M. 2006. "Corrosion Behavior of NiCrFe Alloy 600 in High Temperature, Hydrogenated Water." *Corrosion Science, 48,* 498-521. New York, New York: Elsevier. TIC: 259506.

181408 Ziemniak, S.E.; Jones, M.E.; and Combs, K.E.S. 1998. "Solubility and Phase Behavior of Cr(III) Oxides in Alkaline Media at Elevated Temperatures." *Journal of Solution Chemistry, 27,* (1), 33-66. New York, New York: Plenum Publishing. TIC: 259501.

9.2 CODES, STANDARDS, REGULATIONS, AND PROCEDURES

180319 10 CFR 63. 2007. Energy: Disposal of High-Level Radioactive Wastes in a Geologic Repository at Yucca Mountain, Nevada. Internet Accessible.

147578 ASTM A 20/A20M-99a. 1999. *Standard Specification for General Requirements for Steel Plates for Pressure Vessels.* West Conshohocken, Pennsylvania: American Society for Testing and Materials. TIC: 247403.

165003 ASTM A 240/A 240M-03b. 2003. *Standard Specification for Chromium and Chromium-Nickel Stainless Steel Plate, Sheet, and Strip for Pressure Vessels and for General Applications.* West Conshohocken, Pennsylvania: American Society for Testing and Materials. TIC: 254845.

162723 ASTM A 516/A 516M-01. 2001. *Standard Specification for Pressure Vessel Plates, Carbon Steel, for Moderate- and Lower-Temperature Service.* West Conshohocken, Pennsylvania: American Society for Testing and Materials. TIC: 253997.

154062 ASTM A 887-89 (Reapproved 2000). 2000. *Standard Specification for Borated Stainless Steel Plate, Sheet, and Strip for Nuclear Application.* West

Conshohocken, Pennsylvania: American Society for Testing and Materials. TIC: 249544.

162727 ASTM B 209M-02. 2002. *Standard Specification for Aluminum and Aluminum-Alloy Sheet and Plate Metric.* West Conshohocken, Pennsylvania: American Society for Testing and Materials. TIC: 253985.

168403 ASTM B 932-04. 2004. *Standard Specification for Low-Carbon Nickel-Chromium-Molybdenum-Gadolinium Alloy Plate, Sheet, and Strip.* West Conshohocken, Pennsylvania: American Society for Testing and Materials. TIC: 255846.

103515 ASTM G 1-90 (Reapproved 1999). 1999. *Standard Practice for Preparing, Cleaning, and Evaluating Corrosion Test Specimens.* West Conshohocken, Pennsylvania: American Society for Testing and Materials. TIC: 238771.

IM-PRO-002, *Control of the Electronic Management of Information.*

IM-PRO-003, *Software Management.*

SCI-PRO-001, *Qualification of Unqualified Data.*

SCI-PRO-002, *Planning for Science Activities.*

SCI-PRO-004, *Managing Technical Product Inputs*

SCI-PRO-006, *Models*.

9.3 SOURCE DATA, LISTED BY DATA TRACKING NUMBER

165226 GS030408312272.002. Analysis of Water-Quality Samples for the Period from July 2002 to November 2002. Submittal date: 05/07/2003.

179065 GS060908312272.004. Chemical Analysis of Pore Water Samples Extracted from HD-PERM, USW SD-9, and ESF-SAD-GTB#1 Core for the Period from April 29, 2006 to July 21, 2006. Submittal date: 09/14/2006.

163089 LL010902212241.026. CSNF Alteration Phase Porosity Estimates. Submittal date: 09/21/2001.

150930 MO0005PORWATER.000. Perm-Sample Pore Water Data. Submittal date: 05/04/2000.

151029 MO0006J13WTRCM.000. Recommended Mean Values of Major Constituents in J-13 Well Water. Submittal date: 06/07/2000.

161886 MO0302SPATHDYN.001. Thermodynamic Data Supporting Spreadsheet Files - Data0.YMP.R2. Submittal date: 02/05/2003.

169007 MO0404ANLSF001.001. CSNF Radionuclide Release Model. Submittal date: 04/09/2004.

172059 MO0409SPAACRWP.000. Aqueous Corrosion Rates for Non-Waste Form Waste Package Materials. Submittal date: 09/16/2004.

172830 MO0502ANLGAMR1.016. HLW Glass Degradation Model. Submittal date: 02/08/2005.

177332 MO0608MWDGEOMA.001. Input Files and Model Output Runs: Geochemistry Model Validation Report: Material Degradation and Release Model. Submittal date: 08/07/2006.

180439 MO0701PACSNFCP.000. CSNF Colloid Parameters. Submittal date: 04/17/2007.

180440 MO0701PAIRONCO.000. Colloidal Iron Corrosion Products Parameters. Submittal date: 04/17/2007.

180700 MO0705TSPASEEP.000. Seepage Results from the TSPA-LA Model. Submittal date: 05/02/2007.

181380 MO0706ECTBSSAR.000. Report INL/EXT-07-12633: Electrochemical Corrosion Testing of Borated Stainless Steel Alloys. Submittal date: 06/12/2007.

181613 MO0706SPAFEPLA.001. FY 2007 LA FEP List and Screening. Submittal date: 06/20/2007.

171547 SN0408T0509903.007. In-Drift Condensation: Mathcad Files Used for Calculation. Submittal date: 09/07/2004.

172712 SN0410T0510404.002. Thermodynamic Database Input File for EQ3/6 - DATA0.YMP.R4. Submittal date: 11/01/2004.

178850 SN0612T0502404.014. Thermodynamic Database Input File for EQ3/6 - DATA0.YMP.R5. Submittal date: 12/15/2006.

181228 SN0702T0502404.015. Supporting Spreadsheets and Data Files for Thermodynamic Database Input File for EQ3/6 - DATA0.YMP.R5. Submittal date: 06/01/2007.

181571 SN0703PAEBSPCE.006. Physical and Chemical Environment (PCE) TDIP Water-Rock Interaction Parameter Table and Salt Separation Tables with Supporting Files. Submittal date: 06/27/2007.

180177 SN0703PAEBSPCE.007. Physical and Chemical Environment (PCE) TDIP Uncertainty Evaluations and Supporting Files. Submittal date: 04/06/2007.

9.4 OUTPUT DATA, LISTED BY DATA TRACKING NUMBER

MO0705GEOMODEL.000. Input Files and Model Output Runs: Geochemistry Model Validation Report: Material Degradation and Release Model. Submittal Date: 05/23/2007.

MO0705MODELVAL.000. Model Validation: Corroboration of EQ3/6 and Phreeqc Model Outputs. Submittal date: 05/24/2007.

9.5 SOFTWARE CODES

179458 ASPRIN V. 1.0. 2004. Windows 2000. STN: 10487-1.0-00.

153964 Software Code: EQ3/6 V.7.2b. 1999. UCRL-MA-110662 (LSCR198).

176889 EQ3/6 V. 8.1. 2005. WINDOWS 2000. STN: 10813-8.1-00.

159731 EQ6 V. 7.2bLV. 2002. WINDOWS 2000, NT. STN: 10075-7.2bLV-02.

175698 PHREEQC V. 2.11. 2006. WINDOWS 2000. STN: 10068-2.11-00.

154059 Software Code: SCALE V. 4.3. 1997. HP. 30011 V4.3.

APPENDIX A
SELECTION OF THE CRITICAL REVIEWER FOR PURPOSES OF MODEL VALIDATION

APPENDIX A
SELECTION OF THE CRITICAL REVIEWER FOR PURPOSES OF MODEL VALIDATION

The technical work plan (SNL 2006 [DIRS 179452], Section 2.3) specifies that a critical review for model validation will be conducted in accordance with SCI-PRO-006, *Models*, Section 6.3.2.[1] Dr. Florie A. Caporuscio of Los Alamos National Laboratory was chosen as the technical specialist to conduct the critical review. The requirements for the critical reviewer, as listed in the technical work plan (SNL 2006 [DIRS 179452], p. A-1), and the responses describing Dr. Caporuscio's qualifications are as follows:

1. *Reviewer shall not have contributed to the development, checking, and review of the model documentation.*

   Dr. Caporuscio did not contribute to the development, checking, or review of the model documentation.

2. *Reviewer shall have an appropriate technical background (i.e., advanced degree in an appropriate technical field) and demonstrated expertise in geochemistry.*

   Dr. Caporuscio has 25 years of experience in high-level and transuranic radioactive waste disposal, with primary responsibilities in the characterization of ash flow tuffs, their alternative productions, and the technical analysis of bedded salt deposits. His research specialty is in the crystal chemistry of dense silicates and oxides. To perform that research, he has operated a multitude of analytical facilities, including microbeam analyses (electron, ion, proton), X-ray fluorescence, X-ray diffraction (power, single XL four-sphere). Dr. Caporuscio has experience in various aspects of the nuclear fuel cycle. While at the Los Alamos National Laboratory, he was instrumental in characterizing the mineralogy and stratigraphy of Yucca Mountain. His postdoctoral work at the University of Pavia (Italy) centered on crystallographic controls of trace element distributions (including radionuclides) in minerals. In 1990, while with the Radiation Branch of the Region II Office of the U.S. Environmental Protection Agency, he worked as the staff geologist, with involvement in characterization and remediation of Comprehensive Environmental Response, Compensation, and Liability Act (CERCLA) and Formerly Utilized Sites Remedial Action Program (FUSRAP) sites. As acting section chief for the Waste Isolation Pilot Plant (WIPP) Test and Retrieval Plan, he reviewed the source term and gas generation models. Dr. Caporuscio was also a member of two national peer review panels. He served as a member of the WIPP Conceptual Models Peer Review panel, an independent panel commissioned by the DOE to comply with Environmental Protection Agency 40 CFR Part 194 regulations. This panel met during 1996-1997 and again in 2002-2003. Since 1993, Dr. Caporuscio has been involved in LANL environmental restoration activities at Los Alamos National Laboratory as an expert on the Bandelier

[1] The term "critical review" is used in the latest version of SCI-PRO-006, Revision 2; it replaces the term "independent technical review" which was used in earlier versions of this procedure.

Tuff, where he has investigated a leaking reactor and various radioactive waste disposal sites. He presently works as a geochemist on the Yucca Mountain Project.

3. *Documentation of the selection of the reviewer shall be included as an appendix to the model report.*

   This appendix serves as the documentation of the selection of Dr. Caporuscio as the critical reviewer.

APPENDIX B
CRITICAL REVIEW FOR PURPOSES OF MODEL VALIDATION

APPENDIX B
CRITICAL REVIEW FOR PURPOSES OF MODEL VALIDATION

MEMORANDUM

To: Susan LeStrange, Cliff Howard August 7, 2007
From: Florie Caporuscio, LANL / EES-6

Subject: Validation Technical Review of ANL-EBS-GS-000001 Rev 02B (Material Degradation and Release Model)

This memorandum is written pursuant to *Technical Work Plan for: In-Package Geochemistry for Criticality Evaluations* [TWP-EBS-MD-000014 Rev 05] (SNL 2006 [DIRS 179452], Section 2.3), which specifies a Level I validation designating one method of post development model validation consistent with a model of lower relative importance. The memorandum documents my independent critical review of *Geochemistry Model Validation Report: Material Degradation and Release Model* [ANL-EBS-GS-000001 Rev 02B]. The validation was required to be performed by critical review conducted by a technical specialist in accordance with SCI-PRO-006, Section 6.3.2, 5th dash.

A. The TWP specifies that the validation technical reviewer shall:

1. *Review the validation criteria in the TWP to determine if they are adequate for intended use of the model.*

   As Validation technical reviewer I have found that the validation criteria dictated in the Technical Work Plan to be adequate for the intended use of the model. This determination took into consideration that the level of confidence required was Level I. A Level II confidence measure would have required a higher level of validation criteria.

2. *Review the material degradation and release model in draft.*

   The *Material Degradation and Material Release Model* was extensively reviewed twice in respective draft forms and comments were submitted to the AMR originator. A substantial amount of the comments were editorial in nature and were directed to improve transparency issues. All comments were resolved in *Material Degradation and Material Release Model* Rev. 02B.

3. *Assess whether or not the model as documented in the report meets the validation criteria.*

   This reviewer finds that the model presented in *Material Degradation and Material Release Model* Rev. 02B meets the validation criteria as delineated in Section B (below). The actual validation method is described in Section 7 of the AMR.

4. *Assess whether or not the model is adequate for its intended use. Meet with the author to resolve comments, and recommend actions, as appropriate, to resolve any inadequacies found as part of the review.*

   I find the model adequate for its intended use. I have had a number of discussions with Susan LeStrange (document originator) concerning the list of minerals formed (or suppressed) to inform her of noted inadequacies. All recommended actions were quickly resolved.

5. *Document the final conclusion as to whether the model is valid for its intended use, as a memo to be included as an appendix in the report.*

   This memorandum, included in Appendix B of *Geochemistry Model Validation Report: Material Degradation and Release Model* [ANL-EBS-GS-000001] meets this requirement.

B. The technical specialist shall evaluate the extent to which the following criteria are met:

1. *The use of the thermodynamic database in the EQ3/6 modeling and the choice of mineral suppressions and formations are sufficiently justified and appropriate for the intended use of the model.*

   The mineral formation and suppression lists for the model (Tables 6.3-10 and 6.3-11, respectively of the AMR) were found to be justified and appropriate for the intended use of the model. The minerals chosen for the AMR were supported by multiple experimental studies and natural analog results in peer reviewed journal articles, notably Wronkiewicz etal., 1996, Efurd, etal. 1998, and Pearcy, etal., 1994. The thermodynamic database *data0.ymp.R5* used in EQ3/6 modeling is now especially robust and has been updated to its present form to include realistic Cr, Pu and Np phases. Therefore this database is justified and appropriate for the intended use of the model.

2. *Modeling assumptions are clearly defined, discussed, and justified as appropriate for the intended use of the model.*

   After review, it was determined that all modeling assumptions are clearly defined, discussed, and justified as appropriate for the intended use of the model.

3. *Uncertainties in parameters, processes, and assumptions are appropriately described, and impacts of these uncertainties on the intended use of the model are discussed.*

   As pertains to this AMR, the uncertainties are appropriately described and impacts are discussed. It will be extremely important to track these uncertainties into the criticality AMRs where this data will be used. Such tracking and evaluation of uncertainties will help to prevent the criticality reports from becoming overly "conservative" in nature.

4. *The overall technical credibility of the approach, including assumptions, parameters, and equations, is appropriate for the model's intended use.*

   This very ambitious modeling effort undertaken in *Geochemistry Model Validation Report: Material Degradation and Release Model* [ANL-EBS-GS-000001] provided the appropriate technical credibility for the model's intended use.

In summary, I find that the authors have provided a modeling report that is both adequate and appropriate for its intended use and level of confidence required.

INTENTIONALLY LEFT BLANK

APPENDIX C
SATURATION SENSITIVITY IN EQ6 MODELS

APPENDIX C
SATURATION SENSITIVITY IN EQ6 MODELS

The waste package degradation calculations assume 30% saturation (Section 5.1). However, actual saturation in a breached waste package might be substantially smaller, or even larger (up to 100% in a full bathtub situation). It is therefore important to examine how the choice of percent saturation affects the results of EQ6 calculations.

This appendix compares results of EQ6 calculations at saturations ranging from 3% to 100% of the original package void volume. The variations were achieved by using the *setmwtmax* capability built into EQ6 V. 7.2bLV and V. 8.1 (BSC 2002 [DIRS 173170], Section 10.1; BSC 2005 [DIRS 180678], Section 2.2). A commercial spent nuclear fuel (CSNF) waste package was chosen for the analysis, as representative of the majority of waste packages in the repository.

The CSNF conditions are those used for the batch reactor in Section 6.6.1.1 (the single-cell model used for comparison with the multiple-cell, drip-through model). The igneous scenario is modeled, with the fuel allowed to prereact with water and oxygen, which would be expected in the cool-down of the breached package from magmatic conditions, as outlined in Section 6.2.2. The EQ6 calculation starts in a solid-centered flow-through mode, at 50°C, with a drip rate of 10 L/yr (10 times the base case) and all metal degradation rates at 10 times the base-case values. PuO_2 (hydr, aged) is allowed to form, but PuO_2 and $PuO_2(OH)_2 \cdot 2H_2O$ are suppressed. The *setmwtmax* option is used to vary the effective saturation (the percent of void volume that is water) over 3%, 10%, 30% (the base case), 70%, and 100%. The metal degradation rates were increased above the base-case value to ensure greater production of pH-controlling species (i.e., to stress the system more); the drip rate was increased to ensure that not all the water was consumed by reactions. In addition, the higher drip rate forces greater differentiation of the cases, ensuring that more fluid volumes will be exchanged over 10^4 years of simulation time than in the base case.

The estimated pH and concentration data are plotted in Figures C-1 through C-5. Figures C-1 through C-4 have linear scales on the x- and y-axes. The gadolinium (aqueous) plot is supplied as both linear and log scale (Figures C-4 and C-5). The plots are all very similar for pH and aqueous plutonium, uranium, and gadolinium; in particular, the results for 30% saturation (assumed in the base case) are not very different from 10% and 3% saturation. As expected, there is more tailing with the higher saturation because it takes longer to flush the system (for a fixed drip rate) when the static volume of the fluid is greater; thus the 3% case has sharp edges on the peaks, whereas the 100% case has a tail. However, the peak concentration of plutonium, uranium, and gadolinium, the timing of peak concentration, and the widths of the peak (in time) are very similar, for all saturations up to 100%. Perhaps the greatest apparent difference is seen for gadolinium, primarily because the initial sharp concentration pulse is early in the history of the EQ6 run. The sharp leading edge of the pulse is delayed by approximately 2×10^2 years in the 100% saturation case, versus the 3% saturation case; and the end of the peak is delayed approximately 10^2 years in the 100% case. However, these times are relatively small compared to the 10^4 year calculation time, and the uncertainty in the package breach time. Thus, the percent saturation does not significantly affect the concentration estimates.

The values of percent remaining of gadolinium, plutonium, and uranium for each waste package saturation are listed in Table C-1. The results show that the range of saturation from 3% to 100% has a small affect on the plutonium releases, with no impact on the total Pu/U releases from the waste package. The largest impact is on the gadolinium releases. The base case choice of 30% waste package saturation has a gadolinium retention about 4% higher than the lowest saturation and 10% lower than the highest retention at 100% saturation. Therefore, using the base-case waste package saturation of 30% overestimates the likelihood of a criticality event inside the waste package when a high saturation is likely due to the lower quantity of gadolinium estimated in the waste package and slightly underestimates the likelihood when saturation is below 30% due to the higher quantity of gadolinium estimated in the waste package (up to 4%).

This example is somewhat atypical, because the retention of gadolinium is highly controlled by solid gadolinium phosphate as gadolinium carbonate disappears from the system by ≈2,000 years. In contrast, in the base case EQ6 simulation (*CSNFIG1.6i*), solid gadolinium carbonate persists through the entire 10,000-year time span of the calculation. The greater loss of the solid carbonate in the saturation study is due to the relatively fast steel corrosion rates, which temporarily drive pH below 5. It must be noted that there is significant difference in the probability the solubility product will be exceeded when the solid is a carbonate versus when the solid is a phosphate. This difference is due to the assumption of a constant fugacity of CO_2, which guarantees a fairly constant concentration of aqueous carbonates in the simulations, regardless of whether the system is at 3% or 100% saturation. Thus one part of the solubility product (aqueous carbonate concentration), will be nearly the same at the same time, for both 3% and 100% runs, when the solid is gadolinium carbonate. However, when the solid phase is a phosphate, a very different situation can develop. In the 3% saturation run, the final concentration of aqueous phosphorus (principally as $H_2PO_4^-$) is 7.66×10^{-9} molal, whereas in the 100% saturation run, the final concentration of aqueous phosphorous is 2.50×10^{-7} molal, or 33 times higher. This result is not surprising; the phosphate is supplied by steel degradation at a constant rate in both 3% and 100% runs, but the fluid is exchanged 33 times faster in the 100% run. Thus one component of the solubility product (aqueous phosphate) is lower at lower saturation. The result is that the higher saturation simulation maintains a higher probability of solid gadolinium phosphate saturation.

Table C-1. Saturation Study Results: Gadolinium, Plutonium, and Uranium Percent Remaining

CSNF Waste Package Conditions	Percent Remaining at 10,000 years					
	pH Max	pH Min	Gd	Pu	U	Pu/U Combined
3% saturation	7.12	4.95	29.7	18.0	100.1	99.5
10% saturation	7.08	4.95	30.7	18.0	100.1	99.5
30% saturation	7.09	4.95	33.8	18.3	100.1	99.5
70% saturation	7.09	4.95	40.4	19.6	100.1	99.5
100% saturation	7.09	4.95	44.6	20.5	100.1	99.5

Source: Output DTN: MO0705GEOMODEL.000, folder: Saturation_study, file: *Satur-study-summary.xls*

NOTE: Decay of Pu-239 is included, therefore uranium retention is greater than 100%.

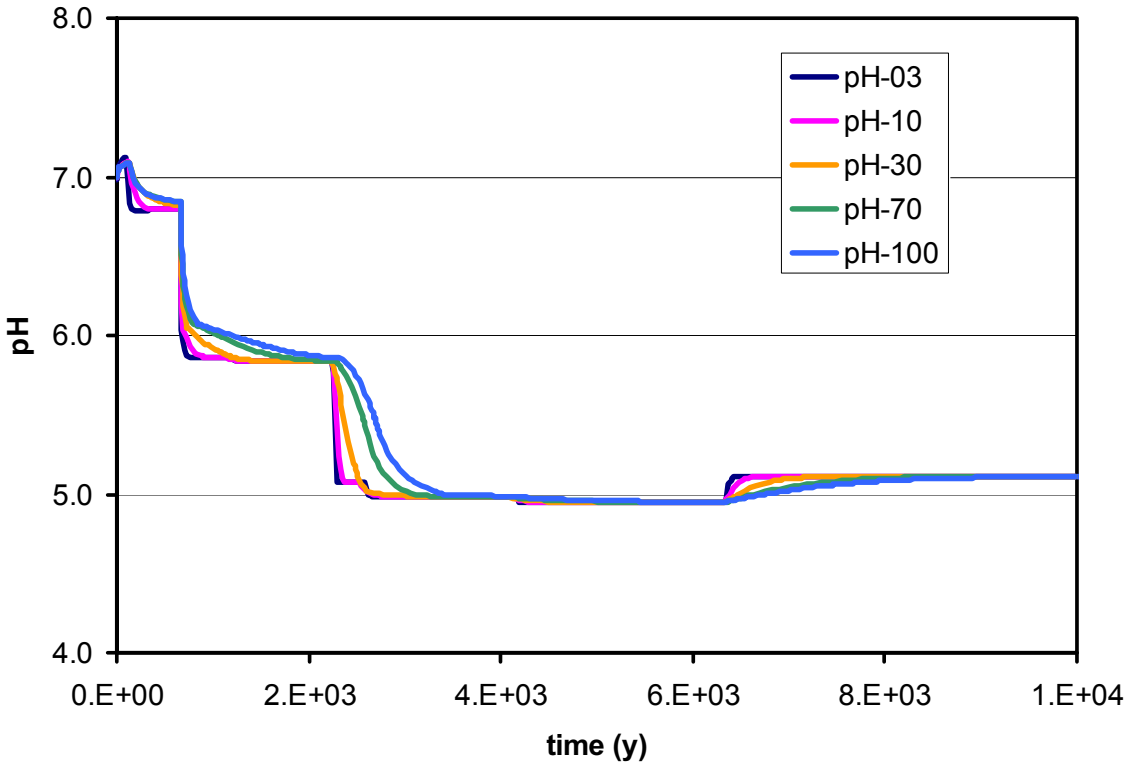

Source: Output DTN: MO0705GEOMODEL.000, file *csnf-ign-satur-study-B.xls.*

NOTES: Saturations vary through 3%, 10%, 30%, 70%, and 100%.
pH-03 = 3%; pH-100 = 100%.

Figure C-1. Comparison of the pH in a Degrading CSNF Package for Various Saturations

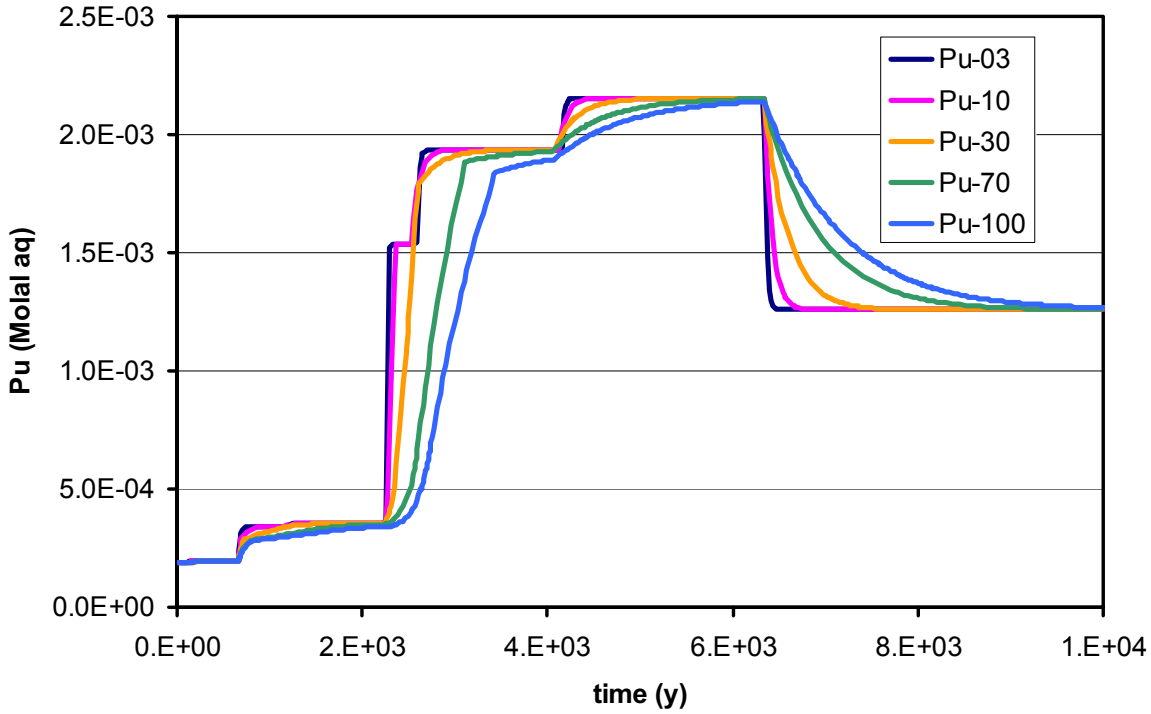

Source: Output DTN: MO0705GEOMODEL.000, file *csnf-ign-satur-study-B.xls*.

NOTES: Saturations vary through 3%, 10%, 30%, 70%, and 100%.
pH-03 = 3%; pH-100 = 100%.

Figure C-2. Comparison of the Aqueous Plutonium Concentration in a Degrading CSNF Package for Various Saturations

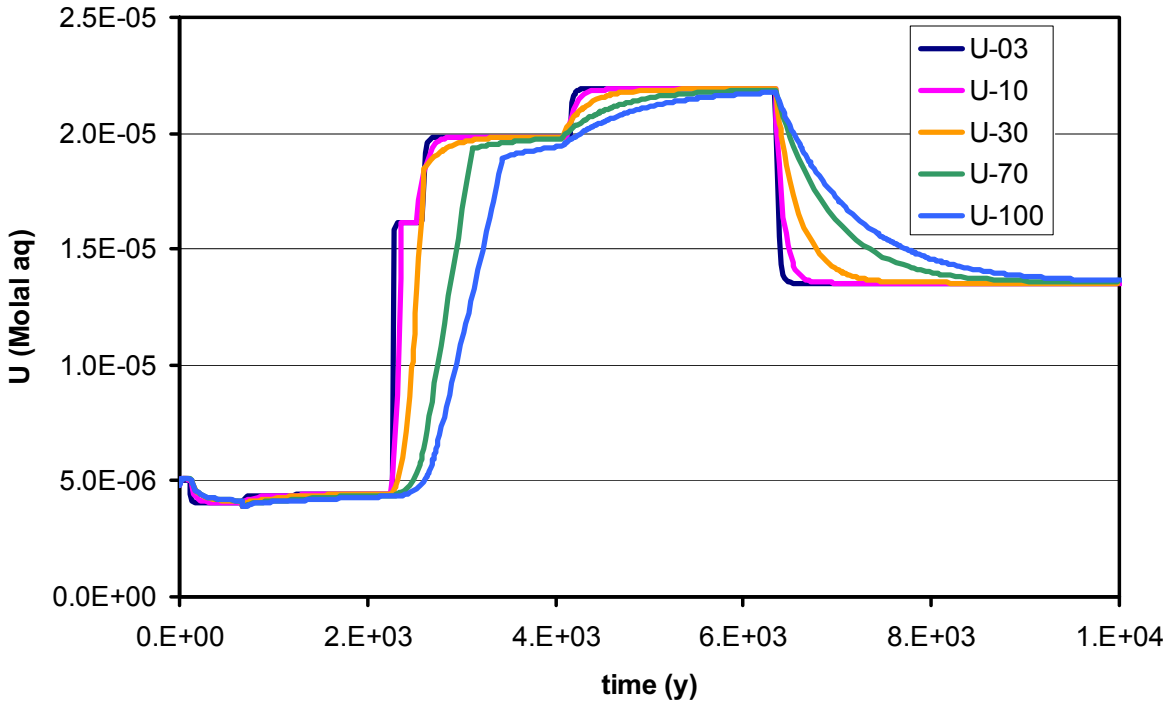

Source: Output DTN: MO0705GEOMODEL.000, file *csnf-ign-satur-study-B.xls*.

NOTES: Saturations vary through 3%, 10%, 30%, 70%, and 100%.
pH-03 = 3%; pH-100 = 100%.

Figure C-3. Comparison of the Aqueous Uranium Concentration in a Degrading CSNF Package for Various Saturations

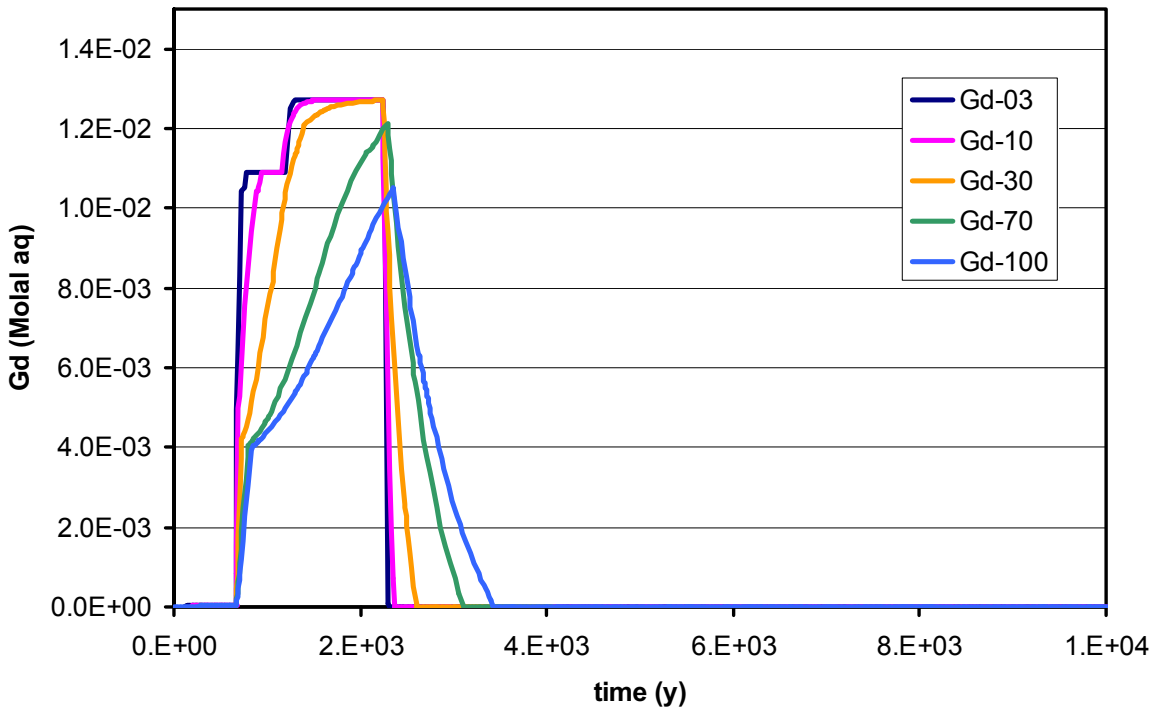

Source: Output DTN: MO0705GEOMODEL.000, file *csnf-ign-satur-study-B.xls*.

NOTES: Saturations varied through 3%, 10%, 30%, 70%, and 100%.
pH-03 = 3%; pH-100 = 100%.
Linear concentration scale is used.

Figure C-4. Comparison of the Aqueous Galodinium Concentration in a Degrading CSNF Package for Various Saturations

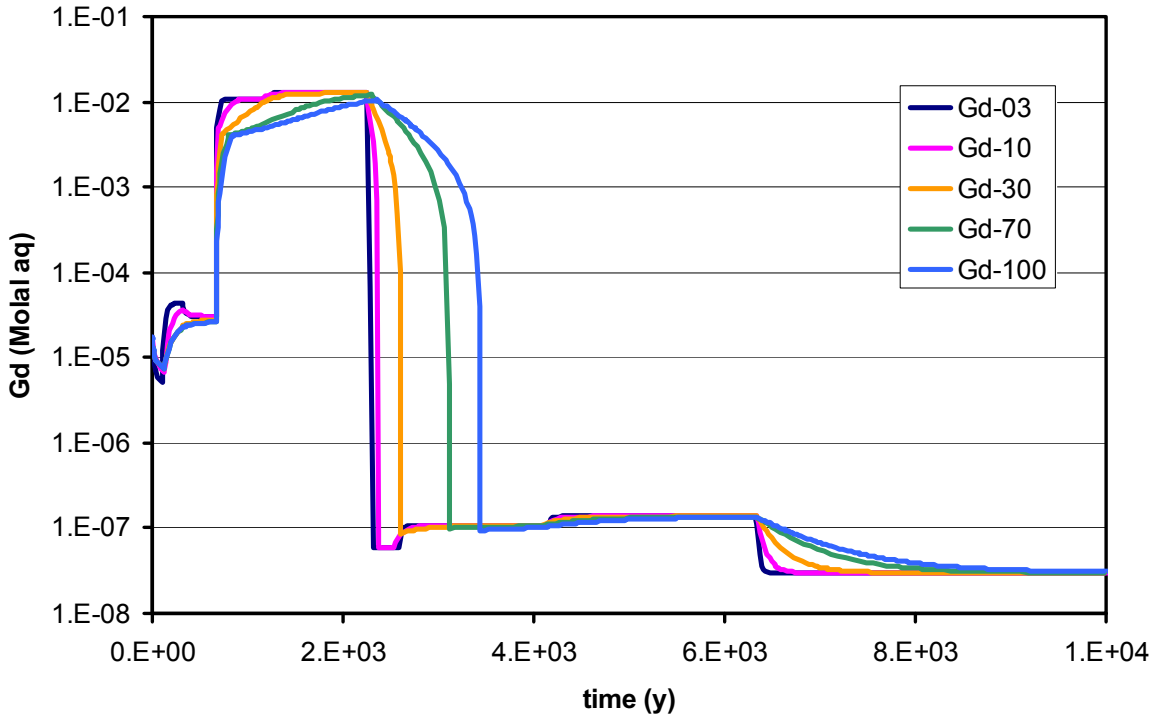

Source: Output DTN: MO0705GEOMODEL.000, file *csnf-ign-satur-study-B.xls*.

NOTES: Saturations vary through 3%, 10%, 30%, 70%, and 100%.
pH-03 = 3%; pH-100 = 100%.
Log concentration scale is used.

Figure C-5. Comparison of the Aqueous Gadolinium Concentration in a Degrading CSNF Package for Various Saturations

INTENTIONALLY LEFT BLANK

APPENDIX D
TEMPERATURE EFFECTS FOR THERMOCHEMICAL DATA

APPENDIX D
TEMPERATURE EFFECTS FOR THERMOCHEMICAL DATA

The *data0.ymp.R5* thermodynamic database (DTN: SN0612T0502404.014 [DIRS 178850]) has few entries for lanthanides at temperatures other than 25°C. The situation is better for some actinides; for uranium, there are extensive data for all solids and dissolved species found to control the solubility of uranium in criticality runs. However, up-temperature data are less complete for plutonium. When EQ6 is used to perform thermodynamic calculations at temperatures other than 25°C (and some involved reactions have only 25°C data), the code simply uses the 25°C values for those reactions.

In this section, the effect of using 25°C data for lanthanides and two plutonium compounds is examined and quantified.

D.1 LANTHANIDE CARBONATES

For concreteness, gadolinium is used in the analysis, as representative of all lanthanides.

The temperature dependence of the reaction is shown in Equation D-1:

$$Gd_2(CO_3)_3\ (solid) + 3H^+ = 2Gd^{3+} + 3HCO_3^- \qquad \text{(Eq. D-1)}$$

and is calculated in the spreadsheet *Solids_j_HWS_Gd.xls*. The methods are essentially identical to those used to calculate the temperature variation for the analogous americium solid in the *solids_j_YC_Am.xls* spreadsheet (DTN: MO0302SPATHDYN.001 [DIRS 161886]; these methods are described in Section 6.1 of *Qualification of Thermodynamic Data for Geochemical Modeling of Mineral-Water Interactions in Dilute Systems* (SNL 2007 [DIRS 177409])). The heat capacity of the solid carbonate is estimated from the heat capacities of component oxides, including a fictive solid CO_2 calculated from heat capacities of well-characterized solid carbonates. This heat-capacity function is then used to extrapolate the logK of reactions to higher temperatures. At lower pH and fCO_2, Gd^{3+} is the dominant aqueous ion, and Equation D.1 suffices to define solubility. However, at higher pH and fCO_2, the gadolinium-carbonate aqueous complexes become more significant.

Cantrell and Byrne (1987 [DIRS 181066]) determined the temperature-dependence of europium carbonate complex stability, through experiments at 15°C, 25°C, and 35°C. Byrne et al. (1988 [DIRS 181088]) extended the temperature dependence found for europium to all other lanthanides, and Wood (1990 [DIRS 181086]) used the Cantrell and Byrne (1987 [DIRS 181066]) data to calculate rare-earth carbonate complexation at much higher temperatures. For the current report, the Cantrell and Byrne results (1987 [DIRS 181066]) were used in spreadsheet *Gd-CO3-complex-augmentk.xls* to calculate the temperature dependence for the reactions in Equations D-2 through D-4:

$$GdCO_3^+ + H^+ = Gd^{3+} + HCO_3^- \qquad \text{(Eq. D-2)}$$

$$Gd(CO_3)_2^- + 2H^+ = Gd^{3+} + 2HCO_3^- \qquad \text{(Eq. D-3)}$$

$$GdHCO_3^{2+} = Gd^{3+} + HCO_3^- \qquad \text{(Eq. D-4)}$$

This spreadsheet calculates the value of the EQ6 input file parameter "AugmentLogK" for 50°C and 90°C, for Equations D-1 through D-4. Use of this parameter forces EQ6 to use the temperature-corrected values for the logK of the reactions. In this manner, a temperature-sensitivity study can be performed at 50°C and 90°C, without altering the *data0.ymp.R5* database itself (DTN: SN0612T0502404.014 [DIRS 178850]).

D.2 LANTHANIDE PHOSPHATES

In EQ6 runs that include degrading steel or HLWG, lanthanide phosphates may limit the solubility of gadolinium and other neutron poisons. These phosphates have the general formula $LnPO_4 \cdot xH_2O$, where *Ln* is any lanthanide element, and *x* varies from 0 to 2 for different values of *Ln*.

In general, the *data0.ymp.R5* database (DTN: SN0612T0502404.014 [DIRS 178850]) contains no logK data for solid $LnPO_4 \cdot xH_2O$, at temperatures other than 25°C. However, various studies (Jonasson et al. 1985 [DIRS 147467]; Cetiner et al. 2005 [DIRS 181082]; Poitrasson et al. 2004 [DIRS 181083]) have suggested that solubility for these compounds is retrograde (i.e., goes down with increasing temperature). Table D-1 compares the 25°C entries from the *data0.ymp.R5* database (DTN: SN0612T0502404.014 [DIRS 178850]) with data from Cetiner et al. (2005 [DIRS 181082]) and Poitrasson et al. (2004 [DIRS 181083]) for varied temperatures. Comparing data from various studies is problematical, as the identification of the stable solid phase (rhabdophane, xenotime, or monazite structure) is not consistent among studies. It is also not practical to perform a general temperature extrapolation as was done for the carbonate species, because data are not available for all lanthanides at more than two temperatures.

However, two points are obvious. First, within experimental uncertainty, the lower temperature logKs from the *data0.ymp.R5* database (DTN: SN0612T0502404.014 [DIRS 178850]) are either close to newer experimental data, or overestimate $LnPO_4 \cdot xH_2O$ solubility. The overestimation is particularly notable for gadolinium. Second, the trend is for lower solubility at higher temperatures. Therefore, limiting the *data0.ymp.R5* database (DTN: SN0612T0502404.014 [DIRS 178850]) to 25°C data will overestimate $LnPO_4 \cdot xH_2O$ solubility for higher temperatures, and will predict waste package conditions in which a criticality event is more likely, since the lanthanides are significant neutron absorbers.

Table D-1. Temperature Dependence of logK for Phosphate Dissolution

$LnPO_4 \cdot xH_2O + H^+ = Ln^{3+} + HPO_4^{2-} + xH_2O$ [a]			
	data0.ymp.R5 [b]	**Literature data**	
Temperature	**25°C**	**23°C**	**50°C**
Lanthanum	−12.3495	−12.3257 ± 0.15 [c]	−13.1856 [c]
Neodymium	−12.1495	−13.4257 ± 0.05 [c]	−14.3856 [c]
Samarium	−12.1495	−12.2257 ± 0.19 [c]	−12.5856 [c]

Table D-1. Temperature Dependence of logK for Phosphate Dissolution (Continued)

$LnPO_4 \cdot xH_2O + H^+ = Ln^{3+} + HPO_4^{2-} + xH_2O$ [a]			
	data0.ymp.R5 [b]	**Literature data**	
Temperature	**25°C**	**21°C**	**70°C**
Neodymium	−12.1495	−13.5318 ± 0.07 [d]	−14.977 ± 0.13 [d]
Gadolinium	−11.9495	−13.4718 ± 0.10 [d]	ND

Sources: [a] The EQ3/6 databaseb was used to convert values in literature references c and d, below, from a PO43− to HPO42− basis, per output DTN: MO0705GEOMODEL.000, file *REE-phosp-T-depend.xls*.

[b] DTNs: SN0612T0502404.014 [DIRS 178850] and SN0702T0502404.015 [DIRS 181228]; lanthanide values in these DTNs are from a compilation by Spahiu and Bruno (1995 [DIRS103804]).

[c] Cetiner et al. 2005 [DIRS 181082], Table 1. Estimated uncertainty is for the solubility product.

[d] Poitrasson et al. 2004 [DIRS 181083], Table 1. Estimated uncertainty is for the solubility product.

NOTE: ND = not determined.

D.3 PLUTONIUM COMPOUNDS

In some runs, particularly those with higher fCO_2, PuO_2CO_3 (aqueous) is calculated to be the dominant soluble species for plutonium. The current *data0.ymp.R5* database (DTN: SN0612T0502404.014 [DIRS 178850]) has no logK estimates for this species, other than at 25°C.

The logK(T) for the reaction is given in Equation D-5:

$$PuO_2CO_3\,(aq) + H^+ = PuO_2^{2+} + HCO_3^- \qquad \text{(Eq. D-5)}$$

at an arbitrary temperature, *T*, and can be estimated by assuming that the difference (logK(25°C) – logK(T)) is the same as for the analogous reaction in Equation D-6:

$$UO_2CO_3\,(aq) + H^+ = UO_2^{2+} + HCO_3^- \qquad \text{(Eq. D-6)}$$

The latter reaction has logK for the entire EQ3/6 data0 temperature grid. Equation D-6 can thus be used to calculate "AugmentLogK" values at 50°C and 90°C for the EQ6 input file as in spreadsheet *Gd-CO3-complex-augmentk.xls*.

The in-package calculations are performed with both crystalline PuO_2 and PuO_2(hydr, aged) as solubility-controlling species. The solid PuO_2 has very low solubility. The sensitivity case in which it is formed is intended for use in calculating internal criticality, as it causes a potential fissile material to remain in the package. The cases in which the more soluble solid PuO_2(hydr, aged) is formed are intended for use in calculating the possibility of external criticality; the higher solubility causes more plutonium to leave the package, possibly to be reprecipitated in the drift or in the cracks and pore space of the tunnel walls.

The effective solubility of PuO_2(hydr, aged) decreases with increasing temperature, from 25°C to 90°C (Efurd et al. 1998 [DIRS 108015]). This decrease may result from the increasing crystallinity of initially amorphous plutonium solids as temperature is increased. Therefore, the solubility of PuO_2(hydr, aged) at higher temperatures (e.g., 50°C and 90°C) is bracketed by the 25°C PuO_2(hydr, aged) data, as well as those for crystalline PuO_2.

APPENDIX E
PLOTS OF BASE-CASE MINERALS FORMED AND UNREACTED COMPONENTS REMAINING IN THE WASTE PACKAGE VERSUS TIME

APPENDIX E
PLOTS OF BASE-CASE MINERALS FORMED AND UNREACTED COMPONENTS REMAINING IN THE WASTE PACKAGE VERSUS TIME

The quantities of minerals formed and unreacted components remaining in the waste package that are presented in Figures E-1 through E-16 in this appendix are plotted as normalized moles. To convert to total moles, the values in the plots must be multiplied by the normalization factor for the specific waste package as listed in Table 6.3-1 (CSNF = 7,664, CDSP (N-reactor) = 5,698, TMI and FFTF = 6,430). These plots are intended to provide a quick assessment of the major minerals formed. Directions for extracting detailed information from the EQ6 output files (such as moles and volume of minerals formed, mass of unreacted waste package components, aqueous concentrations) are provided in Table 6.5-6.

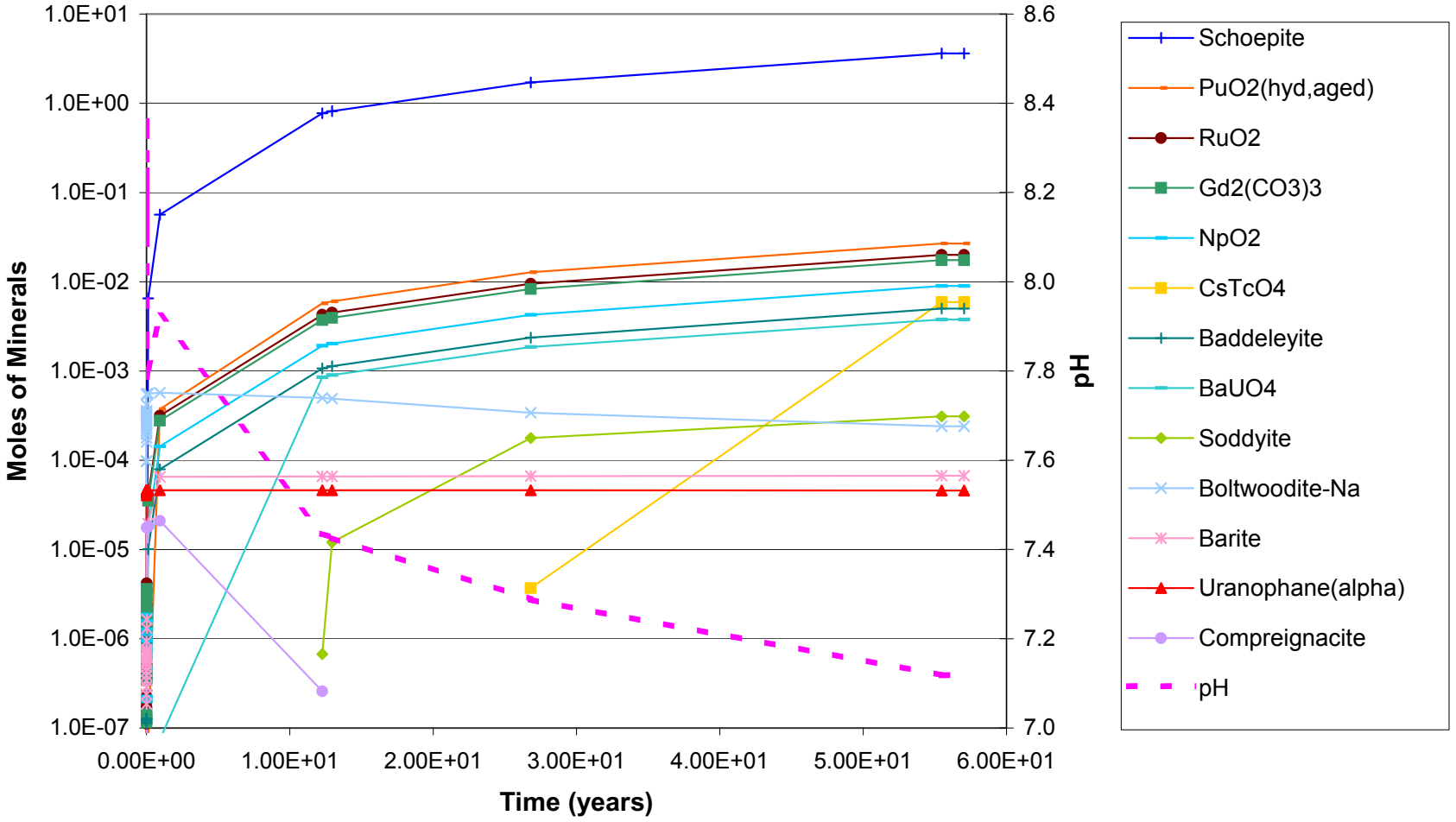

Source: Output DTN: MO0705GEOMODEL.000, folder: CSNF/CSNF Igneous/Base case, file: *CSIGox.min_info.xls*.

Figure E-1. CSNF Igneous, Stage 1 (oxidation of fuel), Minerals Formed

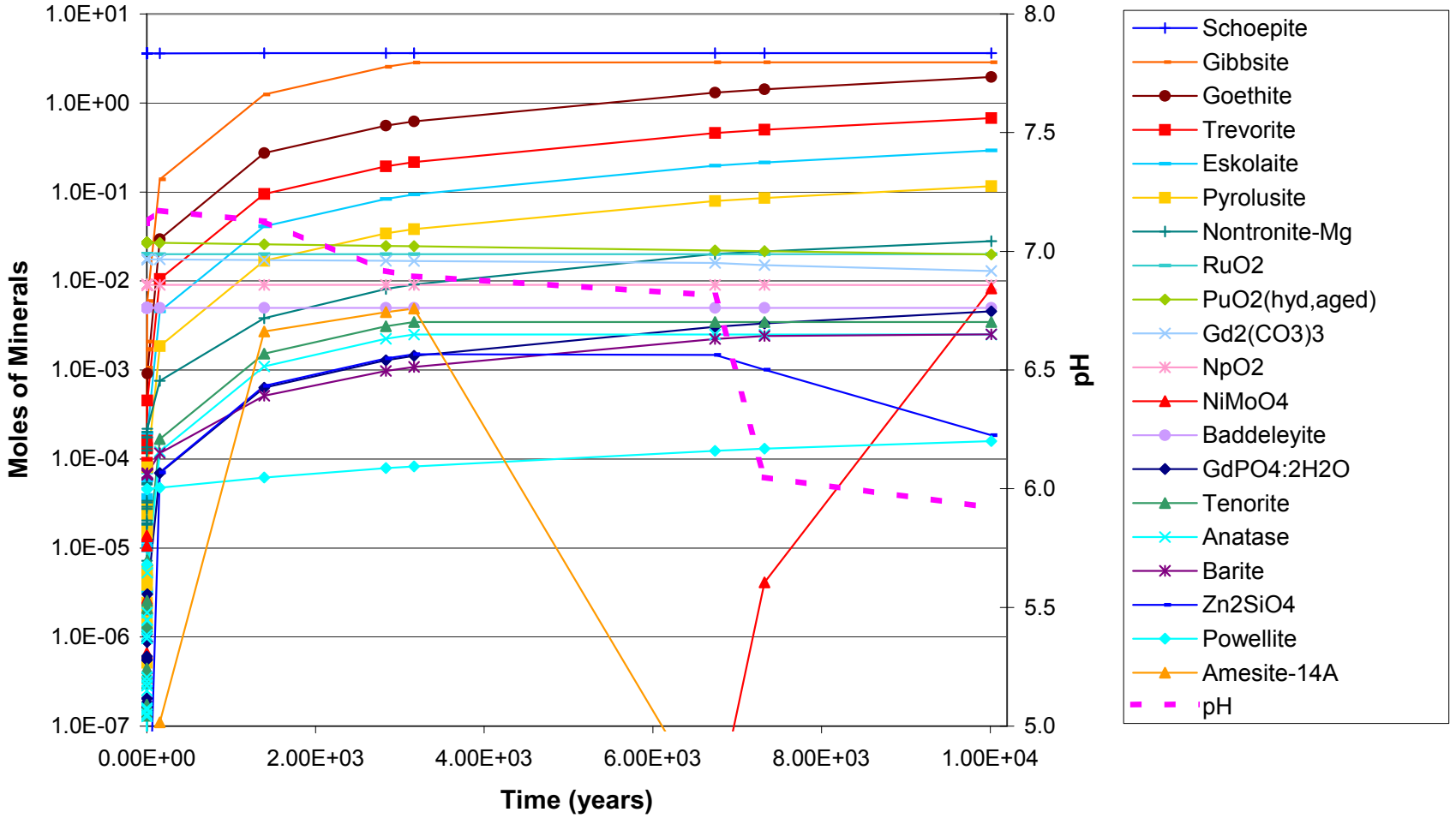

Source: Output DTN: MO0705GEOMODEL.000, folder: CSNF/CSNF Igneous/Base case, file: *CSNFIG1.min_info.xls*.

Figure E-2. CSNF Igneous, Stage 2 (oxidation of waste package components), Minerals Formed

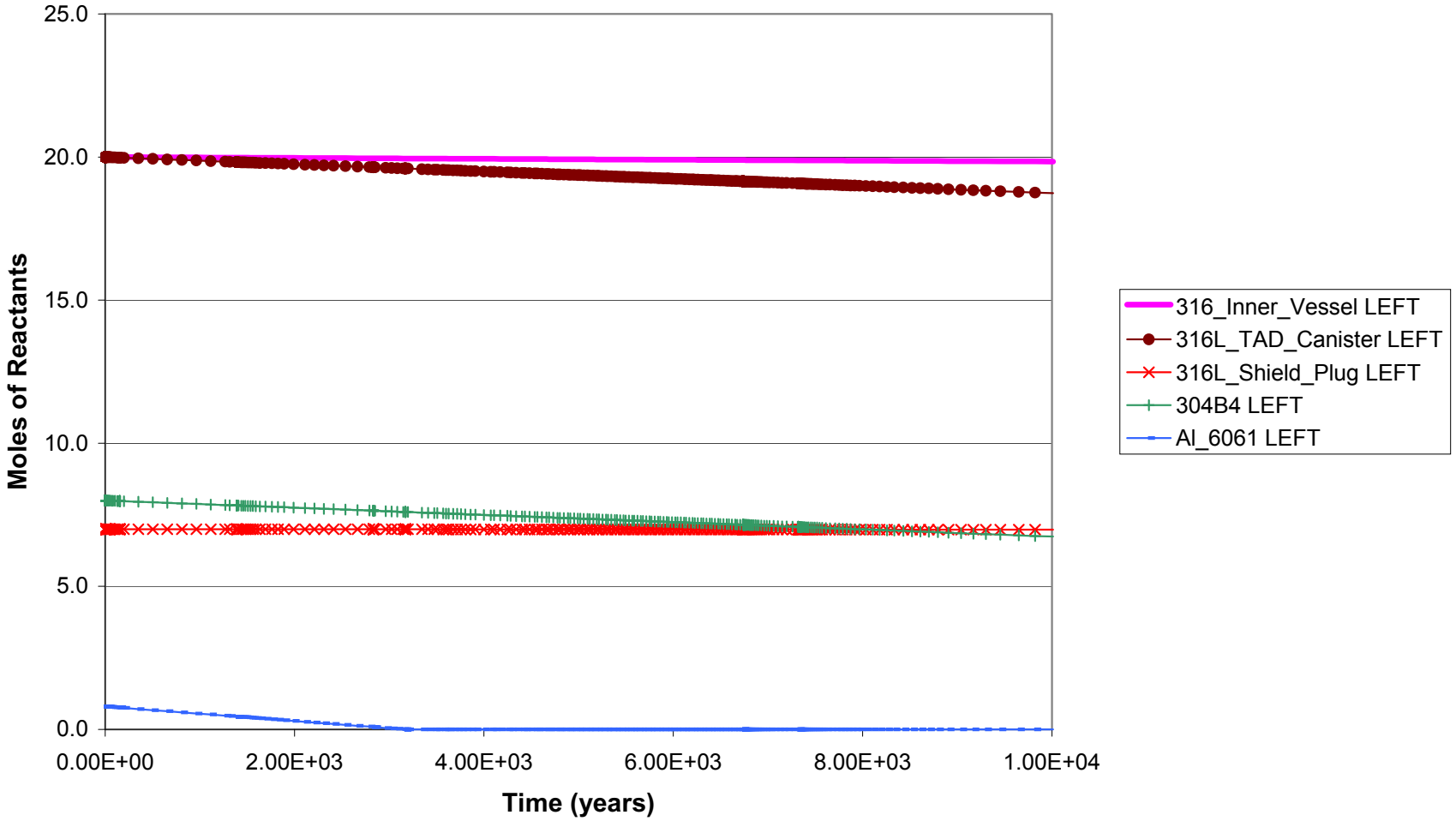

Source: Output DTN: MO0705GEOMODEL.000, folder: CSNF/CSNF Igneous/Base case, file: *reactants.xls*.

Figure E-3. CSNF Igneous, Reactants Remaining

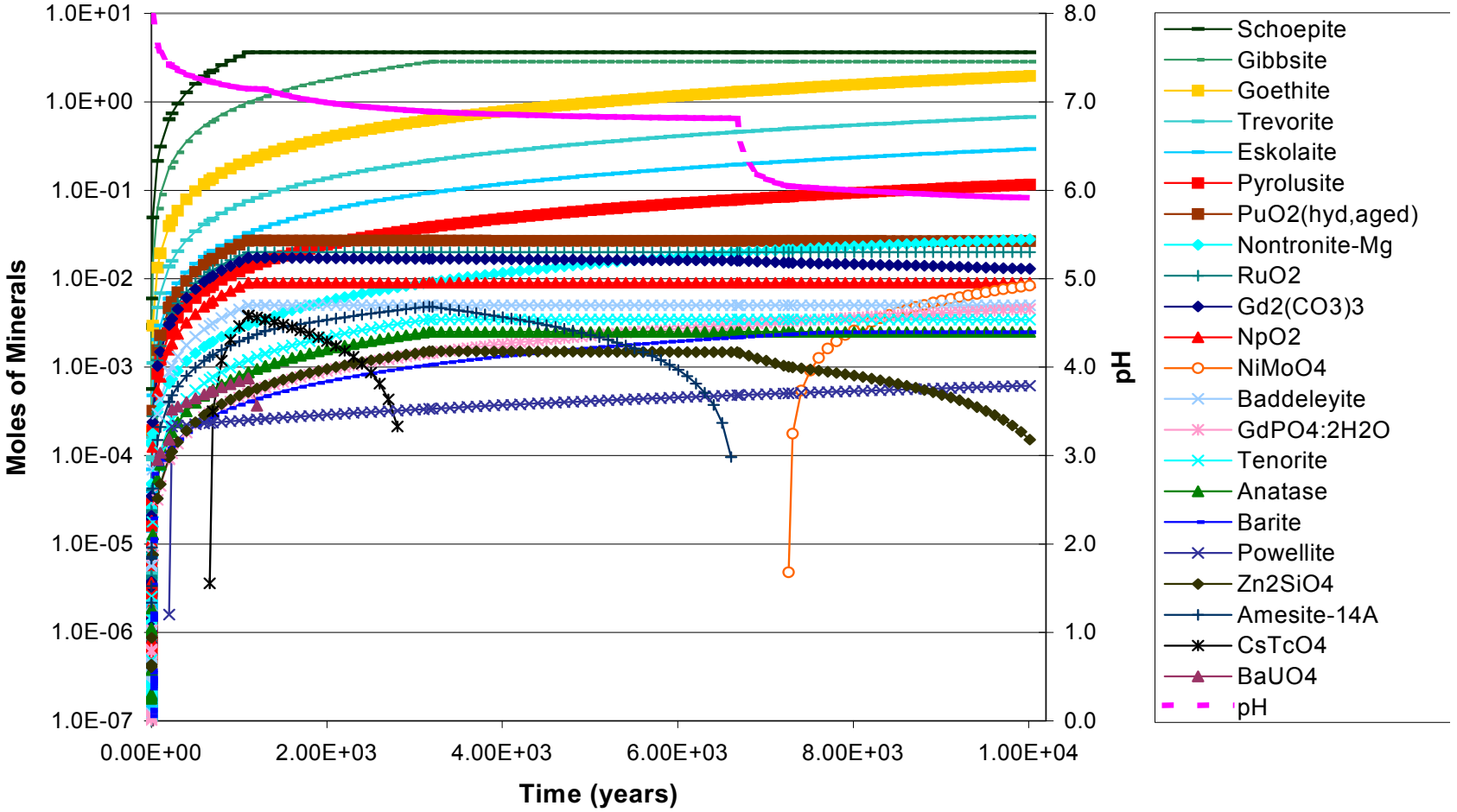

Source: Output DTN: MO0705GEOMODEL.000, folder: CSNF/CSNF Seismic/Base case, file: *CS_S_b.min_info.xls*.

Figure E-4. CSNF Seismic, Minerals Formed

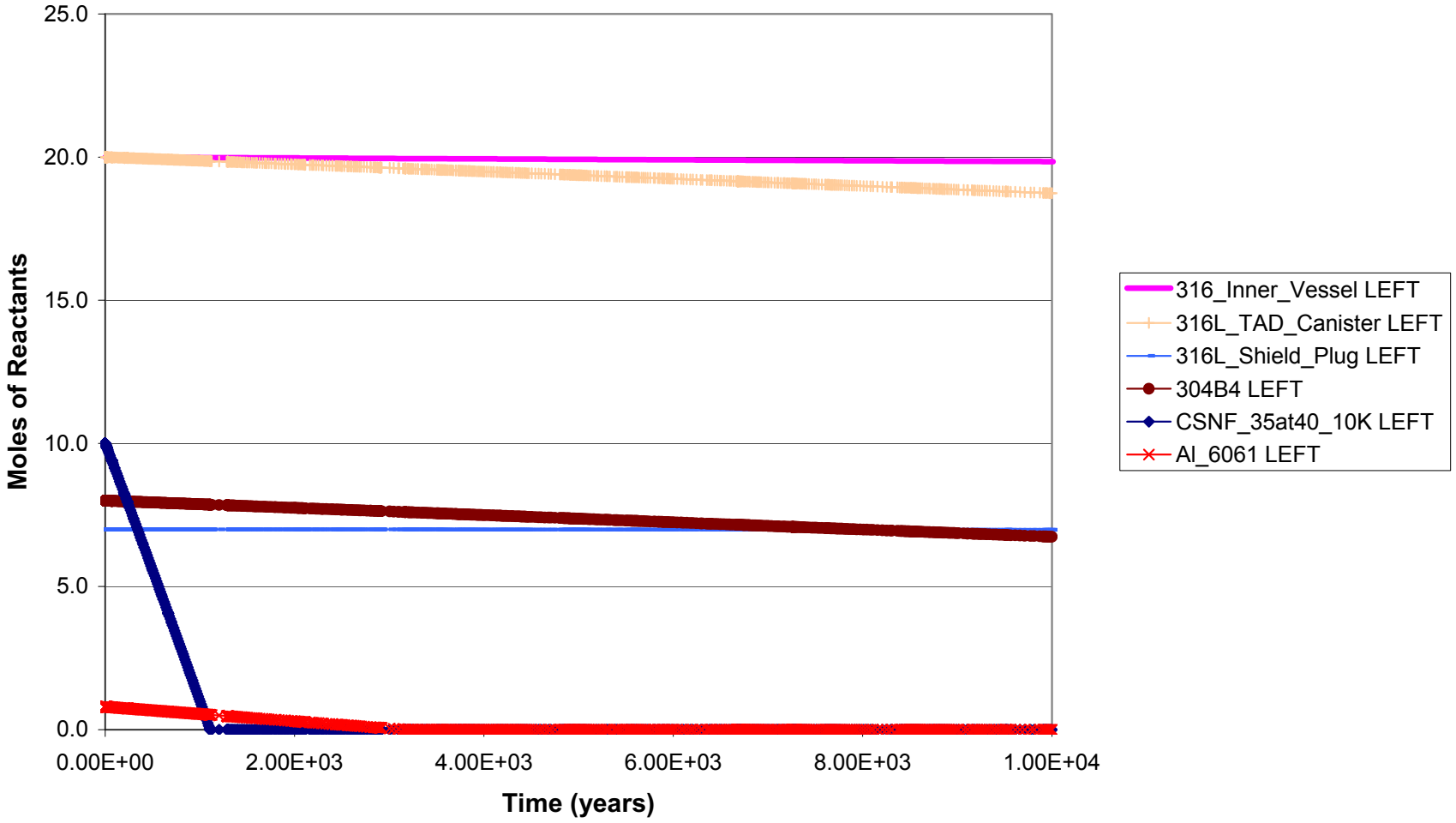

Source: Output DTN: MO0705GEOMODEL.000, folder: CSNF/CSNF Seismic/Base case, file: *CS_S_b Reactants.xls*.

Figure E-5. CSNF Seismic, Reactants Remaining

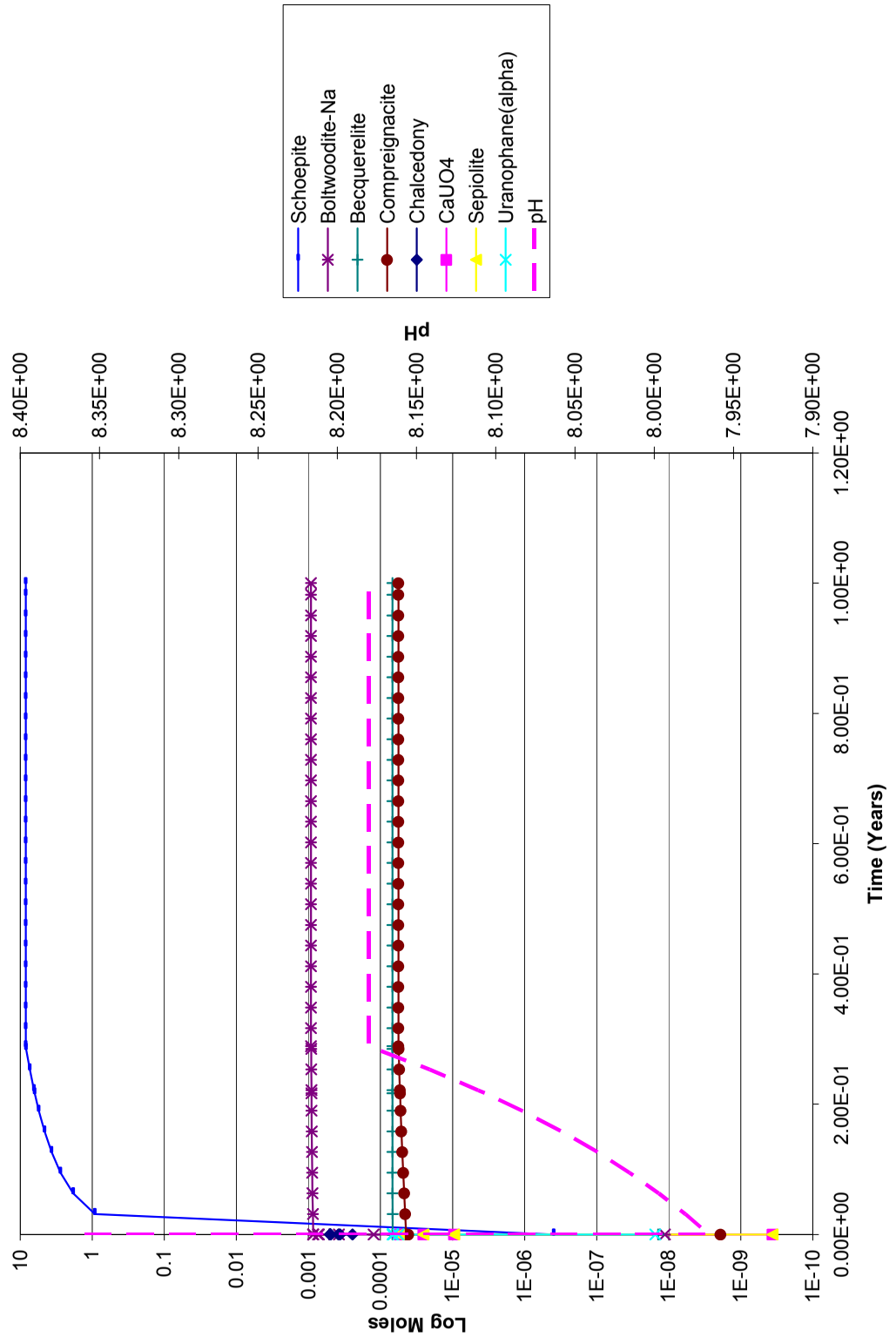

Source: Output DTN: MO0705GEOMODEL.000, folder: CDSP (N-Reactor)/Figures, file: *Fig_CD_I_b.xls*.

Figure E-6. Codisposal Igneous, Stage 1 (oxidation of fuel), Minerals Formed

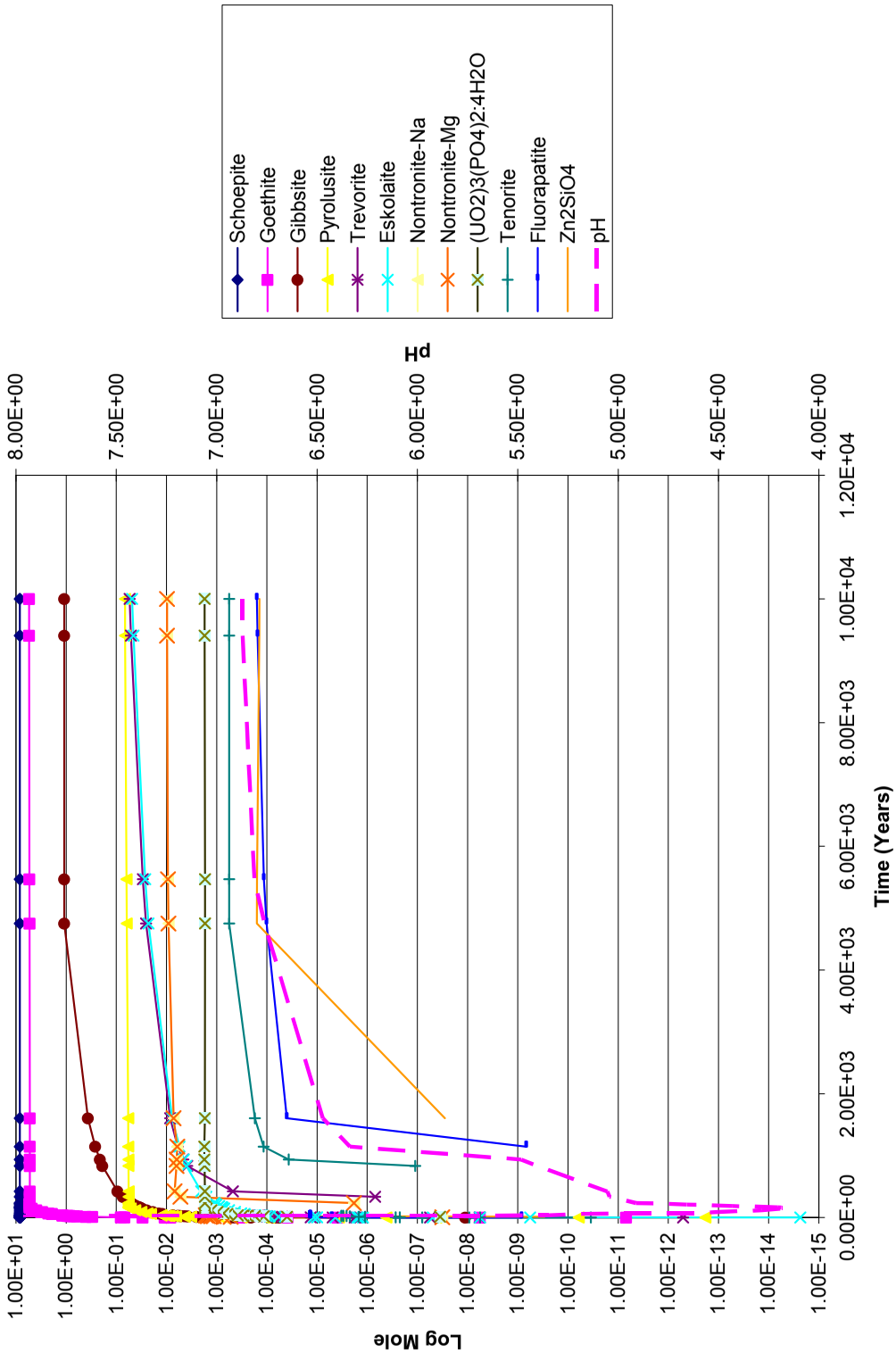

Source: Output DTN: MO0705GEOMODEL.000, folder: CDSP (N-Reactor)/Figures, file: *Fig_CD_I_b.xls*.

Figure E-7. Codisposal Igneous, Stage 2 (oxidation of waste package components), Minerals Formed

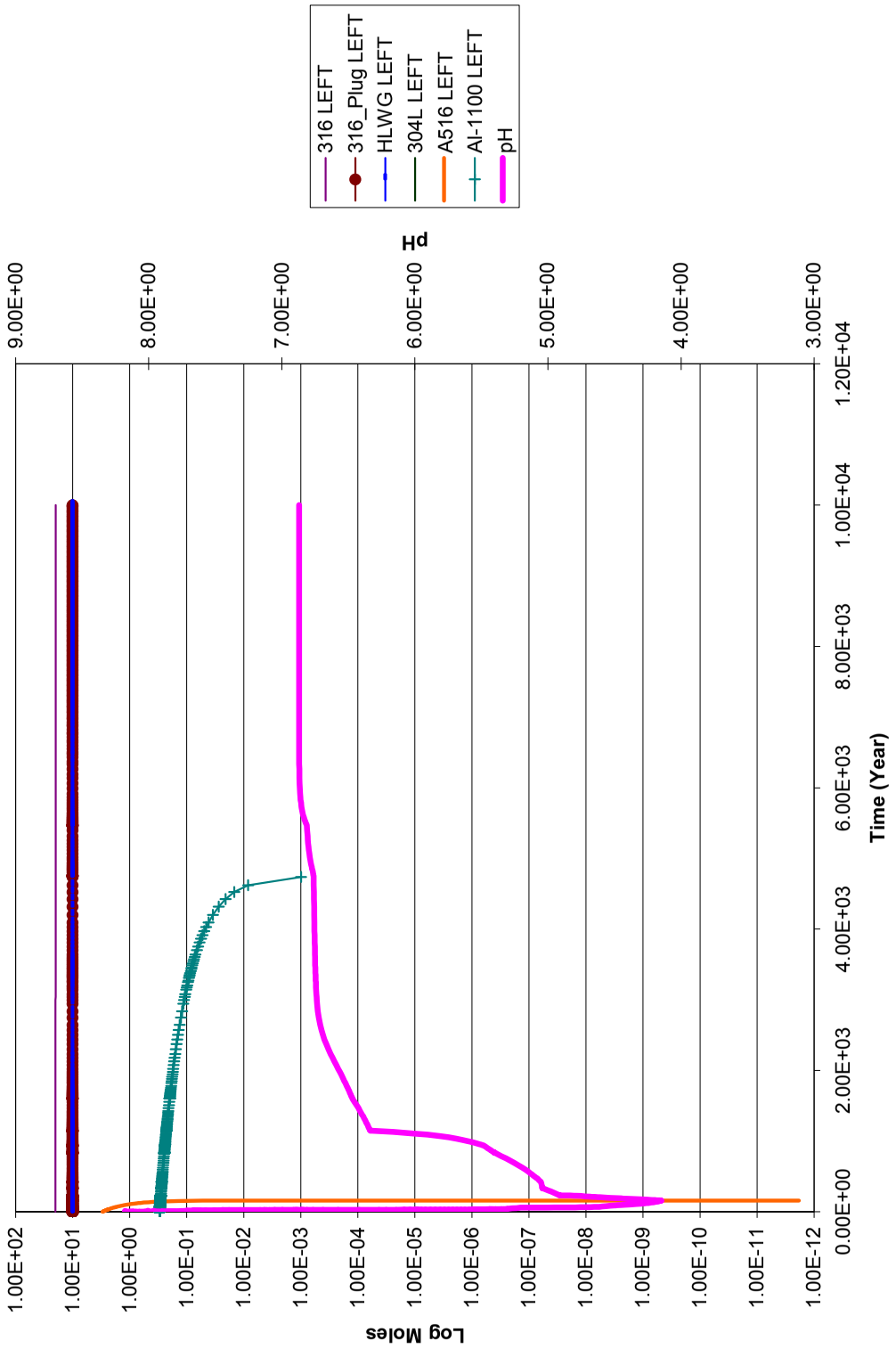

Source: Output DTN: MO0705GEOMODEL.000, folder: CDSP (N-Reactor)/Figures, file: *Fig_reactants_left.xls*.

Figure E-8. Codisposal Igneous, Reactants Remaining

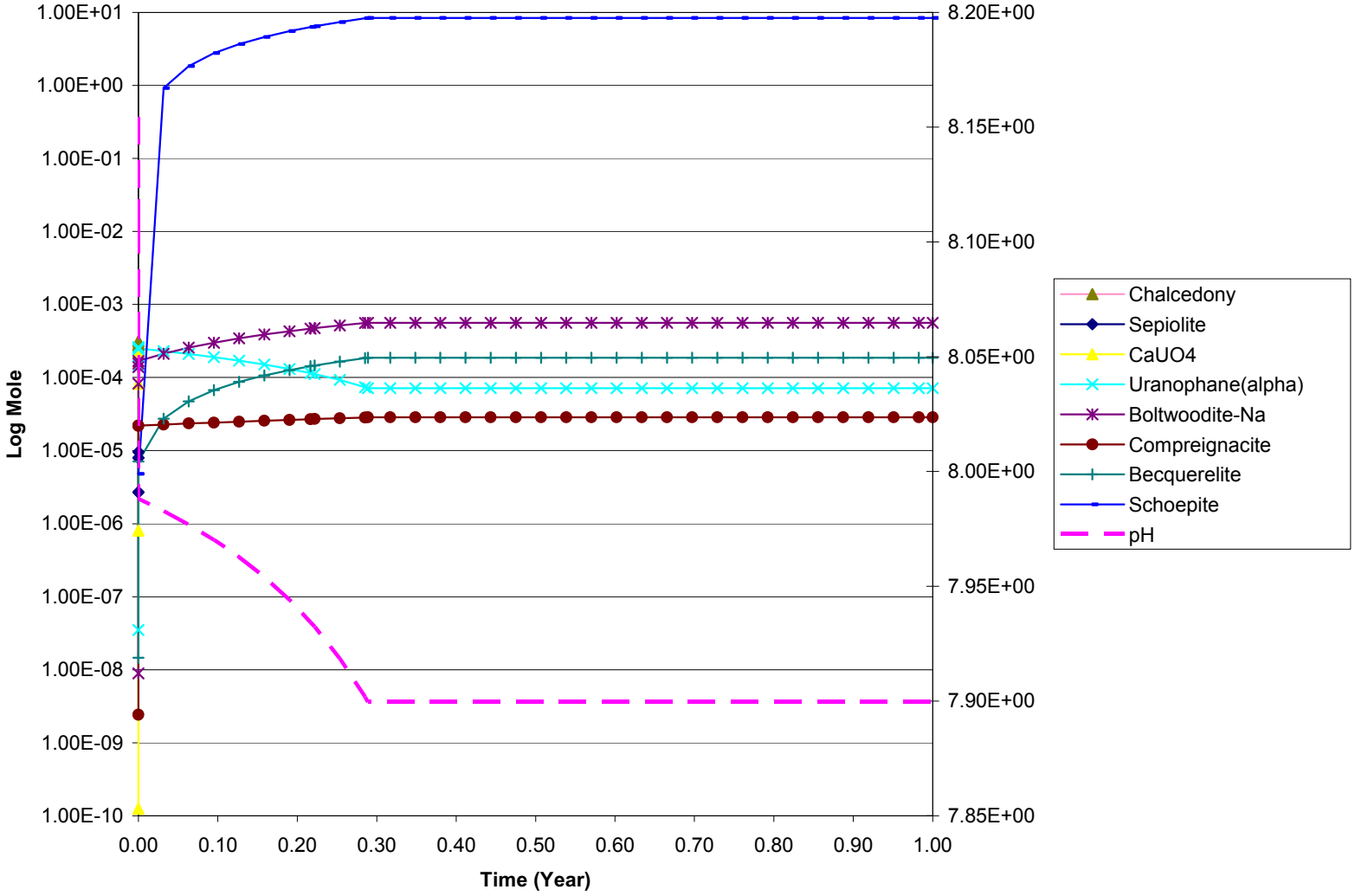

Source: Output DTN: MO0705GEOMODEL.000, folder: CDSP (N-Reactor)/Figures, file: *Fig_CD_S_b.xls*.

Figure E-9. Codisposal Seismic, Stage 1 (oxidation of fuel), Minerals Formed

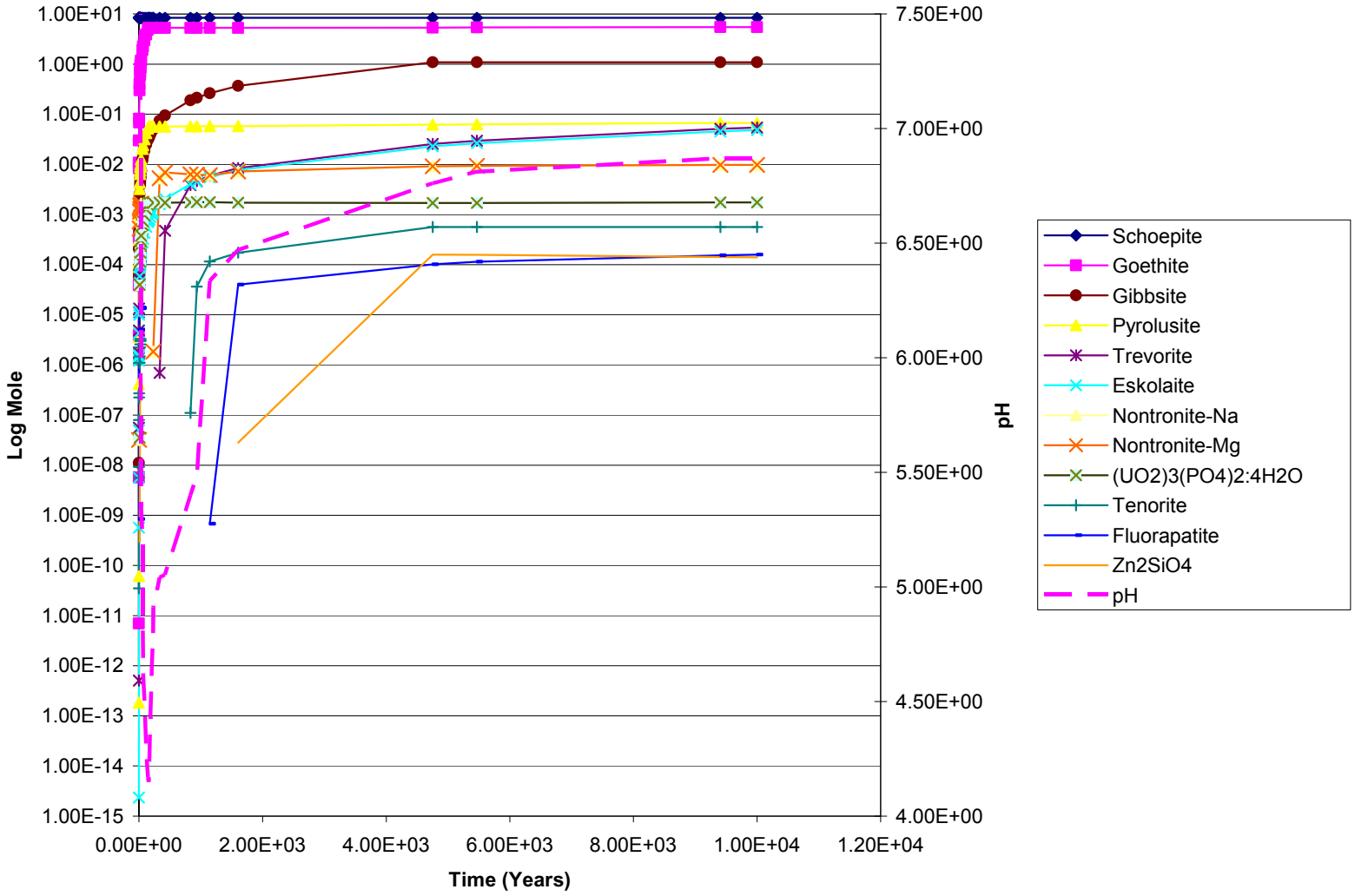

Source: Output DTN: MO0705GEOMODEL.000, folder: CDSP (N-Reactor)/Figures, file: *Fig_CD_S_b.xls*.

Figure E-10. Codisposal Seismic, Stage 2 (oxidation of waste package components), Minerals Formed

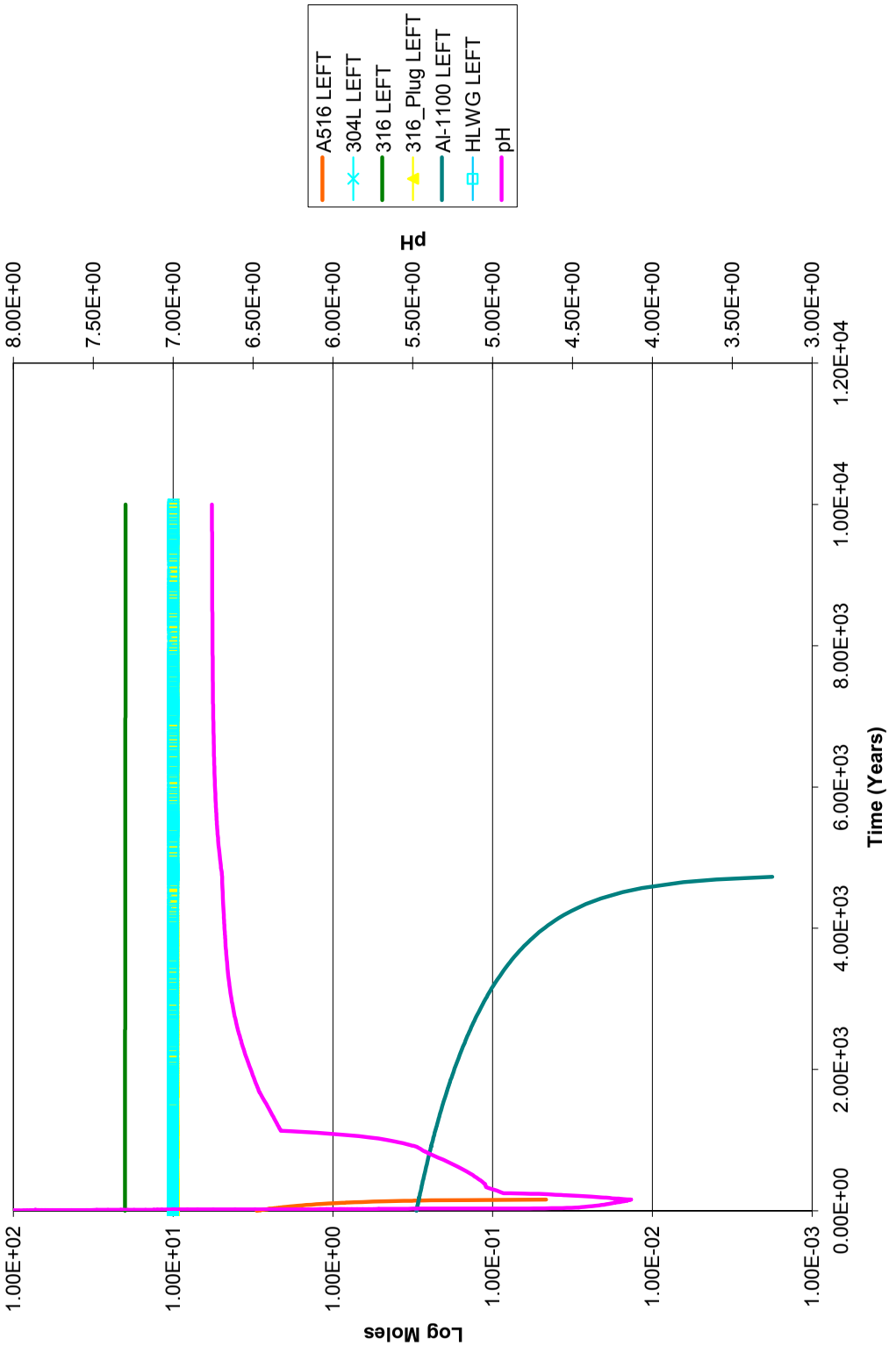

Source: Output DTN: MO0705GEOMODEL.000, folder: CDSP (N-Reactor)/Figures, file: *Fig_reactants_left.xls*.

Figure E-11. Codisposal Seismic, Reactants Remaining

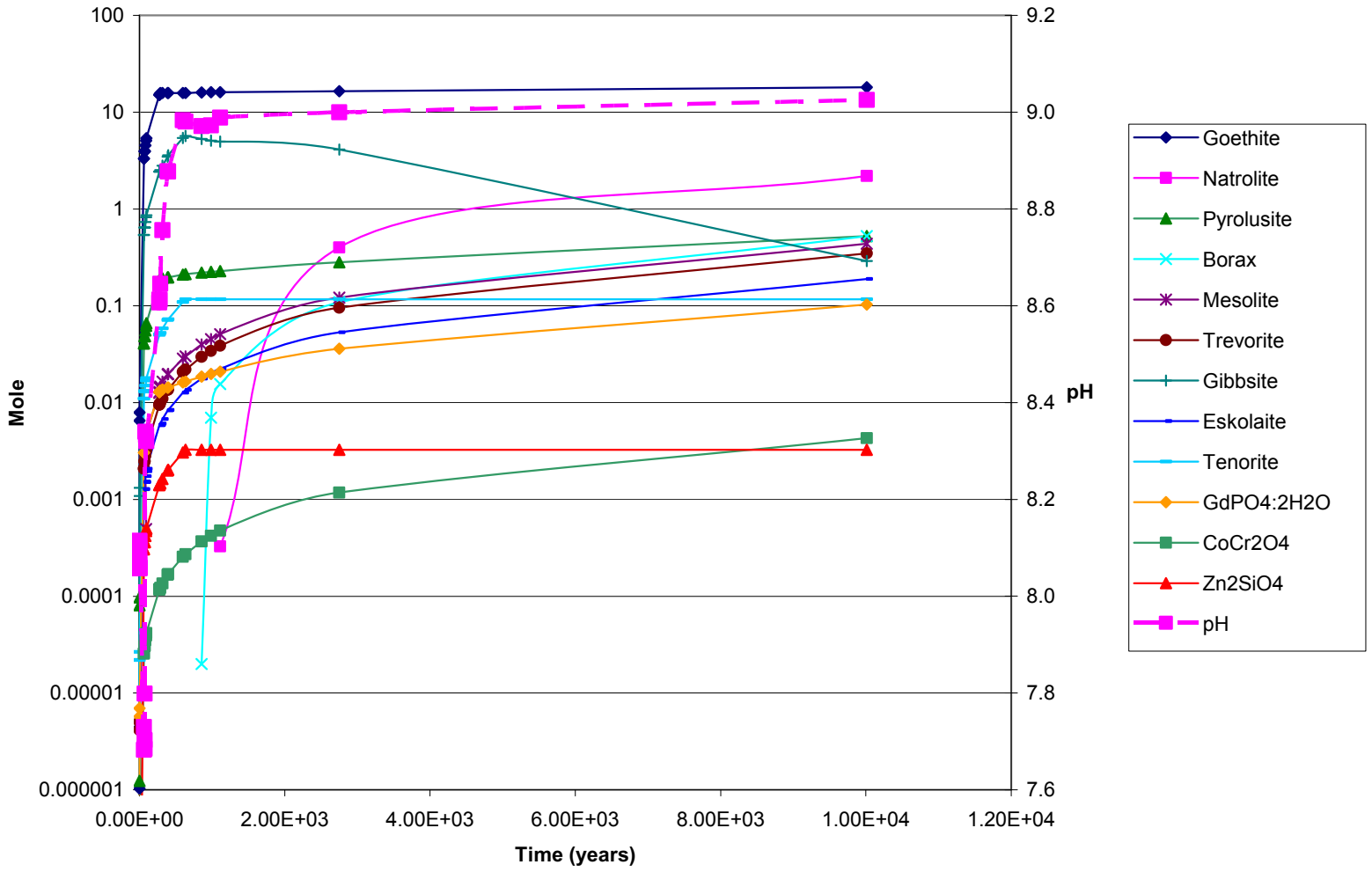

Source: Output DTN: MO0705GEOMODEL.000, folder: FFTF, file: *Fig_FFTF_b.xls*.

Figure E-12. FFTF Igneous, Minerals Formed

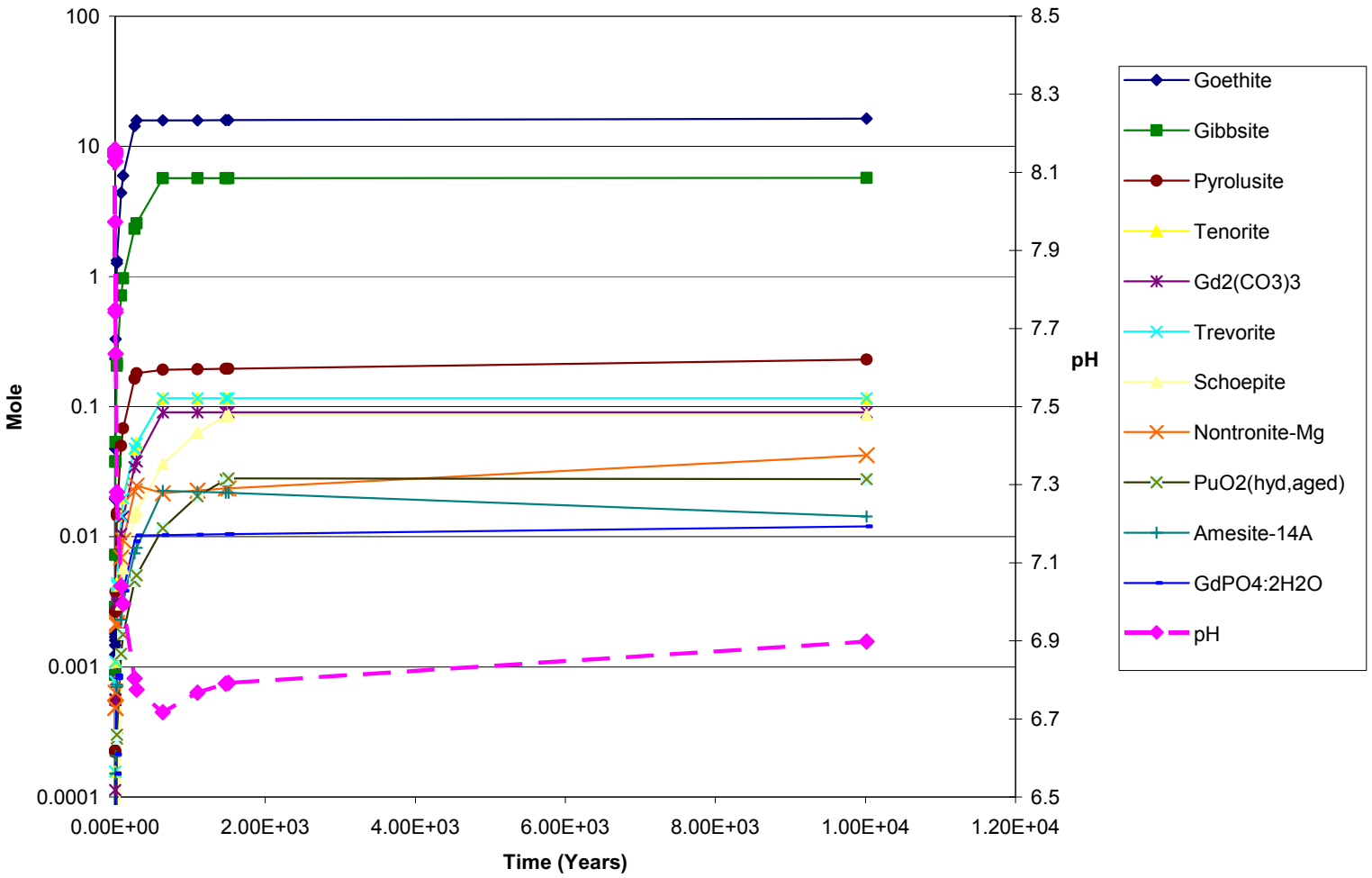

Source: Output DTN: MO0705GEOMODEL.000, folder: FFTF, file: *Fig_FFTF_b.xls*.

Figure E-13. FFTF Seismic, Minerals Formed

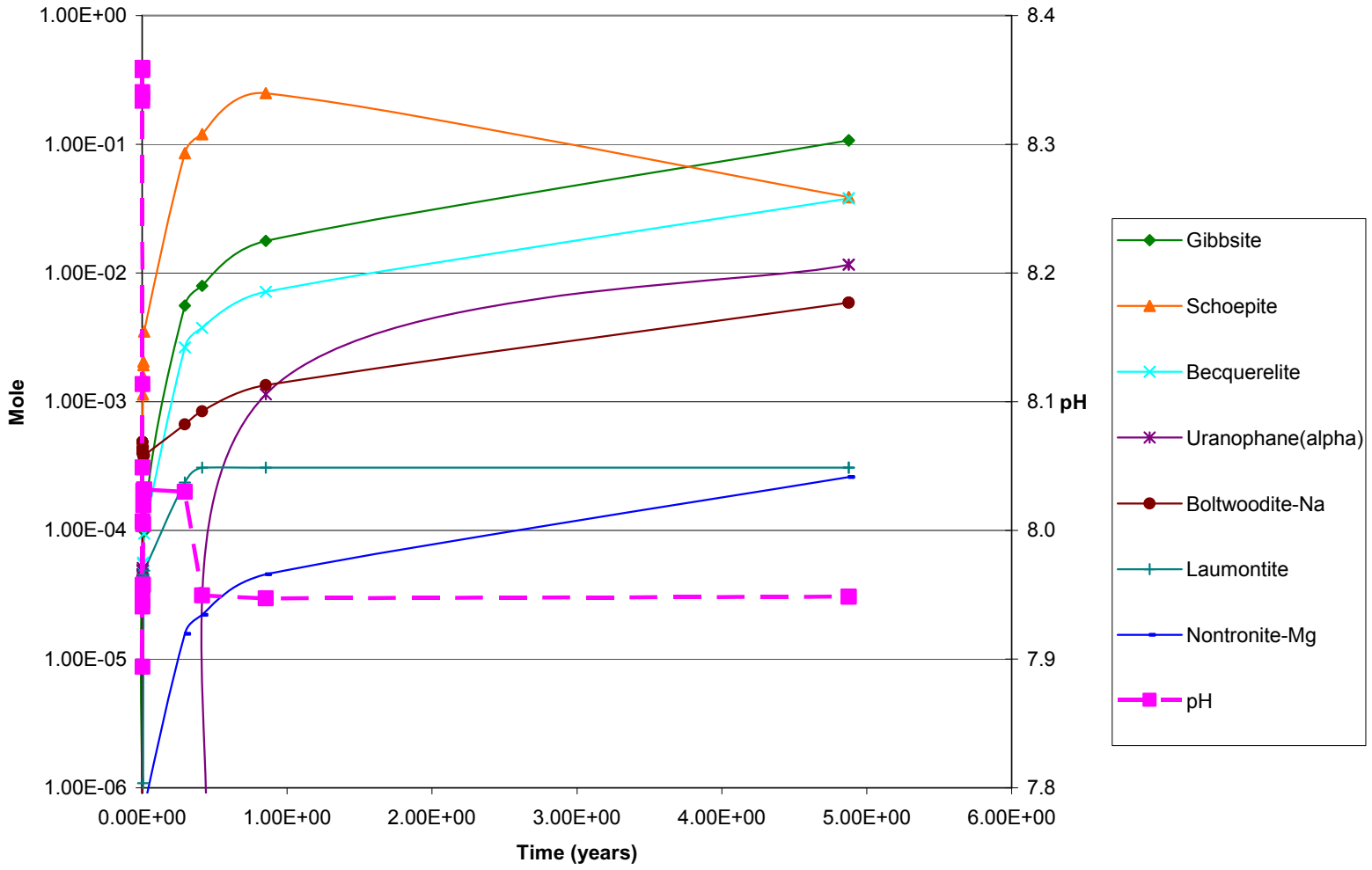

Source: Output DTN: MO0705GEOMODEL.000, folder: TMI, file: *Fig_TMI_b.xls*.

Figure E-14. TMI Igneous, Stage 1, Minerals Formed

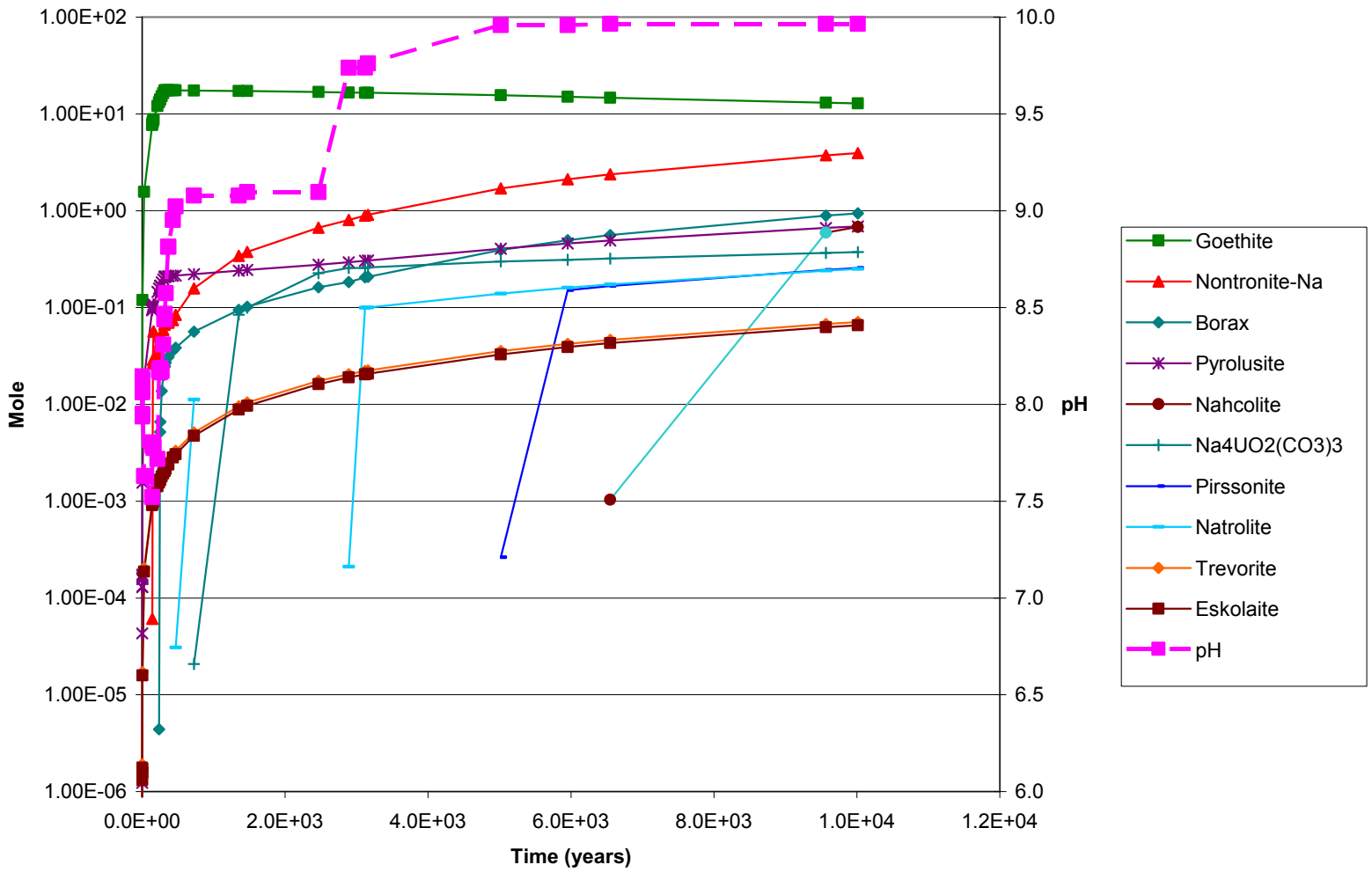

Source: Output DTN: MO0705GEOMODEL.000, folder: TMI, file: *Fig_TMI_b.xls*.

Figure E-15. TMI Igneous, Stage 2, Minerals Formed

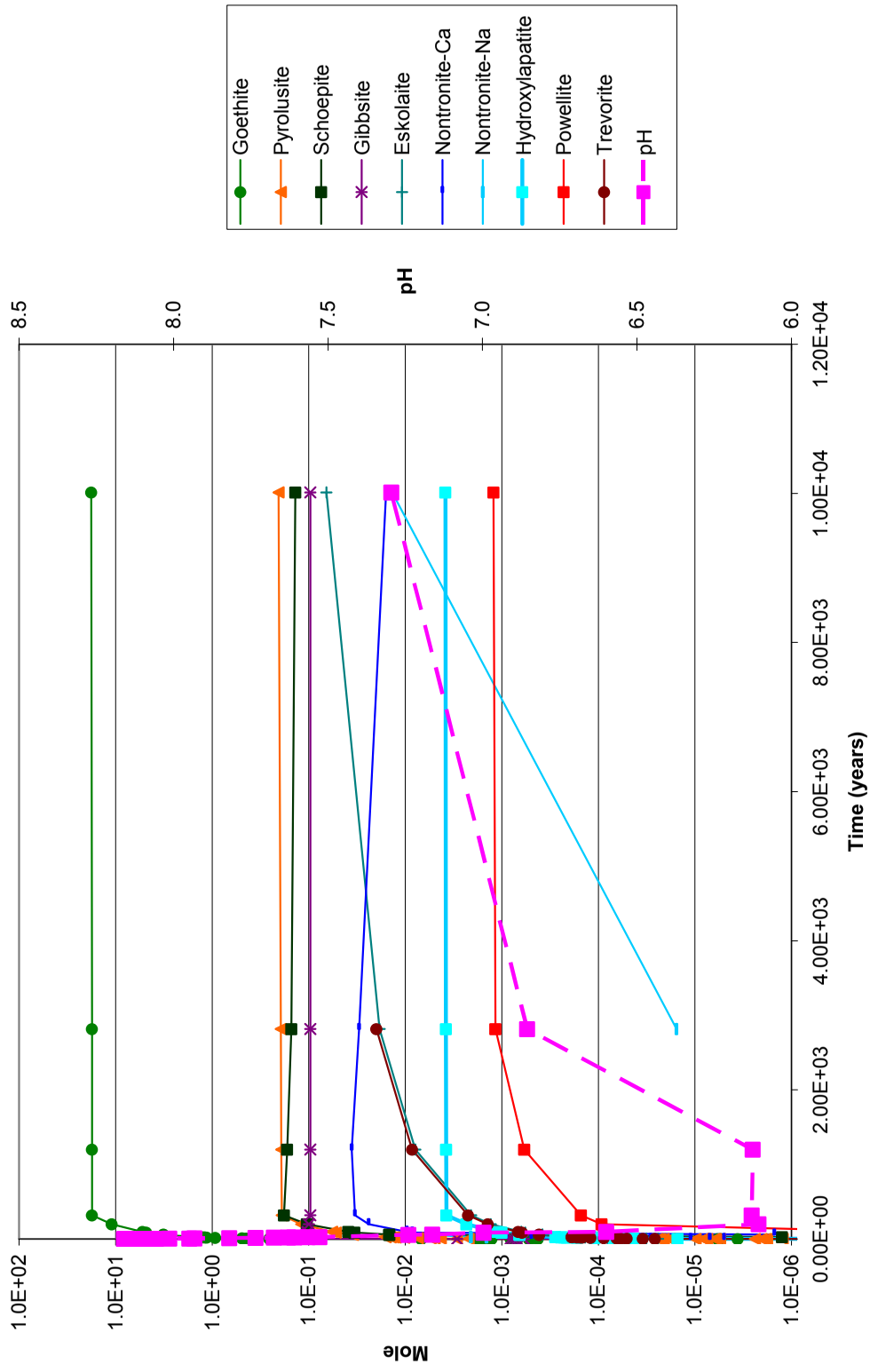

Source: Output DTN: MO0705GEOMODEL.000, folder: TMI, file: *Fig_TMI_b.xls*.

Figure E-16. TMI Seismic, Minerals Formed

INTENTIONALLY LEFT BLANK

APPENDIX F
SEEPAGE RATE SENSITIVITY IN EQ6 MODELS

APPENDIX F
SEEPAGE RATE SENSITIVITY IN EQ6 MODELS

The EQ6 runs described in Section 6.5.1 used two seepage rates: 1 L/yr and 1,000 L/yr. This appendix gives a rationale for choosing those two disparate rates.

Figure F-1 shows the gadolinium, plutonium and uranium retained in the CSNF waste package over 10,000 years (igneous scenario), against the seepage rate used in the calculations. (Here gadolinium is representative of all lanthanides, which are the principal neutron absorbers aside from boron in Stainless Steel Type 304B plates.) The calculation at 1 L/yr is the base-case scenario (represented by file *CSNFIG1.6i*); the other calculations vary only the seepage rate for Basalt 1 water. Seepage rates of 1 L/yr and 1,000 L/yr capture the range of behavior in retention and loss. In particular, at rates of 100 L/yr and above, all plutonium is lost; in the calculations at lower rates, 37% to 74% of the plutonium is retained. At rates of 10 L/yr and above, nearly all the gadolinium is retained; at rates below 10 L/yr, some gadolinium is lost. There is a slight minimum in gadolinium retention at 3 L/yr, but at all seepage rates, more than 85% gadolinium is retained. Therefore the low seepage rates are useful for internal criticality calculations, as the low rates give the greatest retention of fissionable materials and the greatest loss of neutron absorbers.

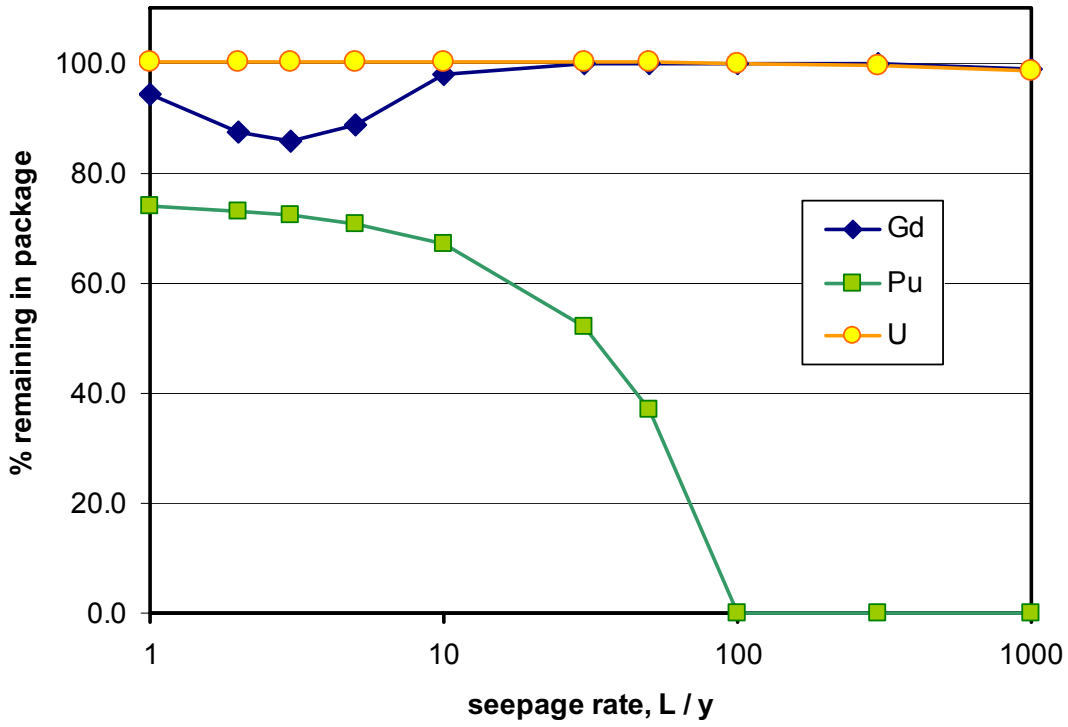

Source: Output DTN: MO0705GEOMODEL.000, folder: seep-sens, file *CSNF-driprate-sens.xls*.

Figure F-1. Comparison of Gadolinium, Plutonium, and Uranium Percent Remaining in the Waste Package for Varied Model Seepage Rates in liters per year, CSNF Igneous Scenario

Figure F-2 shows the gadolinium, plutonium, and uranium retained in the FFTF waste package (igneous scenario) over 10,000 years, against the seepage rate used in the calculations. The calculation at 1 L/yr is the base-case scenario (represented by file *FFTF1_IG.6i*); the other calculations vary only the seepage rate for Basalt 1 water. Seepage rates of 1 L/yr and 1,000 L/yr approximately capture the range of behavior in retention and loss. The highest plutonium retention is at 1 L/yr; at approximately 5 L/yr, the retention of fissionable materials plateaus and stays nearly constant to 1,000 L/yr. At all rates, nearly all the gadolinium is retained. Therefore, the low seepage rates are useful for internal criticality calculations, as the low rates give the greatest retention of fissionable materials.

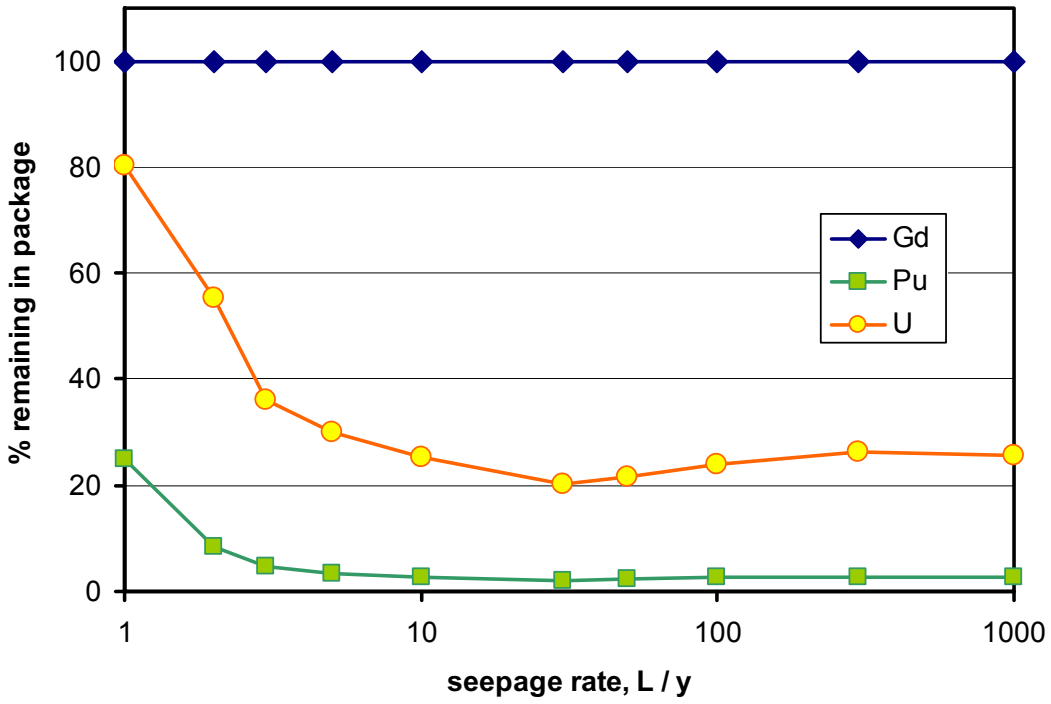

Source: Output DTN: MO0705GEOMODEL.000, folder: seep-sens, file *fftf-driprate-sens.xls*.

NOTE: Seepage rates are given in liters per year.

Figure F-2. Comparison of Gadolinium, Plutonium, and Uranium Percent Remaining in the Waste Package for Varied Model Seepage Rates, FFTF Igneous Scenario

APPENDIX G
QUALIFICATION OF EXTERNAL SOURCES

APPENDIX G
QUALIFICATION OF EXTERNAL SOURCES

This appendix presents planning and documentation for the qualification of external source data used as direct input. Data qualification is performed in accordance with SCI-PRO-006, *Scientific Analyses and Calculations*. The intent of the qualification process is to qualify the data for use only within this report.

Data for Qualification

There are 15 external sources of data used as direct input to this report. These data sources are qualified here for use in this product:

1. Gislason, S.R. and Eugster, H.P. 1987. "Meteoric Water-Basalt Interactions. II: A Field Study in N.E. Iceland." *Geochimica et Cosmochimica Acta*, *51*, 2841-2855. New York, New York: Pergamon. TIC: 259231. [DIRS 179957]

2. Turney, G.L. 1986. *Quality of Ground Water in the Columbia Basin, Washington, 1983*. Water-Resources Investigations Report 85-4320. Tacoma, Washington: U.S. Geological Survey. ACC: LLR.20070321.0001. [DIRS 179852]

3. Allison, J.M. 2004. "Request for Referenceable Information on High-Level Waste (HLW) Radionuclide Inventories in Support of Preparation of the Yucca Mountain Project License Application (Your Letter, JCP-0445, 1/28/04)." Memorandum from J.M. Allison (DOE/SR) to J. Arthur, III (OCRWM), February 26, 2004, 0303040661, with attachment. ACC: MOL.20040317.0265. [DIRS 168734]

4. Blenkinsop, R.D.; Currell, B.R.; Midgley, H.G.; and Parsonage, J.R. 1985. "The Carbonation of High Alumina Cement, Part II." *Cement and Concrete Research, 15,* (3), 385-390. Elmsford, New York: Pergamon Press. TIC: 259450. [DIRS 181193]

5. Dunster, A.M.; Bigland, D.J.; and Holton, I.R. 2000. "Rates of Carbonation and Reinforcement Corrosion in High Alumina Cement Concrete." *Magazine of Concrete Research, 52,* (6), 433-441. London, England: Thomas Telford. TIC: 259448. [DIRS 181194]

6. Pankratz, L.B. 1982. *Thermodynamic Properties of Elements and Oxides.* Bulletin 672. Washington, D. C.: U.S. Bureau of Mines. ACC: LLR.20070522.0016. [DIRS 181065] (Gd_2O_3 section only)

7. Cantrell, K.J. and Byrne, R.H. 1987. "Temperature Dependence of Europium Carbonate Complexation." *Journal of Solution Chemistry, 16,* (7), 555-566. New York, New York: Plenum Publishing. TIC: 259374. [DIRS 181066]

8. DOE (U.S. Department of Energy) 1992. *Characteristics of Potential Repository Wastes*. DOE/RW-0184-R1. Volume 1. Washington, D.C.: U.S. Department of Energy, Office of Civilian Radioactive Waste Management. ACC: HQO.19920827.0001. [DIRS 102812]

9. DOE (U.S. Department of Energy) 2002. *SNF Canister Characteristics for Criticality Analysis of a Dual Canister/Waste Package Disposal Strategy*. DOE/SNF/REP-074, Rev. 0. Idaho Falls, Idaho: U.S. Department of Energy. TIC: 253869. [DIRS 161752]

10. DOE (U.S. Department of Energy) 2003. *Review of Oxidation Rates of DOE Spent Nuclear Fuel Part 2. Nonmetallic Fuel*. DOE/SNF/REP-068, Rev. 0. Idaho Falls, Idaho: U.S. Department of Energy, Idaho Operations Office. ACC: DOC.20030905.0009. [DIRS 166027]

11. DOE (U.S. Department of Energy) 2004. *Interim Report on the Corrosion Performance of a Neutron Absorbing Ni-Cr-Mo-Gd Alloy*. DOE/SNF/REP-086, Rev. 0. Idaho Falls, Idaho: U.S. Department of Energy, Idaho Operations Office. ACC: DOC.20040412.0001. [DIRS 168434]

12. DOE (U.S. Department of Energy) 2000. *N Reactor (U-Metal) Fuel Characteristics for Disposal Criticality Analysis*. DOE/SNF/REP-056, Rev. 0. Washington, D.C.: U.S. Department of Energy, Office of Environmental Management. TIC: 247956. [DIRS 150095].

13. DOE (U.S. Department of Energy) 2000. *Review of Oxidation Rates of DOE Spent Nuclear Fuel, Part 1: Metallic Fuel*. DOE/SNF/REP-054, Rev. 0. Washington, D.C.: U.S. Department of Energy. TIC: 248978. [DIRS 152658]

14. INEEL (Idaho National Engineering and Environmental Laboratory) 2002. *FFTF (MOX) Fuel Characteristics for Disposal Criticality Analysis*. DOE/SNF/REP-032, Rev. 1. Idaho Falls, Idaho: U.S. Department of Energy, Idaho National Operations Office. TIC: 252933. [DIRS 158820]

15. Taylor, L.L. 2005. *Using Fuel Parameters to Predict DOE SNF Canister Loadings*. EDF-NSNF-046, Rev. 0. Washington, D.C.: U.S. Department of Energy, National Spent Nuclear Fuel Program. ACC: LLR.20070515.0108. [DIRS 180657]

Qualification Methods Selected

Three methods were selected for qualification, as outlined in Attachment 3 of SCI-PRO-001, *Qualification of Unqualified Data*:

Method 1, equivalent QA program, is used for reports from DOE and its contactors that describe fuel and associated material characteristics. The rationale for using this method is that the QA programs for the reports can be traced, while all other methods are largely inapplicable; typically these reports cite older, one-of-a-kind records from decommissioned facilities.

Method 2, corroborating data, is used for two reports based on peer reviewed journal articles, as a supplement for Method 5; and for one DOE report, as a supplement to Method 1.

Method 5, technical assessment, is used for seven data sources. The rationale for using this method for these documents is that there is no record of the QA plans under which the data were collected in the original source (i.e., scientific journal or publication). These evaluations were

performed independently from the data collection or data reduction process and by a subject matter expert. For Method 5, two "actions to be taken" from SCI-PRO-001 are considered: (b) determination that confidence in the data is warranted (e.g., by assurances that the processes were collected by qualified professionals), and (c) confirmation that the data have been used in similar applications.

Qualification process attributes used in the technical assessment of the external sources are selected from the list provided in Attachment 4 of SCI-PRO-001, which represent the acceptance criteria used to determine if the data are qualified. Process attributes used specifically for data qualification in this report are:

1. *Qualifications of personnel or organizations generating the data are comparable to qualification requirements of personnel generating similar data under an approved program that supports the YMP License Application process or post closure science;*

2. *The extent to which the data demonstrate the properties of interest (e.g., physical, chemical, geologic, mechanical);*

3. *Prior uses of the data and associated verification processes;*

4. *Prior peer or other professional reviews of the data and their results;*

5. *Extent and quality of corroborating data or confirmatory testing results;*

6. *The extent to which conditions under which the data were generated may partially meet the QA program that supports the YMP License Application process or post closure science.*

Qualification of External Data from Gislason and Eugster 1987 [DIRS 179957]

The data used from this document are the compositions of groundwater from a basalt aquifer in Iceland. These data were used to estimate the composition of influent water in the igneous scenario. Method 5, Technical Assessment (SCI-PRO-001, Attachment 3) is used to qualify these data. The "action to be taken" is (b), determination that confidence is warranted.

The following process attributes were used to assess these external data:

- *Qualifications of personnel or organizations generating the data are comparable to qualification requirements of personnel generating similar data under an approved program that supports the YMP License Application process or post-closure science*

- *The extent to which the data demonstrate the properties of interest (e.g., physical, chemical, geologic, mechanical).*

Justification for the appropriate use of the data: This journal article contains analyses of groundwater samples from springs issuing from a fractured basalt aquifer in Iceland. The researchers are professors at the University of Iceland and Johns Hopkins University, respectively, and have many publications in the area of rock-water interactions to their credit.

The data are published in *Geochimica et Cosmochimica Acta*, one of the oldest and most respected periodicals in the field of geochemistry. All articles are subjected to peer-review by three researchers in the field. The data are for groundwaters in equilibrium with basalt and are used to simulate the water that would be entering a breached waste package after inundation in magma and cooling to less than the boiling temperature of the fluid. The equilibrium concentrations of those hypothesized fluids should be similar to those from basalt aquifers.

Based on this assessment, the basalt water data from Gislason and Eugster (1987 [DIRS 179957]) is qualified for intended use within this report.

Qualification of External Data from Turney 1986 [DIRS 179852]

The data used from this document are the compositions of groundwater from a basalt aquifer in the Columbia Basin, Washington. These data were used to estimate the composition of influent water in the igneous scenario. Method 5, Technical Assessment (Attachment 3, SCI-PRO-001) is used to qualify these data. The "action to be taken" is (b), determination that confidence is warranted.

The following process attributes were used to assess these external data:

- *Qualifications of personnel or organizations generating the data are comparable to qualification requirements of personnel generating similar data under an approved program that supports the YMP License Application process or post-closure science*

- *The extent to which the data demonstrate the properties of interest (e.g., physical, chemical, geologic, mechanical).*

Justification for the appropriate use of the data: This U.S. Geological Survey (USGS) Water-Resources Investigations Report contains analyses of groundwater samples from groundwater wells in a fractured basalt aquifer in the Columbia Basin, Washington. The researcher was a member of the U.S. Geological Survey and has many publications in the area of water resources and quality to his credit. The data are published in Water-Resources Investigations Report 85-4320, one of the standard reports on water resources and quality published by the USGS. All USGS publications are subjected to peer-review by independent USGS researchers in the field and are approved for publication by the Director. The data are for groundwaters in equilibrium with basalt and are used to simulate the water that would be entering a breached waste package after inundation in magma and cooling back to less than the boiling temperature of the fluid. The equilibrium concentrations of those hypothesized fluids should be similar to those from basalt aquifers.

Based on this assessment, the basalt water data from Turney (1986 [DIRS 179852]) are qualified for their intended use within this report.

Technical Assessment of External Data from Allison 2004 [DIRS 168734]

In previous versions of this document, the composition of DHLW glass was estimated from the compositions of waste sludges and the estimates of the components necessary to produce a borosilicate glass waste form. The Savannah River Laboratory (SRL) Defense Waste Processing

Facility generated several tons of DHLW glass in batches and these were sampled and analyzed. The measured DHLW glass compositions were incorporated into this report. Method 5, Technical Assessment (Attachment 3, SCI-PRO-001) is used to qualify these data. The "action to be taken" is (b), determination that confidence is warranted.

The following process attributes were used to assess these external data:

- *Qualifications of personnel or organizations generating the data are comparable to qualification requirements of personnel generating similar data under an approved program that supports the YMP License Application process or post-closure science*

- *The extent to which the data demonstrate the properties of interest (e.g., physical, chemical, geologic, mechanical).*

Justification for the appropriate use of data: The analyses were conducted in accordance with SRL analytical procedures and under the DOE-approved SRL QA program (Fellinger and Bibler 2000 [DIRS 179902]). The technical personnel are internationally recognized in the field of nuclear waste-form chemistry and have many peer-reviewed publications to their credit. The SRL QA program requires multiple analyses of the HLWG samples as an internal quality control check and has procedures for maintenance and calibration of the instrumentation. Thus, the qualifications of the personnel and organization generating these data are comparable to those generating data specifically for the YMP license application.

These data are specifically for the chemical compositions of the HLWG that are slated for disposal in the Yucca Mountain repository. The applicability of the data is direct and requires no interpretation or extrapolation.

Thus, these data are qualified for intended use within this report.

Qualification of External Data from Blenkinsop et al. 1985 [DIRS 181193]

The data used from this document are the rates of carbonation of high alumina cements. These data were used to estimate the corrosion rate for LiCon (light concrete) cement; specifically, the data were used to evaluate temperature dependence. Method 5, Technical Assessment (Attachment 3, SCI-PRO-001) is used to qualify these data. The "action to be taken" is (b), determination that confidence is warranted. Method 2, corroborating data, supplements the qualification.

The following process attributes were used to assess these external data:

- *The extent to which the data demonstrate the properties of interest (e.g., physical, chemical, geologic, mechanical)*

- *Prior peer or other professional reviews of the data and their results*

- *Extent and quality of corroborating data or confirmatory testing results.*

LiCon is a high alumina cement/concrete, and, at the conditions of simulation (constant CO_2 fugacity), carbonation is the principal mechanism of cement alteration. This study was published in a peer-reviewed journal. The two parts of this journal article (only Part II is used here, but Part I provides background material) have been cited nine times, never negatively. The basic mechanism postulated for alteration agrees with the mechanism postulated in Dunster et al. (2000 [DIRS 181194]). The rates extracted from Blenkinsop et al. (1985 [DIRS 181193]) and the following article by Dunster et al. (2000 [DIRS 181194]) agree qualitatively with the rates estimated by Crammond and Currie (1993 [DIRS 181195]).

Thus, these data are qualified for intended use within this report.

Qualification of External Data from Dunster et al. 2000 [DIRS 181194]

The data used from this document are the rates of carbonation of high alumina cements. These data were used to estimate the corrosion rate for LiCon cement. Method 5, Technical Assessment (Attachment 3, SCI-PRO-001), is used to qualify these data. The "action to be taken" is (b), determination that confidence is warranted. Method 2, corroborating data, supplements the qualification.

The following process attributes were used to assess these external data:

- *The extent to which the data demonstrate the properties of interest (e.g., physical, chemical, geologic, mechanical)*
- *Qualifications of personnel or organizations generating the data are comparable to qualification requirements of personnel generating similar data under an approved program that supports the YMP License Application process or post-closure science*
- *Prior peer or other professional reviews of the data and their results*
- *Extent and quality of corroborating data or confirmatory testing results.*

LiCon is a high alumina cement/concrete, and at the conditions of simulation (constant CO_2 fugacity), carbonation is the principal mechanism of cement alteration. The 2000 article by Dunster et al. (2000 [DIRS 181194]) has never been cited, but this is a very narrow field with few practitioners, and the article is relatively recent. However, Dunster has been cited 20 times in the peer-reviewed literature for his studies of cement reactions and is an expert in the field of cement alteration. These two studies (Blenkinsop et al. 1985 [DIRS 181193] and Dunster et al. 2000 [DIRS 181194]) agree with each other on the mechanism of degradation and give overlapping rates; furthermore, they are corroborated qualitatively by field observations described by Crammond and Currie (1993 [DIRS 181195]).

Thus, these data are qualified for intended use within this report.

Qualification of External Data from Pankratz 1982 [DIRS 181065]

These data were used to estimate the heat capacity of $Gd_2(CO_3)_3$ by the oxide summation method, as described in Appendix D. The estimated heat capacities were then used to calculate

the logK(T) for the dissolution of the solid carbonate, via the standard thermochemical methods described in Section 6.1 of *Qualification of Thermodynamic Data for Geochemical Modeling of Mineral-Water Interactions in Dilute Systems* (SNL 2007 [DIRS 177409]). Method 5, Technical Assessment (Attachment 3, SCI-PRO-001), is used to qualify these data. The "action to be taken" is (b), determination that confidence is warranted.

The following process attributes were used to assess these external data:

- *The extent to which the data demonstrate the properties of interest (e.g., physical, chemical, geologic, mechanical)*
- *Qualifications of personnel or organizations generating the data are comparable to qualification requirements of personnel generating similar data under an approved program that supports the YMP License Application process or post-closure science*
- *Prior peer or other professional reviews of the data and their results.*

This source provides exactly the equations for heat capacity of Gd_2O_3; these data are needed for the method outlined in Appendix D. The Pankratz reference is basically a handbook compilation of data from peer-reviewed sources. The primary sources of the lower temperature data (i.e., those needed for the extrapolation) on p. 167 are:

1. A bulletin by K.A. Gschneidner, who has authored more than 300 papers, mostly on rare earth chemistry, in peer-reviewed journals
2. An article by B.H. Justice in the respected *Journal of Physical Chemistry*. This specific article is not cited in journals, probably because the subject is obscure. However, Justice has written 21 articles for peer-reviewed journals. His work on rare earth thermochemistry (as a first or second author) has been cited more than 117 times in the peer-reviewed literature.

For article (1), the author's reputation, as indicated by the citation record, demonstrates his qualifications. Article (2) appeared in a highly respected peer-reviewed journal, and the author's citation record also demonstrates his qualifications.

Thus, these data are qualified for intended use within this report.

Qualification of External Data from Cantrell and Byrne 1987 [DIRS 181066]

The data from this article are used to derive the up-temperature log(K) values for several lanthanide aqueous complexes, as described in Appendix D. Method 5, Technical Assessment (Attachment 3, SCI-PRO-001), is used to qualify these data. The "Action(s) to be taken" are (b), determination that confidence is warranted, and (c), confirmation that the data have been used in similar applications.

The following process attributes were used to assess these external data:

- *The extent to which the data demonstrate the properties of interest (e.g., physical, chemical, geologic, mechanical)*

- *Qualifications of personnel or organizations generating the data are comparable to qualification requirements of personnel generating similar data under an approved program that supports the YMP License Application process or post-closure science*

- *Prior peer or other professional reviews of the data and their results*

- *Prior uses of the data and associated verification processes.*

The Cantrell and Byrne article provides the exact data needed to calculate the up-temperature stability constants. This article appeared in the respected peer-reviewed journal, *The Journal of Solution Chemistry*, and has been cited 24 times in the peer-reviewed literature, never negatively. Cantrell has been cited nearly 600 times in the peer-reviewed literature. Cantrell's related 1987 paper in *Geochimica et Cosmochimica Acta*, "Rare-earth element complexation by carbonate and oxalate ions," alone has been cited 210 times and identifies Cantrell as an expert in this field. Byrne et al. (1988 [DIRS 181088]) extended the temperature dependence for europium to all lanthanides, and Wood (1990 [DIRS 181086]) used the Cantrell and Byrne (1987 [DIRS 181066]) data to calculate rare earth complexation at much higher temperatures. Therefore these data are well-supported by citation and the expertise of the authors.

Thus, these data are qualified for intended use within this report.

Qualification of External Data from DOE 1992 [DIRS 102812]

This report supplies glass pour-canister dimensions and fill volumes. Method 1, Equivalent QA Program (Attachment 3, SCI-PRO-001), is used to qualify these data.

The following process attributes were used to assess these external data:

- *The extent to which the data demonstrate the properties of interest (e.g., physical, chemical, geologic, mechanical)*

- *Qualifications of personnel or organizations generating the data are comparable to qualification requirements of personnel generating similar data under an approved program that supports the YMP License Application process or post-closure science*

- *Prior peer or other professional reviews of the data and their results.*

The DOE 1992 report contains the dimensions and volumes needed to calculate surface areas and masses of reactants for some EQ6 simulations. The adequacy of the QA program is first documented in the report itself (DOE 1992 [DIRS 102812]), which describes the plan for peer review of the data to satisfy OQA requirements for the OCRWM program; and by Cowart and Notz (1992 [DIRS 182747]), who summarize and document the peer review of DOE 1992. The qualifications of the 27 peers are documented in Appendix F of the report by Cowart and Notz.

Thus, these data are qualified for intended use within this report.

Qualification of External Data from DOE 2002 [DIRS 161752]

This report contains the composition and density of LiCon. Method 1, Equivalent QA Program (Attachment 3, SCI-PRO-001), is used to qualify these data.

The following process attributes were used to assess these external data:

- *The extent to which the data demonstrate the properties of interest (e.g., physical, chemical, geologic, mechanical)*
- *Qualifications of personnel or organizations generating the data are comparable to qualification requirements of personnel generating similar data under an approved program that supports the YMP License Application process or post-closure science.*

The report contains the information needed to develop the LiCon reactant for EQ6 simulations of the degradation of TMI packages. There is no other known qualified source of these data. The information for the report was gathered and assessed by the National Spent Nuclear Fuel Program (NSNFP). Brown (2002 [DIRS 182748]) reports that a 2002 audit found the NSNFP QA program compliant with *Quality Assurance Requirements and Description* (QARD) (DOE 2007 [DIRS 182051]).

Thus, these data are qualified for intended use within this report.

Qualification of External Data from DOE 2003 [DIRS 166027]

This report asserts that the dissolution of PuO_2 is approximately 10 times slower than the dissolution of UO_2. Method 1, Equivalent QA Program (Attachment 3, SCI-PRO-001), is used to qualify these data.

The following process attributes were used to assess these external data:

- *The extent to which the data demonstrate the properties of interest (e.g., physical, chemical, geologic, mechanical)*
- *Qualifications of personnel or organizations generating the data are comparable to qualification requirements of personnel generating similar data under an approved program that supports the YMP License Application process or post-closure science.*

This information is needed to develop a reactant dissolution rate for EQ6 simulations; no other qualifiable source of data is known. The full quality assurance audit for 2003 was rescheduled for the first quarter of 2004; the rescheduled audit, which found compliance with the QARD, is documented in a report issued by Robertson (2004 [DIRS 182751]). There was, however, a Quality Assurance Management Assessment for NSNFP in 2003 (Blyth 2004 [DIRS 182750]); that assessment determined the audited aspects of the program were compliant with the QARD.

Thus, these data are qualified for intended use within this report.

Qualification of External Data Sources in DOE 2004 [DIRS 168434]

This source gives corrosion rates for nickel-gadolinium alloys that would potentially be used for neutron control material in certain DOE waste packages. Method 1, Equivalent QA Program (Attachment 3, SCI-PRO-001), is used to qualify these data.

The following process attributes were used to assess these external data:

- *The extent to which the data demonstrate the properties of interest (e.g., physical, chemical, geologic, mechanical)*

- *Qualifications of personnel or organizations generating the data are comparable to qualification requirements of personnel generating similar data under an approved program that supports the YMP License Application process or post-closure science.*

The nickel-gadolinium alloy corrosion rates are needed to determine kinetic characteristics for EQ6 simulations of the degradation of certain DOE waste packages. The data were gathered and checked by the NSNFP. Robertson (2004 [DIRS 182751]) summarizes the 2004 QA audit of NSNFP on March 29 through April 1, 2004 and states that the NSNFP was satisfactorily implementing the QARD at that time. Golan (2004 [DIRS 182752]) reports an additional audit conducted from June 21-24, 2004, which focused on specific aspects of the NSNP. Though the last audit found one significant condition adverse to quality, it was determined that as whole, the specific audited programs were effectively implementing the QARD.

Thus, these data are qualified for intended use within this report.

Qualification of External Data Sources in DOE 2000 [DIRS 150095]

This report gives: (1) N-reactor fuel density and composition; (2) the alloys chosen for the multicanister overpack (Stainless Steel Type 304L) and the basket spacer grids (1100 aluminum); and (3) the dimensions of the MCO baskets. Method 1, Equivalent QA Program (Attachment 3, SCI-PRO-001), is used to qualify these data.

The following process attributes were used to assess these external data:

- *The extent to which the data demonstrate the properties of interest (e.g., physical, chemical, geologic, mechanical)*

- *Qualifications of personnel or organizations generating the data are comparable to qualification requirements of personnel generating similar data under an approved program that supports the YMP License Application process or post-closure science.*

The data were gathered and assessed by the NSNFP. The report gives the exact information needed to develop input for EQ6 simulations. Clarke (2000 [DIRS 182753]) gives a summary letter and enclosure with the full audit report of the NSNFP for 2000. On pages 13 and 14 of the enclosure, every QA program element, as required by the QARD, received an overall satisfactory rating.

Thus, these data are qualified for intended use within this report.

Qualification of External Data Sources in DOE 2000 [DIRS 152658]

This report provides the rate equations for the reaction of N-reactor fuel. Method 1, Equivalent QA Program (Attachment 3, SCI-PRO-001), and Method 2, Corroborating Data, are used to qualify these inputs.

The following process attributes were used to assess these external data:

- *The extent to which the data demonstrate the properties of interest (e.g., physical, chemical, geologic, mechanical)*

- *Qualifications of personnel or organizations generating the data are comparable to qualification requirements of personnel generating similar data under an approved program that supports the YMP License Application process or post-closure science.*

The report gives the kinetic constants necessary to produce input for EQ6 simulations of N-reactor fuel degradation. Actually, N-reactor simulations assume that the fuel degradation is fast (within the first few years), so the report need only conclude that the reaction with water proceeds rapidly. The rate estimates were gathered and assessed under NSNFP. Clarke (2000 [DIRS 182753]) provides a summary letter and enclosure with the full audit report of the NSNFP for 2000. On pages 13 and 14 of the enclosure, every QA program element, as required by the QARD, received an overall satisfactory rating.

The development of the N-reactor fuel reaction rates is found in Section 2.2.3, pp. 49 to 52 of *Review of Oxidation Rates of DOE Spent Nuclear Fuel, Part 1: Metallic Fuel* (DOE 2000 [DIRS 152658]). The discussion starts with a detailed description of uranium/water reaction rates measured before 1960. This report (DOE 2000 [DIRS 152658]) then reanalyzes and evaluates all available uranium/water reactions rate data up to 1999. The results of the analysis are graphically compared in Figure 2-10 and in Arrhenius expressions in Table 2-4, using data from three different authors. It was concluded that the resulting Arrhenius expressions calculated by the report and the other authors and summarized in Figure 2-10 were essentially the same and completely overlayed each other.

The Arrhenius dependence of the uranium/water reaction determined in the report was provided in Equation 2-39. It was determined that the four Arrhenius expressions were essentially the same and were consistent with the graphical overlay observed in Figure 2-10. The authors concluded that "there is high confidence in the validity of the temperature dependent reaction rates." Considering that the MDR needs only to show that the reaction is fast, the agreement of the varied expressions is more than adequate.

Thus, these data are qualified for intended use within this report.

Qualification of External Data Sources in INEEL 2002 [DIRS 158820]

This report gives the dimensions of DOE canister and internals, as well as fuel characteristics and compositions, for FFTF and TMI waste packages. Method 1, Equivalent QA Program (Attachment 3, SCI-PRO-001), was used to qualify the data.

The following process attributes were used to assess these external data:

- *The extent to which the data demonstrate the properties of interest (e.g., physical, chemical, geologic, mechanical)*
- *Qualifications of personnel or organizations generating the data are comparable to qualification requirements of personnel generating similar data under an approved program that supports the YMP License Application process or post-closure science.*

This report gives the exact information needed to prepare input files for EQ6 simulations of waste package degradation. The information for the report was gathered and assessed by the NSNFP. Brown (2002 [DIRS 182748]) reports that a 2002 audit found the NSNFP QA program was compliant with the QARD.

Thus, these data are qualified for intended use within this report.

Qualification of External Data Sources in Taylor 2005 [DIRS 180657]

This report gives dimensions and characteristics for DOE and DSNF canisters and internals. Method 1, Equivalent QA Program (Attachment 3, SCI-PRO-001), was used to qualify the data.

The following process attributes were used to assess these external data:

- *The extent to which the data demonstrate the properties of interest (e.g., physical, chemical, geologic, mechanical)*
- *Qualifications of personnel or organizations generating the data are comparable to qualification requirements of personnel generating similar data under an approved program that supports the YMP License Application process or post-closure science.*

This report gives the exact information needed to prepare input files for EQ6 simulations of waste package degradation. The information for the report was gathered and assessed by the NSNFP. Golan (2005 [DIRS 182754]) reports that a 2005 audit found the NSNFP was satisfactorily implementing the QARD.

Thus, these data are qualified for intended use within this report.